THE ROLE OF POST-TRANSLATIONAL MODIFICATIONS AND ALLOSTERY IN THE RECEPTOR GUANYLYL CYCLASES GC-A AND GC-B

A Dissertation

SUBMITTED TO THE FACULTY OF
UNIVERSITY OF MINNESOTA
BY

Aaron Bradley Edmund

IN PARTIAL FULFILLMENT OF THE REQUIREMENTS
FOR THE DEGREE OF

DOCTOR OF PHILOSOPHY

Advisor: Dr. Lincoln Potter

Degree Conferral: December 2018

ACKNOWLEDGEMENTS

The work in these chapters was supported by the following sources:

National Institutes of Health grants R37HD014939, R01GM098309, T32AR050938, 1K23HD073351, 8UL1TR00017005

March of Dimes award 6-FY12-393

University of Minnesota Academic Health Center grant for Faculty Research Development, Office of the Vice President for Research Grants, Minnesota Partnership for Biotechnology and Medical Genomics Grant

Fund for Science and Hormone Receptor Fund

I would like to thank Dr. Jerid Robinson, Dr. Deborah Dickey, Dr. Laurinda Jaffe, Dr. Gianluigi Veglia, Dr. Nick Levinson, and the graduate students of the Department of Biochemistry, Molecular Biology, and Biophysics at University of Minnesota for their many helpful conversations throughout my graduate studies.

ABSTRACT

The receptor guanylyl cyclases (GC) GC-A and GC-B are complex transmembrane proteins with multiple functional domains and multiple post-translational modifications. GC-A and GC-B are activated by selective natriuretic peptide (NP) hormones binding to their glycosylated extracellular domains and primarily regulate the cardiovascular and skeletal systems, respectively. This binding signal then travels to a highly phosphorylated pseudokinase domain. The pseudokinase domain is phosphorylated prior to NP binding and must be phosphorylated for the binding signal to proceed further. Finally, the binding signal arrives at the guanylyl cyclase domain and simulates the production of cyclic guanosine monophosphate from guanosine triphosphate.

Prior to my research there were many questions centered on the role of glycosylation in receptor maturation, the biological significance of phosphorylation and dephosphorylation, and the role of the pseudokinase domain and its potential interaction with ATP. We now know that dephosphorylation is a *bona fide* mechanism of regulation *in vivo*. Furthermore, ER-mediated glycosylation is required to generate a receptor that can be activated by NP and the only form of the enzyme correlated with GC activity is the most highly glycosylated form. Thus, mutations that inhibit full glycosylation of GC-B cause dwarfism. Finally, the pseudokinase domain functions as a conserved allosteric switch whose output is dependent on multiple input signals; NP binding, ATP binding, and phosphorylation. It accomplishes this integrative switch function through the dynamic assembly and disassembly of the regulatory spine and catalytic spine; hydrophobic core elements conserved in all kinases and pseudokinases. Together, my data substantially advances the field by providing a purpose to these post-translational modifications and a mechanistic function to the PKD.

TABLE OF CONTENTS

Acknowledgements ..... **i**

Abstract ..... **ii**

Table of Contents ..... **iii**

List of Tables ..... **v**

List of Figures ..... **vi**

Chapter 1: Introduction to Activation of the Natriuretic Peptide Receptors and Protein Kinase Allostery **1**

Introduction to Natriuretic Peptides and their Cognate Receptors 2

Introduction to Kinases and Pseudokinases 8

Figures 12

Chapter 2: Dephosphorylation and inactivation of NPR2 guanylyl cyclase in granulosa cells contributes to the LH-induced decrease in cGMP that causes resumption of meiosis in rat oocytes **14**

Summary 15

Introduction 16

Results 18

Discussion 25

Experimental Procedures 27

Supplementary Materials and Methods 29

Figures and Tables 33

Chapter 3: Dephosphorylation of juxtamembrane serines and threonines of the NPR2 guanylyl cyclase is required for rapid resumption of oocyte meiosis in response to luteinizing hormone **50**

Summary 51

Introduction 52

Results 54

Discussion 57

Experimental Procedures 59

Supplementary Materials and Methods 61

Figures 63

Chapter 4: Heterozygous Mutations in Natriuretic Peptide Receptor-B (NPR2) Gene as a cause of Short Stature **73**

Summary 74
Introduction 75
Results 77
Discussion 81
Experimental Procedures 84
Supplementary Materials and Methods 87
Figures and Tables 90
Chapter 5: Catalytically Active Guanylyl Cyclase B Requires Endoplasmic Reticulum-mediated Glycosylation, and Mutations that Inhibit This Process Cause Dwarfism 103
Summary 104
Introduction 105
Results 106
Discussion 111
Experimental Procedures 113
Figures and Tables 116
Chapter 6: The Pseudokinase Domains of Guanylyl Cyclase-A and –B allosterically increase the affinity of their catalytic domains for substrate 127
Summary 128
Introduction 129
Results 132
Discussion 139
Experimental Procedures 142
Supplementary Materials and Methods 146
Figures and Tables 148
Chapter 7: Conclusions and Future Directions 164
Conclusions 165
Future Directions 170
Figures 175
Bibliography 182

LIST OF TABLES

Chapter 2: Dephosphorylation and inactivation of NPR2 guanylyl cyclase in granulosa cells contributes to the LH-induced decrease in cGMP that causes resumption of meiosis in rat oocytes 14

Supplemental Table S1. Primers and fluorescent probes used for qRT-PCR analysis of relative expression levels of PPP family phosphatases 49

Chapter 4: Heterozygous Mutations in Natriuretic Peptide Receptor-B (NPR2) Gene as a cause of Short Stature 73

Table 1. Summary of recent studies searching for heterozygous *NPR2* mutations in cohorts with ISS. 91

Table 2. *NPR2* potentially nonsynonymous variants in short stature patients 92

Table 3. *NPR2* potentially nonsynonymous variants in FINRISK and Estonian Biobank height extreme samples 94

Table 4. Observation of *NPR2* nonsynonymous variants in four cohorts 95

Table 5. Functional characterization of NPR2 nonsynonymous variants in three cohorts 96

Table 6. Fraction of ISS individuals with clearly functional *NPR2* variants 97

Supplemental Table S1. Additional clinical features of patients from short stature cohort #1 102

Chapter 6: The Pseudokinase Domains of Guanylyl Cyclase-A and –B allosterically increase the affinity of their catalytic domains for substrate 127

Table 1. Amino acids that are important for ATP binding and allosteric transmission of the ATP binding signal are conserved between PKA and GC-A and GC-B. 161

LIST OF FIGURES

Chapter 1: Introduction to Activation of the Natriuretic Peptide Receptors and Protein Kinase Allostery 1

Fig. 1. The kinase fold is conserved in the PKDs of GC-A and GC-B. 12

Chapter 2: Dephosphorylation and inactivation of NPR2 guanylyl cyclase in granulosa cells contributes to the LH-induced decrease in cGMP that causes resumption of meiosis in rat oocytes 14

Fig. 1. Rapid decrease in follicle NPR2 guanylyl cyclase activity and cGMP content in response to LH signaling 33

Fig. 2. Rapid dephosphorylation of NPR2 in follicle membranes in response to LH signaling.....35

Fig. 3. Time course of the LH-induced dephosphorylation of NPR2. 37

Fig. 4. Inhibition of the LH-induced dephosphorylation and inactivation of NPR2 and decrease in cGMP content upon the treatment of follicles with the PPP-family phosphatase inhibitor cantharidin.....39

Fig. 5. Rapid phosphorylation of PDE5 in follicles in response to LH signaling.....41

Fig. 6. Relative amounts of each PPP phosphatase catalytic subunit mRNA in isolated granulosa cells 42

Fig. 7. Time course of the decrease in the CNP content of follicles, and the resumption of meiosis in response to LH signaling 43

Fig. 8. LH signaling in rat ovarian follicles decreases NPR2 guanylyl cyclase activity by way of a rapid dephosphorylation of regulatory sites followed by a slower decrease of the levels of the agonist CNP 44

Supplemental Fig. S1. Validation of the specificity of the NPR2 antibody 45

Supplemental Fig. S2. Inhibition of the LH-induced dephosphorylation and inactivation of NPR2 by treatment of follicles with the PPP family phosphatase inhibitor okadaic acid.....46

Supplemental Fig. S3. Blot images for figures 3A and 4A, with red boxes indicating the upper region (more phosphorylated) and lower band (less phosphorylated) for which immunostaining intensity was measured. 48

Chapter 3: Dephosphorylation of juxtamembrane serines and threonines of the NPR2 guanylyl cyclase is required for rapid resumption of oocyte meiosis in response to luteinizing hormone 50

Fig. 1. Diagram of the NPR2 guanylyl cyclase showing the 7 serine and threonine phosphorylation sites that were changed to glutamates (E) in the Npr2-7E mice 63

Fig. 2. Prevention of the LH-induced decrease in CNP-dependent guanylyl cyclase activity in Npr2-7E/7E follicles 64
Fig. 3. Relative amounts of NPR2 protein in wild-type and Npr2-7E/7E follicles, with and without LH, and within different regions of the follicle 65
Fig. 4. Attenuation of the LH-induced cGMP decreases in Npr2-7E/7E follicles 66
Fig. 5. Delay of LH-induced Meiotic resumption in Npr2-7E/7E follicle-enclosed oocytes 67
Supplemental Fig. S1. NPR2 is dephosphorylated in response to LH signaling, and remains dephosphorylated for several hours even when LH is washed out after a brief exposure 69
Supplemental Fig. S2. Generation of knock-in mice with phosphomimetic glutamate mutations in NPR2 70
Supplemental Fig. S3. Similar CNP concentration-dependence of the activity of wild-type and 7E-mutated NPR2 72
Chapter 4: Heterozygous Mutations in Natriuretic Peptide Receptor-B (NPR2) Gene as a cause of Short Stature 73
Fig. 1. Segregation of identified NPR2 nonsynonymous variants in affected families 90
Supplemental Fig. S1. Two Western immunoblots using a polyclonal antibody to rat NPR2 showing no protein detected from mutants with no functional activity in one assay 98
Supplemental Fig. S2. Growth chart for Patient 1 99
Supplemental Fig. S3. Growth chart for Patient 2 100
Supplemental Fig. S4. Growth chart for Patient 4 101
Chapter 5: Catalytically Active Guanylyl Cyclase B Requires Endoplasmic Reticulum-mediated Glycosylation, and Mutations that Inhibit This Process Cause Dwarfism 103
Fig. 1. AMDM mutants are not processed to the fully glycosylated and phosphorylated form of GC-B 116
Fig. 2. The AMDM mutants bind ^{125}I-CNP on the surface of live cells 117
Fig. 3. Microscopic immunofluorescence detection indicates that the AMDM mutants are on the cell surface 118
Fig. 4. The AMDM mutants have markedly reduced activated guanylyl cyclase activity 120
Fig. 5. Reduced phosphorylation does not explain the inactivation of the AMDM mutants 121
Fig. 6. N-linked glycosylation in the ER is required for stimulated GC-B activity 123
Fig. 7. Mutation of the Asn-24 glycosylation site decreases the guanylyl cyclase activity and increases the electrophoretic migration of GC-B 124

Fig. 8. Incomplete glycosylation in the Golgi apparatus does not reduce CNP- or detergent-dependent guanylyl cyclase activity of GC-B 125
Fig. 9. Enzymatic deglycosylation after normal processing does not inhibit GC-B activity.....126
Chapter 6: The Pseudokinase Domains of Guanylyl Cyclase-A and –B allosterically increase the affinity of their catalytic domains for substrate 127
Fig. 1. The regulatory and catalytic spines and residues the directly bind and transmit the allosteric ATP-binding signal in PKA are conserved in the PKD of GC-A 148
Fig. 2. Structural alignment of the PKD of GC-A with crystal structures from other kinases 149
Fig. 3. Decreased NP-dependent guanylyl cyclase activity in Lys and Asp mutants is not explained by changes in protein abundance or phosphorylation 150
Fig. 4. The GC-B-K551A mutant has reduced CNP-dependent GC activity that is not explained by changes in phosphorylation or protein levels.....152
Fig. 5. Conserved Lys and Asp residues in PKD's are required for ctivation of GC-A and GC-B by ATP but not NP.....153
Fig. 6. A GC-A mutant lacking the pseudokinase domain contains a cooperative, ATP binding, allosteric site 155
Fig. 7. The Lys and Asp mutations increase the Michaelis constants for GC-A and GC-B.....156
Fig. 8. The GC-A-A533W mutation partially mimics the ATP bound state of GC-A 158
Fig. 9. The GC-B-M571F mutation increases GC activity at sub-saturating concentrations of CNP 159
Fig 10. The GC-B I583W mutation increases stimulation by either ATP or CNP alone 160
Supplementary Fig. S1. 8-azido-2'/3'-biotinyl-ATP binding.....162
Supplementary Fig. S2. ATP-agarose interaction assay 163
Chapter 7: Conclusions and Future Directions.....164
Fig. 1. A conserved patch of basic residues in the PKD is positioned to interact with known phosphorylation sites in a hypothesized BRAF-like dimer 175
Fig. 2. Mutation of conserved basic sites reduces activation similar to dephosphorylation.....176
Fig. 3. Preliminary data suggests αC-helix motion controls NP sensitivity 177
Fig. 4. Preliminary data shows F566 positions R562 for optimal regulatory interactions 178
Fig. 5. Preliminary data shows removing negative charge in the activation loop does not mimic the R562Q mutation.....179
Fig. 6. Hypothesized interactions between the N-terminal Linker and the PKD.....180
Fig. 7. Representative models of the PKD C-terminal hinge helix 181

CHAPTER 1:

Introduction to Activation of the Natriuretic Peptide Receptors and Protein Kinase Allostery

INTRODUCTION TO NATRIURETIC PEPTIDES AND THEIR COGNATE RECEPTORS

In 1984, atrial natriuretic peptide (ANP) was discovered in atrial homogenates that lowered blood pressure through increased sodium and water excretion by the kidneys (*1*). In 1988 and 1990, respectively, B-type natriuretic peptide (BNP) and C-type natriuretic peptide (CNP) were purified from brain extracts based on their ability to relax smooth muscle (*2, 3*). Natriuretic peptides act primarily through one of two single, membrane spanning guanylyl cyclase (GC) receptors, although it has been reported that some functions are mediated by a clearance receptor that lacks GC activity (*4*). GC-A, also known as NPR-A or Npr1, was purified by multiple groups from various tissues in the 1980s (*5-7*), and molecularly cloned from rat and humans shortly thereafter (*8, 9*). GC-A is activated by ANP and BNP but not CNP (*10*). Activation of GC-A regulates many physiologic processes including renal sodium and water excretion, vasorelaxation, endothelial permeability, lipolysis, and cardiac hypertrophy. Guanylyl Cyclase-B (GC-B), also known as NPR-B or Npr2, was discovered by molecular cloning using a low stringency screen with a sea urchin GC cDNA probe against a rat brain cDNA library (*11*). GC-B is activated by CNP but not by ANP or BNP. Activation of GC-B stimulates endochondral ossification in long bones, meiotic arrest in mammalian ovarian follicles, sensory axon bifurcation in the spinal cord, and vascular relaxation.

GC-A and GC-B are identical topologically. The minimal functional catalytic unit of the receptor is a homodimer, although higher oligomers of each receptor are possible. Unlike tyrosine kinase linked growth factor receptors, there is no further oligomerization upon ligand binding (*12*). Each monomer begins at the N-terminus with a large extracellular NP-binding domain and spans the cell membrane with a single alpha helix. Intracellularly, GC-A and GC-B are 78% identical and chimeric receptor studies have demonstrated that their intracellular domains are interchangable (*13, 14*). Immediately following the transmembrane helix, a short linker sequence precedes a pseudokinase domain (PKD) region. The PKD has strong conservation of secondary and tertiary structure elements of known kinases and pseudokinases despite only having about 25-30% identity across the kinase superfamily. The PKD is followed by a coiled-coil domain implicated in dimerization of intracellular domains and a C-terminal GC catalytic domain responsible for generating the 3'-5'-cyclic guanosine monophosphate (cGMP) second messenger in response to NP stimulation (*12, 15*). Phylogenetic analysis of domain sequences demonstrated the coiled-coil region coevolved with the guanylyl cyclase domain in all class III nucleotidyl

cyclases and the PKD coevolved with these domains in the membrane guanylyl cyclase family (*16*).

The hormone activated membrane guanylyl cyclases are a complex family of proteins with multiple internal functions that must be properly coordinated to produce the second messenger cGMP that mediates their physiologic functions. To better illustrate this principle, we compare the GC-A-cGMP signal transduction pathway to the first second messenger identified, 3'-5'-cyclic adenosine monophosphate (cAMP). Using the example of the β-adrenergic system, epinephrine binds to and induces a conformational change in a seven-pass-transmembrane domain receptor on the cell surface, which causes the dissociation of the β-γ subunits from the α subunit of the heterotrimeric G-protein, The free Gsα monomer then binds to membrane bound adenylyl cyclase to stimulate the conversion of adenosine triphosphate (ATP) into cAMP and pyrophosphate. This pathway includes one polypeptide acting as a receptor, three polypeptides acting as a regulatory molecular switch, and one polypeptide generating the second messenger cAMP. In contrast, hormone-activated membrane guanylyl cyclases encompass all five of these functions in a single polypeptide chain that forms a functional dimer. The extracellular ligand-binding domain binds the activating peptide, the intracellular PKD functions as a molecular switch that is regulated by a nucleotide, and the C-terminal guanylyl cyclase catalytic domain functions as the enzyme that generates the second messenger. This is consistent with the biological role of kinases and some pseudokinases acting as allosterically regulated molecular switches.

Co- and Post-translational modifications of GC-A and GC-B

The extracellular domains of both GC-A and GC-B are N-glycosylated (*17*), and the extracellular domain of GC-B was reported to be O-glycosylated in developing rat brain tissue . Because Golgi-mediated N- and O-glycosylation is enzymatic, not template-driven, this gives rise to receptors with considerable size heterogeneity due to differing numbers of extracellular sugars. In contrast, ER-mediated N-glycosylation uses a pre-formed oligosaccharide substrate that is transferred to specific template sites which gives discrete molecular weight shifts. The role of extracellular glycosylation is disputed with some groups finding that glycosylation affects NP binding (*18, 19*) and some finding it has no effect on NP binding (*20*). My work has shown when receptors are expressed in the presence of tunicamycin, which blocks the first committed step in N-linked glcosylation, only the lowest molecular weight species of GC-B is observed and the receptor cannot be activated naturally by natriuretic peptides or synthetically by detergent (*17*).

This is consistent with previous observation showing that when interactions between GC-A and HSP-90 are blocked with geldanamycin, the receptor cannot be activated. It is also consistent with the well-known role of ER-mediated N-glycosylation in promoting interactions with chaperones (*21*). However, when GC-B is expressed in 293 cells lacking N-acetylglucosaminyl transferase 1 (293-Gnt1$^-$), a primary enzyme involved in Golgi-mediated N-glycosylation, it is still activated to the same extent as receptors expressed in wild type 293 cells, although it is lacking the highest molecular weight species. One explanation for these findings is that GC-B in these cells is incompletely glycosylated but is still trafficked through the Golgi and is posttranslationally modified like the wild type completely glycosylated receptor in these cells.

The N-termini of the pseudokinase domains in GC-A and GC-B are highly phosphorylated, which is essential for hormonal activation (*22, 23*). Importantly, in receptors expressed under normal conditions only the highest molecular weight species of the receptor is phosphorylated. Mutation of four or more phosphorylation sites results in a form of the receptor which cannot be activated by NP and loses positive cooperativity in the absence of ATP (*14, 24*). The underlying mechanism behind the effect of phosphorylation in these receptors is not known, but my recent work is consistent with a model where the phosphorylated serines and threonines participate in salt-bridges with conserved lysines and arginines to form a conformation of the pseudokinase domain that is capable of transmitting the NP binding signal to the GC catalytic domain in a cooperative manner.

Long-term stimulation of cultured cells expressing GC-A and GC-B with their cognate NP activator results in homologous desensitization of the GC receptors through a general loss of phosphorylation at all sites as demonstrated by reduced phosphate levels but similar tryptic phosphopeptide maps for receptors isolated from control and NP exposed cells (*22, 25*). Antagonizing hormone pathways also inactivate GC-A and GC-B through decreasing receptor phosphate content. Treating cells expressing GC-A and GC-B with phorbol esters (PMA) results in a net decrease in phosphorylation, but an increase in phosphorylation at Ser-518 in GC-B is also observed as a result of PMA treatment (*26*). Heterologous desensitization is biologically significant and has been demonstrated by knocking-in a "constitutively phosphorylated" form of GC-B in which all known phosphorylation sites are mutated to glutamate (GC-B-7E)(*27*) at the endogenous genetic locus in mice (*28*). This dephosphorylation-resistant form of GC-B is refractory to PMA-dependent or prolonged NP-dependent receptor inactivation, but retains WT-like activation by NPs and substrate affinity when expressed in 293 cells (*27*). Ovarian follicles from GC-B$^{7E/7E}$ knock-in mice treated with luteinizing hormone (LH) do not demonstrate

decreased GC-B activity whereas GC-B in ovarian follicles from GC-B$^{WT/WT}$ mice is dephosphorylated and loses 50% of its CNP-stimulated GC activity after the same LH treatment (*28*). Similarly, recent work in rat chondrosarcoma cells has shown fibroblast growth factor receptor-3 activation inhibits WT GC-B through dephosphorylation but fails to inhibit the dephosphorylation-resistant GC-B-7E mutant form of the enzyme (*29*). Importantly, GC-B$^{7E/7E}$ mice have longer bones than GC-B$^{WT/WT}$ mice (*30*), which is consistent with the notion of long bone length being regulated by fibroblast growth factor-3 dependent changes in GC-B phosphorylation.

Activation by ATP

The exact role of ATP in the activation of GC-A and GC-B has been difficult to determine for a number of reasons. First, there are multiple nucleotide binding sites present in different domains in the receptor. Because the PKD retains all ATP-interacting residues except the catalytic base, it has been widely assumed, but not demonstrated until now, that this site is involved in allosteric regulation of the GC catalytic domain. Both Focco Van den Akker's group using the hinge-catalytic region of GC-A expressed in bacteria (*31*) and Dr. Jerid Robinson, a previous student in the Potter laboratory (*32*), using full length GC-A, identified a pseudosymmetric site in the catalytic domain of GC-A that preferentially binds ATP, but binds GTP in the absence of ATP, resulting in positive cooperativity. ATP has multiple functions in GC activity assays. It serves as a phosphate donor for phosphorylation of GC-A and GC-B (*33*), and it allosterically decreases the Michaelis constant (Km), a measure of substrate affinity, approximately 10-fold in a NP-dependent manner (*34*). Finally, since it binds the allosteric site, it reduces the cooperativity of the enzyme and causes the kinetic profile to shift from positive-cooperative to hyperbolic (*32*). In early experiments, it was not known that these receptors were phosphorylated, so membrane samples were prepared without phosphatase inhibitors, which led to dephosphorylated and inactive receptors (*35, 36*). When ATP was added to GC activity assays containing the dephosphorylated enzymes, it served as a phosphate donor and led to phosphorylation and activation of the enzymes (*33, 35*). However, the increased activity was initially thought to result from direct ATP binding to the enzyme and not phosphorylation. However, later experiments conducted in the presence of phosphatase inhibitors showed that the maximal velocity (Vmax) of the enzyme is increased in the presence of NP regardless of the presence or absence of ATP (*34, 37*). Of the remaining two effects, allosteric reductions in the Km and reductions in the Hill slope, it has been difficult to elucidate which effect is due to which

ATP binding site. ATP regulation of GTP affinity is essential for physiologic function of GC-A and GC-B because ATP-dependent allosteric reductions in the Km bring the affinity for GTP substrate within the range of physiologic GTP concentrations (*32*). Thus, without both NP-activation and ATP-dependent allostery, these hormone receptors would not generate sufficient cGMP to serve as a second messenger and carry out the many physiologic functions associated with NPs.

Activation by Natriuretic Peptides

Natriuretic peptides increase GC activity in GC-A and GC-B by binding to the extracellular domain in a stoichiometry of one molecule of natriuretic peptide to two molecules of receptor (*38, 39*), but how the NP binding signal is transduced through the intracellular domains is not well understood. A rotation mechanism in the extracellular domain of GC-A involving a 24º counterclockwise rotation of one monomer relative to the other has been reported (*38*), but it is not known how this signal is propagated throughout the intracellular domains. As stated above, phosphorylation is required for this binding signal to reach the GC catalytic domain (*14, 24*). Constructs of GC-A lacking the PKD are constitutively active and are not activated by NP (*40*). This supports a long-standing model in which the PKD represses GC activity under basal conditions and NP binding to the extracellular domain de-represses GC catalytic activity (*40*). In substrate-velocity activity assays using membranes where phosphorylation was preserved, NP stimulation in the absence of ATP increases Vmax 23-fold over basal activity for WT GC-A and 13-fold for WT GC-B with no significant change in the Km or the Hill slope (*32*). However, in the presence of ATP, NP stimulation results in both an increase in Vmax as well as a 10-fold decrease in the Km. Because ATP cannot stimulate GC activity by itself in WT receptors and NP cannot decrease the Km to effective physiologic concentrations of GTP without ATP, it is logical to conclude that the effects of ATP and NP stimulation on GC activity are tightly coupled. If and how these two activators are coupled has not been studied to my knowledge.

Contrasts with other membrane guanylyl cyclases

GC-A and GC-B are not the only members of the membrane guanylyl cyclase family. There are five membrane guanylyl cyclases in humans (*41*), seven in mice and rats, and at least 26 in *C. elegans (42)*. Each corresponding member of the mammalian membrane guanylyl cyclase family contains the same receptor topology as GC-A and GC-B, although the mechanisms of activation vary between receptors. Phylogenetic analysis of amino acid sequences has

suggested the PKDs co-evolved with their corresponding guanylyl cyclase domain (*16*), which is consistent with variations in activation mechanisms and regulation between members of the membrane guanylyl cyclase family.

GC-C is the receptor for the endogenous peptides guanylin and uroguanylin as well as the heat stable enterotoxin from *E. coli* and is found primarily in intestinal epithelial cells (*43*). It is also the target of the gastrointestinal drug, linaclotide (*44*). Interestingly, the PKD domain of GC-C is not phosphorylated, but the same region in GC-C that corresponds to the known phosphorylation sites in GC-A and GC-B contains a high number of acidic residues that may contribute to a stabilizing mechanism similar to the phosphorylation sites in GC-A and GC-B. GC-C's PKD also lacks the conserved catalytic base found in protein kinases, but retains other ATP-interacting residues and conserved hydrophobic core elements similarly to GC-A and GC-B. However, chimeric constructs in which the PKD of GC-C was replaced with the PKD from GC-A were not activated by NP (*13*), which is consistent with the notion of the PKD and GC domains of membrane GCs coevolving (*16*). Importantly, ATP binding to the PKD of GC-C has been demonstrated and this binding increased the Vmax rather than reducing the Km as observed for GC-A and GC-B (*45*). Furthermore, mutation of K516 in GC-C, which corresponds to K72 in PKA, K535 in GC-A and K551 in GC-B, resulted in a loss of activity and a loss of ATP binding, suggesting that ATP binding to the PKD is required for activation of GC-C.

GC-E and GC-F are found in the retina and participate in cGMP regeneration during the dark cycle. Unlike the other membrane GCs, there is no known extracellular activator of GC-E and GC-F. Instead, they are activated by cytosolic guanylyl cyclase activating proteins (GCAPs) binding intracellularly to their PKD and the coiled coil region (*46, 47*). The PKD of GC-E also lacks the conserved catalytic base of protein kinases and has a tryptophan substituted for alanine in the β3 strand, a substitution which would be predicted to block ATP binding. Nonetheless, ATP also increases GC activity under conditions mimicking physiologic activation, but like GC-C, substrate velocity assays demonstrated that ATP increased Vmax without affecting the Km (*48*). Interestingly, one report described residual autophosphorylating kinase activity in GC-E (*49*) and mutation of the conserved Mg-chelating aspartate in the ATP-binding pocket decreased the phosphorylation of GC-E (*50*). Finally, although GC-E is phosphorylated, phosphorylation does not appear to regulate physiologic activation by GCAPs as is observed for NP activation of GC-A and GC-B (*50*).

INTRODUCTION TO KINASES AND PSEUDOKINASES

The first protein kinase, casein kinase, was described in 1954 by Burnett and Kennedy (*51*) with studies by Krebs and Fischer demonstrating the regulatory importance of protein phosphorylation of phosphorylase kinase following in 1956 (*52*). Further studies by Rabinowitz and Lipmann demonstrated the substrate specificity of protein kinases in 1960 by showing phosphorylase *b* was not a suitable substrate for egg yolk phosphoprotein kinase and egg yolk phosphoprotein was not a suitable substrate for phosphorylase kinase (*53*). In 1988 Hunter and Hanks identified eleven conserved sequence elements termed "subdomains" in proteins with demonstrated kinase activity. Two years later, Susan Taylor's group obtained the first crystal structure of protein kinase A (PKA) (*54*), which provided a structural basis for why the specific subdomains were conserved. In 2002, Manning and colleagues annotated the entire human kinome consisting of 518 protein kinases, of which about 50 were predicted to be inactive due to the absence of one of three "highly conserved or invariant" residues thought to be important for catalysis (K72, D166, and D184 in PKA) (*55*). One of the primary functions of protein kinases in biology is catalyzing the transfer of the gamma phosphate from ATP to hydroxyl groups on serines, threonines or tyrosine residues within the intracellular portion of proteins (*55-57*). This occurs through a ternary complex involving the kinase enzyme, Mg^{2+}ATP, and the protein substrate to be phosphorylated on a serine, threonine, or tyrosine (*58, 59*). With one known exception (*60*), kinases require divalent metals such as Mg^{2+} or Mn^{2+} in complex with ATP for ATP to bind to the enzyme active site, so all references to ATP refer to the metal-ATP complex. Some kinases show preference for binding ATP first, while others show no preference between ATP or their protein substrate (*61, 62*). Initially large conformational changes were found to be important for the underlying activation mechanisms of protein kinases, but recent work from many groups has refined this model to emphasize the role of dynamic, coordinated motions between hydrophobic core elements in the protein kinase fold conserved in three-dimensional space rather than in linear sequence (*63*).

Conserved catalytic elements of kinases and pseudokinases

Crystallographic analysis of many kinases has confirmed a highly conserved bilobed fold for all protein kinases and a common theme of structural elements underlying their catalytic activity. The Gly-loop between the β1 and β2 strands (G50-G55 in PKA) is critical for ATP binding in most protein kinases. The amide backbone is involved in hydrogen bonds with the triphosphate tail of ATP and flexibility afforded by multiple glycines in this loop is necessary for

efficient function of many protein kinases. The invariant lysine in the β3 strand (K72 in PKA) is important for multiple reasons, and as such, alanine substitutions for this lysine are the most commonly used kinase-inactivating mutation. One function of this lysine is that it forms a salt bridge with a conserved glutamate in the αC-helix (E91 in PKA), which is a hallmark of the active state conformation of all protein kinases. Another function is that in some crystal structures, it interacts with the α- and β-phosphates of ATP to help facilitate proper positioning of the γ-phosphate for nucleophilic attack by the substrate hydroxyl group that receives the phosphate. The catalytic loop (Y164-N171 in PKA) contains the catalytic base (D166 in PKA) as well as a Mg-interacting asparagine (N171 in PKA). The catalytic base is responsible for deprotonation of the protein substrate hydroxyl group prior to nucleophilic attack of the gamma phosphate of ATP. The DFG-loop, also called the Mg-chelating loop, includes the invariant aspartate (D184 in PKA) that chelates magnesium for ATP binding and positioning. Another variable but important element is the activation loop (A188-T197 in PKA). This loop is of variable length and sequence among protein kinases but phosphorylation of this loop commonly plays a significant role in activation of protein kinases (*64*). Immediately following the activation loop is a more conserved element important for peptide substrate recognition and binding; the P+1 loop (L198-E208 in PKA). Mutations in this region are frequently associated with disease as kinases with these mutations will not efficiently bind either substrate or pseudosubstrate (PKA-L205R). Alternatively, these mutations abrogate allosteric increases in ATP binding affinity known to occur with peptide substrate binding (PKA-Y204A) (*65, 66*). Figure 1 highlights these elements in PKA and compares them to the PKDs of GC-A and GC-B.

The dynamic hydrophobic core mechanism of allostery in protein kinases

In PKA, allosteric coupling of protein substrate binding and ATP binding have been described where binding of one of the two substrates increases the enzymes affinity for the other substrate (*65*). In the RAF kinases, dimerization allosterically activates the kinase for phosphotransfer (*67*). In pseudokinases, allostery is preserved despite the loss of catalytic phosphotransfer function (*68-70*). It was further noted that the apo-kinase is much more flexible and dynamic than the ternary complex when studied using non-hydrolyzable ATP analogs(*63*). Molecular dynamics and nuclear magnetic resonance studies revealed a dynamically coordinated hydrophobic core with multiple non-canonical structural elements conserved across the kinase superfamily (*63, 71-73*). The regulatory (R)-spine was identified first (*71*). The R-spine spans both lobes of the kinase and includes residues in loops and other secondary structure features

known to be important to kinase function and regulation. In PKA, beginning in the C-lobe and working upwards through the N-lobe these residues are D220/RS0 in the αF-helix, Y164/RS1 in the catalytic loop, F185/RS2 in the Mg-chelating loop, L95/RS3 in the αC-helix, and L106/RS4 in the β4 strand. RS1-4 were discovered first (*71*), with RS0 coming two years later (*73*). In PKA and many other kinases, phosphorylation of the activation loop underlies R-spine assembly, although many diverse mechanisms exist. Upon assembly, the R-spine locks the necessary components for catalysis into position and these pieces now move together in a dynamically coordinated fashion. A further hydrophobic core element, the Shell, was later identified that plays a supporting role to the R-spine and bridges the gap between RS3/RS4 and the N-lobe portion of the C-spine (*72*). In PKA, the Shell consists of Sh1/V104 in the αC-β4 loop, and Sh2/M120 (also called the gatekeeper residue) and Sh3/M118 in the β5 strand.

Another "spine," the catalytic (C)-spine, was identified two years later that interacts with and drives dynamic changes in the kinase in response to ATP (*73*). This spine also spans both lobes of the kinase and is anchored to the αF-helix. In PKA, the C-lobe portion consists of L227 and M231 in the αF-helix, L172-I174 on the β7 strand, M128 on the αD-helix. The N-lobe portion consists of V57 and A70 in the β2 and β3 strands, respectively. These two portions exist as separate entities in the absence of ATP and line the adenine binding pocket of the kinase active site. Upon ATP binding, the adenine ring of ATP bridges the gap between the N-lobe and C-lobe portions of the C-spine, thus forming a single, contiguous hydrophobic element.

The αF-helix is an important hydrophobic core element as well because it is the anchor site for both spines in the C-lobe (*72, 73*). It is almost entirely hydrophobic and other residues on the αF-helix between the R- and C-spines likely play a role in communication between the two spines. Through the bridging provided in the N-lobe by the Shell and the αF-helix in the C-lobe, the R- and C-spines together are able to rigidify the entire kinase and slow the timescale of motions to that of catalysis (*63*), thus providing the synchronized motion of all components necessary for catalysis. In pseudokinases, the same transitions from flexible and nonsynchronous to rigid and synchronized also occur and can be biologically significant in the absence of catalysis (*68-70*). It has been suggested that pseudoenzymes of biological significance fulfill their biological role through one of following four possible mechanisms: 1) allosterically modulate the activity of their binding partners. 2) Competitively bind substrates to prevent access to other signaling proteins. 3) anchor binding partners to specific subcellular locations. 4) integrate multiple components from different signaling pathways or multiple activators in a single cascade

(*74*). Through my work and the work of others,' the latter integrative role of these PKDs is now becoming clear.

FIGURES

Figure 1. The kinase fold is conserved in the PKDs of GC-A and GC-B.

PKA (PDB:1atp) and models of GC-A and GC-B were structurally aligned in PyMol to determine the exact conservation in 3D space and is shown as a primary amino acid sequence alignment. The amino acid groupings used to identify strong similarity were [ILVM], [FYW], [DE], [RKH], [NQST], [AG], [P], [C]. The amino acid groupings used to identify weak similarity were [ILVMFYWAG], [FYWH], [DENQ]. The secondary structure of PKA is indicated above the alignment, and the secondary structure of the GC-A and GC-B models is shown below the alignment. Regions of importance are indicated in blue and described in the boxes surrounding the alignment. Amino acid positions mentioned in the text of this chapter or those used as sites of mutations in further chapters are indicated.

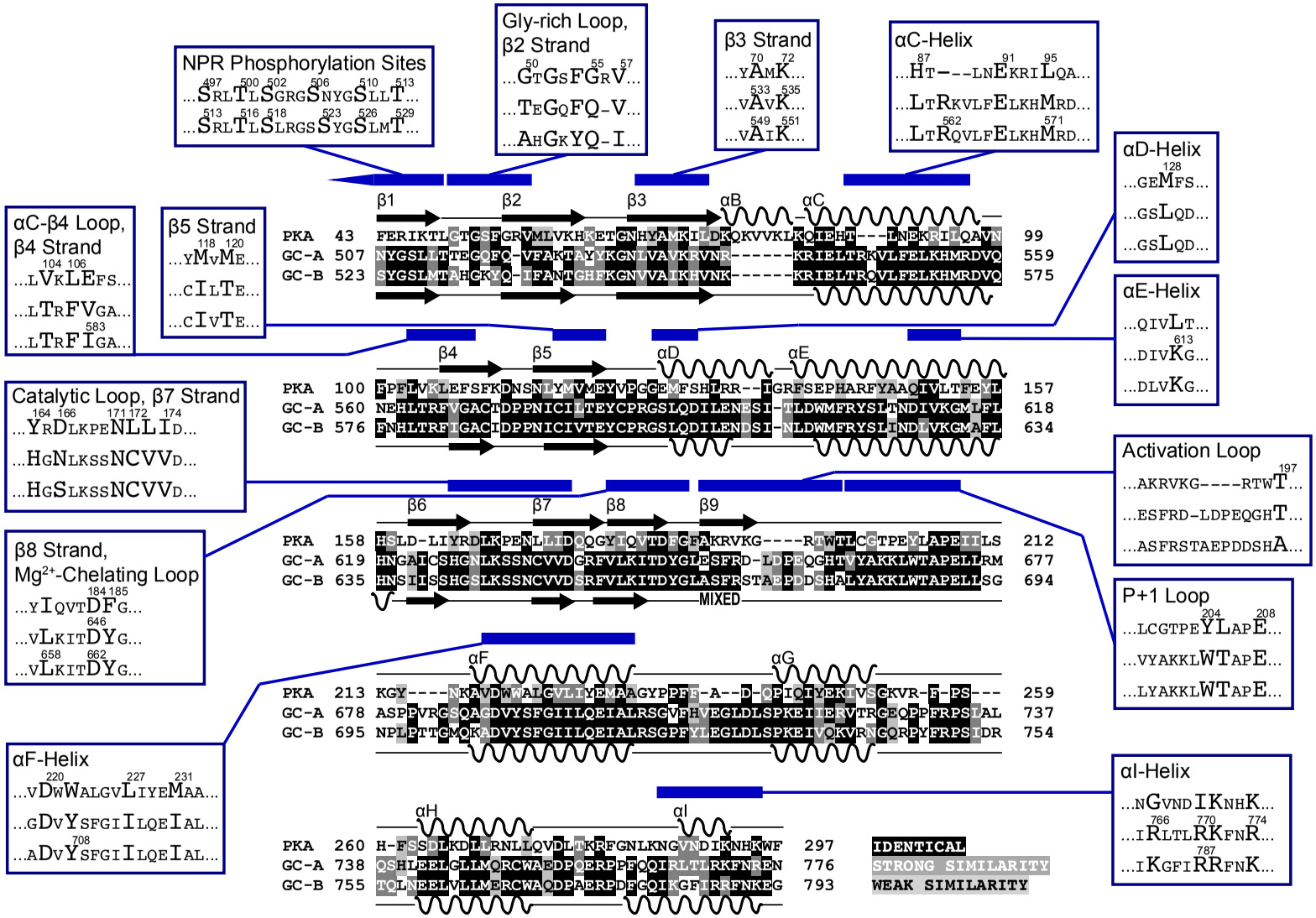
NPR Phosphorylation Sites
...SRLTLSGRGSNYGSLLT...
...SRLTLSLRGSSYGSLMT...
Gly-rich Loop, β2 Strand
...GTGSFGRV...
...TEGQFQ-V...
...AHGKYQ-I...
β3 Strand
...YAMK...
...VAVK...
...VAIK...
αC-Helix
...HT--LNEKRILQA...
...LTRKVLFELKHMRD...
...LTRQVLFELKHMRD...
αD-Helix
...GEMFS...
...GSLQD...
...GSLQD...
αE-Helix
...QIVLT...
...DIVKG...
...DLVKG...
αC-β4 Loop, β4 Strand
...LVKLEFS...
...LTRFVGA...
...LTRFIGA...
β5 Strand
...YMVME...
...CILTE...
...CIVTE...
β1 β2 β3 αB αC
PKA 43 FERIKTLCTGSFGRVMLVKHKETGNHYAMKILDKQKVVKLKQIEHT---LNEKRILQAVN 99
GC-A 507 NYGSLLTTEGQFQ-VFAKTAYYKGNLVAVKRVNR------KRIELTRKVLFELKHMRDVQ 559
GC-B 523 SYGSLMTAHGKYQ-IFANTGHFKGNVVAIKHVNK------KRIELTRQVLFELKHMRDVQ 575
β4 β5 αD αE
PKA 100 PPFLVKLEFSFKDNSNLYMVMEYVPGGEMFSHLRR--IGRFSEPHARFYAAQIVLTFEYL 157
GC-A 560 NEHLTRFVGACIDPPNICILTEYCPRGSLQDILENES I-TLDWMFRYSLTNDIVKGMLFL 618
GC-B 576 ENHLTRFIGACIDPPNICIVTEYCPRGSLQDILENDS I-NLDWMFRYSLINDLVKGMAFL 634
Catalytic Loop, β7 Strand
...YRDLKPENLLIID...
...HGNLKSSNCVVD...
...HGSLKSSNCVVD...
Activation Loop
...AKRVKG----RTWT...
...ESFRD-LDPEQGHT...
...ASFRSTAEPDDSHA...
β6 β7 β8 β9
PKA 158 HSLD-LIYRDLKPENLLIDQQGYIQVTDFGFAKRVKG----RTWTLCGTPEYLAPEIILS 212
GC-A 619 HNGAICSHGNLKSSNCVVDGRFVLKITDYGLESFRD-LDPEQGHTVYAKKLWTAPELLRM 677
GC-B 635 HNSIISSHGSLKSSNCVVDSRFVLKITDYGLASFRSTAEPDDSHALYAKKLWTAPELLSG 694
MIXED
β8 Strand, Mg2+-Chelating Loop
...YIQVTDFG...
...VLKITDYG...
...VLKITDYG...
P+1 Loop
...LCGTPEYLAPE...
...VYAKKLWTAPE...
...LYAKKLWTAPE...
αF αG
PKA 213 KGY----NKAVDWWALGVLIYEMAAGYPPFF-A--D-QPIQIYEKIVSGKVR-F-PS--- 259
GC-A 678 ASPPVRGSQAGDVYSFGIILQEIALRSGVFHVEGLDLSPKEIIERVTRGEQPPFRPSLAL 737
GC-B 695 NPLPTTGMQKADVYSFGIILQEIALRSGPFYLEGLDLSPKEIVQKVRNGQRPYFRPSIDR 754
αF-Helix
...VDWWALGVLIYEMAA...
...GDVYSFGIILQEIAL...
...ADVYSFGIILQEIAL...
αH αI
PKA 260 H-FSSDLKDLLRNLLQVDLTKRFGNLKNGVNDIKNHKWF 297
GC-A 738 QSHLEELGLLMQRCWAEDPQERPPFQQIRLTLRKFNREN 776
GC-B 755 TQLNEELVLLMERCWAQDPAERPDFGQIKGFIRRFNKEG 793
IDENTICAL
STRONG SIMILARITY
WEAK SIMILARITY
αI-Helix
...NGVNDIKNHK...
...IRLTLRKFNR...
...IKGFIRRFNK...

CHAPTER 2:

Dephosphorylation and inactivation of NPR2 guanylyl cyclase in granulosa cells contributes to the LH-induced decrease in cGMP that causes resumption of meiosis in rat oocytes.

This chapter is a reprint of an original publication with minor alterations, used with permission:

Jeremy R. Egbert, Leia C. Shuhaibar, **Aaron B. Edmund**, Dusty A. Van Helden, Jerid W. Robinson, Tracy F. Uliasz, Valentina Baena, Andreas Geerts, Frank Wunder, Lincoln R. Potter and Laurinda A. Jaffe. Dephosphorylation and inactivation of NPR2 guanylyl cyclase in granulosa cells contributes to the LH-induced decrease in cGMP that causes resumption of meiosis in rat oocytes. *Development.* (2014) 141(18):3594-604

Aaron Edmund collected, interpreted, and analyzed data in Figures 1 and 4.

SUMMARY

In mammals, the meiotic cell cycle of oocytes starts during embryogenesis and then pauses. Much later, in preparation for fertilization, oocytes within preovulatory follicles resume meiosis in response to luteinizing hormone (LH). Before LH stimulation, the arrest is maintained by diffusion of cyclic (c)GMP into the oocyte from the surrounding granulosa cells, where it is produced by the guanylyl cyclase natriuretic peptide receptor 2 (NPR2). LH rapidly reduces the production of cGMP, but how this occurs is unknown. Here, using rat follicles, we show that within 10 min, LH signaling causes dephosphorylation and inactivation of NPR2 through a process that requires the activity of phosphoprotein phosphatase (PPP)-family members. The rapid dephosphorylation of NPR2 is accompanied by a rapid phosphorylation of the cGMP phosphodiesterase PDE5, an enzyme whose activity is increased upon phosphorylation. Later, levels of the NPR2 agonist C-type natriuretic peptide decrease in the follicle, and these sequential events contribute to the decrease in cGMP that causes meiosis to resume in the oocyte.

INTRODUCTION

Oocytes in mammalian preovulatory follicles are held in meiotic prophase arrest by cyclic (c)GMP that is produced in the granulosa cells surrounding the oocyte, which then diffuses into the oocyte through gap junctions (*75, 76*). Luteinizing hormone (LH), which is released from the anterior pituitary during each reproductive cycle, acts on a G-protein coupled receptor in the outer granulosa cells of the follicle (*77, 78*) (see Fig. 1A), to relieve the inhibition of the prophase-to-metaphase transition. LH acts by lowering the levels of cGMP in the granulosa cells, thus reducing cGMP in the oocyte. Although this regulatory system is best understood in mice (*75, 76, 79-83*), there is evidence that similar mechanisms operate in other mammals (*84-87*), including women (*80, 88*). The LH-induced resumption of the meiotic cell cycle leads into a series of events by which the oocyte matures to become a fertilizable egg (*89-93*).

As a consequence of the initial cGMP decrease in the mural granulosa cells, cGMP diffuses out of the oocyte into the surrounding granulosa cells, and the decrease in cGMP in the oocyte re-initiates the meiotic cell cycle (*75, 76*). The direct effect of the cGMP decrease in the oocyte is to relieve the inhibition of the cAMP phosphodiesterase PDE3A, which is competitively inhibited by cGMP. Thus, the cGMP reduction causes the levels of cAMP to decrease. cAMP, which is produced in the oocyte (*94-98*), maintains meiotic prophase arrest through activation of protein kinase A (PKA) (*99, 100*). PKA activity inhibits the CDC25B phosphatase and stimulates the WEE1B and MYT1 kinases, and this keeps the CDK1 kinase that controls the prophase-to-metaphase transition phosphorylated and inactive (*89, 91, 92*). When LH signaling reduces oocyte levels of cGMP, and in turn cAMP, meiosis resumes.

cGMP is produced in the granulosa cells of mice by natriuretic peptide receptor 2 (NPR2), also known as guanylyl cyclase-B (*79-83*). NPR2 appears to be the only relevant guanylyl cyclase in mouse follicles because follicle-enclosed oocytes in the ovaries of mice with non-functional NPR2 resume meiosis spontaneously (*79, 82, 83*) and an inactivating mutation in NPR2 reduces the cGMP content of the follicle to an undetectable level (*83*). Gene expression analysis and enzyme assays have indicated that other guanylyl cyclases are present at levels much lower than those of NPR2 (*81*). NPR2 is located throughout the granulosa cells of the follicle, in both the mural granulosa and the cumulus cells directly surrounding the oocyte; it is not expressed in the oocyte (*79, 101*). The agonist of NPR2, C-type natriuretic peptide (CNP, released from a precursor protein that is encoded by the Nppc gene) is produced only in the mural granulosa cells (*79*).

NPR2 is a single transmembrane-spanning enzyme that is activated by the binding of CNP to its extracellular domain (*41, 102*). In order for the CNP activation signal to be transmitted to the catalytic domain, the juxtamembrane intracellular region of NPR2 must be phosphorylated on some combination of five serine residues and two threonine residues that have been identified as regulatory (*22, 24, 27, 103*). However, unlike many growth factor receptors, NPR2 phosphorylation is not increased upon binding to its agonist CNP (*22*). Thus, there are at least two separate mechanisms by which signaling pathways could increase or decrease the guanylyl cyclase activity of NPR2 – changing the amount of CNP or changing the level of receptor phosphorylation.

LH signaling is known to decrease the amount of CNP in rat and mouse ovaries (*80, 81, 88, 104*) and in human and porcine follicular fluid (*80, 87*); the decrease in the levels of CNP is associated with a decrease in Nppc mRNA (*80, 82, 88*). However, in the mouse ovary, where the kinetics are best characterized, the CNP decrease is first detected at 2 h (*81, 88*), whereas the decrease in cGMP is detected at 15 to 20 min (*88, 105*). Guanylyl cyclase activity in mouse follicle membranes decreases to approximately half of the basal level at 20 min after LH application, and this is independent of any change in CNP (*81, 88*). Cultured human granulosa cells also show a rapid decrease in cGMP production, measured in the presence of a constant concentration of CNP (*88*).

The mechanism underlying this early decrease in guanylyl cyclase activity is unknown. Here, we show that the rapid reduction in NPR2 activity in rat follicles in response to LH signaling is caused by the dephosphorylation of NPR2, which is mediated by a process that requires the activity of the protein phosphatases of the phosphoprotein phosphatase (PPP) family, the most likely candidates being PPP1, PPP2 and/or PPP6. The rapid dephosphorylation of NPR2 is accompanied by a rapid phosphorylation of the cGMP phosphodiesterase PDE5 (also known as PDE5A), an enzyme whose activity is increased upon phosphorylation. Later, CNP levels decrease in the follicle, and these sequential events contribute to the decrease in cGMP that causes meiosis to resume in the oocyte.

RESULTS

LH signaling reduces NPR2 activity and cGMP content in rat ovarian follicles

Previous studies demonstrating an LH-induced decrease in guanylyl cyclase activity in ovarian follicles have been conducted using mice (*81*), but the amount of protein that can be obtained from mouse follicles is small. We therefore tested whether a similar regulatory system operates in rats, from which an order of magnitude more follicle protein per animal can be obtained, making analysis of changes in phosphorylation feasible.

To test whether LH causes a decrease in NPR2 guanylyl cyclase activity in rat follicles, and to investigate the time course of the decrease as a basis for subsequent mechanistic studies, isolated preovulatory rat follicles were incubated for various times with or without LH. Because NPR2 is located in the plasma membrane, the follicles were then homogenized to obtain a crude membrane fraction. The membranes were assayed for guanylyl cyclase activity, with and without the NPR2 agonist CNP; CNP-dependent activity indicates the activity of NPR2 (Fig. 1B,C). By 30 min after LH exposure, the CNP-dependent guanylyl cyclase activity decreased to ~50% of the initial level and stayed at this reduced level for at least 4 h, without any additional change (Fig. 1B,C). Approximately 40% of the decrease to the plateau level had occurred by 10 min (Fig. 1C). No change in CNP-dependent guanylyl cyclase activity was seen in follicles incubated for 4 h without LH (Fig. 1C). The cGMP content of the follicle also decreased rapidly in response to LH – most of the change had occurred by 10 min (Fig. 1D).

The LH-induced decrease in CNP-dependent guanylyl cyclase activity was not explained by a reduction in the affinity of NPR2 for CNP because the fraction by which the activity decreased in response to LH, when it was measured in the presence of 50 nM CNP, was similar to that measured in the presence of 1 μM CNP (Fig. 1B). LH had no effect on guanylyl cyclase activity when it was measured in the presence of 1% Triton X-100 and 5 mM MnCl2 (Fig. 1B), a condition that activates guanylyl cyclase activity independently of natriuretic peptide and phosphorylation and that is indicative of guanylyl cyclase protein levels (*106, 107*). Because the predominant guanylyl cyclase in ovarian follicles is NPR2, this indicates that the LH-induced decrease in CNP-stimulated activity is not due to a decrease in the amount of NPR2 protein.

LH signaling causes rapid dephosphorylation of NPR2

To investigate whether the rapid LH-induced decrease in NPR2 activity correlated with a decrease in NPR2 phosphorylation, we first considered the use of ^{32}PO4 metabolic labeling. However, because the expression level of NPR2 in native tissues is low, this approach has only

been feasible for overexpressing cells (*22*). The NPR2 fraction of the total cell protein in ovarian follicles is ~5% of that in the 3T3 cells which had been transfected with NPR2 and used in previous ^{32}PO4 labeling studies, based on the relative levels of enzyme activity (*22*). To obtain the same amount of NPR2 protein used in the transfected 3T3 cell studies, this would have required ~10 mg of follicle membrane protein, corresponding to dissection of follicles from ~30 rats, for a single gel lane. Likewise, detection of changes in phosphorylation by mass spectrometry (*108*) would require much more NPR2 protein than is practical to obtain from rat follicles.

We then investigated whether an LH-induced shift in NPR2 migration could be detected using standard SDS-PAGE, as a previous study showed that dephosphorylation results in a small shift in the electrophoretic migration of the closely related guanylyl cyclase natriuretic peptide receptor 1 (NPR1) (*23*). In standard SDS-PAGE gels, NPR2 from rat follicles migrated as a predominant band at the same position as rat NPR2 from stably transfected HEK-293T cells, at the typically observed size of ~130 kDa (*22*). The fuzziness of this band is primarily due to multiple glycosylation sites (*109*). There was also a minor band at ~115 kDa, which is thought to represent the polypeptide chain that has not been post-translationally modified (*22, 109*) (Fig. 2A). However, treatment with LH did not result in a consistent shift in the electrophoretic migration of NPR2 under the conditions that we used (Fig. 2A).

As an alternative approach to investigate whether LH exposure led to dephosphorylation of NPR2, we used gels including Phos-tag acrylamide and MnCl2. In these gels, phosphorylated proteins transiently interact with the Mn2+-Phos-tag complex, which retards their migration relative to less-phosphorylated or nonphosphorylated forms (*110-113*). NPR2 was purified from the membranes by using sequential immunoprecipitation and fractionation on gels containing Phos-tag acrylamide and was visualized by western blotting. In these gels, NPR2 from untreated follicles migrated as multiple bands, indicating the presence of multiple phosphorylated forms of the enzyme (Fig. 2B; see also Fig. 3A, Fig. 4A). Although molecular weight standards are not accurate indicators of relative molecular mass on a Phos-tag gel, they are useful as descriptive markers; the NPR2 bands migrated in a region that extended from above the 150 kDa marker to approximately the 250 kDa marker.

Controls that were performed using pre-immune serum (Fig. S1), and co-migration of the immunoreactive bands from follicles with those from a HEK cell line that stably expressed NPR2 (Fig. 2A, Fig. 3A), validated the specificity of the antibody. The relative amount of NPR2 staining in a sample of follicle membranes was 2-7% of that in a sample from overexpressing

HEK cells (normalized to the amount of membrane protein loaded per lane), and this corresponded closely to the relative amount of NPR2 activity (2-4% of that reported for this cell line) (*32, 114*), further confirming the antibody specificity. The use of Phos-tag gel migration as an indicator of the phosphorylation state of NPR2 was validated by showing that incubation of follicle membranes under conditions that promoted or inhibited phosphatase activity resulted in faster or slower migrating forms of NPR2 (Fig. 2E-G).

Exposure of the follicles to LH dramatically compressed the majority of the NPR2 into a predominant lower band, indicating dephosphorylation (Fig. 2B; see also Fig. 3A, Fig. 4A). The shift in migration was quantified by measuring the total amount of NPR2 immunostaining in the upper region relative to that in the region of the lower band (Fig. 2C,D). Most of the decrease in the relative amount of immunoreactive material in the upper region had occurred by 10 min after LH exposure, and a minimum level was reached at 30 min (Fig. 3A,B). The dephosphorylation persisted for at least 4 h (Fig. 3A,B), as did the reduction of NPR2 activity (Fig. 1C).

No decrease in NPR2 phosphorylation occurred in follicles that had been incubated for 4 h in the absence of LH (Fig. 3A,B). When LH was applied for 30 min and then washed out, the NPR2 dephosphorylation and activity measured 4 h later were the same as when LH was present continuously (two independent experiments, data not shown). Based on measurements of the total immunoreactive protein, no change in the total amount of NPR2 protein was detected when comparing membranes from follicles with or without treatment with LH (Fig. 3C). This conclusion is also supported by our earlier finding that LH did not affect the amount of guanylyl cyclase activity measured in the presence of Triton X-100 and MnCl2 (Fig. 1B).

Most of the decrease in NPR2 phosphorylation had occurred by 10 min after application of LH (Fig. 3B), whereas only approximately 40% of the decrease in guanylyl cyclase activity had occurred by this time, compared with that measured at 30 min (Fig. 1C). The cause of the delay between the decreases in NPR2 phosphorylation and enzyme activity is unknown, but one possibility is that dephosphorylation of a particular serine or threonine residue that is crucial for the activity decrease occurs late in a series of dephosphorylation events, all of which are detected by the Phos-tag method. Consistent with this hypothesis, the individual phosphorylation sites in NPR2 have varying effects on the activity of the enzyme (*24, 27*).

The LH-induced decrease in NPR2 activity is prevented by inhibiting NPR2 dephosphorylation with PPP-family protein phosphatase inhibitors

To test whether preventing the LH-induced dephosphorylation of NPR2 inhibits the decrease in NPR2 activity, and to begin to distinguish which of the approximately 30 known serine-threonine phosphatase catalytic subunits are required for dephosphorylation of NPR2, we treated the follicles with specific phosphatase inhibitors. Serine-threonine phosphatases belong to two main families – PPP or PPM (protein phosphatase Mg2+ or Mn2+ dependent); in addition, there is a smaller family (FCP) whose only known function is to dephosphorylate RNA polymerase II (*115, 116*). Among these, only the PPP family is inhibited by the natural toxins cantharidin and okadaic acid (*115, 117*). PPM family phosphatases (also known as PP2C) are not inhibited by 100 μM cantharidin (*118*) or by 10 μM okadaic acid (*119*).

Pre-incubation of follicles for 1 h with cantharidin (100 μM) or okadaic acid (10 μM) prevented the LH-induced dephosphorylation and decrease in guanylyl cyclase activity of NPR2 (Fig. 4, S2). These results indicate that the activity of PPP family phosphatases is required for the dephosphorylation of NPR2 in response to LH and that dephosphorylation is required for the LH-induced decrease in NPR2 activity. Among the PPP family phosphatases, our results with cantharidin argue against an important function for PPP3 (also known as PP2B or calcineurin) because PPP3 is insensitive to 100 μM cantharidin (*117, 120*).

These toxin results do not distinguish between other PPP family phosphatases because PPP1, PPP2, PPP4, PPP5 and PPP6 are all inhibited by the concentrations of cantharidin and okadaic acid that we applied to the follicles (*115, 117*). Other toxins with greater specificities for particular PPP-family phosphatases (fostriecin, cytostatin and rubratoxin) were also tested and found to have no consistent effects under the conditions used (data not shown). However, these results were not definitive because we could not determine whether significant amounts of these toxins penetrated into the cytoplasm of the follicle cells.

The LH-induced decrease in follicle cGMP content is attenuated by inhibiting the decrease in NPR2 guanylyl cyclase activity

To determine the effect of preventing the LH-induced decrease in NPR2 guanylyl cyclase activity on the LH-induced cGMP decrease, we measured the cGMP content of follicles that had been pre-treated with 100 μM cantharidin for 1 h and then treated for 30 min with LH. Without cantharidin pre-treatment, LH caused cGMP content to decrease to 7% of the control level (Fig. 1D and Fig. 4D). Cantharidin pre-treatment attenuated the LH-induced decrease – cGMP content only decreased to 56% of the control level (Fig. 4D).

The effect of phosphatase inhibition on the LH-induced decrease in cGMP content is consistent with the conclusion that the LH induced decrease in NPR2 phosphorylation and guanylyl cyclase activity contributes to the cGMP decrease. However, the finding that phosphatase inhibition did not completely prevent the LH-induced cGMP decrease, whereas it did completely prevent the LH-induced decrease in NPR2 phosphorylation and activity (Fig. 4A-C), indicates that LH must also induce another change in the follicle, such as an increase in cGMP phosphodiesterase activity. The finding that most of the cGMP decrease had occurred by the 10 min time point after treatment with LH (Fig. 1D), whereas only 40% of the NPR2 activity decrease had occurred by this time point (Fig. 1C), also suggests that LH induces an increase in cGMP phosphodiesterase activity in parallel with the decrease in NPR2 guanylyl cyclase activity.

LH signaling causes phosphorylation of the cGMP phosphodiesterase PDE5

An important component of the cGMP phosphodiesterase activity in mouse granulosa cells is contributed by PDE5 (*76*). PDE5 activity is stimulated by phosphorylation (*121, 122*); therefore, we examined whether LH signaling increased PDE5 phosphorylation in rat follicles. In gels without Phostag, PDE5 migrated as a band at ~90 kDa, and treating follicles with LH did not change this migration (Fig. 5A). However, in Phos-tag containing gels, PDE5 migrated as two separate bands, and treatment of the follicles with LH for 10 or 30 min increased the fraction of PDE5 in the upper band, indicating phosphorylation (Fig. 5B,C). PDE5 remained phosphorylated until at least 4 h after stimulation with LH (data not shown). In vitro phosphorylation of PDE5 in follicle lysates with the catalytic subunit of PKA also caused a shift of PDE5 to the upper band, confirming that the LH-induced shift was due to phosphorylation (Fig. 5D).

Although the effect of LH on the cGMP phosphodiesterase activity of PDE5 in rat follicles is unknown, the rapid phosphorylation of PDE5 in response to LH is expected to increase PDE5 activity based on in vitro studies (*121, 122*). An increase in PDE5 activity could contribute to the LH-induced cGMP decrease in the follicle, acting in parallel with the decrease in the production of cGMP that results from the dephosphorylation of the NPR2 guanylyl cyclase.

Analysis of PPP family phosphatase gene expression in granulosa cells

To distinguish the PPP-family phosphatases that might contribute to the dephosphorylation of NPR2, we investigated which of these are expressed in granulosa cells. The rat genome contains 13 PPP family genes, encoding seven subfamilies of PPP-family phosphatases (*117*). We detected mRNA encoding all of these phosphatases, although the

fractions of those encoding PPP4, PPP5 and PPP7 were each <2% of the total (Fig. 6). mRNA encoding PPP1, PPP2, PPP3 and PPP6 constituted 61%, 11%, 19% and 6% of the total, respectively. Although the amount of mRNA is not directly proportional to the amount of the protein they encode, and although the localization of a particular phosphatase could affect its functional significance, these measurements point to a role for PPP1, PPP2, PPP3 and/or PPP6, rather than PPP4, PPP5 or PPP7. Because our earlier findings with cantharidin argue against a function of PPP3 in the LH-induced decrease in NPR2 activity, PPP1, PPP2 and/or PPP6 are the phosphatases that are most likely to be important in this signaling cascade.

LH signaling gradually reduces the follicle content of the NPR2 agonist CNP, contributing to the decrease in cGMP production that triggers resumption of meiosis

The guanylyl cyclase assays described above were performed using membranes in the presence of a saturating concentration of CNP (1 μM), so the observed decreases in NPR2 activity occurred independently of any changes in CNP. However, previous studies in several species have shown that on a time scale of hours after hormone injection to activate LH receptors in vivo, CNP levels decrease (see Introduction). To integrate our findings regarding the dephosphorylation of NPR2 with this previous knowledge of another component of the regulatory system, we directly compared the kinetics of the decrease of CNP levels in the same experimental system that we had used for the phosphorylation studies. CNP content, as measured using ELISA, did not change during the initial 2 h after the application of LH to follicles, but by 4 h, CNP levels had decreased to 56% of the baseline level (Fig. 7A). CNP content in the follicles did not change during parallel incubations without LH (Fig. 7B). The LH-induced CNP decrease would further decrease NPR2 activity, beginning 2-4 h after the initial dephosphorylation. However, the magnitude of this subsequent activity decrease is unknown because the ELISA measurements detect the CNP peptide, as well as its biologically inactive precursor protein.

Because the significance of the decrease in guanylyl cyclase activity is to reduce cGMP and re-initiate meiosis in the oocyte, we also examined the time course of nuclear envelope breakdown (the first morphologically detectable event in the resumption of meiosis) following the addition of LH to isolated follicles in our culture system. The time by which 50% of the oocytes had undergone nuclear envelope breakdown was ~4 h, with a marginally significant decrease observed at 2 h; almost all oocytes had resumed meiosis 12-24 h after LH exposure (Fig. 7C). This time course is similar to that previously observed using a slightly different follicle culture system or after injection of LH into rats (*123*). The effect of phosphatase inhibitors on LH-

induced resumption of meiosis could not be determined because these inhibitors also act on phosphatases in the oocyte, causing meiosis to resume independently of LH (*124*).

DISCUSSION

The results described here show that LH signaling decreases guanylyl cyclase activity in rat ovarian follicles by two sequential processes: rapid dephosphorylation of NPR2, detectable at 10 min after treatment with LH, and a slower decrease in the NPR2 agonist CNP, detectable at 4 h after treatment with LH (Fig. 8). Phosphorylation of the cGMP phosphodiesterase PDE5 at 10 min after LH exposure indicates that, in parallel, PDE5 activity may be rapidly increased. This would also contribute to the LH-induced cGMP decrease in the follicle, together with the decrease in the production of cGMP that results from the dephosphorylation of the NPR2 guanylyl cyclase. The decrease of cGMP in the follicle leads to the resumption of meiosis in the oocyte.

In addition, LH induces other changes in the follicle that would further decrease cGMP levels in the oocyte. One such change is a delayed decrease in cGMP generation by the inner granulosa (cumulus) cells of mouse follicles, detected 2-3 h after LH receptor stimulation, measured in the presence of a constant concentration of CNP (*81, 88*). Another factor that could contribute to the decrease in oocyte cGMP levels is that LH causes a transient decrease in gap junction permeability between the granulosa cells (*125-127*). However, at least in mouse follicles, gap junction closure is not essential for the cGMP decrease (*75*), although it could be a 'fail-safe' mechanism if other mechanisms are defective.

How activation of the LH receptor is coupled to dephosphorylation of NPR2, and how dephosphorylation results in inactivation of NPR2, are unknown. The LH receptor activates Gs, as well as other G-proteins (*78, 93*), and through one or more of these G-proteins, LH signaling must activate phosphatases and/or inactivate kinases, or possibly change the conformation of NPR2 such that it is a better or worse substrate for either enzyme. Although the kinases involved have not been identified, our results indicate that the phosphatases that are important for this dephosphorylation belong to the PPP family, and not to the PPM or FCP families. Among the PPP family, our findings using cantharidin argue against an important function for PPP3 (PP2B or calcineurin). Because PPP3 is activated by Ca2+, this conclusion is consistent with the finding that deletion of Gαq/11 in mouse granulosa cells, and the resulting prevention of LH-induced inositol phosphate accumulation, does not inhibit meiotic progression in response to LH (*128*). Taken together with our gene expression analysis, PPP1, PPP2 and/or PPP6 emerge as the most likely candidates for mediating the LH-induced dephosphorylation of NPR2.

Studies of rat granulosa cells in culture have shown that LH activation of Gs leads to the PKA-dependent activation of PPP2 and that PPP2 is associated with the MAP2D A-kinase

anchoring protein (*129*). One possible scenario, although not the only one, is that NPR2 could also be associated with MAP2D, such that it might be dephosphorylated by PPP2 in response to LH-Gs- PKA signaling. Because NPR2 contains multiple phosphorylation sites, and the sequences surrounding these sites differ, the regulation of other phosphatases (and kinases) might also be important in initiating or maintaining the dephosphorylation and inactivation of NPR2 in response to LH.

In particular, EGF receptor signaling is required for part of the LH-induced decrease in the cGMP content and the resumption of meiosis in mouse follicles; how much of the cGMP decrease depends on EGF receptor kinase activity is variable in different studies (*76, 87, 105, 130, 131*). The release of EGF receptor ligands from the outer mural granulosa cell layers where the LH receptors are located provides a mechanism for paracrine signaling to cells in the interior of the follicle. In rats, the EGF receptor dependence of the LH-induced cGMP decrease has not been determined, but EGF receptor kinase activity is required over a period of hours for LH-induced resumption of meiosis (*132, 133*).

Signaling through various other hormones and growth factors also reduces the guanylyl cyclase activity of NPR2 in other cells, for example, vasopressin (*134*), PDGF (*107, 135*), lysophosphatidic acid (*107, 136*), sphingosine-1-phosphate (*137*), and thyrotropin-releasing hormone (*138*). In studies of sphingosine-1-phosphate acting on cultured fibroblasts that overexpress NPR2 (*137*), there is a correlation between dephosphorylation and the decrease in guanylyl cyclase activity. However, LH signaling in the ovarian follicle is the first example of a physiological pathway that is mediated by such a mechanism.

Other developmental processes that are regulated by the activity of NPR2 and the closely related natriuretic peptide receptor NPR1 could be controlled similarly. In particular, bone growth is affected by mutations in Npr2 or the Nppc gene that encodes CNP; increased NPR2 activity results in longer bones, whereas decreased activity results in shorter bones (*83, 139-143*). Natriuretic peptide receptors also function in the development of the nervous system (*144*) and heart (*145*). Some of the actions of growth factors and hormones that affect chondrocyte differentiation, axon bifurcation and cardiomyocyte proliferation might involve the regulation of natriuretic peptide receptor phosphorylation and/or levels of natriuretic peptides, as seen for LH-mediated regulation of meiosis in the ovary.

EXPERIMENTAL PROCEDURES

Isolation and culture of rat ovarian follicles

Ovaries were obtained from 25- to 26-day-old CD-Sprague-Dawley rats (Charles River Laboratories); procedures were approved by the animal care committee of the University of Connecticut Health Center. Rats were injected with 12 U of equine chorionic gonadotropin 48 h before ovary collection to stimulate follicle growth and LH receptor expression. Preovulatory follicles, 700-900 μm in diameter, were dissected from the ovaries and cultured as previously described for mouse follicles (*125*) with some modifications (see supplementary Materials and Methods).

Cantharidin was obtained from Tocris Bioscience (R&D Systems) and prepared as a 50 mM stock in dimethylsulfoxide (DMSO). Okadaic acid was obtained from LC Laboratories and was prepared as a 1 mM stock in DMSO.

Preparation of crude membranes from rat follicles and measurement of guanylyl cyclase activity

Crude membranes were prepared from rat follicles, and guanylyl cyclase assays were conducted as previously described for mouse follicles (*81, 114*). cGMP production was measured after a 9-min assay period and was approximately linear over this period (*81*). Basal activity without CNP was subtracted from the activity in the presence of CNP to obtain the CNP-dependent activity. Additional details are described in the supplementary Materials and Methods.

Immunoprecipitation, Phos-tag acrylamide gel electrophoresis and western blotting

Immunoprecipitation was used to purify the low-abundance NPR2 protein from rat follicle membranes. NPR2 was immunoprecipitated by incubation with a rabbit polyclonal antiserum (6328) made against the ten C-terminal amino acids of NPR2 (*134*). Phosphorylated forms of NPR2 were separated by electrophoresis on SDS-PAGE gels made with 6% acrylamide that had been co-polymerized with 25 μM Phos-tag-acrylamide (WAKO Chemicals) and 100 μM MnCl2. Blots were probed with the 6328 antiserum. Phosphorylated forms of PDE5 were separated from follicle lysates, using Phos-tag gels as described for NPR2. The blots were probed with an affinity-purified rabbit polyclonal antibody made against a C-terminal sequence from human PDE5 (catalog no. 2395, Cell Signaling Technology). Additional details, as well as protocols for the generation of dephosphorylated NPR2 and phosphorylated PDE5 controls, are described in the supplementary Materials and Methods.

Images were analyzed using ImageJ software. As an indicator of changes in NPR2 phosphorylation, the intensity of the immunostaining was measured within boxes surrounding the upper region and the lower band (see Fig. 2C, S3). The background intensity of each lane was collected from a box below the NPR2 signal and subtracted. The background-corrected intensity of the upper region was then divided by that of the lower band. This ratio method corrects for variability in the amount of protein that was immunoprecipitated and loaded in each lane. As a measure of total immunoreactive protein, we added the intensity of the upper region and the lower band and then subtracted the background intensity.

ELISA measurements of cGMP and CNP in follicles

The cGMP and CNP contents of rat follicles were measured as previously described (*75, 81*) by using ten follicles per sample and ELISA kits from Enzo Life Sciences (no. ADI-900-014 for cGMP) and Phoenix Pharmaceuticals (no. FEK-012-03 for CNP). Data were analyzed using Prism software (GraphPad).

Measurement of relative amounts of phosphatase mRNAs in granulosa cells

RNA was extracted from mural granulosa cells, mRNAs were reverse transcribed using random hexamers, and quantitative TaqMan analysis was performed as previously described (*81*). Primer sequences are listed in supplementary material Table S1.

Statistics

Differences between a single treatment and control were analyzed by paired t-test using Prism software. Other data were analyzed by either repeated measures ANOVA using Prism (where sample sizes between groups were equal) or by repeated measures mixed models in IBM SPSS (v. 21.0). Post-hoc t-tests were corrected for multiple comparisons by the Holm–Bonferroni method (*146*). *P*-values<0.05 were considered to indicate a significant difference.

SUPPLEMENTARY MATERIALS AND METHODS

Isolation and culture of rat ovarian follicles

Preovulatory follicles, 700 - 900 μm in diameter, were dissected from the ovaries of rats that had been injected 48 hours previously with equine chorionic gonadotropin. Approximately 30 follicles were obtained per rat. The follicles were placed on Millicell culture inserts (PICMORG50, Millipore, Billerica, MA; 10-30 follicles per insert). MEMα medium (Invitrogen, Carlsbad, CA) was supplemented with 25 mM $NaHCO_3$, 3 mg/ml BSA, 5 μg/ml insulin, 5 μg/ml transferrin, 5 ng/ml selenium, 50 μg/ml streptomycin, and 75 μg/ml penicillin G. The follicles were cultured at 37ºC in 5% CO_2 in air, and experimental procedures were started one to 4 hours after isolation. LH and other reagents were applied to the medium under the culture membrane, and 200-400 μl was also added to the top of the membrane to ensure rapid exposure of the follicles. Ovine LH and equine chorionic gonadotropin, purified from biological sources, were obtained from A.F. Parlow (National Hormone and Peptide Program, Torrance, CA). LH was used at a saturating concentration (10 μg/ml; approximately 350 nM). The kinetics of nuclear envelope breakdown in response to LH were determined by incubating isolated follicles with LH, and at various times afterwards, opening them with 30 gauge needles to release the cumulus-oocyte complex for observation of the presence or absence of the nucleus and nucleolus.

Preparation of crude membranes from rat follicles

To prepare crude membranes from rat follicles, 20-100 follicles were washed in PBS and then lysed in phosphatase inhibitor buffer (buffer A) containing 25 mM Hepes (pH 7.4), 50 mM NaCl, 50 mM NaF, 2mM EDTA, 20% glycerol, 1 μM microcystin-LR (Cayman Chemical Co., Ann Arbor, MI), and protease inhibitors (complete Mini, EDTA-free; Roche Applied Science), in a 0.1 ml glass homogenizer (Wheaton, Millville, NJ) on ice. The follicle wash procedure was done at room temperature and was started 3 minutes before the homogenizer was placed on ice. LH incubation times refer to the times at which the homogenizer was chilled. The homogenate (200-400 μl volume) was centrifuged at 10,000xg for 20 minutes at 4ºC; the pellet was resuspended in buffer A using a probe sonicator. Protein content was determined by a BCA assay (Thermo Fisher Scientific, Rockford, IL). The crude membrane fraction contained approximately 10 μg of protein per follicle. Aliquots were frozen in liquid N_2 and stored at – 80ºC. Crude membranes were also prepared from HEK-293T cells stably expressing NPR2, from plates of cells at 70-80% confluency that had been serum starved for >2 hours.

Measurement of guanylyl cyclase activity in follicle membranes

Guanylyl cyclase assays were conducted as previously described (*114*). Assays were performed at 37ºC using 3-20 µg of follicle protein per assay tube, in the presence or absence of CNP (1 µM except as indicated). The reaction mixture contained 25 mM Hepes (pH 7.4), 50 mM NaCl, 0.1% BSA, 1 mM EDTA, 0.5 µM microcystin, 5 mM $MgCl_2$, as well as 1 mM of the allosteric activator, ATP, and 1 mM of the substrate, GTP. 5 mM creatine phosphate and 0.1 mg/ml creatine kinase were included in the reaction mixture to maintain ATP and GTP concentrations. 0.5 mM isobutylmethylxanthine was included to inhibit cGMP phosphodiesterase activity.

Immunoprecipitation of NPR2 from rat follicle membranes

Crude membrane samples (130-230 µg protein) were diluted to 400 µl in immunoprecipitation buffer containing 50 mM Tris-HCl (pH 7.5), 100 mM NaCl, 50 mM NaF, 10 mM NaH_2PO_4, 2 mM EDTA, 1% NP-40, 0.1% SDS, 0.5% sodium deoxycholate, 1 µM microcystin-LR, and protease inhibitors. NPR2 was immunoprecipitated by incubation with 0.6 µl of 6328 rabbit polyclonal antiserum made against the 10 C-terminal amino acids of NPR2 (*134*) for one hour at 4ºC, and then with 25 µl of washed protein AG magnetic beads (Thermo Fisher Scientific, Rockford, IL) overnight at 4ºC. The beads were washed and resuspended in Laemmli sample buffer with 75 mM dithiothreitol. Protein was eluted by heating at 70ºC for 10 minutes. Approximately 50% of the membrane NPR2 was recovered after immunoprecipitation.

Phos-tag acrylamide gel electrophoresis and Western blotting

Phosphorylated forms of NPR2 or PDE5 were separated by electrophoresis on SDS-PAGE gels made with 6% acrylamide copolymerized with 25 µM Phos-tag-acrylamide (WAKO Chemicals USA, Richmond, VA) and 100 µM $MnCl_2$ (145 x 160 x 1.5 mm gel dimensions). Gels containing 6% acrylamide, but without Phos-tag-acrylamide or $MnCl_2$, were used for comparison. Immunoprecipitated NPR2, or lysates of follicles that had been washed in PBS and then sonicated in Laemmli sample buffer with 75 mM dithiothreitol, were electrophoresed at 25 mA/gel for 6-8 hours at 4ºC. The gels were then incubated for 20 minutes in 400 ml transfer buffer (100 mM Tris, 192 mM glycine, no SDS or methanol) containing 1 mM EDTA to chelate Mn^{2+}, and then washed for 20 minutes in 400 ml transfer buffer alone to remove Mn^{2+}-EDTA. Protein was transferred to a nitrocellulose membrane for 17-20 hours with 500 mA constant current at 4ºC. The membrane was stained with Ponceau-S, and blocked with 0.1% Tween and 2% milk. Blots

for NPR2 were probed overnight at 4ºC with a 1:50,000 dilution of the 6328 antiserum (see main text), and then with a 1:500 dilution of Clean-Blot IP Detection Reagent coupled to HRP (Thermo Fisher Scientific, Rockford, IL). Blots for PDE5 were probed overnight with a 1:500 dilution of the 2395 antibody from Cell Signaling Technology (see main text) and then with a 1:5000 dilution of a goat-anti-rabbit antibody coupled to HRP (catalog # sc-2004; Santa Cruz Biotechnology Inc., Dallas, TX). Blots were developped using ECL Prime (GE Healthcare Bio-Sciences, Piscataway, NJ), and imaged using a charge-coupled device camera (G:Box Chemi XT4, Syngene, Frederick, MD).

In vitro dephosphorylation of NPR2 in follicle membranes

To confirm that the LH-induced acceleration of NPR2 migration in a Phos-tag gel was due to dephosphorylation (Fig. 2E, F), follicle membranes were incubated at 30ºC for 30 min, either with phosphatase inhibitors (50 mM NaF + 2 mM EDTA + 1 μM microcystin-LR), or under conditions that promoted phosphatase activity (no phosphatase inhibitors, and 2 mM $MgCl_2$) (*147*). NPR2 was then immunoprecipitated and separated on a gel containing Phos-tag acrylamide; NPR2 was visualized by western blotting. To prepare membranes for these assays, follicles were homogenized in buffer A without microcystin-LR, to avoid irreversible modification of phosphatases. After centrifugation, the membranes were suspended in a buffer containing 25 mM Hepes, 50 mM NaCl, 20% glycerol, and protease inhibitors. After incubation under the indicated conditions, aliquots were frozen for immunoprecipitation and western blotting (Fig. 2 E, F), and for guanylyl cyclase assays (Fig. 2G).

In vitro phosphorylation of PDE5 in follicle lysates

To confirm that the LH-induced retardation of PDE5 migration in a Phos-tag gel was due to phosphorylation (Fig. 5D), a lysate of follicles was incubated with the catalytic subunit of protein kinase A (PKA_c, kindly provided by Jackie Corbin, Vanderbilt University), following the procedure described by Rybalkin et al., 2002. The follicles were lysed in a glass homogenizer in a buffer containing 50 mM Tris, pH 7.5, 1.5 mM EDTA, 25 mM NaF, 0.2 mM Na vanadate, and protease inhibitors (Roche complete Mini) followed by sonication. Aliquots containing 100 μg protein were then incubated at 30ºC for 30 minutes with 4 μM PKA_c, or with the buffer in which the PKA_c was dissolved. Reactions were performed with or without 10 μM cGMP, which is required for phosphorylation of PDE5 by PKA_c (*121*). The samples were then spin-dialyzed into a buffer compatible with Phos-tag gel electrophoresis (50 mM Tris, pH 7.5, 25 mM NaF, 0.2 mM

Na vanadate, and protease inhibitors), using a 0.5 ml, 10K Amicon Ultra centrifugal filter (EMD Millipore, Billerica, MA).

FIGURES AND TABLES

Fig. 1. Rapid decrease in follicle NPR2 guanylyl cyclase activity and cGMP content in response to LH signaling.

(A) Diagram showing the cell layers of a rat ovarian follicle. (B) Guanylyl cyclase activity in follicle membranes in the presence or absence of CNP. Membranes were prepared from follicles with or without treatment with LH for 30 min. Each point shows the mean±s.e.m. for four separate membrane preparations, each assayed in triplicate. In the presence of 50 nM or 1 μM CNP, 30 min of treatment with LH caused a decrease in activity to ~50% of the initial level. 1% Triton X-100 and 5 mM MgCl2 was used as a control condition that fully activates the enzyme (see text). (C) Time course of the LH-induced decrease in NPR2 activity, as determined in the presence of 1 μM CNP. The open circle represents measurements from follicle membranes incubated for 240 min in the absence of LH. Each point shows the mean±s.e.m. for (n) separate membrane preparations, each assayed in triplicate. (D) Time course of the LH-induced decrease in follicle cGMP content. Error bars are not visible for some points because they are smaller than the data point markers. C,D, *measurements that were significantly different ($P<0.05$) from the control without LH. Measurements at 30 and 240 min after LH exposure were not significantly different.

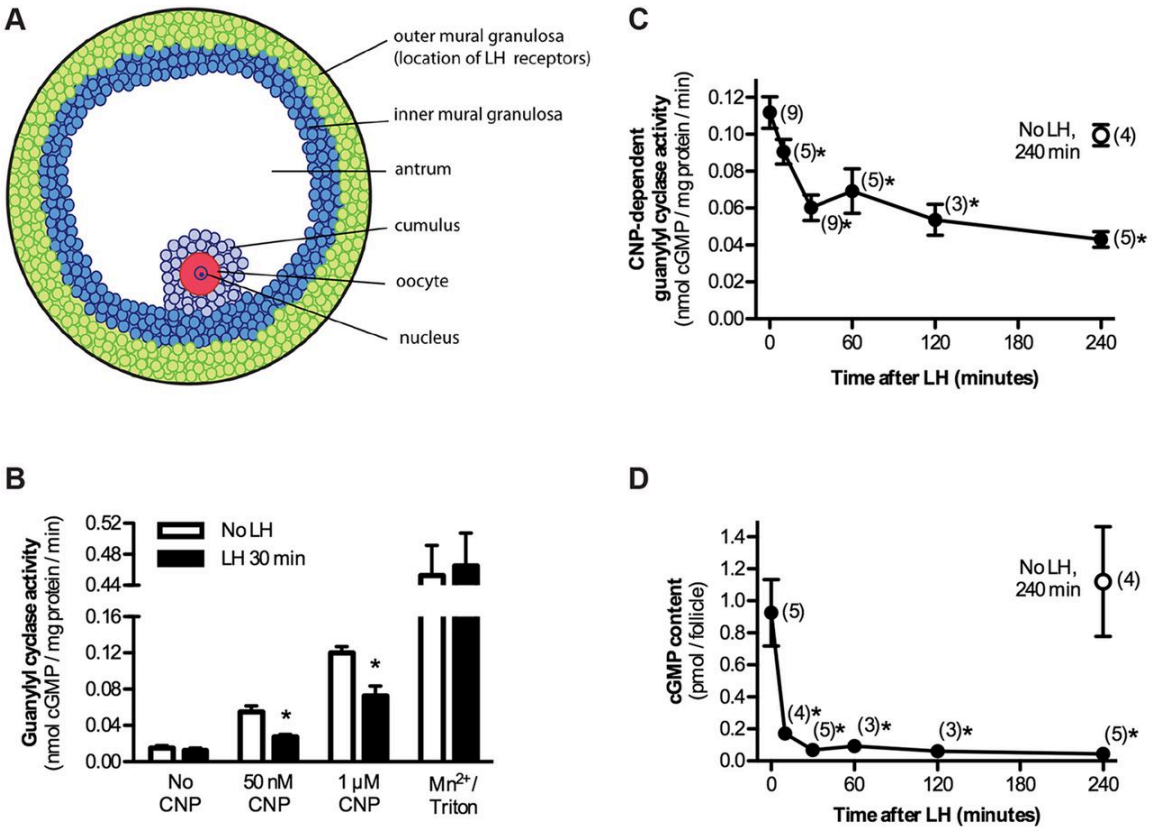
A
outer mural granulosa
(location of LH receptors)
inner mural granulosa
antrum
cumulus
oocyte
nucleus
C
CNP-dependent
guanylyl cyclase activity
(nmol cGMP / mg protein / min)
0.12
0.10
0.08
0.06
0.04
0.02
0.00
(9)
(5)*
(9)*
(5)*
(3)*
No LH,
240 min
(4)
(5)*
0
60
120
180
240
Time after LH (minutes)
B
Guanylyl cydase activity
(nmol cGMP / mg protein / min)
0.52
0.48
0.44
0.16
0.12
0.08
0.04
0.00
No LH
LH 30 min
*
*
No
CNP
50 nM
CNP
1 µM
CNP
Mn2+/
Triton
D
cGMP content
(pmol / follicle)
1.4
1.2
1.0
0.8
0.6
0.4
0.2
0.0
(5)
(4)*
(5)*
(3)*
(3)*
(5)*
No LH,
240 min
(4)
0
60
120
180
240
Time after LH (minutes)

Fig. 2. Rapid dephosphorylation of NPR2 in follicle membranes in response to LH signaling. (A) A western blot of a standard SDS-PAGE gel that had been probed with NPR2 antiserum; for each lane, NPR2 was immunoprecipitated from 145 μg of membrane protein from follicles with or without treatment with LH for 20 min, or from 10 μg of membrane protein from HEK-293T cells that stably expressed NPR2. (B) A western blot of an SDS-PAGE gel containing 25 μM Phos-tag acrylamide that had been probed with NPR2 antiserum; NPR2 was immunoprecipitated from 175 μg of membrane protein from follicles with or without treatment with LH for 30 min. Molecular weight standards are shown for reference, but do not indicate relative molecular mass on a Phos-tag gel. (C) Method for quantifying the LH-induced shift in NPR2 migration on Phos-tag gels. Boxes show the upper region (more phosphorylated) and lower band (less phosphorylated) for which background-corrected total immunostaining intensity was measured. The upper region was defined as the region extending from just above the lower band to the top of the dense zone near the 250-kDa marker. (D) Ratios of the intensity of the upper region to that of the lower band; mean±s.e.m. for 20 blots similar to that shown in B. (E-G) Validation of the shift in Phos-tag gel migration as an indicator of NPR2 dephosphorylation. Follicle membranes were incubated at 30°C for 30 min, with or without phosphatase inhibitors (see supplementary Materials and Methods). In the absence of phosphatase inhibitors, NPR2 was dephosphorylated (E). (F) Quantification of the shift in NPR2 migration caused by dephosphorylating conditions (mean±s.e.m. for four experiments). (G) Dephosphorylating conditions resulted in a decrease in NPR2 guanylyl cyclase activity (mean±s.e.m. for three experiments). *$P<0.05$.

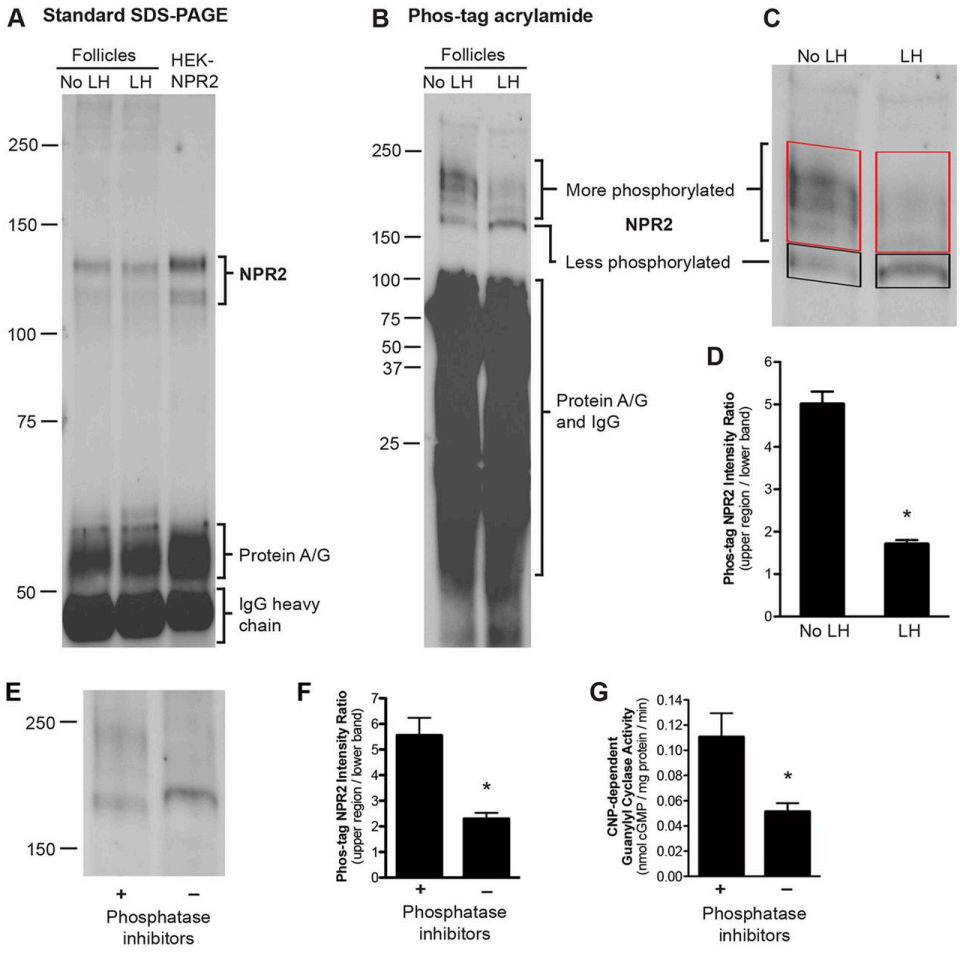
A
Standard SDS-PAGE
Follicles
No LH
LH
HEK-NPR2
250
150
100
75
50
NPR2
Protein A/G
IgG heavy chain
B
Phos-tag acrylamide
Follicles
No LH
LH
250
150
100
75
50
37
25
More phosphorylated
NPR2
Less phosphorylated
Protein A/G and IgG
C
No LH
LH
D
Phos-tag NPR2 Intensity Ratio
(upper region / lower band)
No LH
LH
E
250
150
+
–
Phosphatase inhibitors
F
Phos-tag NPR2 Intensity Ratio
(upper region / lower band)
+
–
Phosphatase inhibitors
G
CNP-dependent Guanylyl Cyclase Activity
(nmol cGMP / mg protein / min)
+
–
Phosphatase inhibitors

Fig. 3. Time course of the LH-induced dephosphorylation of NPR2.

(A) Follicles were incubated with LH for various times. Crude membranes were then isolated and used for immunoprecipitation of NPR2 (from 190 μg of membrane protein per lane), Phos-tag gel electrophoresis and immunoblotting for NPR2. Samples from follicles without treatment with LH were prepared in parallel, at 30 min and 240 min after starting the incubation. The regions used for quantification are shown in supplementary material Fig. S3A. The righthand lane sample was prepared using the same methods, instead using 10 μg of membrane protein from HEK-293T cells that stably expressed NPR2. (B) Time course of the LH-induced dephosphorylation of NPR2, quantified as shown in Fig. 2C. The open circle represents measurements from follicle membranes incubated for 240 min in the absence of LH. Each point shows the mean±s.e.m. for the number of experiments shown in parentheses. *$P<0.05$, measurements that were significantly different from the control without LH. Measurements at 30 and 240 min after LH exposure were not significantly different. (C) The total amount of NPR2 immunoreactive material in follicle membranes did not change during the first 4 h after treatment with LH. Measurements were made from the same set of blots used for B, by drawing a box around the entire NPR2 region of the blot (the sum of the red and black boxes shown in Fig. 2C).

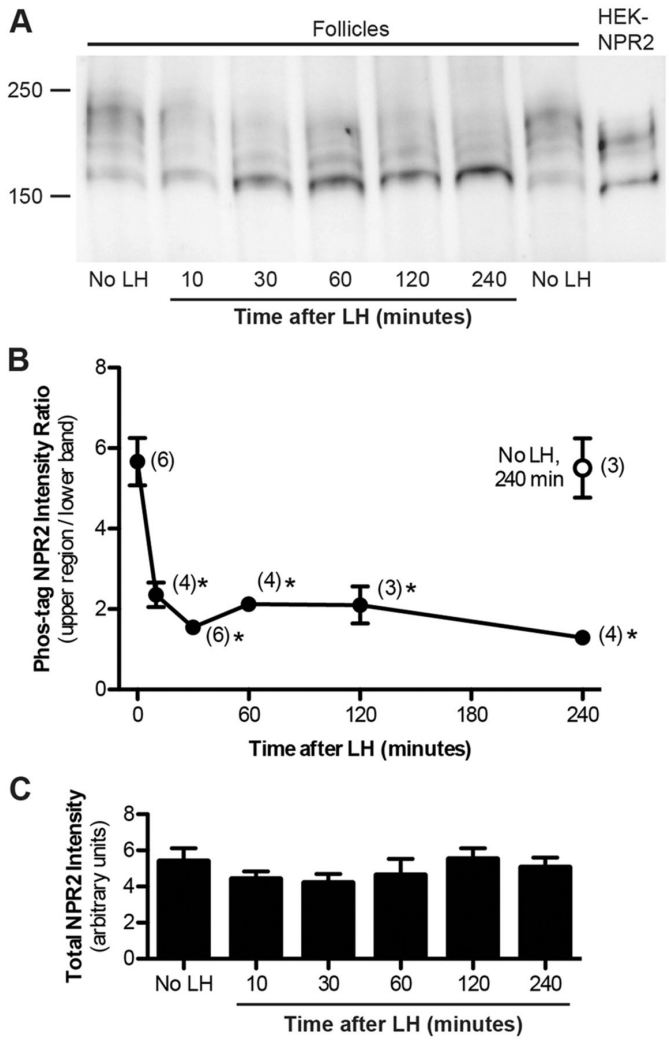
A
Follicles
HEK-NPR2
250
150
No LH
10
30
60
120
240
No LH
Time after LH (minutes)
B
Phos-tag NPR2 Intensity Ratio
(upper region / lower band)
8
6
4
2
0
(6)
No LH,
240 min
(3)
(4)*
(4)*
(3)*
(6)*
(4)*
0
60
120
180
240
Time after LH (minutes)
C
Total NPR2 Intensity
(arbitrary units)
8
6
4
2
0
No LH
10
30
60
120
240
Time after LH (minutes)

Fig. 4. Inhibition of the LH-induced dephosphorylation and inactivation of NPR2 and decrease in cGMP content upon the treatment of follicles with the PPP-family phosphatase inhibitor cantharidin.

(A) Follicles were incubated with or without 100 μM cantharidin for 1 h, then with or without LH for 30 min. Crude membranes were isolated and used for immunoprecipitation, Phos-tag gel electrophoresis and immunoblotting for NPR2. In the presence of cantharidin, the ratio of NPR2 in the upper region and lower band did not change in response to LH, indicating that cantharidin inhibited the LH-induced dephosphorylation of NPR2. The regions used for quantification are shown in supplementary material Fig. S3B. (B) A graph showing the results of three experiments similar to that shown in A (mean±s.e.m.). (C) Membranes from follicles treated with or without cantharidin followed by LH, as described above, were assayed for NPR2 guanylyl cyclase activity. The graph shows the results from three experiments. (D) Follicles treated with or without cantharidin followed by LH, as described above, were assayed for cGMP content. The graph shows the results from seven experiments. Values not indicated by the same letter are significantly different ($P<0.05$).

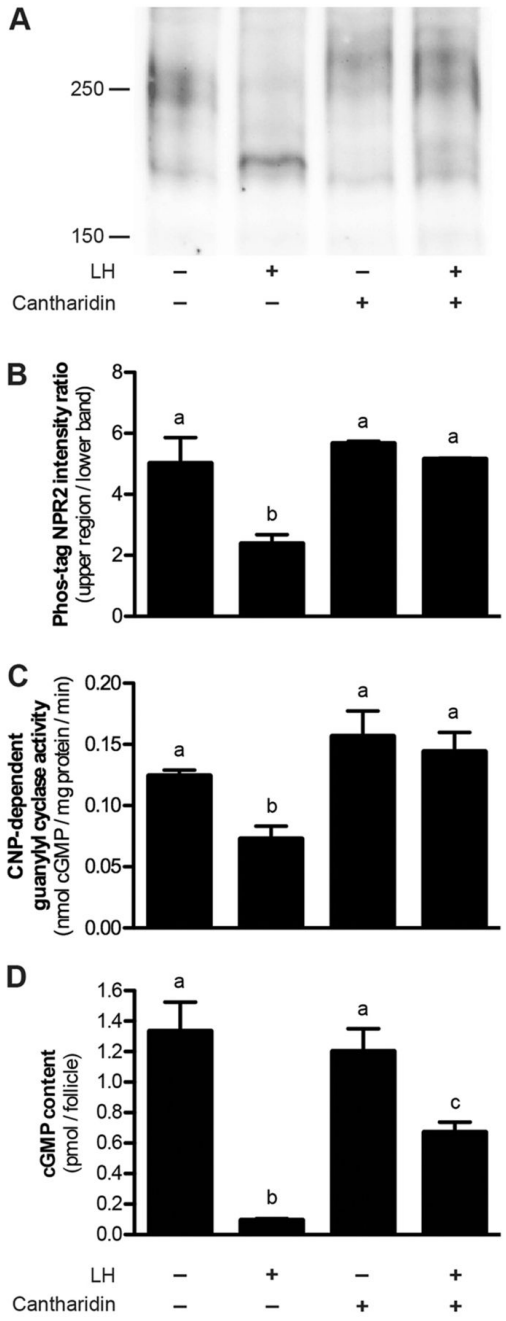
A
250
150
LH
Cantharidin
B
Phos-tag NPR2 intensity ratio
(upper region / lower band)
C
CNP-dependent
guanylyl cyclase activity
(nmol cGMP / mg protein / min)
D
cGMP content
(pmol / follicle)
a
b
c

Fig. 5. Rapid phosphorylation of PDE5 in follicles in response to LH signaling.

(A,B) Western blots of proteins from follicles with or without 10 or 30 min of treatment with LH, which were probed with an antibody against PDE5. (A) Standard SDS-PAGE gel, 30 μg protein per lane; (B) SDS-PAGE gel containing 25 μM Phos-tag acrylamide, 20 μg protein per lane. Molecular weight standards are shown for reference, but do not indicate relative molecular mass on a Phos-tag gel. (C) Ratios of the intensity of the upper band to that of the lower band; mean±s.e.m. for four blots similar to that shown in B. (D) Phos-tag gel separation and immunoblotting for PDE5 in follicle lysates that had been incubated with or without the catalytic subunit of PKA (PKAc). Incubations were performed with or without 10 μM cGMP (see supplementary Materials and Methods); cGMP binds to an allosteric site on PDE5 and is required for PKAc to phosphorylate PDE5 (Corbin et al., 2000; Rybalkin et al., 2002). In the presence of PKAc and cGMP, the migration of PDE5 was retarded, indicating phosphorylation.

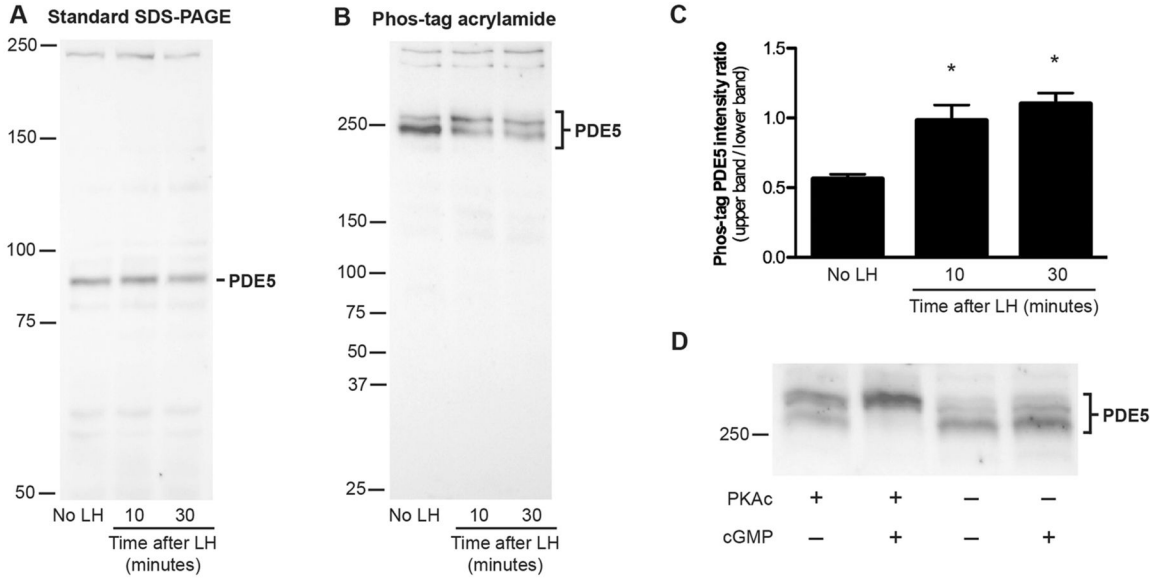

Fig. 6. Relative amounts of each PPP phosphatase catalytic subunit mRNA in isolated granulosa cells.

(A) The graph shows the mean±s.e.m. for four independent preparations of granulosa cell RNA. The PPP1 bar shows the total for mRNA encoded by Ppp1ca, Ppp1cb and Ppp1cc. The PPP2 bar shows the total for Ppp2ca and Ppp2cb. The PPP3 bar shows the total for Ppp3ca, Ppp3cb and Ppp3cc. The PPP7 bar shows the total for Ppef1 and Ppef2. (B) Data for each individual gene.

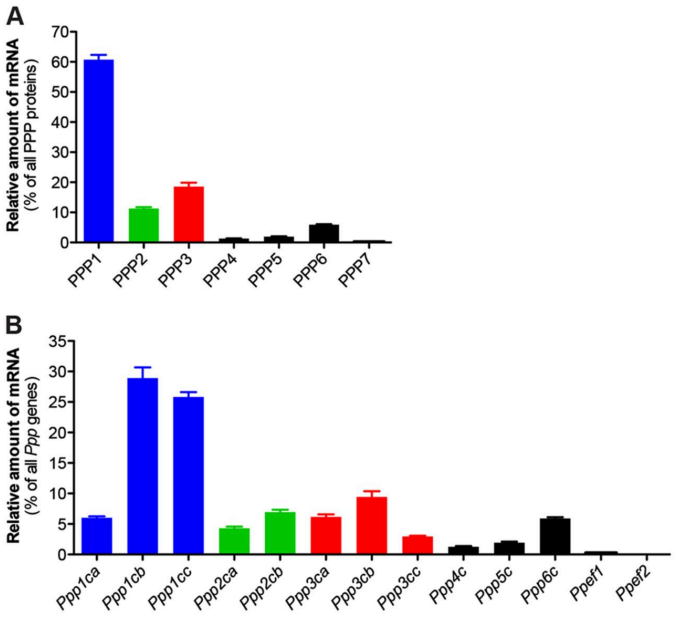

Fig. 7. Time course of the decrease in the CNP content of follicles, and the resumption of meiosis in response to LH signaling.

(A) A time course of the decrease in CNP content of follicles that had been treated with LH. (B) There was no change in the CNP content of follicles that had been incubated for 2-6 h without LH. (C) A time course of nuclear envelope breakdown in follicles that had been treated with LH. Values indicate the mean±s.e.m. for the indicated number of experiments (above each bar). A total of 386 follicles were examined for C. A,C, the 'no LH' data combine results from follicles that had been incubated without LH for times corresponding to the times of LH exposure. *P<0.05, measurements that are significantly different from controls without LH.

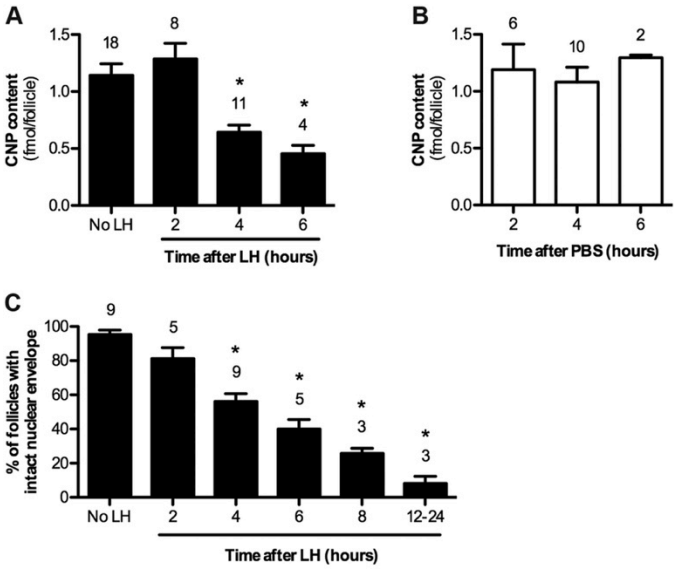

Fig. 8. LH signaling in rat ovarian follicles decreases NPR2 guanylyl cyclase activity by way of a rapid dephosphorylation of regulatory sites followed by a slower decrease of the levels of the agonist CNP.

The functional domains of the homodimeric transmembrane protein NPR2 are shown in gray. Binding of CNP (green) to the extracellular domain and phosphorylation of seven juxtamembrane regulatory sites (red) both increase the catalytic activity of the enzyme. LH signaling acts by way of a PPP-family phosphatase to dephosphorylate some of these sites; dephosphorylation occurs by 10 min and persists for at least 4 h. By 4 h after LH exposure, the CNP content of the follicle decreases. Both of these changes decrease guanylyl cyclase activity, contributing to the decrease in cGMP that restarts meiosis.

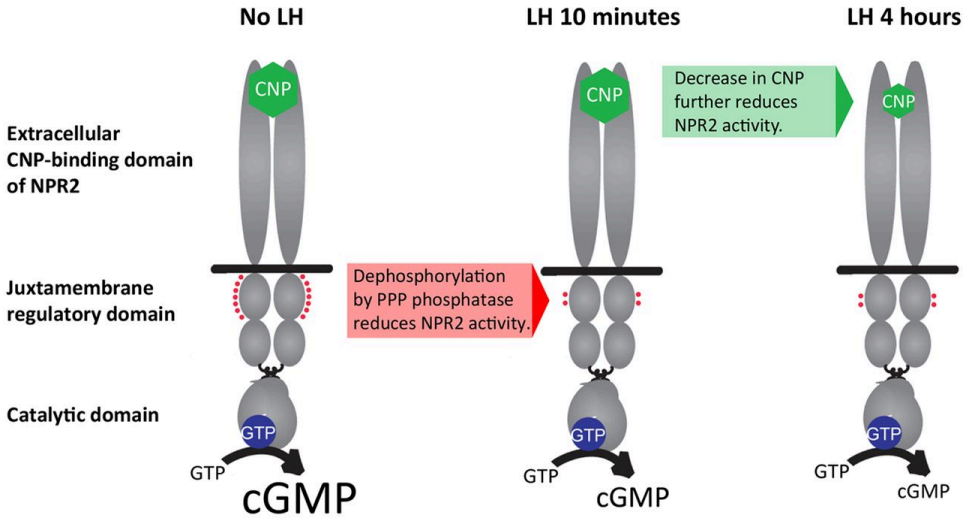

Supplementary Figure S1. Validation of the specificity of the NPR2 antibody.

Blot showing the lack of immunoreactivity when the immunoprecipitation and western blot of follicle membranes were done with preimmune serum instead of the 6328 antibody against a C-terminal peptide from NPR2. The follicles were treated with or without LH for 30 minutes.

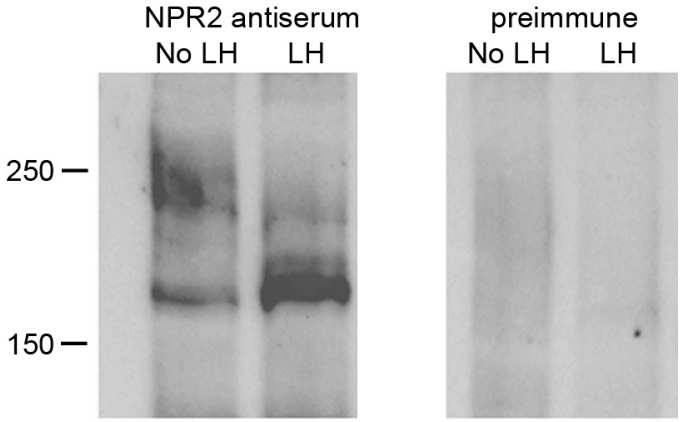

Supplementary Figure S2. Inhibition of the LH-induced dephosphorylation and inactivation of NPR2 by treatment of follicles with the PPP family phosphatase inhibitor okadaic acid. (A) Follicles were incubated with or without 10 μM okadaic acid for one hour, then with or without LH for 30 minutes. Crude membranes were isolated and used for immunoprecipitation, Phos-tag gel electrophoresis, and immunoblotting for NPR2. In the presence of okadaic acid, basal phosphorylation of NPR2 increased, but LH did not change the ratio of NPR2 in the upper region and lower band, indicating that okadaic acid inhibited the LHinduced dephosphorylation of NPR2. (B) Graph showing the results of 4 experiments like that shown in A (mean ± s.e.m.). (C) Membranes from follicles treated with or without okadaic acid followed by LH, as described above, were assayed for NPR2 guanylyl cyclase activity (4 experiments). Values not indicated by the same letter are significantly different. We also attempted to determine the effect of okadaic acid on the LH-induced decrease in cGMP, but these experiments were not interpretable because okadaic acid alone caused cGMP to decrease in some of the trials.

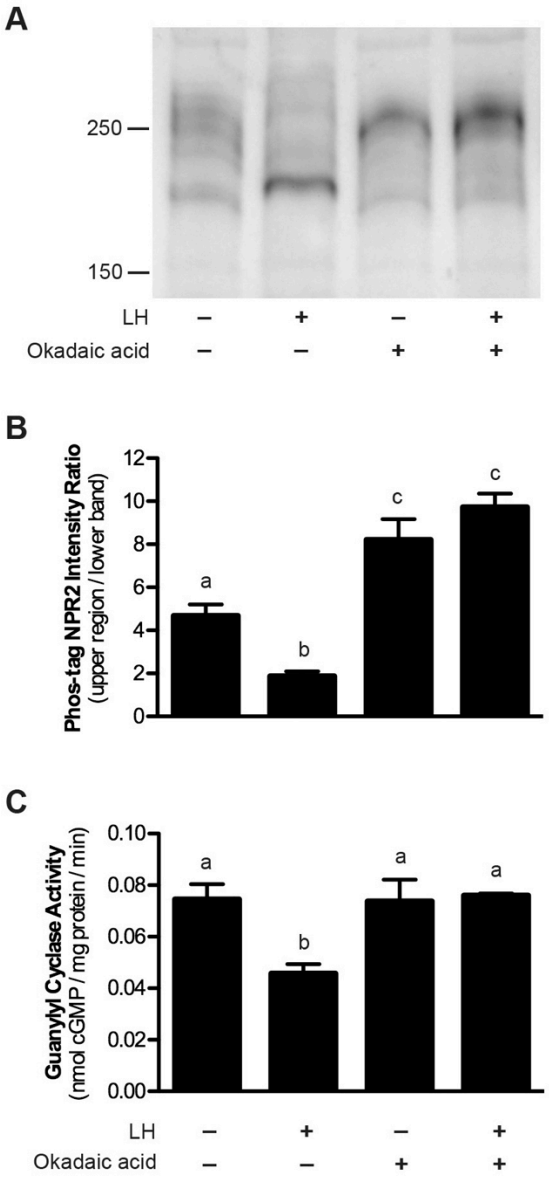
A
250
150
LH – + – +
Okadaic acid – – + +
B
Phos-tag NPR2 Intensity Ratio
(upper region / lower band)
12
10
8
6
4
2
0
a
b
c
c
C
Guanylyl Cyclase Activity
(nmol cGMP / mg protein / min)
0.10
0.08
0.06
0.04
0.02
0.00
a
b
a
a
LH – + – +
Okadaic acid – – + +

Supplementary Figure S3. Blot images for figures 3A and 4A, with red boxes indicating the upper region (more phosphorylated) and lower band (less phosphorylated) for which immunostaining intensity was measured.

(A) Figure 3A. (B) Figure 4A.

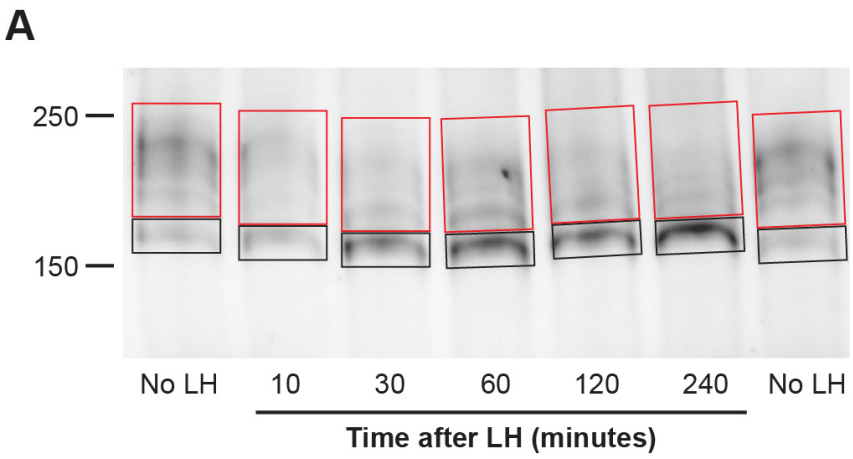

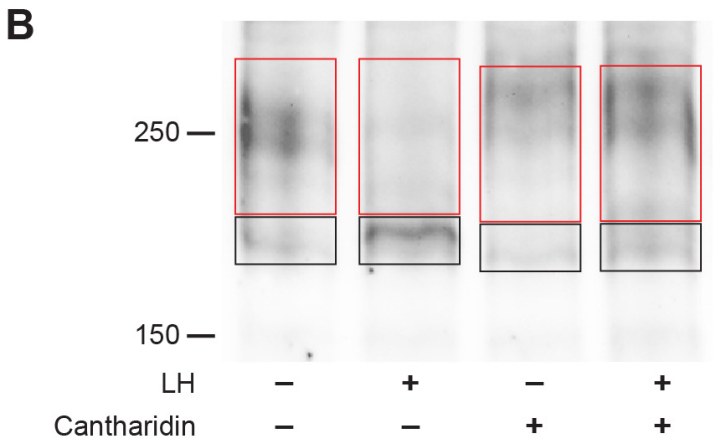

Supplementary Table S1. Primers and fluorescent probes used for qRT-PCR analysis of relative expression levels of PPP family phosphatases.

gene name	forward primer, 5'-3'	probe, 5'-3'	reverse primer, 5'-3'
Ppp1ca	AAGGGGAAGTATGGGCAGTT	AGGCCGTCCCATCACTCCACC	TTTCTTGGCTTTGGCAGAAT
Ppp1cb	ACCAGTATGGTGGGCTGAAT	CTGTCACTCCGCCTCGAACAGCTAA	TTCACCTTTTCTTCGGTGGA
Ppp1cc	CCCAACTACTGTGGCGAGTT	AATGCGGGCGCCATGATGAGT	AGCACATGAGGGTCTCATCC
Ppp2ca	CGTAGAGGCGAGCCACA	CTCGTCGTACCCCAGACTACTTCCTG	TTCATGGCAATACTGTACAAGG
Ppp2cb	CGTCGTGGAGAGCCTCAT	CCGGCGCACCCCAGACTACTTC	AGGTCCTGGGGAGGAATTTA
Ppp3ca	ACGCCAACCTTAACTCCATC	TCGCCTCAGAGACTAACGGCACAGA	TGCTGCTATTACTGCCGTTG
Ppp3cb	AGGAGAGTGAAAGCGTGCTG	AAGGGCCTGACTCCCACAGGGAT	CCAGCCAACACTCCACTAGG
Ppp3cc	TTGAAGAAGCCCGAGGTCTA	TGAGAGAATGCCACCCCGAAAAGAG	GTGTCTTTCCTGCATCATGG
Ppp4c	GGCAGCCATCTTAGAACTGG	TTCATCATCTTCGAGGCTGCACCC	GGATGCCACGTGTCTCTTG
Ppp5c	GACCAGATGGGAAACAAAGC	ACATCCACCTCCAGGGCTCCGAC	CACTGCTGTGAATTGGTGGA
Ppp6c	CGTCAACACGAGAGAACCAA	TCCGAGCAGTTCCAGATTCAGAACG	CGTGGTTCTGGGAGGAATAA
Ppef1	TGTGGAAACTTTTCAATGCTCA	ATGATTCCCAAATTGATGAGCTTGCC	TTGTTGGAGTCCATTGTGCT
Ppef2	CATCTGTGACCTTGCCAGAA	TTCAACAAGGACGGCCACATCGATA	AAGGCCTCCAGGAACTCATT
Rpl32	GAAAGAGCAGCACAGCTGGC	TCAGAGTCACCAATCCCAACGCCA	TCATTCTCTTCGCTGCGTAGC

CHAPTER 3:

Dephosphorylation of juxtamembrane serines and threonines of the NPR2 guanylyl cyclase is required for rapid resumption of oocyte meiosis in response to luteinizing hormone.

This chapter is a reprint of an original publication with minor alterations, used with permission:

Leia C. Shuhaibar, Jeremy R. Egbert, **Aaron B. Edmund**, Tracy F. Uliasz, Deborah M. Dickey, Siu-Pok Yee, Lincoln R. Potter, Laurinda A. Jaffe. Dephosphorylation of juxtamembrane serines and threonines of the NPR2 guanylyl cyclase is required for rapid resumption of oocyte meiosis in response to luteinizing hormone. *Developmental Biology.* (2016) 409(1):194-201.

Aaron Edmund collected, interpreted, and analyzed data in Figure 2.

SUMMARY

The meiotic cell cycle of mammalian oocytes starts during embryogenesis and then pauses until luteinizing hormone (LH) acts on the granulosa cells of the follicle surrounding the oocyte to restart the cell cycle. An essential event in this process is a decrease in cyclic GMP in the granulosa cells, and part of the cGMP decrease results from dephosphorylation and inactivation of the natriuretic peptide receptor 2 (NPR2) guanylyl cyclase, also known as guanylyl cyclase B. However, it is unknown whether NPR2 dephosphorylation is essential for LH-induced meiotic resumption. Here, we prevented NPR2 dephosphorylation by generating a mouse line in which the seven regulatory serines and threonines of NPR2 were changed to the phosphomimetic amino acid glutamate (*Npr2*–7E). *Npr2*–7E/7E follicles failed to show a decrease in enzyme activity in response to LH, and the cGMP decrease was attenuated; correspondingly, LH-induced meiotic resumption was delayed. Meiotic resumption in response to EGF receptor activation was likewise delayed, indicating that NPR2 dephosphorylation is a component of the pathway by which EGF receptor activation mediates LH signaling. We also found that most of the NPR2 protein in the follicle was present in the mural granulosa cells. These findings indicate that NPR2 dephosphorylation in the mural granulosa cells is essential for the normal progression of meiosis in response to LH and EGF receptor activation. In addition, these studies provide the first demonstration that a change in phosphorylation of a transmembrane guanylyl cyclase regulates a physiological process, a mechanism that may also control other developmental events.

INTRODUCTION

Meiosis in mammalian oocytes begins during embryonic development and is paused at prophase until, beginning at puberty, luteinizing hormone (LH) that is secreted from the pituitary gland during each reproductive cycle acts on the ovarian follicle to release the arrest. In the preovulatory follicle, meiotic arrest is maintained by cGMP that is produced outside of the oocyte, in the granulosa cells surrounding it; cGMP diffuses into the oocyte through gap junctions (*75, 76, 79, 148*). In the oocyte, cGMP acts by inhibiting the cAMP phosphodiesterase PDE3A, resulting in a high level of cAMP that maintains the CDK1 kinase in a phosphorylated and inactive form, thus inhibiting the prophase-to-metaphase transition (*89, 91*). LH signaling induces meiotic resumption by lowering cGMP in the granulosa cells and, as a consequence of equilibration through gap junctions, decreases cGMP in the oocyte (*75, 76, 88, 148*). Thus cAMP in the oocyte decreases and meiosis resumes, initiating the series of events by which chromosomes segregate in preparation for fertilization (*149*).

cGMP in the follicle is produced by natriuretic peptide receptor 2 (NPR2), also known as guanylyl cyclase B, which is expressed in both the mural granulosa and cumulus cells, but not in the oocyte or in the theca cells surrounding the follicle (*79, 82, 83, 104*). Based on studies of mutant mice with defective NPR2, it has been established that NPR2 is essential for maintaining meiotic arrest (*79, 82, 83, 150*). NPR2 is also essential for other developmental processes including chondrocyte differentiation (*83, 151*) and axon bifurcation (*144*). It is not well understood for any of these processes how other regulators, such as hormones and growth factors, are coordinated with NPR2 regulation, but recent studies of ovarian follicles have begun to identify these mechanisms (*88, 152*).

NPR2 is a homo-oligomeric transmembrane protein, probably a dimer, that is activated by C-type natriuretic peptide (CNP). NPR2 consists of an extracellular CNP-binding domain, a single-membrane spanning region, a juxtamembrane regulatory region, a kinase homology domain, a dimerization domain, and a guanylyl cyclase catalytic domain (*41*) (Fig. 1). Phosphorylation of serine and threonine sites in the juxtamembrane domain and the beginning of the kinase homology domain is required for CNP-dependent activation of NPR2, and dephosphorylation is a mechanism of inactivation (*22, 23, 27, 41, 103*).

LH activates a G-protein coupled receptor in the outer (mural) granulosa cells (*77, 93, 153*) , and this leads to dephosphorylation and inactivation of NPR2 by 10 min after LH exposure, thus reducing cGMP production in mouse and rat follicles (*81, 152*). The dephosphorylation persists for at least 4 h, even if LH is washed out after a brief exposure (*152*). More slowly,

between one and 2 h after LH exposure, levels of the NPR2 agonist CNP begin to decrease, presumably further lowering NPR2 activity (*80-82, 88*). In parallel with these events that decrease NPR2 activity, the cGMP phosphodiesterase PDE5 becomes phosphorylated, which is likely to increase its hydrolytic activity (*152*). In addition, LH signaling increases EGF receptor kinase activity, which by means that are not understood, contributes to the cGMP decrease and is essential for rapid resumption of meiosis in response to LH (*88, 105, 130, 131*).

The complexity of these processes raises the question of whether NPR2 dephosphorylation is essential for LH-induced resumption of meiosis. While a previous study showed that inhibiting NPR2 dephosphorylation with phosphatase inhibitors reduced the LH-induced decrease in guanylyl cyclase activity (*152*), other proteins would also have been prevented from being dephosphorylated by the broad specificity phosphatase inhibitors. In particular, these inhibitors also act on phosphatases in the oocyte, causing meiosis to resume independently of LH (*124*). Thus this approach did not provide information as to whether the rapid dephosphorylation and inactivation of NPR2 is essential for meiotic resumption in response to LH or EGF receptor activation. Here we investigate these questions using a genetically modified mouse in which the 7 juxtamembrane serine and threonine residues in NPR2 are changed to glutamates in both endogenous alleles encoding NPR2 (*Npr2*–7E/7E) (Fig. 1), such that the enzyme behaves as if it is constitutively phosphorylated. Our results indicate that dephosphorylation is necessary for NPR2 inactivation, and for the rapid resumption of meiosis in response to signaling by luteinizing hormone and the EGF receptor ligand epiregulin.

RESULTS

NPR2 dephosphorylation in the mural granulosa cells is required for the LH-induced decrease in guanylyl cyclase activity

To investigate if dephosphorylation of the 7 regulatory serines and threonines of NPR2 is required for the LH-induced decrease in guanylyl cyclase activity, we developed a genetically modified mouse in which the 7 regulatory phosphorylation sites of NPR2 are changed to glutamates, such that the enzyme behaves as if it is constitutively phosphorylated. Using this mouse line, we compared CNP-dependent NPR2 activity in wild-type and *Npr2*–7E/7E follicles. In untreated follicles, NPR2 activity was the same for wild-type and *Npr2*–7E/7E (Fig. 2A). However, while wild-type follicles that had been treated with LH for 20 min showed an approximately 50% decrease in NPR2 activity (Fig. 2B, left), LH caused no significant change in NPR2 activity in membranes from *Npr2*–7E/7E follicles (Fig. 2B, right). These findings indicate that dephosphorylation of these regulatory serines and threonines of NPR2 is necessary for the hormonal regulation of guanylyl cyclase activity in the ovarian follicle.

To test if NPR2 protein levels were the same in *Npr2*–7E/7E and wild-type follicles, we measured guanylyl cyclase activity in the presence of 1% Triton X-100 and 5 mM $MnCl_2$ (Fig. 2C), which yields near maximal NPR2 guanylyl cyclase activity that is independent of CNP or phosphorylation (*24*). Based on these assays, as well as western blots (Fig. 3A, B), neither the 7E mutations nor a 20 min LH treatment changed the amount of NPR2 protein per follicle.

Although it is known that *Npr2* RNA is present in both mural granulosa and cumulus cells (*79, 82, 150*), the relative amount of NPR2 protein in these 2 regions has not been investigated. In some models, NPR2 protein is depicted as being located primarily in the cumulus cells (*79*), which would be difficult to reconcile with our activity measurements from whole follicles. For this reason, we investigated the NPR2 protein distribution by comparing NPR2 levels in whole follicles and cumulus–oocyte complexes. Our results indicated that 97% of the total NPR2 protein in the follicle is located in the mural granulosa cells (Fig. 3C), implying that the LH-induced decrease in NPR2 phosphorylation and activity occurs primarily in the mural cells, where the LH receptors are located (*77, 93, 153*). Our results comparing NPR2 activity in membranes from follicles of *Npr2*–7E/7E and wild-type mice are consistent with measurements showing that the 7E mutations have little or no effect on substrate-binding and maximal catalytic activity of NPR2 in transfected HEK cells, but result in resistance to phosphorylation-dependent inactivation (*27*). The 7E mutations also have no effect on the CNP concentration required to activate NPR2 to half its maximum value (EC_{50}) (Fig. S3).

NPR2 dephosphorylation is required for part of the LH-induced decrease in cGMP

To investigate the effect of the 7E mutations on the LH-induced decrease in cGMP levels, we used *Npr2*–7E/7E and wild-type follicles that co-expressed the cGMP FRET sensor cGi500 (*148, 154*). With this sensor, the CFP/YFP emission ratio provides a measure of cytosolic cGMP. Live follicles were imaged with a confocal microscope, and CFP/YFP ratios were measured in the mural granulosa cells. The cGi500 CFP/YFP emission ratios before LH treatment were similar for the two genotypes, indicating that the 7E mutations do not alter the basal concentration of cGMP in the granulosa cell cytosol (Fig. 4). However, in *Npr2*–7E/7E follicles, the LH-induced decrease in cGMP was attenuated (Fig. 4). Thus the dephosphorylation-mediated decrease in NPR2 guanylyl cyclase activity is an important cause of the LH-induced decrease in cGMP in the follicle, although it appears not to be the only cause, since a partial cGMP decrease occurred in the *Npr2*–7E/7E follicles. An LH-induced increase in cGMP phosphodiesterase activity might account for the residual cGMP decrease seen when LH was applied to *Npr2*–7E/7E follicles (*152*).

NPR2 dephosphorylation is required for the rapid resumption of meiosis in response to LH or epiregulin

To investigate whether the LH-induced dephosphorylation and inactivation of NPR2 is required for meiotic resumption, we isolated *Npr2*–7E/7E and wild-type follicles and observed them in culture before and after addition of LH. The *Npr2*–7E/7E follicles had normal morphology, and by 8h after stimulation with LH, the cumulus cell region underwent the normal expansion that results from secretion of a hyaluronan-rich extracellular matrix between the cells, in preparation for ovulation (*155, 156*) (Fig. 5A).

However, follicle-enclosed oocytes from *Npr2*–7E/7E mice showed a delay in resumption of meiosis in response to LH, as indicated by a delay in nuclear envelope breakdown (NEBD) (Fig. 5B). In control wild-type follicles, NEBD occurred between 2 and 6 h after LH exposure. In contrast, in *Npr2*–7E/7E follicles, no NEBD occurred in the first 6 h following treatment with LH. The 7E mutations had no effect on meiotic resumption in response to isolating oocytes from the follicle (Fig. 5C), consistent with the lack of NPR2 expression in the oocyte (*79*). Thus, dephosphorylation and inactivation of NPR2 is needed for the rapid LH-induced meiotic resumption, but not for the meiotic resumption that occurs when oocytes are disconnected from the granulosa cells that are the source of the inhibitory cGMP. The signaling pathways

leading to the dephosphorylation of NPR2 in response to LH are incompletely understood, but one likely factor is activation of the EGF receptor, since EGF receptor activity is required for rapid resumption of meiosis, and for a component of the cGMP decrease, in response to LH (*88, 105, 130, 131, 148*). Application of the EGF receptor ligand epiregulin to isolated follicles caused meiosis to resume (Fig. 5D), and as with LH, meiotic resumption in response to epiregulin was delayed in *Npr2*–7E/7E follicles (Fig. 5D). Thus EGF receptor signaling is likely to contribute to establishing and/or maintaining dephosphorylation of NPR2.

Although meiotic resumption was delayed by the 7E mutations, it did occur eventually. By 8 h after LH application, NEBD had occurred in approximately 40% of *Npr2*–7E/7E follicle-enclosed oocytes, and in approximately 90% by 12 h (Fig. 5B). Compared to the timecourse of NEBD in wild-type follicles, NEBD in the *Npr2*–7E/ 7E follicles occurred with a 5 h delay. A similar delay was seen when epiregulin was used to stimulate meiotic resumption (Fig. 5D). Consistent with the eventual resumption of meiosis, the 7E mutations caused no obvious defect infertility (Fig. 5E); however, further studies would be needed to determine if there is a subtle defect.

A possible cause of the eventual resumption of meiosis is the disruption of gap junction communication due to cumulus expansion (*155, 157*); cumulus expansion occurred similarly in *Npr2*–7E/7E and wild-type follicles (Fig. 5A, F). Loss of communication between the oocyte and granulosa cells would remove the source of inhibitory cGMP and allow meiosis to resume (*75, 76*).

DISCUSSION

These studies contribute three new findings about how LH signaling causes meiosis to resume in the oocyte: 1) dephosphorylation of the NPR2 guanylyl cyclase is required for the rapid resumption of meiosis in response to LH; 2) dephosphorylation of NPR2 is a component of the pathway by which EGF receptor activation mediates LH signaling; and 3) most of the NPR2 protein in the follicle is located in the mural granulosa cells. These findings indicate that NPR2 dephosphorylation in the mural granulosa cells is essential for the normal progression of meiosis in response to LH and EGF receptor activation.

If LH-induced dephosphorylation ofNPR2 fails to occur, as in the *Npr2*–7E/7E mice, meiosis still resumes eventually, possibly due to disruption of gap junction communication during cumulus expansion, as mentioned above. Other LH-induced changes that could contribute to the eventual resumption of meiosis in the *Npr2*–7E/7E follicles include: 1) decreasing levels of NPR2 (*104*) and the RNA encoding it (*82, 150*), detectable by 3 h after LH receptor stimulation; 2) decreasing levels of the NPR2 agonist CNP, detectable after 2 h of LH treatment and continuing to decrease over the next several hours (*80-82, 88*); and 3) LH-induced activation of cGMP phosphodiesterase activity (*152*). Correspondingly, under the conditions of our experiments, the 7E mutations caused no obvious defect infertility. Whether there are subtle defects, not detected here, remains to be examined. Because meiotic progression is essential for reliable fertility, mechanisms for LH induction of meiotic resumption involve coordinated fail-safe processes, of which NPR2 dephosphorylation is only one. Thus reduction of the function of a single path way may have little effect on fertility. For example, various mutations that result in reduced EGF receptor signaling have been reported to have only small effects (*131, 158*) or no detectable effect (*159, 160*) on fertility; one such mutant line was reported to have highly reduced fertility, but interpretation was complicated by possible effects outside of the ovary (*158*).

Using recombinant protein expressed in HEK cells, previous studies have shown that phosphomimetic, glutamate-substituted versions of transmembrane guanylyl cyclases are resistant to dephosphorylation-dependent inactivation (*27, 106, 136*). However, it has not been previously demonstrated that this mechanism is physiologically significant. This is the first report to show that a biological signal is transduced by dephosphorylation of a guanylyl cyclase. Our studies establish that in the ovarian follicle, normal progression of meiosis in response to LH requires dephosphorylation ofNPR2.

Another developmental process that could be regulated by NPR2 dephosphorylation is longitudinal growth of bones in limbs and vertebrae. Chondrocyte growth and differentiation in

the growth plate is dependent on NPR2 activity (*139, 151*), and cGMP production by NPR2 in a chondrocyte cell line is decreased by FGF receptor 3 signaling (*161*), suggesting that FGF could regulate NPR2 activity by way of dephosphorylation. Axon bifurcation also requires NPR2 (*144*), and this process could potentially be regulated by NPR2 dephosphorylation. Thus our demonstration that LH signaling regulates meiosis by way of NPR2 dephosphorylation provides a model for future investigations of regulation of guanylyl cyclases in other developmental systems.

EXPERIMENTAL PROCEDURES

Mice, follicle culture, and microscopy

Generation of the *Npr2*–7E mouse line, globally expressing 7 glutamate substitutions, is described in the Supplementary Materials and Methods and Fig. S2. The cGi500 mouse line was provided by Robert Feil (*154*). Ovaries were obtained from pre-pubertal mice (22–25 days old). All experiments were conducted as approved by the University of Connecticut Health Center Animal Care Committee.

Antral follicles (~300–400 μm in diameter) were isolated using fine forceps and were cultured for 24–30h on Millicell organotypic membranes before use, as described (*125*) except that 3mg/ml BSA was included in the culture medium in place of serum. 10ng/ml of follicle stimulating hormone was included in the medium to stimulate follicle growth and expression of LH receptors. LH was used at a concentration of 10 μg/ml. Ovine LH and ovine follicle stimulating hormone were obtained from A.F. Parlow (National Hormone and Peptide Program, Torrance, CA). Epiregulin (R&D Systems) was used at a concentration of 100 nM. For some experiments, cumulus–oocyte complexes were isolated from the cultured follicles, by slitting them with a 30 gauge needle. Oocytes were isolated from cumulus–oocyte complexes by aspiration through a glass pipet with an approximately 80 μm diameter opening.

Observations of follicles on Millicell membranes were made using a 20x/0.4 NA long-working distance objective. LH was applied to the medium in the dish holding the Millicell membrane, and oocytes within follicles were observed for the presence or absence of a nuclear envelope and nucleolus a 1 h intervals. At 8 and 12 h after LH application, the oocyte was not visible within the follicle due to the secretion of extracellular matrix by the cumulus cells; therefore follicles were opened to isolate and observe the oocyte. Photographs were taken using a Canon EOS M camera.

Guanylyl cyclase activity assays

For guanylyl cyclase activity measurements, crude membranes were prepared and assayed as previously described (*81, 114*). For each membrane preparation, 80–100 antral follicles from 5–8 *Npr2*–7E/7E or *Npr2*–+/+ mice were divided into 2 equal groups, and half were exposed to LH for 20 min, before preparing and freezing membrane samples in phosphatase inhibitor buffer to preserve the phosphorylation state ofNPR2. Assays were performed in the presence of 1 μM CNP, 1 mM ATP, 1 mM GTP, and 5 mM $MgCl_2$, or 1% Triton X-100, 1mM

GTP, and 5mM $MnCl_2$, for 9 min at 37 °C. 0.5 mM IBMX was included in the assay buffer to inhibit cyclic nucleotide phosphodiesterase activity.

Western blotting and deglycosylation

Amounts of NPR2 protein were compared by western blotting, using an antibody provided by Hannes Schmidt (*144*). To deglycosylate NPR2, 10 µg of follicle protein was incubated with Peptide: N-glycosidase F (PNGaseF, New England Bio Labs, Ipswich, MA) following the manufacturer's protocol. Immunodensities of western blot bands were determined using ImageJ software (http://imagej.nih.gov/ij/).

cGMP measurement

To examine the effect of LH on cytosolic cGMP, mice expressing the cGi500 sensor for cGMP (EC_{50} = 500nM) (*154*) were bred with mice from the *Npr2*–7E line, to obtain mice of either the *Npr2*–7E/7E or *Npr2*–+/+ genotype, expressing one copy of the cGi500 transgene. Follicles were imaged by confocal microscopy in a 200 mm-thick glass-bottomed chamber, before and after perfusion with LH (*148*). cGMP binding to cGi500 decreases FRET between CFP and YFP, such that higher CFP/YFP emission ratios after CFP excitation indicate higher cGMP concentrations (*154, 162*). CFP and YFP images were collected every 30s, and intensities in the mural granulosa region were measured from a 25 µm-wide band just inside the basal lamina.

Statistical analysis

Differences between treatment conditions were analyzed by unpaired or paired t-tests, or by one-way ANOVA with the Tukey adjustment for multiple comparisons, using Prism software (GraphPad).

SUPPLEMENTARY MATERIALS AND METHODS

Generation of knock-in mice with phosphomimetic glutamate mutations in NPR2

A sequence encoding the 7E point mutations, located in exon 8 and 9, was introduced into the endogenous *Npr2* gene by homologous recombination (Fig. S2A). The targeting vector was prepared by recombineering (*163*). Briefly, we first retrieved approximately 9.2 kb of the *Npr2* genomic sequence spanning introns 2 to 12 from the BAC vector, RP24-306K11 (Children's Hospital Oakland Research Institute), into a vector containing the negative selectable marker PGKdta, by gap repair. We then inserted a single LoxP site into exon 8 together with a unique restriction site, PmeI. An 800 bp genomic fragment spanning intron 7 to 9 with the 7E mutations S489E, S513E, T516E, S518E, S523E, S526E, and T529E, was prepared by PCR and inserted into the targeting vector to replace the single LoxP. Unique site elimination, by PmeI digestion, was used to remove plasmids that did not undergo recombineering to generate the p*Npr2*-7E.dta vector (*164*). We then inserted a single LoxP with two unique restriction sites, SalI and AscI, in the 3' end into intron 8. A fragment containing a wild-type *Npr2* minigene with a unique SalI site and 200 bp of intron 8 and cDNA from exons 8 to 22 was prepared by overlapping PCR using the BAC and a full length *Npr2* cDNA as initial templates. The mini-cDNA was then inserted into pSK+ and sequenced to confirm its identity. A DNA fragment containing IRESeGFP followed by *Npr2* 3'UTR and the Frt-PGK-Neo-Frt-LoxP cassette was prepared by a combination of PCR and conventional cloning. This fragment, which contains a unique AscI in the 3' end, was inserted 3' to the *Npr2* mini-cDNA plasmid. The final DNA fragment was then released from pSK+ and inserted into 3' to the single LoxP site in the p*Npr2*-7E.dta vector by restriction digestion and ligation to generate the final targeting vector.

This vector, which contains approximately 5.3 kb and 4 kb of 5' and 3' arms, respectively, was linearized and electroporated into mouse ES cells derived from F1 (129Sv/C57BL6/J) blastocysts. Electroporated ES cells were cultured for 48 hour prior to drug selection using G418. Drug resistant colonies were picked and screened by long range PCR using primers corresponding to sequences outside the arms and specific to the 5'LoxP site, and eGFP fluorescence to identify targeted ES clones. These targeted ES clones were then further analyzed by PCR and sequencing to confirm the presence of the 7E mutations prior to using them for the generation of chimeric animals by ES cell-morula aggregation (*165*). Chimeric animals were then bred with *Hprt-Cre* mice (*166*) to generate global knock-in mice. Cre recombinase excises the *Npr2* wild-type mini-gene and IRES-eGFP sequences, leaving a single LoxP site in intron 7, and

inducing expression of the *Npr2* gene with the 7E mutations (*Npr2*-7E). We performed PCR and sequencing of positive F1 pups to confirm the 7E knock-in mutation (Fig. S2B).

The single LoxP located approximately 900 bp 5' of exon 9 serves as a convenient marker for PCR genotyping. All subsequent PCR-based genotyping was performed using genomic DNA isolated from ear biopsies with the following primers, located as shown by the purple arrows.

LoxF(forward): 5'- CATCCTAGGTATTTATCTTGC

LoxF(reverse): 5'- TAAAAACTACTTCTTTTTTAAAAAATCCTTA

These primers amplify a 399-bp fragment of the wildtype sequence, and a 496-bp fragment of the 7E-mutated sequence.

FIGURES

Figure 1. Diagram of the NPR2 guanylyl cyclase showing the 7 serine and threonine phosphorylation sites that were changed to glutamates (E) in the Npr2–7E mice.

Binding of CNP (green) to the extracellular domain and phosphorylation of 7 serine or threonine residues (red) increase catalytic activity. Dephosphorylation of these regulatory sites decreases catalytic activity; the 7E mutations result in a protein that cannot be dephosphorylated. (For interpretation of the references to color in this figure legend, the reader is referred to the web version of this article.)

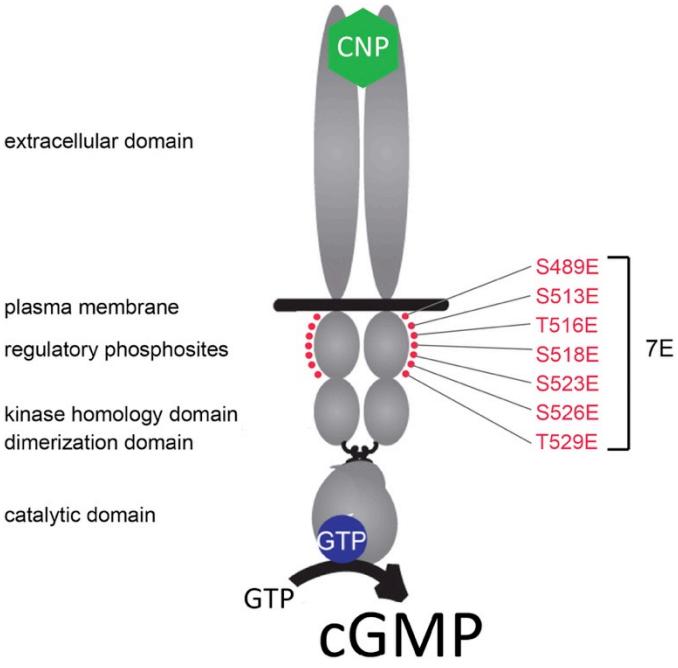

Figure 2. Prevention of the LH-induced decrease in CNP-dependent guanylyl cyclase activity in Npr2–7E/7E follicles.

(A) CNP-dependent guanylyl cyclase activity in membranes from wild-type and *Npr*2–7E/7E follicles, without LH treatment. (B) CNP-dependent guanylyl cyclase activity in membranes from wild-type and *Npr2*–7E/7E follicles, treated with or without LH for 20 min. Data were normalized to the no LH value for each experiment. LH treatment significantly decreased the CNP-dependent guanylyl cyclase activity in wild-type ($p < 0.05$), but not in *Npr2*–7E/7E follicles (NS). (C) Guanylyl cyclase activity in wild-type and *Npr2*–7E/7E follicles from the same membrane preparations as in (B), measured with 5 mM Mn2. and 1% Triton X-100 in place of CNP, ATP, and Mg2., to determine the relative amounts of NPR2 protein. The activity levels in wild-type and *Npr2*–7E/7E follicles were not significantly different, and neither activity value changed in response to LH. For A–C, each value shows the mean ± SEM for 4–5 membrane preparations.

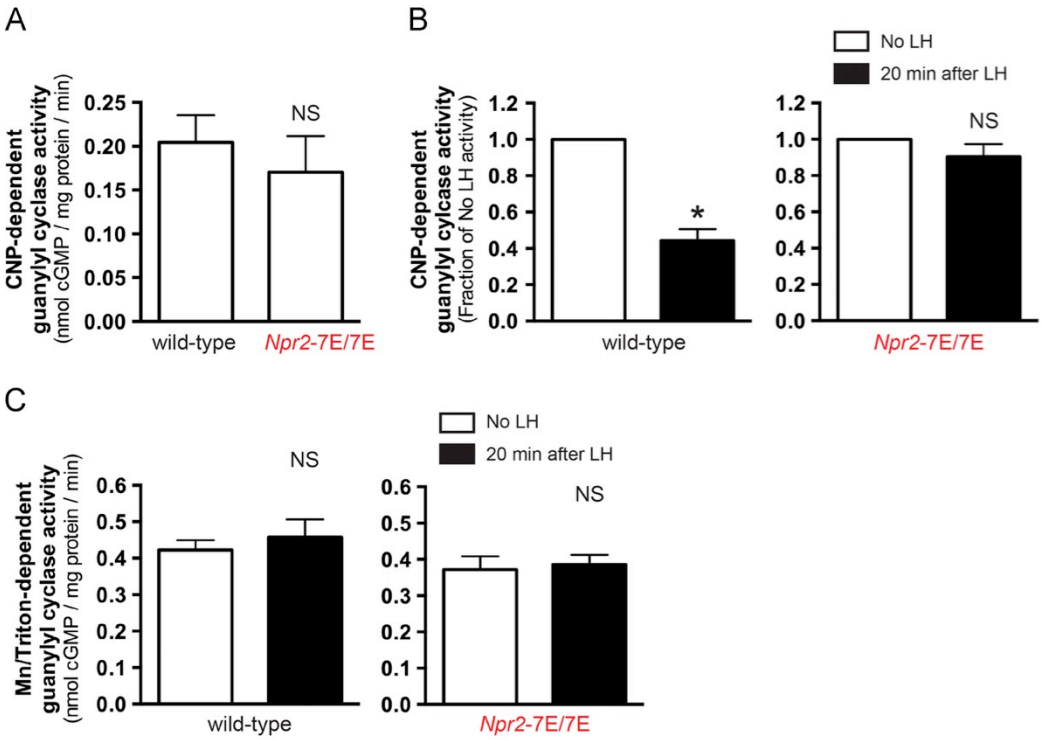

Figure 3. Relative amounts of NPR2 protein in wild-type and Npr2–7E/7E follicles, with and without LH, and within different regions of the follicle.

(A) Western blot indicating that the amount of NPR2 protein is the same in wild-type and *Npr2*–7E/ 7E follicles, and is unchanged by a 20-min LH treatment. (B) Effect of glycosidase treatment of follicle lysates, showing that the 2 immunoreactive bands correspond to NPR2 with different amounts of glycosylation (*167, 168*). (C) Comparison of the immunodensity of NPR2 in 40 cumulus–oocyte complexes (COCs) with that in amounts of lysate from 1 or 2 follicles, showing that ~3% of the NPR2 protein in a follicle is in the COC. Since Npr2 RNA is not detectable in the theca cells or oocyte (*79, 82, 104*), this indicates that ~97% of the NPR2 protein is in the mural granulosa cells.

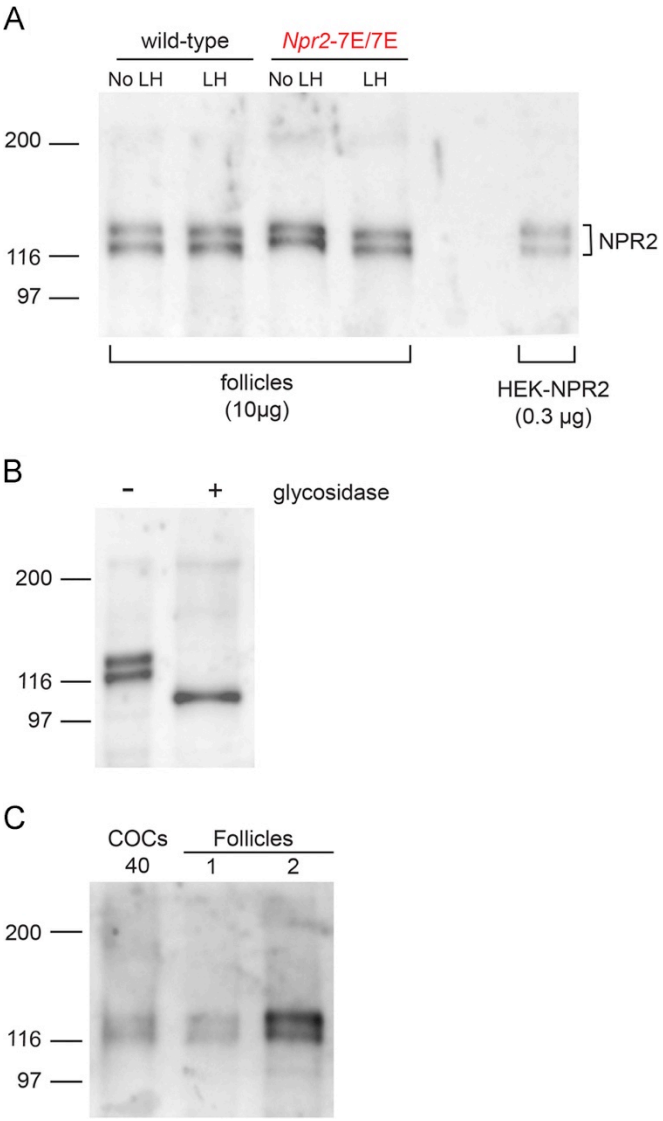

Figure 4. Attenuation of the LH-induced cGMP decreases in Npr2–7E/7E follicles. Representative records showing LH-induced decreases in cytosolic cGMP in mural granulosa cells of follicles expressing the cGi500 sensor, comparing wild-type (A) and *Npr2*–7E/7E (B). (C) Measurements before and at 20 min after LH treatment. LH decreased the CFP/YFP ratio in the *Npr2*–7E/7E follicles to 1.72 ± 0.04 compared to 1.38 ± 0.03 in wild-type follicles (mean ± SEM, n.9 and 7 follicles, respectively). Values with different letters are significantly different ($p < 0.05$).

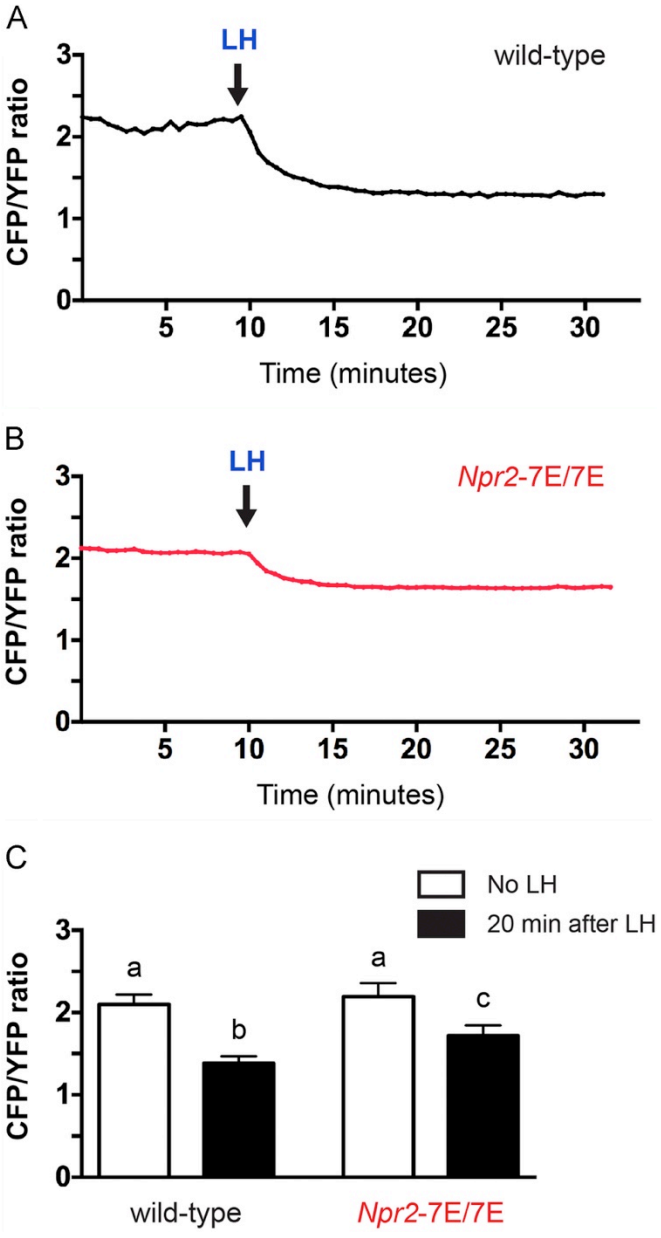

Figure 5. Delay of LH-induced meiotic resumption in Npr2–7E/7E follicle-enclosed oocytes. (A) An *Npr2*–7E/7E follicle before LH treatment, with the oocyte arrested in prophase (left), and at 8 h after LH treatment, when the oocyte is no longer visible due to cumulus expansion (right). (B) Time course of LH-induced nuclear envelope breakdown in *Npr2*–7E/7E and wild-type follicles. (C) Time course of nuclear envelope breakdown after isolating oocytes from *Npr2*–7E/7E and wild-type follicles without LH treatment. (D) Time course of epiregulin-induced nuclear envelope breakdown in *Npr2*–7E/7E and wild-type follicles. (E) No obvious defect in fertility of *Npr2*–7E/7E mice, as judged by the number of pups produced by 7E/7E x 7E/7E breeding pairs, compared with wild-type pairs. The graph shows the number of pups produced by individual breeding pairs as a function of maternal age (7 pairs for WT, and 6 pairs for 7E/7E). (F) Time course of the initiation of LH-induced cumulus expansion, as scored by loss of a clear image of the oocyte periphery, in *Npr2*–7E/7E and wild-type follicles. B,C,D, and F show the mean ± SEM for 3–8 sets of measurements at each time point. Each set of measurements included an average of 12 follicles.

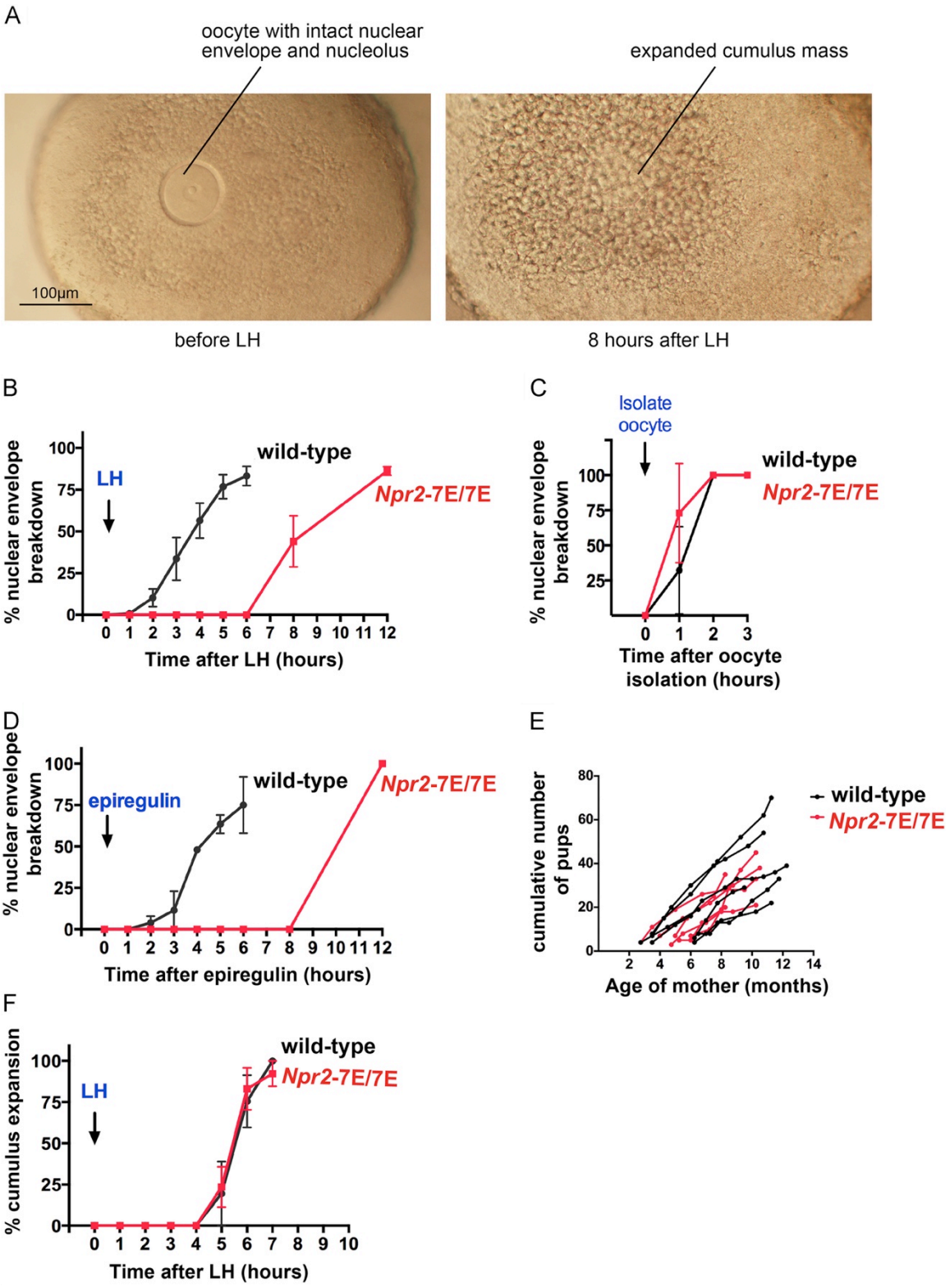
A
oocyte with intact nuclear envelope and nucleolus
expanded cumulus mass
100µm
before LH
8 hours after LH
B
% nuclear envelope breakdown
LH
wild-type
Npr2-7E/7E
Time after LH (hours)
C
Isolate oocyte
% nuclear envelope breakdown
wild-type
Npr2-7E/7E
Time after oocyte isolation (hours)
D
% nuclear envelope breakdown
epiregulin
wild-type
Npr2-7E/7E
Time after epiregulin (hours)
E
cumulative number of pups
wild-type
Npr2-7E/7E
Age of mother (months)
F
% cumulus expansion
LH
wild-type
Npr2-7E/7E
Time after LH (hours)

Supplementary Figure S1. NPR2 is dephosphorylated in response to LH signaling, and remains dephosphorylated for several hours even when LH is washed out after a brief exposure.

Experiments were done using follicles from rats, using methods as described previously (*152*). Preovulatory follicles without LH treatment were compared with follicles that were treated with LH for 30 or 240 min, or treated with LH for 30 min, then washed 5 times in medium without LH for a total of 20 min, and incubated without LH until 240 min after the initial treatment. The western blot shows NPR2 that was immunoprecipitated from crude follicle membranes and run on a gel containing Phos-tag, which retards the migration of phosphorylated proteins. Without LH, most of the NPR2 signal is represented by several slower-migrating bands, indicating phosphorylation. Upon treatment with LH for 30 or 240 min, the upper bands collapse into a single lower band, indicating NPR2 dephosphorylation. NPR2 remains dephosphorylated for several hours after removal from a 30-min LH treatment. These results are representative of 2 similar experiments. The findings indicate that a brief exposure to LH may induce persistent signaling (*133*), perhaps as a consequence of receptor endocytosis (*169*). It is also possible that since LH binds with high affinity to its receptor (*170*), it remains bound despite extensive washing.

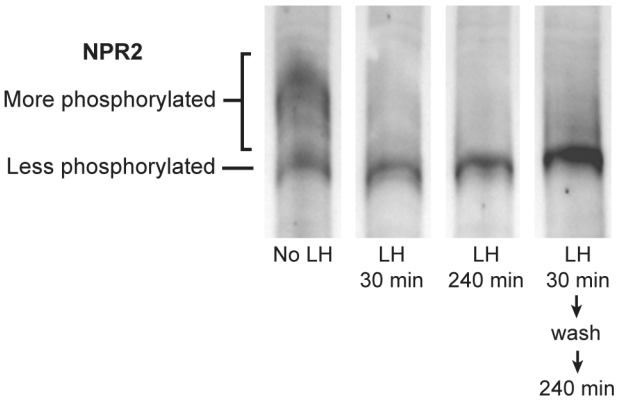

Supplementary Figure S2. Generation of knock-in mice with phosphomimetic glutamate mutations in NPR2.

(A) Outline of the strategy. A sequence encoding the 7E point mutations (red asterisks), located in exon 8 and 9, was introduced into the endogenous *Npr2* gene by homologous recombination. (B) Sequencing chromatographs from an *Npr2*-7E/+ mouse, confirming the point mutations in the seven serine and threonine sites of the *Npr2* gene.

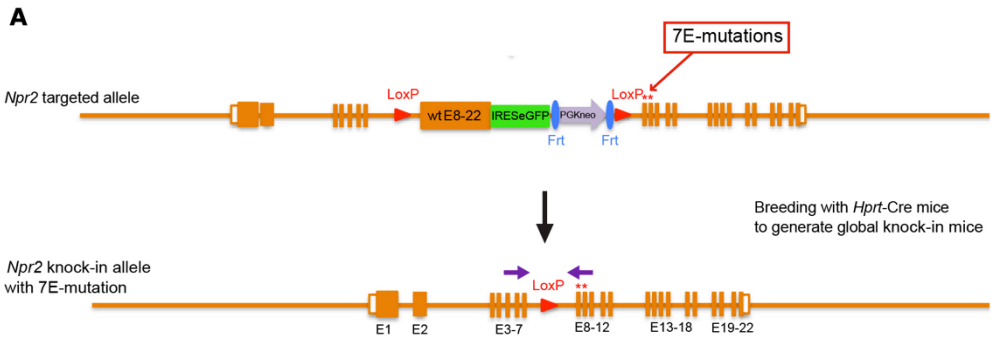
A
7E-mutations
Npr2 targeted allele
LoxP
wt E8-22
IRESeGFP
PGKneo
Frt
Frt
LoxP**
Breeding with Hprt-Cre mice
to generate global knock-in mice
Npr2 knock-in allele
with 7E-mutation
LoxP
**
E1
E2
E3-7
E8-12
E13-18
E19-22

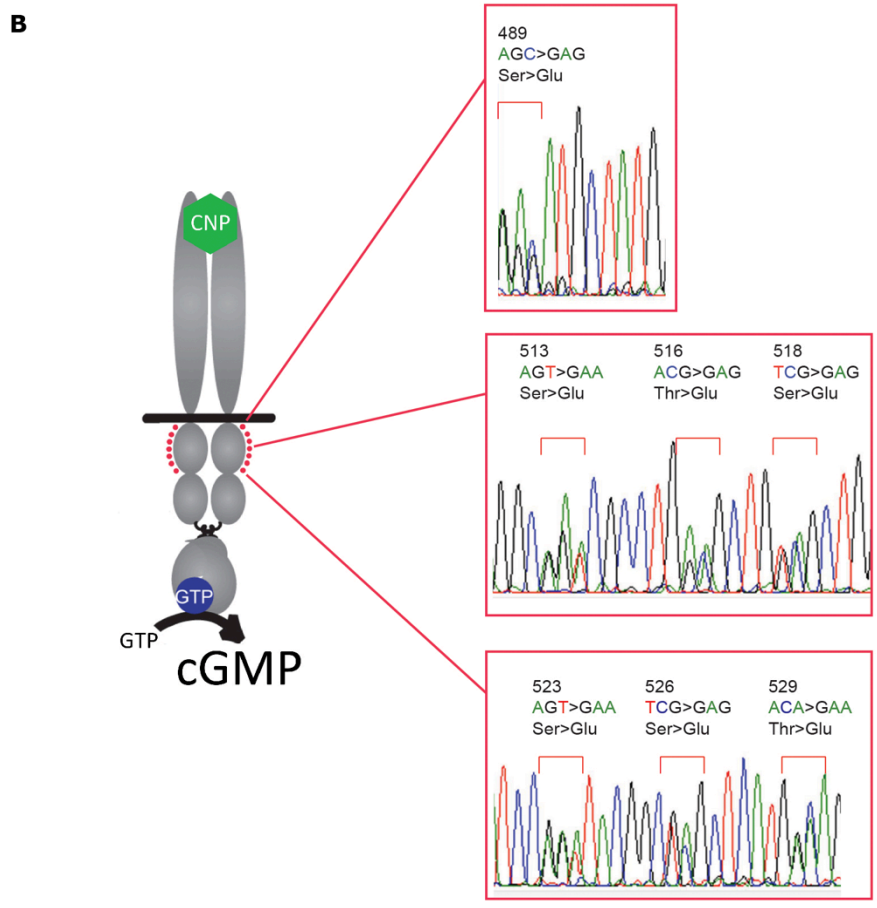
B
CNP
GTP
GTP
cGMP
489
AGC>GAG
Ser>Glu
513
AGT>GAA
Ser>Glu
516
ACG>GAG
Thr>Glu
518
TCG>GAG
Ser>Glu
523
AGT>GAA
Ser>Glu
526
TCG>GAG
Ser>Glu
529
ACA>GAA
Thr>Glu

Supplementary Figure S3. Similar CNP concentration-dependence of the activity of wild-type and 7E-mutated NPR2.

HEK-293T cells transiently transfected with either wild-type or 7E-mutated NPR2 were seeded in 48-well plates and serum starved for 4 hours. Medium containing 1 mM of the cyclic nucleotide phosphodiesterase inhibitor isobutylmethylxanthine was added to the cells for 10 min and then this medium was aspirated and replaced with the same medium containing the indicated concentrations of CNP. After 1 min, the medium was aspirated and the reaction was stopped by adding 80% ice-cold ethanol. Cyclic GMP concentrations in the ethanolic extracts were determined by radioimmunoassay. Vertical bars represent SEM (n = 18).

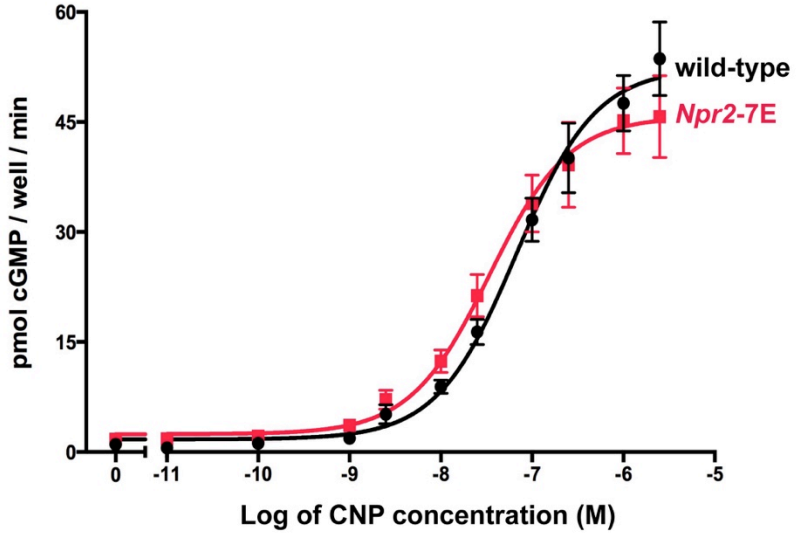

CHAPTER 4:

Heterozygous Mutations in Natriuretic Peptide Receptor-B (NPR2) Gene as a Cause of Short Stature

This chapter is a reprint of an original publication with minor alterations, used with permission:

Sophie R. Wang, Christina M. Jacobsen, Heather Carmichael, **Aaron B. Edmund**, Jerid W. Robinson, Robert C. Olney, Timothy C. Miller, Jennifer E. Moon, Veronica Mericq, Lincoln R. Potter, Matthew L. Warman, Joel N. Hirschhorn, and Andrew Dauber. Heterozygous Mutations in Natriuretic Peptide Receptor-B (NPR2) Gene as a Cause of Short Stature. *Human Mutation.* (2015) 36(4):474-81

Aaron Edmund collected, interpreted, and analyzed data for Patients 2-7 and both FINRISK bio-bank tall extreme variants in Table 5 and Supplemental Figure S1.

SUMMARY

Based on the observation of reduced stature in relatives of patients with acromesomelic dysplasia, Maroteaux type (AMDM), caused by homozygous or compound heterozygous mutations in natriuretic peptide receptor-B gene (NPR2), it has been suggested that heterozygous mutations in this gene could be responsible for the growth impairment observed in some cases of idiopathic short stature (ISS). We enrolled 192 unrelated patients with short stature and 192 controls of normal height and identified seven heterozygous NPR2 missense or splice site mutations all in the short stature patients, including one de novo splice site variant. Three of the six inherited variants segregated with short stature in the family. Nine additional rare nonsynonymous NPR2 variants were found in three additional cohorts. Functional studies identified eight loss-of-function mutations in short individuals and one gain-of-function mutation in tall individuals. With these data, we were able to rigorously verify that NPR2 functional haploinsufficiency contributes to short stature. We estimate a prevalence of NPR2 haploinsufficiency of between 0 and 1/26 in people with ISS.

INTRODUCTION

C-type natriuretic peptide (CNP, gene natriuretic peptide precursor C, NPPC; MIM# 123830) is a small, secreted peptide and a member of the natriuretic peptide family. CNP binds to a homodimeric transmembrane receptor named natriuretic peptide receptor-B (NPR-B, gene NPR2; MIM# 108961), which functions as a guanylyl cyclase to generate cGMP in chondrocytes, female reproductive organs, and endothelial cells (*102, 171*). In the growth plate chondrocytes, binding of CNP to NPRB stimulates chondrocyte differentiation and hypertrophy as well as increases matrix synthesis. This occurs in part through NPR-B signaling inhibiting MAP kinase signaling by FGFR3 (*140, 172, 173*).

Several lines of evidence indicate that CNP/NPR-B signaling is an important regulator of skeletal growth. CNP-overexpressing mice exhibit excessive growth (*140*), whereas defects of the Nppc (*143*) or Npr2 (*139*) gene lead to impairment of skeletal development. In humans, biallelic loss-of-function mutations in NPR2 cause acromesomelic dysplasia, Maroteaux type (AMDM; MIM# 602875). This autosomal recessive skeletal dysplasia is characterized by dwarfism and short limbs (*151*). On the other hand, overproduction of CNP due to a chromosomal translocation has been reported in association with a skeletal dysplasia characterized by tall stature (*174, 175*). In addition, gain-of-function mutations of NPR2 have been identified in several families and are associated with an overgrowth disorder with only mild skeletal features (*142, 176-178*).

Interestingly, in the first report of biallelic NPR2 mutations causing AMDM, parents of patients with AMDM (obligate heterozygotes) were noted to be shorter than expected for their population of origin (*151*), although these individuals came from a wide range of geographic and ethnic backgrounds, which complicated the interpretation of these findings. Another study that evaluated a single family with an AMDM proband showed that the heterozygous carriers had a mean height 1.4 SD lower than their non-carrier family members (*179*). In this single family study, the proband's parents share a common ancestor, so it is possible that the heterozygous carriers share some other mutation causing short stature, and the level of evidence of a heterozygous effect was limited by the size of the family. Based on these two studies, it is presumed that heterozygous NPR2 loss-of-function mutations can mildly impair long bone growth. It has further been hypothesized that one person in 30 with idiopathic short stature (ISS) will carry a NPR2 mutation (*151, 179*).

Recent studies searched for heterozygous NPR2 mutations in cohorts with ISS (Table 1). One study of 47 independent Brazilian patients identified heterozygous NPR2 mutations in 6% of patients (*180*). Another study on 101 unrelated Japanese patients with short stature identified

heterozygous NPR2 mutations in 2% of patients (*168*). Although providing observational data consistent with the hypothesis that a monoallelic NPR2 mutation could cause short stature, these studies did not include controls without short stature, and were based on a relatively small number of patients. Hence, the hypothesis that NPR2 haploinsufficiency leads to short stature has not been rigorously verified. Analyses of larger cohorts, including controls, are needed to more clearly define the role of heterozygous NPR2 defects in patients with ISS.

RESULTS

Discovery of NPR2 variants in patients with short stature and controls using pooled sequencing

We selected 192 patients with short stature (more than 2 SD below the mean for age and sex) and 192 controls of matching ancestry from the middle of the Framingham Heart Study height distribution (height z scores between –0.7 and +0.7). Characteristics of the subjects were described previously (*181*); 104 subjects fit strict criteria for ISS with no evidence of GH deficiency, significant medical comorbidity, developmental delay, or suspected syndromic cause for their short stature. Pooled targeted sequencing of the exons of 1,077 candidate genes was performed (*181*). We detected 11 variants in NPR2. Of these, two were synonymous SNPs found in multiple patients and controls, and two were synonymous variants found only in patients. We focused on the seven potential loss-of-function variants, which included one splice site and six missense variants, all found in patients only (Table 2). These seven variants were all validated via traditional Sanger sequencing and confirmed to be heterozygous in each individual carrier.

Family analyses and clinical phenotypes

The splice site mutation is c.1352-1G>A in a highly conserved base pair in the acceptor splice site at the 5' end of exon 7, carried in a single patient (Patient 1, Table 2). Sanger sequencing of the proband, his parents, and a brother confirmed that the variant is found in the patient but not in his mother, father, or brother. These results were confirmed by a second round of sequencing, and paternity was confirmed by SNP genotyping. There was no family history of short stature (Fig. 1), consistent with the hypothesis that the de novo variant in NPR2 is contributing to short stature in this patient.

We also detected six missense variants in NPR2; of these, four were private variants not found in the public databases (Patients 2–5, Table 2). Sequencing of relatives demonstrated that three of these novel variants segregated with the short stature phenotype (Patients 2–4, Fig. 1). The mother of Patient 5, who did not have short stature, did not carry the NPR2 variant, but the father's DNA was not available to further confirm the segregation. Of note, one of the three segregating variants (Patient 2) was found in a male patient who was also found to carry a known TRPV4 mutation (c.1858G>A (p.V620I)) previously reported as causal for brachyolmia type 3 (*182*). The patient carries a clinical diagnosis of brachyolmia and features consistent with this disease, including platyspondyly of the cervical spine. We previously reported the presence of this likely pathogenic variant in this patient (*181*). The NPR2 variant was present in the patient's mother, who does not carry the TRPV4 variant, and in two sisters, the elder of which also carries

the TRPV4 variant. The mother and both sisters had short stature with height SDS scores below –2.5, and the sister carrying both variants had a height SDS score of –3.1. Notably the patient's father is deceased but also was reported to have had short stature (–3.1 SDS) and presumably carried the TRPV4 variant. Thus, this patient and one of his sisters inherited the NPR2 variant from his mother and the TRPV4 variant from his father, presumably resulting in severe short stature with skeletal dysplasia.

We also detected two rare missense variants present in the public databases (Patients 6–7). Neither of these variants has been reported to be pathogenic, and both are reported to be relatively rare (minor allele frequency 0.02% and 0.16%). The mother of Patient 6, who also had short stature, did not carry the NPR2 variant, but DNA was not available from the sibling or father for further segregation analysis. Patient 7 was adopted from China, so the family history of short stature was unknown and testing for segregation of the variant was not possible.

Discovery of NPR2 variants in one additional clinical short stature cohort

To further refine the estimate of the fraction of ISS individuals with functional NPR2 variants, we screened for rare nonsynonymous NPR2 variants in a second short stature cohort (n = 216) from the Lilly GeNeSIS Study and a number of pediatric endocrinology clinics. Patients were diagnosed by the treating provider with ISS and had height more than 2 SD below the mean for age. The exons and intron/exon boundaries of the NPR2 genewere sequenced using Sanger sequencing.

Four nonsynonymous variants in the coding region were identified, one nonsense and three missense variants (Table 2). One of the missense variants (rs180950551: c.1802G>C (p.R601P)) was seen in three separate patients. An in silico analysis suggested that one variant (c.316G>T(p.A106S)) is benign and the other two (rs180950551: c.1802G>C (p.R601P) and rs114115939: c.1517G>A (p.R506H)) are probably damaging.

Screening for NPR2 mutations in population-based cohorts of individuals from the extremes of the height distribution

We then went on to screen for rare nonsynonymous NPR2 variants in two additional cohorts. The first cohort of individuals (n = 272) was selected from the extremes (<1st percentile or >99th percentile) of height distribution from four FINRISK surveys (~33,000 samples in total). Pooled targeted sequencing of the exons of 1,077 candidate genes was performed. We detected three variants in NPR2. Of these variants, one was a common synonymous SNP (observed in the

short stature patients and FHS controls as well), which we did not pursue further. The other two were missense variants, which we validated by genotyping and confirmed to be heterozygous in tall extremes only (Table 3). Neither variant was found in the public databases. An in silico analysis suggested that one mutation is benign (c.739A>G (p.N247D)) and the other is probably damaging (c.1685G>A (p.R562Q)).

The second cohort of individuals (n = 1,000) was taken from the extremes (<1.25th percentile or >98.75th percentile) of height distribution from the Estonian Biobank (~52,000 samples in total). Pooled targeted sequencing of the exons of four candidate genes was performed. As before, we did not attempt to validate or further evaluate the potential synonymous or intronic variants. One missense variant (c.739A>G (p.N247D)), previously identified in one FINRISK tall extreme sample, was observed in both tall extreme and short extreme samples. The remaining three missense variants (Table 3) were each found in single short individuals. These allelic variants were not found in the public databases. An in silico analysis suggested that the three missense mutations are possibly damaging (c.2449G>A (p.E817K)), benign (c.2338G>A (p.G780R)), and probably damaging (c.1982C>A (p.T661K)), respectively.

Functional characterization of NPR2 variants

Overall, across four cohorts, we observed and validated 16 NPR2 nonsynonymous variants (14 missense, one nonsense, and one splice site), 14 in short stature samples, one in a tall extreme sample, one which was present in both short and tall extreme samples, and none in normal height controls (Table 4). To further examine the functional consequences of the identified NPR2 nonysnonymous variants, we assessed the CNP-dependent cGMP-producing capacities of the 14 missense variants by transfecting HEK 293T cells, which do not normally express NPR2, using at least one of two methods. Relative guanylyl cyclase activities (±SD) of these variants compared with wild type are listed in Table 5. The whole cell lysate method was less sensitive at detecting partial loss of function mutations. The de novo splice variant (c.1352-1G>A) and the nonsense variant (c.2710A>T (p.K904∗)) were not tested and are presumed to be loss of function variants.

To characterize the variants as likely nonpathogenic, variants of unknown significance, and likely pathogenic, we considered both the functional results and the pattern of segregation in the families, where available. For the six missense variants identified in the first short stature patient cohort, three of them segregate with short stature (Patient 2–4). For the variants in Patient 2–4, we observed decreased functional activity in at least one of the assays, strongly suggesting

that these are pathogenic variants. The variant from patient 4 also showed decreased expression by Western blot (Supp. Fig. S1). For the variant in Patient 5, the segregation is unknown and the functional data are negative. The variant in Patient 7, a known rare population variant, also had unchanged functional activity. We conclude that these two variants are unlikely to be pathogenic. The variant in Patient 6, which showed a slight increase in activity in the whole cell lysate assay and decreased activity in the enzyme based assay, was characterized as variant of unknown significance. Interestingly, three of the pathogenic variants were found amongst the 22 cases of familial ISS thus providing a diagnostic yield of 13.6%. However, only a single pathogenic variant, the de novo variant, was found amongst the 77 cases of non-familial ISS leading to a much lower diagnostic yield of 1.3%.

One of three missense variants in the second clinical short stature cohort (rs114115939: c.1517G>A (p.R506H)) decreased NPR-B activity likely secondary to decreased expression of the mutated receptor as seen on Western blot (Supp. Fig. S1). Two out of three missense variants in the Estonian short extremes decreased NPR-B activity (c.2449G>A (p.E817K) and c.1982C>A (p.T661K)). Interestingly, one of two missense variants identified in FINRISK tall extremes showed increased NPR-B activity in both assays (c.1685G>A (p.R562Q)), strongly suggesting this is a gain of function variant contributing to the individuals' tall stature. The second variant, which showed increased NPR-B activity only in the whole cell lysate assay, was also observed in Estonian short extreme samples, making it even less likely to be pathogenic.

Verifying the role of heterozygous functional NPR2 variants in ISS individuals

To test formally whether there are more loss of function NPR2 variants in short stature individuals than in controls without short stature, we combined observations from the three cohorts that have control samples (in other words, excluding the second clinical short stature cohort), considering validated variants seen either only in cases or only in controls. In total, there are six likely loss-of-function mutations (five missense and one splice site) based on segregation and functional evidence, all observed in short samples, and one gain-of-function mutation in tall samples. Assuming that all variants are equally likely to occur in short stature samples and tall extreme samples (or control samples of normal height) under the null hypothesis, this observation gives a P value of 0.008 (one-tailed test, p value is the probability of the observed outcome, i.e., 6:0 plus 0:1 and all more extreme). The estimated prevalence of loss of function NPR2 variants in ISS individuals ranged from 1/26 to 0, and no variants were observed in the cohort of 136 short individuals from Finland (Table 6).

DISCUSSION

To explore the role of NPR2 variation in short stature,we screened for nonsynonymous NPR2 variants in four different cohorts (Table 4). Familial segregation analyses in the short stature patient cohort supported the hypothesis that rare heterozygous NPR2 loss of function variants contribute strongly to short stature in individuals carrying these variants. We also identified rare nonsynonymous NPR2 variants in three additional cohorts, where family data are not available. Functional studies of the NPR2 missense variants identified eight loss-of-function mutations in short stature samples and one gain-of-function mutation in tall stature samples. The frequencies of heterozygous mutation carriers in ISS individuals varied across cohorts from 1/26 to 0, and no variants were observed in the short individuals from Finland. This variability may be due to different ancestries, variable sample selection criteria, and statistical fluctuation. Of note, for the second short stature cohort, coverage was not 100% for 5 out of 22 exons and exon 3 was not evaluated. This can reduce the observed frequency of allelic variants found in this group of patients.

In contrast with homozygous mutations in NPR2, which produces a severe short stature and body disproportion, heterozygous mutations in NPR2 seem to be associated with mild and variable growth impairment without a distinct skeletal phenotype. In our studies, the severity of short stature, body proportions, and presence of nonspecific skeletal abnormalities varied across individuals (Supp. Table S1), consistent with previous observations (*179, 180*). This variability is likely due to differences in the nature of NPR2 mutations carried by the individuals, as well as variable expressivity. Data was available on GH response in three of our patients with pathogenic NPR2 variants and response was quite variable (Supp. Figs. S2–S4).

Previously, a study of 47 Brazilian patients identified heterozygous NPR2 mutations in 6% of patients (*180*), whereas another study on 101 short stature Japanese patients identified mutations in 2% of patients (*168*). Functional analyses were performed in both studies to evaluate the pathogenicity and elucidate the molecular mechanisms of the identified mutations. However, both studies included small numbers of patients and lacked the controls needed to formally show an enrichment of loss of function variants in ISS patients. Our study, including much larger cohorts, controls, family data, and functional analyses, is a more comprehensive assessment of heterozygous mutations in NPR2 as a potential cause of growth impairment in ISS patients.

Our study does show that different methods of analyzing the function of NPR2 variants can produce different results. The whole cell lysate method under the conditions specified is less sensitive at detecting partial loss of function mutations compared to a more rigorous enzyme

based assay conducted on membrane fractions of transfected cells using known concentrations of substrate. However, the enzyme based assay is performed in crude membranes from broken cell preparations and cannot evaluate the ability of the mutations to affect the concentrations of the receptors that are properly targeted to the cell surface. Therefore, mutations that reduce activity in the enzyme assay are likely to be damaging but this assay may not detect mutations that reduce activity due to inappropriate plasma membrane targeting or mutations that affect receptor degradation.

The functional assays used do have limitations. Although the rat NPR2 construct is >98% identical to human NPR2 and identical at each of the amino acids mutated in this study, there remains the possibility that non-identical residues located near mutant residues could affect protein function. In addition, the assays do not provide mechanistic data for why these heterozygous mutations reduced NPR2 function. Neither assay is able to differentiate between loss-of-function due to haploinsuffiency and loss of function due to dominant negative effect of the mutant allele.

The frequency of heterozygous carriers of AMDM mutations was previously estimated to be about 0.14% (*179*). In the NHLBI Exome Sequencing Project, the cumulative frequency of all nonsynonymous NPR2 variants is approximately 0.4% in ~4,000 European American samples. The discrepancy between these two allele frequencies highlights the importance of functional studies, which can help distinguish neutral background variants from true loss of function variants. In our study, out of 14 rare nonsynonymous NPR2 variants that were functionally tested, only six showed decreased functional activity. Although the variants with no in vitro functional consequences may still contribute to short stature, our in vitro findings are consistent with the threefold higher frequency of nonsynonymous variants in the population database compared with expectation based on estimated AMDM carrier rates.

Despite the rarity of AMDM mutations (and nonsynonymous NPR2 variants in general), these loss-of-function alleles likely have relatively large effect sizes (loss-of-function alleles were previously estimated to reduce height by _1.8 SD (*179*). Assuming an effect size of 1.8 SD and a cumulative population allele frequency of 0.14%, these maximum-likelihood estimates predict that ~2.6% of individuals with height below –2 SD would have a loss of function NPR2 variant and that ~4.2% of individuals with height below the 1st percentile would carry such a variant. These estimates are somewhat higher than our empirical findings in the two clinical short stature cohorts combined (1.9%), and also substantially higher than our estimates from the Finnish and Estonia cohorts (0.3% of individuals below the ~1st percentile), suggesting that the effect size or

the population allele frequencies previously estimated for loss-of-function NPR2 variants are inflated. The higher reported rates of NPR2 mutations in previous studies (*168, 180*) could also be due to population differences, or more stringent selection criteria in earlier studies that made it more likely to ascertain individuals carrying NPR2 loss of function mutations (such as high rates of familial short stature). Interestingly, we also identified one gain-of-function NPR2 variant in tall extremes of FINRISK height distribution, suggesting NPR2 gain of function may be a more common cause of tall stature than previously recognized.

AMDM patients have been posited to have an abnormality in the GH/IGF-1 system, characterized by low insulin-like growth factor 1 (IGF-1; MIM# 147440) levels, high GH levels, and lack of a response to GH treatment (*179*). However, IGF-1 levels were not low in either the carriers of AMDM mutations (*168, 179, 180*) or in the subjects in our cohort with loss of function mutations for whom data were available. Larger prospective studies are needed to determine whether heterozygous carriers of clearly pathogenic NPR2 variants will respond to growth hormone. Regardless, NPR2 loss-of-function variants likely account for approximately 0.4%–4% of all patients with short stature (height < –2 SD), and should be considered in the diagnostic evaluation of patients presenting with ISS. Interestingly, we identified NPR2 loss-of-function variants in 13.6% of familial cases, suggesting that such variants will provide a frequent explanation for patients with familial ISS.

EXPERIMENTAL PROCEDURES

Subjects

Short stature patient cohort and Framingham Heart Study controls

Patients (192) with short stature (height more than 2 SD below the mean for age and sex) (*183*) but without defined etiology, were recruited from the endocrinology and genetics clinics at Boston Children's Hospital. Subjects (104) fit strict criteria for ISS with no evidence of growth hormone (GH) deficiency, significant medical comorbidity, developmental delay, or suspected syndromic cause for their short stature. Of these 104 patients, height data were available for both parents in 99 cases. 22 of these 99 subjects (22.2%) had at least one parent with a height below –2 SD and were defined as having familial ISS. In addition, 192 control subjects were chosen from the middle of the Framingham Heart Study (FHS) height distribution (height z scores between –0.7 and +0.7). More detailed description of the cohort is reported in Wang et al. (*181*).

Second short stature patient cohort

Patients (216) were taken from the Genetics and Neuroendocrinology of Short Stature International Study (GeNeSIS), sponsored by Eli Lilly andCompany and various pediatric endocrinology clinics in Jacksonville, FL and Santiago, Chili. Patients were diagnosed by the treating provider with ISS and had height < –2 SD below the mean for age and sex.

FINRISK height extreme cohort

Subjects (272) were chosen from the extremes (<1st percentile or >99th percentile) of the FINRISK surveys (FINRISK 1992, FINRISK 1997, FINRISK 2002, FINRISK 2007) height distribution. The FINRISK cohorts comprise the respondents of representative, cross-sectional population surveys that are carried out every 5 years since 1972, to assess the risk factors of chronic diseases and health behavior in the working age population, in five large study areas of Finland (*184*).

Estonian Biobank height extreme cohort

Subjects (1000) were selected from the extremes (<1.25th percentile or >98.75th percentile) of the Estonian Biobank height distribution. The Estonian Biobank cohort is a volunteer-based sample of the Estonian resident adult population (age ~18 years). The age, sex, and geographical distribution closely reflect those of the Estonian adult population and encompass close to 5% of the entire adult population of Estonia (*185*).

Pooled Sequencing Protocol

For the first short stature cohort and the FINRISK and Estonian cohorts, DNA samples from multiple subjects were pooled for DNA sequencing using previously described methods available at the Broad Institute (*186*). To identify variants present only in a single individual (hereafter referred to as singleton variants), we applied a simple overlapping pooling design as described previously (*181*).

Sequencing was performed on the Illumina HiSeq platform. Variant calling was performed using a likelihood-based calling strategy we developed as described previously (*181*). Variants were annotated for functional effect using SnpEff 2.0.5 (http://snpeff.sourceforge.net/). The reference sequence used for numbering nucleotide change and amino acid change was NM 003995.3 and ENSP00000341083. Nucleotide numbering uses +1 as the A of the ATG translation initiation codon in the reference sequence, with the initiation codon as codon 1. Variant allele frequency data were obtained from two publicly available databases: 1) Integrated variant call set of 1000 Genomes samples (*187*) [May 2013 release]; 2) National Heart, Lung, and Blood Institute Exome Variant Server (NationalHeart, Lung). Maximal allele frequency from the two sources was used. Novel variants are those not observed in either of these databases. Confirmation of variants found in NPR2 through pooled sequencing was done via Sanger sequencing or Sequenom MassArray genotyping. Each variant was sequenced in the proband and in all related family members for whom DNA samples were provided. Sanger sequencing of NPR2 was performed in the second short stature cohort. For details of all sequencing protocols, see the Supp. Methods. The variants reported have been submitted to http://www.lovd.nl/NPR2.

In silico prediction of mutation effects

To identify the potential effects of sequence variants identified in NPR2 on protein function or structure, the wild-type and variant sequences were assessed using PolyPhen-2 (software version 2.2.2, http://genetics.bwh.harvard.edu/pph2) [Ramensky et al., 2002]. The options used were: Classifiermodel [HumDiv], Genome aseembly [GRCh37/hg19], Transcripts [CCDS], Annotations [All].

Assaying wild-type and mutant NPR2 activity

Missense mutations in NPR2 were generated by site-directed mutagenesis kit (Agilent Technologies) using the wild-type rat NPR2 expression construct pRK5-NPR-B. Activity in HEK

293T cells was measured by at least one of two assays, one on whole cell lysate and another enzyme based assay done on membrane fractions of transfected cells, as described elsewhere (*114, 188*). For details of the assay, see the Supp. Methods. Variants showing loss of activity in vitro in either assay were characterized as loss-of-function. Variants showing normal in vitro activity in the whole cell lysate assay were tested in the more sensitive enzyme based assay. Variants showing clear increases in activity in both assays were characterized as gain-of-function.

SUPPLEMENTAL MATERIALS AND METHODS

Sequencing protocol

False-negative rates of pooled sequencing

As described in Wang, et al. (*181*), we estimated the false-negative rate of pooled sequencing by comparing pooling data with data from exome sequencing previously performed in 6 of the short stature subjects. False negative results were those observed in exome data but not in either of the 2 relevant pools. The estimated overall false-negative rate was 0.1%.

Short stature patient cohort

The samples from short stature subjects and control samples were each arranged into a 14 . 14 matrix of 28 pools, with 13 to 14 samples in each pool. The coding regions of *NPR2* were sequenced along with ~1000 height candidate genes (*181*). The targeted exons of the candidate genes were enriched using a custom Agilent SureSelect hybrid selection system. The mean target coverage of *NPR2* is 297 reads per pool, resulting in 21 reads per subject in a pool of 14 subjects or 42 total reads per subject, as each subject is present in 2 pools. Coverage was 100% for all 22 exons; 97.5% the targeted regions had at least 10 reads per subject.

Second short stature cohort

The exons of the NPR2 gene in each of the samples were sequenced using Sanger sequencing. Sequencing primers are available upon request. Coverage was 100% in at least one direction in 17 of 22 exons. No coverage was obtained of exon 3, even after resequencing with new primers.

FINRISK height extreme cohort

The FINRISK DNA samples were whole-genome amplified. The short extreme subjects and the tall extreme subjects were each arranged into a 12 ´12 matrix of 24 pools, with 11-12 samples in each pool. The coding region of *NPR2* was enriched as described above for short stature patient cohort. The mean target coverage of *NPR2* is 377 reads per pool, resulting in 31 reads per subject in a pool of 12 subjects or 62 total reads per subject. Coverage was 100% for all 22 exons; 94.3% the targeted regions had at least 10 reads per subject.

Estonian Biobank height extreme cohort

The samples from short extreme subjects and tall extreme subjects were each arranged into a 24 ´ _24 matrix of 48 pools, with 19-24 samples in each pool. The coding regions of *NPR2* were

sequenced along with three other genes. The targeted exons of all four genes were enriched using PCR-based fluidigm Access Array system. The mean target coverage of *NPR2* is 2735 reads per pool, resulting in 114 reads per subject in a pool of 24 subjects or 228 total reads per subject. Coverage was 100% for all 22 exons; 100% the targeted regions had at least 10 reads per subject.

Assaying wild-type and mutant NPR2 activity

The mutations from the first and second short stature cohorts as well as the FINRISK cohort were tested as follows: HEK 293T cells were grown to ~60% confluency on poly-D-lysine coated plates and then transfected overnight with 3-5 µg of plasmid DNA using the Hepes calcium phosphate method as previously described. Transfection efficiency was ~50-60% as estimated by the fluorescence of cells transfected with a plasmid expressing GFP compared to control cells. Cells were incubated with serum free medium for 4 hours then cells were washed with phosphate buffered saline, scraped off the plate into 600µl/plate of PIB, sonicated 3 times for 1 second, centrifuged for 15 minutes at 20,000 x g to pellet the membranes. The supernatant was aspirated and membranes were then resuspended in 400µl/plate of PIB. The resulting membranes were then centrifuged again for 15 minutes at 20,000 x g. The supernatant was aspirated and membranes were then resuspended in 400µl/plate of PIB. Guanylyl cyclase assays were performed at 37ºC in a reaction mixture containing 20µl activation mix, and 60µl cocktail buffer (0.1mM GTP, 25mM Hepes pH 7.4, 50mM NaCl, 0.5mM isobutylmethyl xanthine (IBMX), 1mM EDTA, 0.5µM microcystin, 0.1% BSA). Activation mixes yielded reaction conditions of 1mM ATP and 5mM MgCl2 (Basal), 1mM ATP, 50nM CNP and 5mM MgCl2 (50nM CNP), 1mM ATP, 1µM CNP, and 5mM MgCl2 (1µM CNP), or 1% Triton X-100 and 5mM MnCl2 (Mn/Triton). Reactions were stopped after 3 minutes with 0.4ml of cold 50mM sodium acetate buffer with 5mM EDTA. Cyclic GMP concentrations were determined by radioimmunoassay as described before (*114*).

The mutations from the first short stature cohort, FINRISK cohort and Estonian biobank cohort were tested as follows: 1 x 10^{-5} cells were seeded in 12-well plates in Dulbecco's modified Eagle medium (DMEM) with 10% fetal bovine serum (FBS). The cells were transfected 24 hrs later with 0.5 mg of expression construct with Fugene 6 (Promega). 24 hours after transfection, cells were starved for 24 h prior to CNP exposure (48 h after transfection). Cells were treated with 0.5mM IBMX (Sigma) for 10 minutes, then exposed to 1 x 10^{-7} M CNP (Bachem) for 10 min. Signaling was terminated by aspirating the CNP-containing media and adding 0.1N HCL to the cells. The supernatant was collected and the amount of cGMP was measured by use of a

cGMP assay kit (Cayman Chemical). Each construct was transfected a minimum of three times and each supernatant was assayed in triplicate. Statistical analysis comparing mutant *NPR2* to wild type was done using student's t-test.

Western Blotting

Fifty mg of membrane fractions described above were fractionated on an 8% polyacrylamide gel and then blotted to an Immobilon membrane for 1 h at 100 V at 4ºC. The membrane was rinsed in Tris buffered saline with 0.1% Tween detergent (TBST), then incubated in 1:1 mixture of phosphate buffered saline with Odyssey blocking buffer for 1 h. The membrane was then incubated for 1 h with the rabbit polyclonal antibody to the last 10 C-terminal residues of NPR2 in blocking buffer at a dilution of 1/20,000. The membrane was then washed with TBST 3 times for 5 minutes and incubated at a dilution of 1/20,000 with a goat anti-rabbit IR dye 680-conjugated antibody to detect the NPR2-primary antibody complex. The results were visualized on a Li-Cor instrument.

FIGURES AND TABLES

Figure 1. Segregation of identified NPR2 nonsynonymous variants in affected families. Numbers below the individuals denote the height z scores. + indicates family members who also carry the TRPV4 mutation causal of brachyolmia. ˆ indicates that this family member was treated with growth hormone therapy prior to this height measurement and had a nadir height of −2.8 SDS. ∗ indicates that the height was estimated by a family member. All other values were measured. Individuals with short stature are indicated as black circles (females) or squares (males). The arrow points to the affected proband in each family.

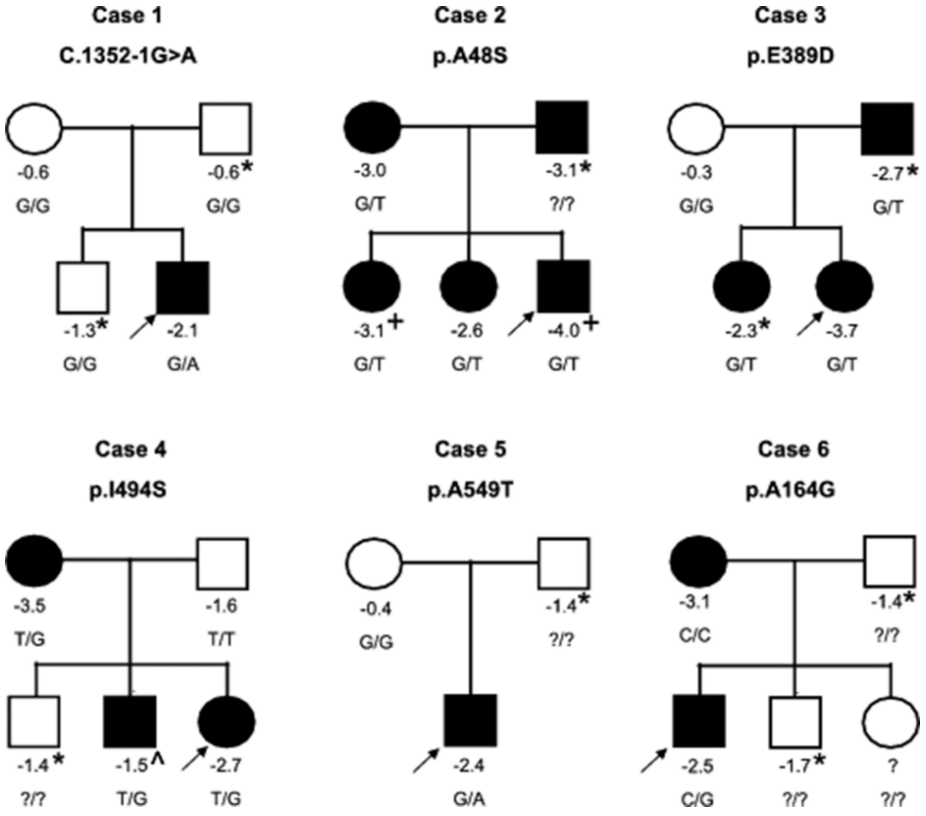

Table 1. Summary of recent studies searching for heterozygous *NPR2* mutations in cohorts with ISS.

Cohort	# of functional *NPR2* variants	# of ISS individuals	Fraction of ISS individuals with functional *NPR2* variants	Reference
Brazilian patients with ISS	3	47	6%	Vasques *et. al.* (2013)
Japanese patients with short stature	2	101	2%	Amano *et. al.* (2014)

Table 2. *NPR2* potentially nonsynonymous variants in short stature patients.

Abbreviations: F, female; M, male; GH, growth hormone; IGF-1, insulin-like growth factor; yr, years old; N/A, not available. Normal age and gender specific ranges for IGF-1 are provided in parentheses. GenBank reference sequence used for *NPR2* is NM_003995.3.

Cohort	Subject	Sex	Variant	Minor allele frequency	PolyPhen2 prediction	Nadir height SDS	Current height SDS	GH therapy	IGF-1 level (ng/ml)
Short stature patient cohort	Patient 1	M	c.1352-1G>A	Novel	N/A	-3.14	-2.15	Yes	53 @ 7 yr (44 - 211)
	Patient 2	M	c.142G>T (p. A48S) (brachyloma with known TRP4 variant)	Novel	1.00	-4.15	-3.91	No	NA
	Patient 3	F	c.1167G>T (p.E389D)	Novel	0.00	-3.84	-3.14	Yes	53 @ 6 yr (47 - 217)
	Patient 4	F	c.1481T>G (p.I494S)	Novel	0.997	-3.57	-1.79	Yes	115 @ 6 yr (47 - 217)
	Patient 5	M	c.1645G>A (p.A549T)	Novel	0.988	-3.88	-2.70	Yes	34 @ 4 yr (25 - 157)
	Patient 6	M	rs62637657: c.491C>G (p.A164G)	0.02%	0.065	-2.53	-2.16	IGF-1 therapy	72 @ 9 yr (61 - 252)
	Patient 7	F	rs114147262: c.2359C>T (p.R787W)	0.16%	0.998	-2.92	-2.41	No	61 @ 7 yr (55 - 238)
Second short stature cohort	Patient	NA	c.316G>T (p.A106S)	Novel	0.189	N/A	N/A	N/A	N/A
	3 Patients	NA	rs180950551: c.1802G>C (p.R601P)	0.02%	1.00	N/A	N/A	N/A	N/A
	Patient	NA	c.2710A>T (p.K904*)	Novel	N/A	N/A	N/A	N/A	N/A
	Patient	NA	rs114115939: c.1517G>A (p.R506H)	0.06%	0.959	N/A	N/A	N/A	N/A

Table 3. *NPR2* potentially nonsynonymous variants in FINRISK and Estonian Biobank height extreme samples.

GenBank reference sequence used for *NPR2* is NM_003995.3.

Variant	Observation	Minor allele frequency	PolyPhen2 prediction
c.739A>G (p.N247D)	FINRISK tall extreme (also observed in Estonian tall extreme and short extreme)	Novel	0.002
c.1685G>A (p.R562Q)	FINRISK tall extreme	Novel	0.995
c.2449G>A (p.E817K)	Estonain short extreme	Novel	0.609
c.2338G>A (p.G780R)	Estonain short extreme	Novel	0.013
c.1982C>A (p.T661K)	Estonain short extreme	Novel	0.999

Table 4. Observation of *NPR2* nonsynonymous variants in four cohorts.

Cohort	Observation of nonsynonymous variants	Note
Short Stature patients and FHS controls	7 variants in 192 short stature patients	Patient 1: de novo mutation
	0 variants in 192 FHS controls	Patients 2-4: all heterozygous relatives had short stature (height SDS < -2)
		Patient 5: variant not present in average height mother and father's DNA unavailable
		Patient 6: variant not present in short mother and father's DNA unavailable
		Patient 7: no family data available
Second short stature cohort	4 variants in 216 short stature patients	No control samples
Extremes of FINRISK height distribution	0 variants in 136 short extremes	No family data available
	2 variants in 136 tall extremes	
Extremes of Estonian Biobank height distribution	3 variants in 500 short extremes	No family data available
	0 variants in 500 tall extremes	

Table 5. Functional characterization of *NPR2* nonsynonymous variants in three cohorts.

* $P < 0.05$. GenBank reference sequence used for *NPR2* is NM_003995.3.

Variant	Observation	Minor allele frequency	Segregation within family	Relative guanylyl cyclase activity % (±SD) - enzyme assay with 1μM CNP	Relative guanylyl cyclase activities % (±SD) - whole cell lysate
c.1352-1G>A	Patient 1	Novel	De novo	N/A	N/A
c.142G>T (p. A48S)	Patient 2	Novel	Yes	36.6 (14.9) *	93.5 (15.4)
c.1167G>T (p.E389D)	Patient 3	Novel	Yes	57.0 (12.0) *	108.5 (24.6)
c.1481T>G (p.I494S)	Patient 4	Novel	Yes	< 6 *	54.3 (8.6) *
c.1645G>A (p.A549T)	Patient 5	Novel	Unknown	68.7 (26.9)	111.2 (9.6)
rs62637657: c.491C>G (p.A164G)	Patient 6	0.02%	No	25.9 (10.3) *	130.6 (15.5) *
rs114147262: c.2359C>T (p.R787W)	Patient 7	0.16%	N/A	62.8 (36.6)	90.9 (14.0)
c.316G>T (p.A106S)	Patient	Novel	N/A	83.9 (32.5)	N/A
rs180950551: c.1802G>C (p.R601P)	Patient	0.02%	N/A	64.5 (12.9)	N/A
c.2710A>T (p.K904*)	Patient	Novel	N/A	N/A	N/A
rs114115939: c.1517G>A (p.R506H)	Patient	0.06%	N/A	< 6 *	N/A
c.739A>G (p.N247D)	FINRISK tall extreme (also observed in Estonian tall extreme and short extreme)	Novel	N/A	69.1 (37.3)	246.9 (66.5) *
c.1685G>A (p.R562Q)	FINRISK tall extreme	Novel	N/A	145.7 (31.6) *	711.8 (238.2) *
c.2449G>A (p.E817K)	Estonain short extreme	Novel	N/A	N/A	31.1 (0.3) *
c.2338G>A (p.G780R)	Estonain short extreme	Novel	N/A	N/A	98.3 (11.9)
c.1982C>A (p.T661K)	Estonain short extreme	Novel	N/A	N/A	65.7 (19.1) *

Table 6. Fraction of ISS individuals with clearly functional *NPR2* variants.

Cohort	# of functional *NPR2* variants	# of ISS individuals	Fraction of ISS individuals with functional *NPR2* variants
Short stature patients and FHS controls	4	104	1/26
Second short stature cohort	2	216	1/108
Extremes of FINRISK height distribution	0	136	0
Extremes of Estonian Biobank height distribution	2	500	1/250

Supplementary Figure S1. Two Western immunoblots using a polyclonal antibody to rat NPR2 showing no protein detected from mutants with no functional activity in one assay. A. No protein is seen in membrane fractions obtained from cells transfected with the I494S mutant or GFP negative control. NPR2 is seen in cells transfected with WT NPR2 and a mutant with normal function (A48S). B. No protein is seen in membrane fractions obtained from cells transfected with the R506H mutant or GFP negative control. NPR2 is seen in cells transfected with WT NPR2 and a mutant with normal function (A106S).

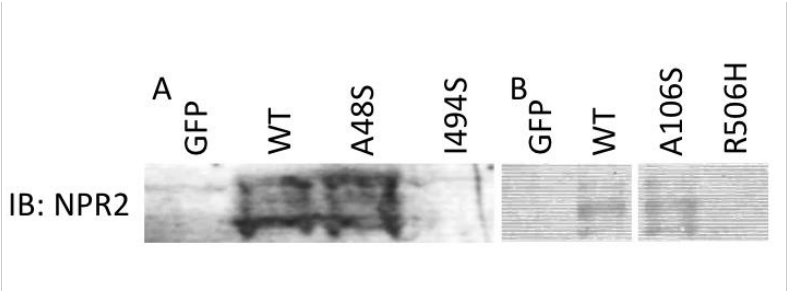

Supplementary Figures S2-S4. Growth charts for the three patients with pathogenic *NPR2* variants who were treated with growth hormone and for whom longitudinal growth data was available.

Supplementary Figure S2. Growth chart for Patient 1.

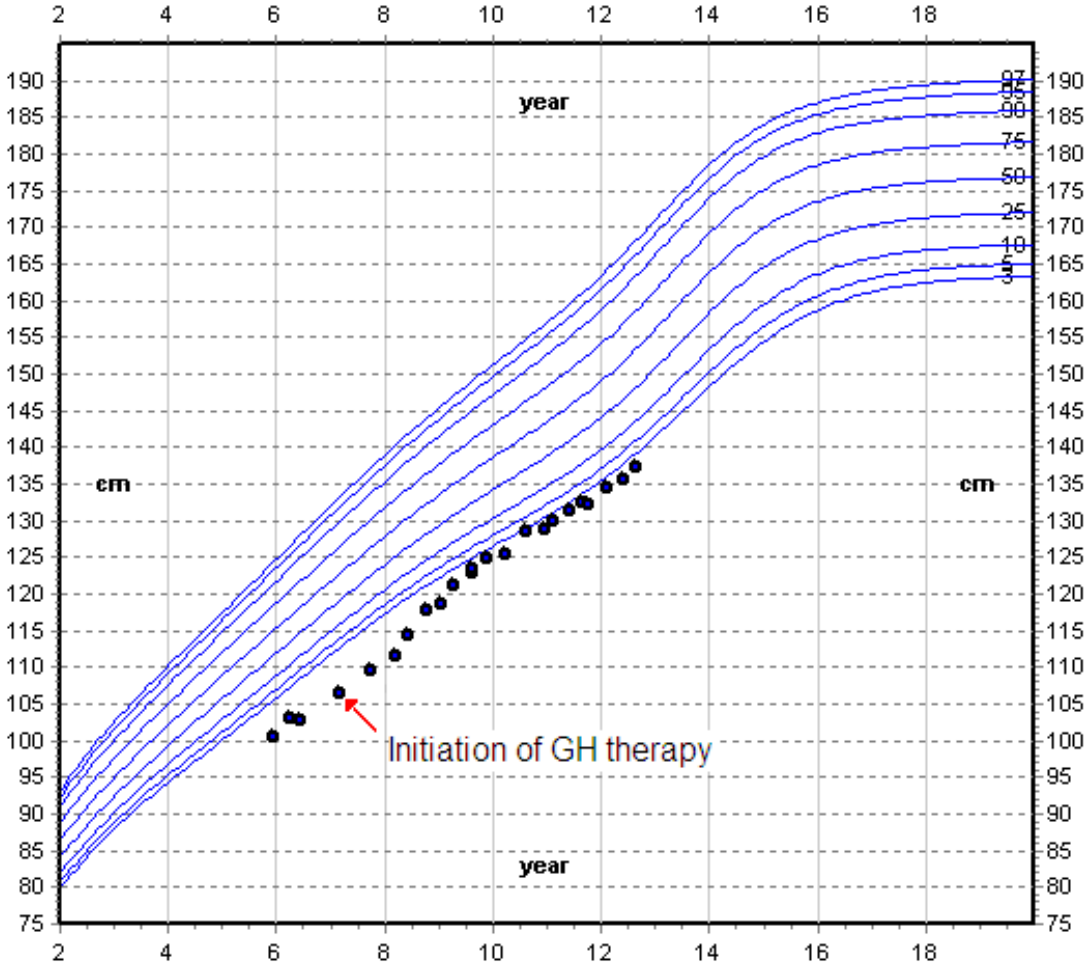

Supplementary Figure S3. Growth chart for Patient 3.

Pubertal suppression was performed with a gonadotropin releasing hormone agonist.

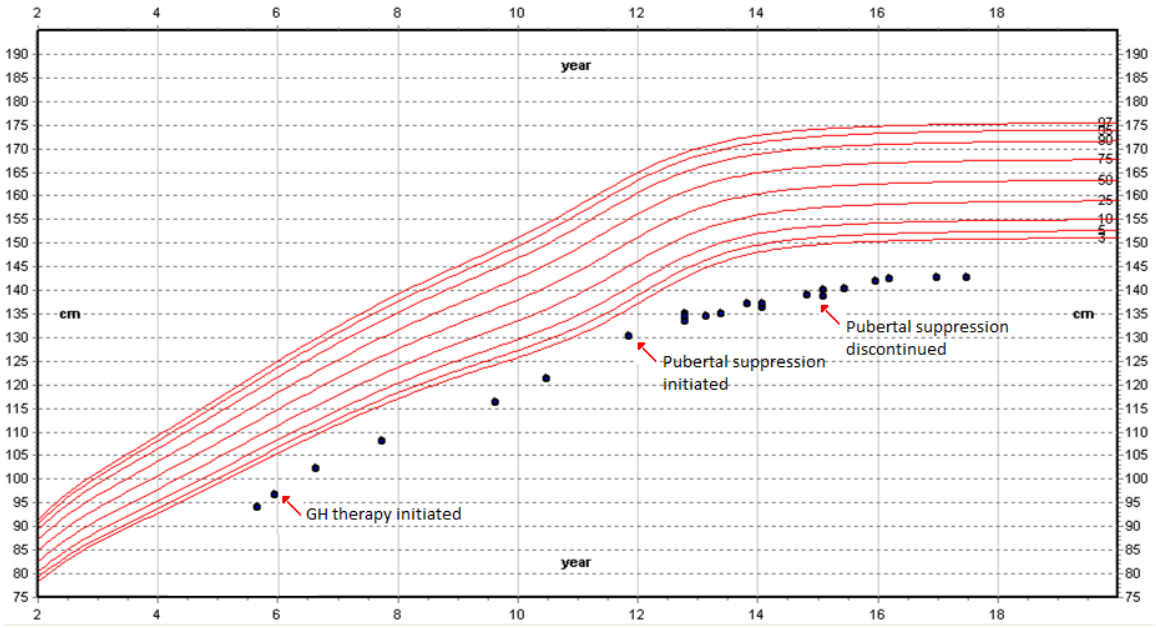

Supplementary Figure S4. Growth chart for Patient 4.

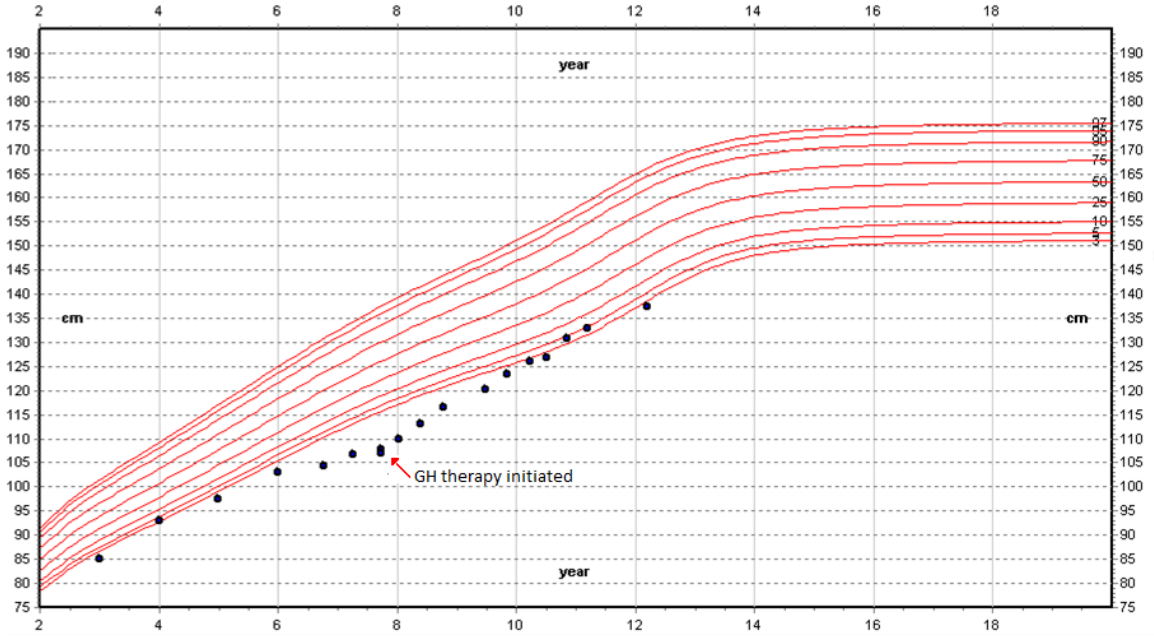

Supplementary Table S1. Additional clinical features of patients from short stature cohort #1.

SGA: small for gestational age.

Subject	Sex	Variant	SGA	Clinodactyly	Upper/ Lower Ratio
Patient 1	M	c.1352-1G>A	No	No	1.08 >+2 SDS
Patient 2	M	c.142G>T; p.A48S (brachyolmia with known TRPV4 variant)	No	Yes	1.17 >+2 SDS
Patient 3	F	c.1167G>T; p.E389D	Yes	No	0.91 -1 SDS
Patient 4	F	c.1481T>G; p.I494S	No	No	0.96 0 SDS
Patient 5	M	c.1645G>A; p.A549T	Yes	No	1.02 +1-2 SDS
Patient 6	M	rs62637657: c.491C>G; p.A164G	No	Yes	1.11 >+2 SDS
Patient 7	F	rs114147262: c.2359C>T; p.R787W	N/A	Yes	1.06 >+2 SDS

CHAPTER 5:

Catalytically Active Guanylyl Cyclase B Requires Endoplasmic Reticulum-mediated Glycosylation, and Mutations That Inhibit This Process Cause Dwarfism.

This chapter is a reprint of an original publication with minor alterations, used with permission:

Deborah M. Dickey, **Aaron B. Edmund**, Neil M. Otto, Thomas S. Chaffee, Jerid W. Robinson, and Lincoln R. Potter. Catalytically Active Guanylyl Cyclase B Requires Endoplasmic Reticulum-mediated Glycosylation, and Mutations That Inhibit This Process Cause Dwarfism. *Journal of Biological Chemistry.* (2016) 291(21):11385-93.

Aaron Edmund collected, interpreted, and analyzed data and created Figures 6 and 8 and also contributed to the writing of the manuscript.

SUMMARY

C-type natriuretic peptide activation of guanylyl cyclase B (GC-B), also known as natriuretic peptide receptor B or NPR2, stimulates long bone growth, and missense mutations in GC-B cause dwarfism. Four such mutants (L658F, Y708C, R776W, and G959A) bound 125I-C-type natriuretic peptide on the surface of cells but failed to synthesize cGMP in membrane GC assays. Immunofluorescence microscopy also indicated that the mutant receptors were on the cell surface. All mutant proteins were dephosphorylated and incompletely glycosylated, but dephosphorylation did not explain the inactivation because the mutations inactivated a "constitutively phosphorylated" enzyme. Tunicamycin inhibition of glycosylation in the endoplasmic reticulum or mutation of the N24 glycosylation site decreased GC activity, but neither inhibition of glycosylation in the Golgi by N-acetylglucosaminyltransferase I gene inactivation nor PNGase F deglycosylation of fully processed GC-B reduced GC activity. We conclude that endoplasmic reticulum mediated glycosylation is required for the formation of an active catalytic, but not ligand-binding domain, and that mutations that inhibit this process cause dwarfism.

INTRODUCTION

C-type natriuretic peptide (CNP)2 is a paracrine factor that stimulates long bone growth and axonal path finding and inhibits meiosis in the oocyte (*41, 189, 190*). The biologic signaling receptor for CNP is guanylyl cyclase B (GC-B) (*79, 139, 191*).

GC-B is a homo-oligomer, possibly a dimer, containing a glycosylated extracellular ligand-binding domain, a single membrane-spanning region, and intracellular kinase homology, dimerization, and C-terminal catalytic domains (*192*). Phosphorylation of the region leading into and at the beginning of the kinase homology domain is required for CNP activation of GC-B, and dephosphorylation inactivates the enzyme (*22, 24, 27, 28, 103, 136, 137*).

Homozygous inactivating mutations in GC-B result in acromesomelic dysplasia, type Maroteaux (AMDM) dwarfism (*151, 193-195*), and heterozygous inactivating mutations in GC-B cause non-pathological reductions in stature (*179*). Heterozygous inactivating mutations in GC-B are also associated with short stature observed in Léri-Weill dyschondrosteosis (*196*). Conversely, genetic mutations that increase GC-B activity result in skeletal overgrowth (*142, 176, 177*).

At least 29 unique inactivating missense mutations in GC-B have been identified in humans (*151, 168, 179, 180, 193-195, 197, 198*). These mutations are randomly distributed from the N terminus (P32) to the C terminus (G959A) of the enzyme, consistent with two potential mechanisms. The first involves multiple processes like disruption of CNP or GTP binding to the enzyme. The second more general mechanism involves conformational changes in the structure of GC-B that preclude catalytic domain formation or activation.

Previous investigators reported that 11 of 12 (*197*), two of three (*180, 198*), or one of two (*168*) missense mutations inhibited the transport of GC-B to the cell surface because of defective cellular trafficking and retention in the ER, as indicated by reduced immunofluorescence imaging of GC-B associated with the plasma membrane. Thus, the current model is that AMDM mutations disrupt intracellular trafficking of GC-B.

Here we characterized four intracellular missense AMDM mutations in GC-B. In contrast to previous reports, we found that all mutants were on the cell surface. However, the GC activity of each mutant was severely reduced or abolished. The mutant receptors migrated as incompletely glycosylated species when fractionated by SDS-PAGE, and inhibition of glycosylation in the ER, but not in the Golgi, produced enzymes with similarly reduced catalytic activity.

RESULTS

AMDM Mutants Are Incompletely Processed

Posttranslational processing of four intracellular AMDM causing mutants (L658F, Y708C, R776W, and G959A) was compared with WTGC- B and GC-B-7A, a mutant containing alanine substitutions for the seven known phosphorylation sites (*24*), in reduced SDS gels containing immunoprecipitated receptors from transiently transfected 293T cells. Coomassie staining (Fig. 1, top panel) of WT-GC-B revealed a slower migrating, diffuse species (top band) that is maximally glycosylated and phosphorylated and a second, faster migrating species (bottom band) that is incompletely glycosylated and not phosphorylated. A fainter, fastest migrating form corresponding to the unprocessed polypeptide is visible in some lanes (Fig. 7) (*22, 24*). The upper band was also present in GC-B-7A, indicating that the majority of the migration difference between the two species is not due to changes in phosphorylation. In contrast, the upper band was markedly diminished or undetectable in samples from the AMDM mutants. ProQ Diamond staining, a dye that binds GC-B in a phosphate-dependent manner (*199*), of the same gel indicated that only the slower-migrating, upper species of the WT receptor was phosphorylated (Fig. 1, bottom panel).

The GC-B AMDM Mutants Bind CNP on the Surface of Cells

^{125}I-CNP binding assays were performed on live 293T cells transfected with the individual AMDM mutants, WT-GC-B as a positive control, and GFP as a negative control (Fig. 2, top panel). Low radiation levels in GFP-transfected cells and in GC-B-expressing cells exposed to excess non-radioactive CNP (nonspecific binding) confirmed that the binding was specific for GC-B. All four mutants specifically bound ^{125}I-CNP, consistent with GC-B being on the cell surface. Total ^{125}I-CNP binding to each mutant was variable and less than that observed for the WT receptor, which is expected because the mutants have reduced protein levels because of the lack of the completely processed and phosphorylated upper protein species only seen with WT-GC-B (Fig. 1, top panel). Competition binding assays indicated that the affinity of each mutant for CNP was similar to that of WT-GC-B (Fig. 2, bottom panel). These data indicate that all four mutants are on the cell surface and that glycosylation of GC-B is neither required to bind CNP nor required for GC-B to adopt a conformation capable of binding CNP.

Microscopic Detection Indicated That All Mutants Are on the Cell Surface

To verify that the mutants were on the cell surface, each mutation was introduced into an amino-terminally HA-tagged version of the human GC-B cDNA (*178*) and transiently expressed along with HA-WT-human GC-B in HeLa cells (Fig. 3). GC-B was detected by probing non-permeabilized and permeabilized cells with a monoclonal antibody to the extracellular HA epitope (Fig. 3, green). The plasma membrane was stained with wheat germ agglutinin (Fig. 3, red), and the nucleus was stained with DAPI (Fig. 3, blue). In the non-permeabilized cells (Fig. 3, left panels), no GC-B surface staining was observed on untransfected HeLa cells. However, a clear extracellular signal (Fig. 3, green) was detected for all receptors when probed with an antibody against the N-terminal GC-B HA epitope. Furthermore, the signal for the plasma membrane marker (Fig. 3, red) co-localized with all HA-tagged receptors (Fig. 3, yellow, merged). For cells permeabilized with saponin (Fig. 3, right panels), extracellular staining was more diffuse, and receptor staining was also observed in intracellular nonnuclear regions. Again, receptor staining colocalized with plasma membrane staining (Fig. 3, yellow). However, for the L658F and Y708C mutants, much more cytoplasmic staining was observed in the permeabilized cells than with the WT enzyme or the R776W or G959A mutants. Together, these data verified that all mutants were on the cell surface.

AMDM Mutants Have Severely Reduced Guanylyl Cyclase Activity

The ability of the GC-B mutants to form active catalytic domains was examined in membranes from transfected 293 cells (Fig. 4). GC activity was measured under basal, CNPstimulated, and detergent and manganese-stimulated conditions. The latter condition activates the enzyme independently of NP or phosphorylation and is an excellent indicator of total activated GC-B catalytic domain formation (*24*). CNP increased the activity of WT-GC-B 568-fold over basal levels but only increased the activity of GC-B-G959A 36-fold and completely failed to activate the other three mutants. Triton X-100 and manganese increased WT-GC-B activity 704-fold over basal levels, but the AMDM causing mutant forms of GC-B were activated by detergent to less than 16% of WT levels. In contrast, the mutations had no effect on basal GC activity.

Lack of Phosphorylation Does Not Explain the Inactivity of the AMDM Mutants

Because phosphorylation is required for CNP-dependent activation of GC-B (*24*), we tested whether lack of phosphorylation caused the mutant enzymes to be inactive. If this hypothesis was true, then the mutations should fail to inactivate a “constitutively phosphorylated”

form of the enzyme, known as GC-B-7E, that contains glutamate substitutions for the seven known phosphorylation sites (*27*). Introduction of the AMDM mutations in a plasmid expressing GC-B-7E resulted in incompletely processed enzymes that bind CNP on the cell surface but lack GC activity, as observed when the mutations were examined in the WT phosphorylated form of GC-B (Fig. 5). These data indicate that the AMDM mutation-dependent loss in GC activity is independent of GC-B phosphorylation.

Blocking Glycosylation in the ER Inhibits CNP- and Detergent- stimulated Guanylyl Cyclase Activity

To test the effect of blocking ER mediated glycosylation on GC-B activity, WT-GC-B, GC-B-7E, GC-B-L658F, and GC-B-G959A were transfected in 293T cells in duplicate and incubated with or without tunicamycin, a chemical that inhibits the rate-limiting step of N-linked glycosylation in the ER (*200*). Western blotting indicated that tunicamycin inhibited glycosylation of GC-B at a very early stage because cells treated with the drug only produced the fastest-migrating, unmodified doublet species and lacked the fainter upper most active species denoted by the large arrowhead in Fig. 6B. We have never seen the doublet lower species before but hypothesize that it represents the naked polypeptide chain of GC-B with and without the signal peptide sequence, although we cannot rule out the possibility that it results from palmitoylation (*201*). Consistent with glycosylation being required for the formation of a stimulated catalytic domain, CNP- and detergent-dependent guanylyl cyclase activities of the WT and mutant GC-B enzymes were dramatically reduced by tunicamycin treatment, whereas basal activity was unaffected. The reduction in stimulated activity was much greater for WT-GC-B and GC-B-7E because these enzymes were more glycosylated in the absence of tunicamycin (Fig. 6B, top arrowhead) compared with GC-B-L658F and GC-B-G959A.

Mutation of the N24 Glycosylation Site Reduces Guanylyl Cyclase Activity

Mutagenesis studies identified five N -linked glycosylation sites in GC-B, and the one that had the greatest effect on migration was Asn-24 (*202*). Therefore, we mutated N24 to Asp or Gln in WT-GC-B and the L658F AMDM mutant and assessed the guanylyl cyclase activity of the resulting enzymes in membranes from transfected 293 cells (Fig. 7). As expected, both Asp and Gln substitutions for N24 reduced CNP and detergent-dependent GC activity as well as the slower migrating form of GC-B when introduced into the WT-GC-B backbone. However, the activity reduction observed for GC-B-L658F was greater than that observed for either N24

mutation, which is expected given that the L658F mutant likely is missing multiple glycosylation sites based on the large increase in electrophoretic mobility compared with the WT enzyme. Importantly, ablating the N24 glycosylation site did not increase the electrophoretic migration of the GC-B-L658F mutant, consistent with this mutant lacking glycosylation at that site.

Blocking Glycosylation in the Golgi Apparatus Does Not Inhibit GC Activity

To test the effect of Golgi-dependent glycosylation on guanylyl cyclase activity, WT-GC-B was expressed in regular 293T cells and a mutant 293 cell line lacking the Golgi enzyme, N -acetylglucosaminyltransferase I (Gnt1$^-$). This enzyme adds complex sugars to proteins that have been trimmed of high mannose sugars added in the ER (Fig. 8). WT-GC-B isolated from the Gnt1$^-$ cells lacked the fully processed, slowest migrating (upper) species and showed an increase in the incompletely processed middle form. However, total expression of GC-B in the Gnt1$^-$ cells was similar to total GC-B expression in the 293T cells that express the Gnt1 I gene (Fig. 8, top panel). Importantly, CNP-stimulated and detergent-stimulated activities were similar regardless of Gnt1 gene expression and Golgi-dependent glycosylation of GC-B.

Enzymatic Deglycosylation of Fully Processed GC-B Does Not Reduce Enzymatic Activity

Finally, WT and mutant enzymes immunoprecipitated and bound to protein-A-agarose beads were incubated with or without PNGase F, which cleaves the covalent bond between the innermost GlcNAc and asparagine of the enzyme. The receptors were then purified by SDS-PAGE and visualized by Western blotting or assayed for guanylyl cyclase activity in the presence of Mn^{2+}GTP and Triton X-100 (Fig. 9, top panels). The electrophoretic migration of the WT enzyme increased the most because it was more highly glycosylated. However, the electrophoretic mobility of the mutants also increased because they were partially glycosylated. Importantly, the electrophoretic mobility of the PNGase F-treated WT enzyme was the same as the mobility of the PNGase F-treated mutants. Thus, deglycosylation completely explains the increased migration of the mutant enzymes. However, PNGase F had no effect on the guanylyl cyclase activity of the WT or mutant enzymes.

To evaluate the effect of deglycosylation on CNP-dependent activity, membranes from 293T cells transfected with WT-GC-B were incubated with PNGase F and then assayed for CNP- and detergent-dependent GC activity or purified by immunoprecipitation and SDS-PAGE. The appearance of a faster-migrating species indicated that 12.2% of the total amount of GC-B was deglycosylated, and the corresponding decrease in the second band indicated that only the

incompletely glycosylated form of GC-B was cleaved by PNGase F in membranes. Incomplete deglycosylation in the membranes compared with purified GC-B bound to protein-A-agarose is expected because the membranes contain more substrates for PNGase F. Nonetheless, no reduction in GC activity measured under CNP or detergent conditions was observed in membranes that were exposed to PNGase F, which is expected given that the upper completely glycosylated and active species was not cleaved. Taken together, these data are consistent with a model where N-linked glycosylation in the ER is required for proper folding of the catalytic but not the NP-binding domain of GC-B. However, when folded, terminal glycosylation is no longer required to produce a stimulated catalytic unit.

DISCUSSION

Post-translational modifications regulate the activity and location of proteins. Here we report that glycosylation is required for the formation of an activated catalytic domain but that it does not regulate the cellular location of GC-B or its ability to bind CNP. Importantly, we connect mutations that result in deglycosylated forms of GC-B to a disease for the first time.

Previous studies on the role of glycosylation on GC-A and GC-B were conflicting. Incompletely glycosylated GC-A was initially reported to lack the ability to bind ^{125}I-ANP (*18*). In contrast, Miyagi et al. (*20*) identified five N -linked glycosylation sites in GC-A but found that glycosylation was not required for ANP binding. A third report demonstrated that incompletely glycosylated mutants of GC-A bound but could not be activated by ANP (*109*). Regarding GC-B, mutagenesis of five of the seven potential N -linked glycosylation sites in the bovine receptor revealed that N24 is a conserved glycosylation site and that mutagenesis of this site inhibits CNP-dependent cGMP elevations but does not affect the affinity of CNP for the membrane exposed receptor (*202*). Here we determined that the single N24 mutation decreased both the CNP- and detergent-dependent activity of GC-B, consistent with the notion of glycosylation being required for maximum enzymatic activity of GC-B. Our data are consistent with the majority of previously published observations showing that reduced glycosylation of GC-A and GC-B decreases cGMP generation but not natriuretic peptide binding.

Experiments employing tunicamycin and N -acetylglucosaminyltransferase I-deficient cells allowed the effects of GC-B glycosylation in the ER versus the Golgi apparatus to be tested independently of the AMDM mutations. Because only tunicamycin treatment decreased catalytic activity, we conclude that glycosylation in the ER is required for the catalytic domain to fold into an active conformation, consistent with glycosylation increasing the solubility and chaperone binding of proteins (*203*). In contrast, neither blocking terminal glycosylation in the Golgi nor enzymatically removing sugar residues from the completely processed enzyme reduced the activity of GC-B. Interestingly, because the level of the lower, more rapidly migrating species of GC-B is unchanged between the WT and mutant enzymes, this suggests that the mutants are selectively degraded in a membrane-limited compartment of the cell, possibly by the incompletely glycosylated form being exported out of the ER and degraded in the cytoplasm.

A previous study using site-directed mutants correlated deglycosylated forms of GC-A with decreased guanylyl cyclase activity. However, because these mutants were also dephosphorylated, whether the loss of activity was due to lack of glycosylation or phosphorylation could not be determined (*109*). Our experiments employing the constitutively

phosphorylated GC-B-7E enzyme allowed the effects of phosphorylation and glycosylation to be separated for the first time. When inactivating AMDM mutations were engineered into a GC-B-7E backbone, the resultant enzymes were inactive. As a result of this report, we can now say that both processes are required for activation of GC-B, with each modification having a different purpose. Phosphorylation is required for transduction of the NP binding signal to the catalytic domain but not required for glycosylation, and it does not affect the formation of functional ligand binding or catalytic domains (*14, 24*). In contrast, glycosylation is required for formation of a stimulated catalytic domain because prevention of glycosylation in the ER inhibits NP- and detergent-dependent but not basal GC activity.

Immunofluorescence imaging studies on mutant forms of GC-B in the initial AMDM report led to the conclusion that the mutations disrupted targeting of GC-B to the cell surface (*197*). However, Amano et al. (*168*) subsequently showed that the Q417E dwarfism mutation did not affect surface expression of GC-B. Positive detection by Amano et al. (*168*) is likely explained by their use of an N-terminal versus C-terminal HA GC-B tag, which allowed surface protein detection in the absence of membrane- permeating agents. Our ^{125}I-CNP binding and immunofluorescence experiments on live cells clearly indicated that all four mutants are on the cell surface. The immunofluorescence data also indicated that the L658F and Y708C mutants have a partial trafficking defect, although this did not explain the loss of GC activity. Consistent with our results, Hachiya et al. (*193*) found that HA-tagged-GC-B-L658F bound ^{125}I-CNP when expressed in whole cells but lacked GC activity. Finally, we point out that, of the three bands commonly seen for GC-B on Western blots, it is only the uppermost band that correlates with guanylyl cyclase activity. Hence, in future studies, only the upper band should be measured when investigating the GC activity of the enzyme.

We conclude that ER-mediated glycosylation is required for CNP- and detergent-stimulated catalytic activity of GC-B. Furthermore, we report that four unique AMDM missense mutants produce a conformation that is incompatible with ER-mediated glycosylation and result in proteins that bind CNP on the cell surface but lack stimulated guanylyl cyclase activity. Thus, our data refute the current "defective trafficking" hypothesis to explain the lack of activity of AMDM mutants. Finally, we predict that any homozygous mutation that inhibits ER-mediated glycosylation of GC-B will inactivate the enzyme and result in skeletal undergrowth.

EXPERIMENTAL PROCEDURES

Reagents

^{125}I-cGMP radioimmunoassay kits and ^{125}I-CNP-22 were from Perkin Elmer Life Sciences. Non-radioactive natriuretic peptides were from Sigma. ProQ Diamond dye and wheat germ agglutinin were from Life Technologies. Tunicamycin was from Millipore Corp. (Billerica, MA).

Cell Culture, Transfections, and cDNAs

293T-GC-B cells were maintained as described previously (*204*). GnT1 293 cells lacking the Golgi N-acetylglucosaminyltransferase I enzyme (*205*) were purchased from the ATCC (Manassas, VA). 293T cells were transfected using the calcium/phosphate method as described previously (*32*). For HeLa cells, a 1:2 mass ratio of plasmid DNA to Lipofectimine2000 was incubated in 0.5 ml of Opti-MEM for 20 min before addition to cells. The mutants used for CNP binding and guanylyl cyclase assays were generated in the rat cDNA backbone. The mutants used for the immunofluorescence studies were generated in the HA-tagged human GC-B cDNA (*193*).

Immunofluorescence

HeLa cells were fixed with 4% formaldehyde in PBS for 15 min at room temperature and stained for the plasma membrane with wheat germ agglutinin 594 at 5 µg/ml for 10 min. Cells were then incubated in PBS containing 2% BSA for 30 min. Cells were then incubated with a 1/1000 dilution of the anti-HA monoclonal antibody AFC-101P (Covance) overnight at 4 °C. Cells were rinsed and incubated with Alexa Fluor 488-conjugated anti-mouse IgG (Life Technologies, A-11001) at 1/500 dilution for 30 min at room temperature to visualize immunocomplexes. Nuclei were stained with a 1/10,000 dilution of DAPI (Invitrogen, D-1306). Images were obtained using a Deltavision Personal DV microscope (Applied Precision). Where indicated, 0.5% saponin was added to permeabilize the plasma membrane.

Immunoprecipitations and SDS-PAGE

Transfected 293T cells from one 10-cm plate were lysed with 1 ml of immunoprecipitation buffer containing phosphatase inhibitors, immunoprecipitated with 3 µl of rabbit 6327 antiserum overnight, and fractionated on an 8% resolving gel as described previously (*136*).

Western Blotting

293T cells were transfected with the indicated constructs, and equal amounts of crude membranes were normalized to total protein, or immunoprecipitated complexes were fractionated by reducing SDS-PAGE and blotted to a Immobilon membrane for immunodetection as described previously (*137*). The blot was blocked and probed with a 1/5000 dilution of rabbit serum 6328 followed by incubation with a 1/20,000 dilution of goat anti-rabbit IRDye 680-conjugated antibody and visualized on a LI-COR instrument as described previously (*206*).

Gel Staining

Resolving gels were fixed in a 30-ml solution of 50% methanol and 10% acetic acid for 30 min with gentle rocking. The solution was changed once for a total of two washes in the fixing solution. The gels were then washed three times in 100 ml of water for 10 min. 10 ml of Pro-Q Diamond phosphoprotein gel stain was added, and gels were rocked for 1.5 h in the dark. The gels were then destained with 80 ml of a solution of 20% acetonitrile, 50 mM sodium acetate (pH 4.0) for 15 min three times. The gels were then rinsed in water and scanned with a 532-nm laser on a Typhoon FLA 9500 imager (GE Life Sciences) (*199*). After imaging, the gel was rinsed and stained with Coomassie Brilliant Blue.

Guanylyl Cyclase Assays

Crude membranes were prepared in phosphatase inhibitor buffer from 293T-GC-B cells as described previously (*114*). All assays were performed at 37 °C in a mixture containing 25mM Hepes (pH 7.4), 50mM NaCl, 0.1% BSA, 0.5 mM isobutylmethyl xanthine, 1 mM EDTA, 0.5 μM microcystin, 10 mg/ml creatine kinase, 5 mM creatine phosphate, and 5 mM MgCl2 . The time each reaction was incubated at 37 °C is indicated in the figure legends. Unless otherwise indicated, 1 mM ATP and 0.1 mM GTP were included in the reaction solutions. Reactions were initiated by adding 60 μl of prewarmed reaction mixture to 20 μl of crude membranes suspended in 20 μl of phosphatase inhibitor buffer alone (basal) or producing final concentrations of 1 μM CNP or 1% Triton X-100 and 5 mM $Mn^{2+}Cl_2$, which was substituted for $MgCl_2$. Reactions were stopped with 0.4 ml of ice-cold 50 mM sodium acetate buffer containing 5 mM EDTA. Cyclic GMP concentrations were determined by radioimmunoassay (*134*).

^{125}I-CNP Binding Assays

Equal numbers of transiently transfected 293 cells were seeded in 24-well plates and grown to 70–90% confluence. Cells were incubated for 1 h in DMEM containing 0.2% BSA at 37 °C. Binding medium containing 1% BSA and 30 pM (20 nanocuries) of 125 I-CNP was added to each well and incubated at 4 °C for 1 h. For nonspecific binding wells, 1 μM of non-radioactive CNP was included in the binding buffer. For the competition binding assays, increasing concentrations of non-radioactive CNP were included in the binding buffer. The cells were washed with ice-cold PBS to remove nonspecifically bound 125 I-CNP. The cells were removed from the plate with 0.5 ml of 1 N NaOH, and the radioactivity of the cell extract was determined in a γ counter.

Tunicamycin Treatment

Four hours after 293T cells were transiently transfected, they were incubated with 2 μg/ml tunicamycin for 24 h, and then membranes were prepared in phosphatase inhibitor buffer for analysis.

Statistical Analysis

Statistics and graphs were generated with Prism 5 software. *p* Values were obtained using Student's paired t test, and $p \leq 0.05$ was considered significant. The error bars within the symbols represent standard error.

FIGURES

Figure 1. AMDM mutants are not processed to the fully glycosylated and phosphorylated form of GC-B.

WT and the indicated missense versions of GC-B were isolated from transiently transfected 293T cells by sequential immunoprecipitation/SDS-PAGE purification. The resulting gel was incubated with ProQ Diamond dye to determine GC-B phosphate levels (bottom panel). The same gel was then washed and stained with Coomassie Brilliant Blue dye to determine the amount of GC-B protein present (top panel). Molecular mass in kilodaltons is shown for protein standards on the left. *7A*, GC-B containing alanine substitutions for all seven known phosphorylation sites. The figure is representative of three experiments.

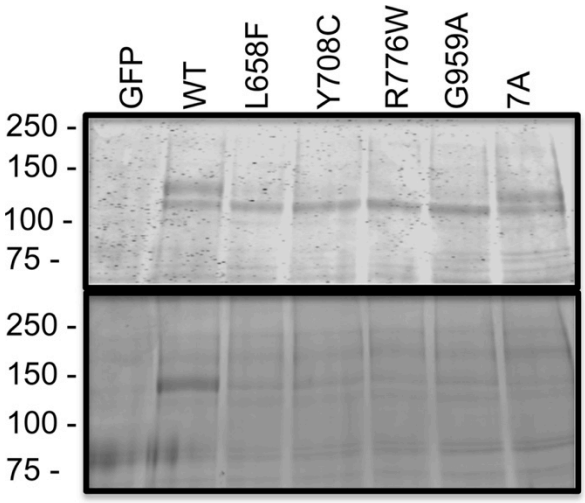

Figure 2. The AMDM mutants bind ^{125}I-CNP on the surface of live cells.

293 cells were transiently transfected with plasmids containing GFP, WT-GC-B, or the indicated mutants. Equal numbers of cells were seeded in the wells and then incubated for 1 h at 4 °C with 30 pM ^{125}I-CNP in the presence or absence of 1 μM (top panel) or increasing concentrations (bottom panel) of non-radioactive CNP. The cells were rinsed with binding medium to remove nonspecific 125I-CNP, removed from the plate with NaOH, and subjected to γ counting to determine the amount of specifically bound ^{125}I-CNP. The error bars and symbols represent the standard error, where n = 3. B/Bo = specific binding over nonspecific binding; conc. = concentration.

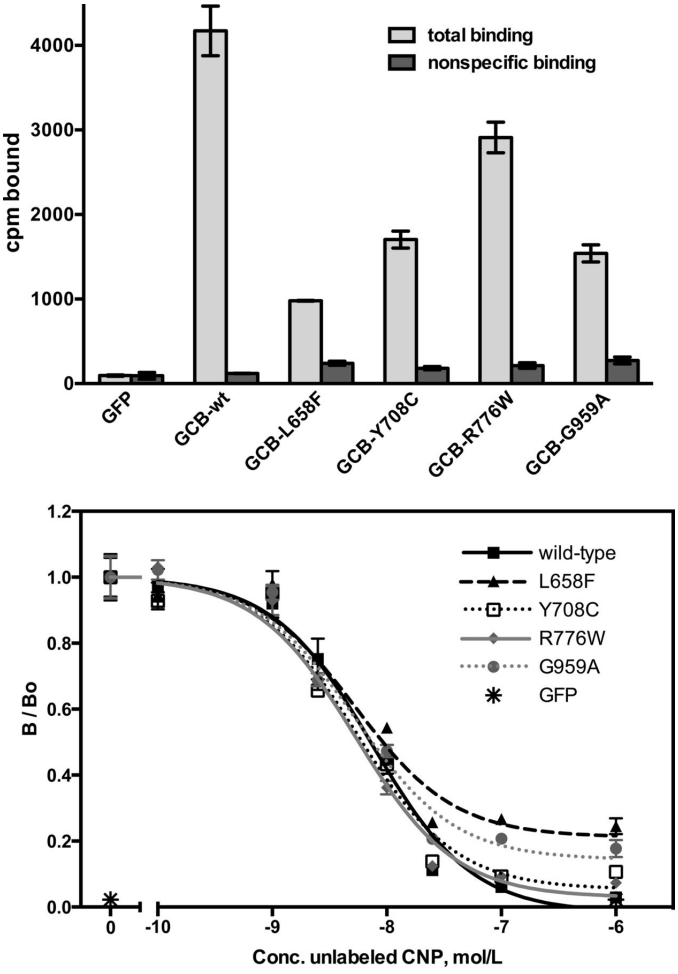

Figure 3. Microscopic immunofluorescence detection indicates that the AMDM mutants are on the cell surface.

HeLa cells were transiently transfected with HA-tagged WT-GC-B, the indicated HA-tagged ADMA mutants, or no plasmid DNA. Cells were fixed and stained as described under "Materials and Methods" and then visualized using a Deltavision Personal DV microscope (Applied Precision). A, D, G, J, L, and O. Non-permeabilized staining using an antibody against the HA epitope (green). B, E, H, K,M, and P. Non-permeabilized plasma membrane staining using wheat agglutinin 594 (red). C, F, I, L, N, and Q. Non-permeabilized colocalization of the HA-stain and plasma membrane stain (yellow). R, U, X, AA, DD, and GG. Permeabilized staining using an antibody against the HA epitope (green). S, V, Y, BB, EE, and HH. Permeabilized plasma membrane staining using wheat agglutinin 594 (red). T, W, Z, CC, FF, and II. Permeabilized colocalization of the HA stain and plasma membrane stain (yellow).

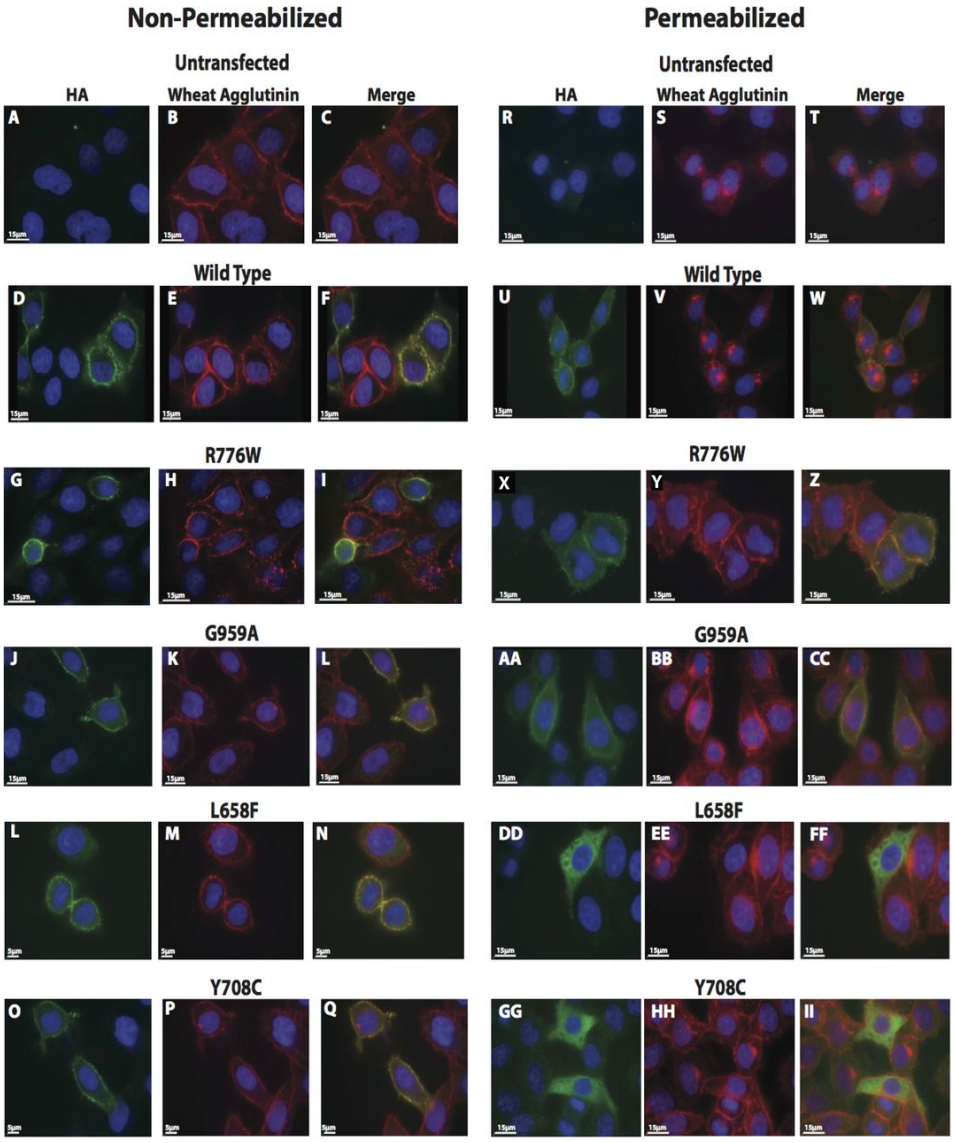
Non-Permeabilized
Permeabilized
Untransfected
HA
Wheat Agglutinin
Merge
A
B
C
R
S
T
Wild Type
D
E
F
U
V
W
R776W
G
H
I
X
Y
Z
G959A
J
K
L
AA
BB
CC
L658F
L
M
N
DD
EE
FF
Y708C
O
P
Q
GG
HH
II

Figure 4. The AMDM mutants have markedly reduced activated guanylyl cyclase activity. 293T cells were transiently transfected with plasmids containing GFP, WT-GC-B, or the indicated GC-B mutants. Crude membranes were prepared from the transfected cells and assayed for guanylyl cyclase activity under basal, CNP-stimulated, or Triton X-100 and manganese-stimulated conditions. The error bars represent the standard error, where n = 6 from three experiments.

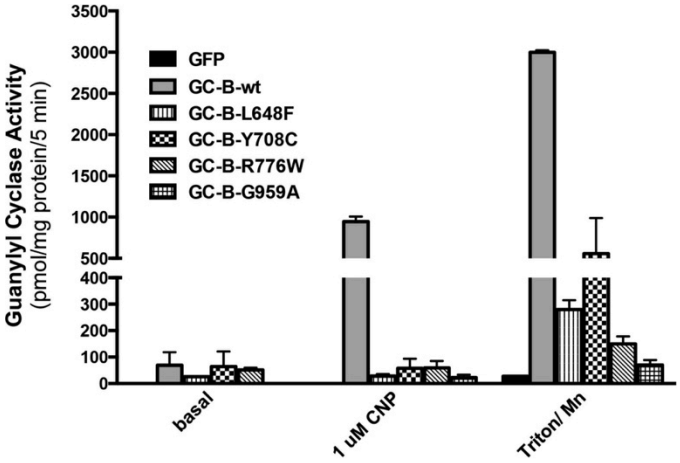

Figure 5. Reduced phosphorylation does not explain the inactivation of the AMDM mutants.

293T cells were transiently transfected with plasmids encoding GFP, WT-GC-B, or the indicated GC-B mutants. A. GC-B proteins were isolated by sequential immunoprecipitation/SDS-PAGE purification followed by Western blotting detection. Peptide block indicates that the peptide antigen was or was not included in the immunoprecipitation reaction to specifically block binding to GC-B. B, equal numbers of cells were incubated for 1 h at 4 °C with 30 pM ^{125}I-CNP in the presence or absence of non-radioactive CNP. The cells were rinsed with binding medium to remove nonspecific ^{125}I-CNP, removed from the plate with NaOH, and subjected to γ counting to determine the amount of specifically bound ^{125}I-CNP. The error bars represent the standard error, where n = 3. C, crude membranes were prepared from the transfected cells and assayed for guanylyl cyclase activity under the indicated conditions. The error bars represent the standard error, where n = 5 from three experiments.

A).

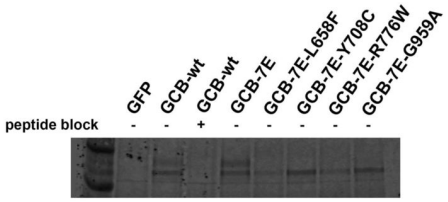
GFP
GCB-wt
GCB-wt
GCB-7E
GCB-7E-L658F
GCB-7E-Y708C
GCB-7E-R776W
GCB-7E-G959A
peptide block
- - + - - - - -

B).

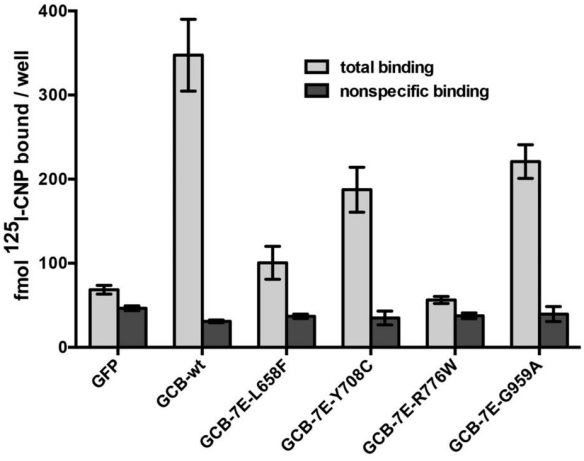
fmol 125I-CNP bound / well
400
300
200
100
0
total binding
nonspecific binding
GFP
GCB-wt
GCB-7E-L658F
GCB-7E-Y708C
GCB-7E-R776W
GCB-7E-G959A

C).

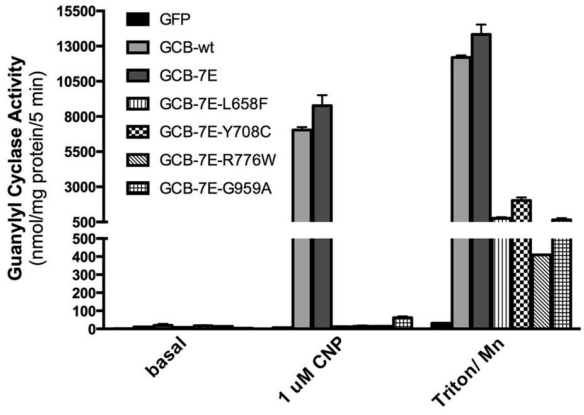
Guanylyl Cyclase Activity
(nmol/mg protein/5 min)
15500
13000
10500
8000
5500
3000
500
500
400
300
200
100
0
GFP
GCB-wt
GCB-7E
GCB-7E-L658F
GCB-7E-Y708C
GCB-7E-R776W
GCB-7E-G959A
basal
1 uM CNP
Triton/ Mn

Figure 6. N-linked glycosylation in the ER is required for stimulated GC-B activity.
A and B. 293T cells were transiently transfected with plasmids encoding GFP, WT-GC-B, GC-B-7E, GC-B-L658F, or GC-B-G959A and incubated in the presence (+) or absence (-) of tunicamycin before preparing membranes and assaying them for guanylyl cyclase activity under the condition shown (A) or changes in molecular mass by sequential immunoprecipitation and Western blotting analysis (B). The error bars represent the range of duplicate determination. The Western blot is representative of three individual experiments. The GC results shown are representative of four similar experiments. Arrowheads indicate the three commonly observed electrophoretic forms of GC-B, with the large arrowhead representing the most highly glycosylated and active form.

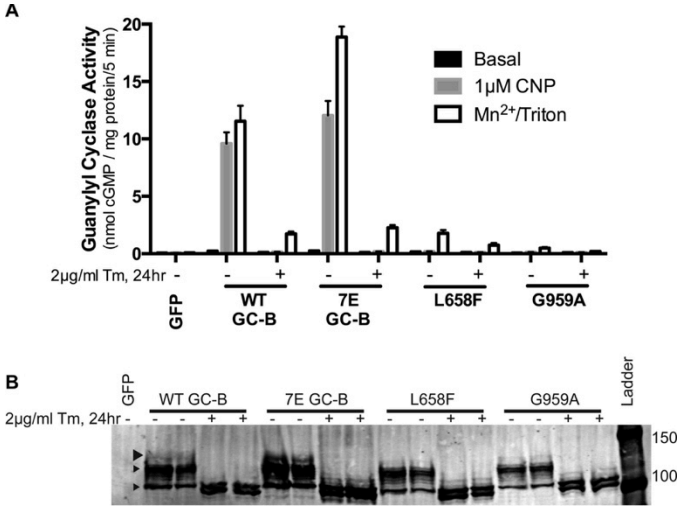

Figure 7. Mutation of the Asn-24 glycosylation site decreases the guanylyl cyclase activity and increases the electrophoretic migration of GC-B.

293T cells were transiently transfected with plasmids containing GFP, WTGC- B, or the indicated GC-B mutants. Crude membranes were prepared from the transfected cells, and GC-B migration was analyzed by Western blotting analysis (top panel) or assayed for guanylyl cyclase activity (bottom panel) under basal, CNP-stimulated, or Triton X-100 and manganese-stimulated conditions. The error bars represent the standard deviation, where n = 4 and is representative of three experiments.

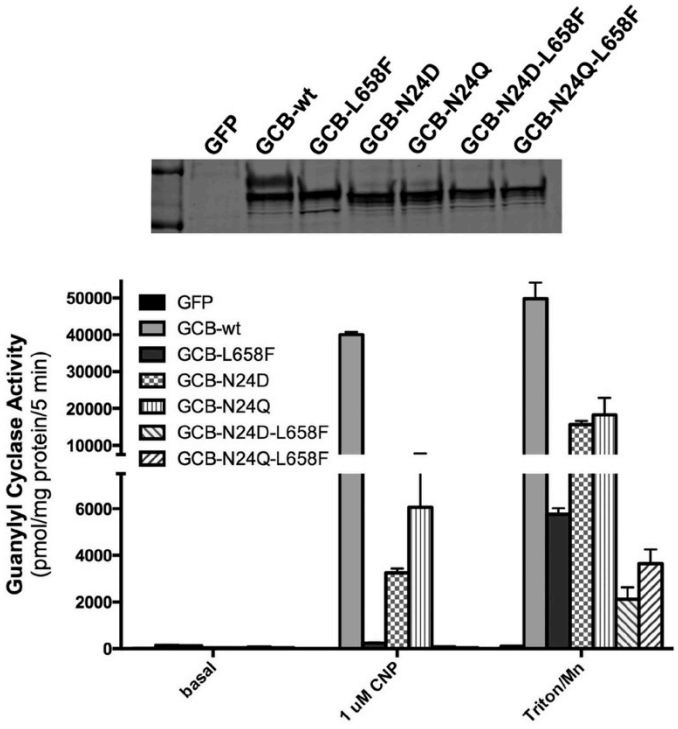

Figure 8. Incomplete glycosylation in the Golgi apparatus does not reduce CNP- or detergent-dependent guanylyl cyclase activity of GC-B.

A plasmid expressing WT-GC-B was transiently transfected into 293T or 293S Gnt1$^-$ cells. GC-B was then purified by sequential immunoprecipitation and SDS-PAGE and detected by Western blotting (top panel), or membranes were prepared from these cells and assayed for guanylyl cyclase activity under the indicated conditions. The error bars represent the standard error, where n = 4. The experiment is representative of three similar experiments.

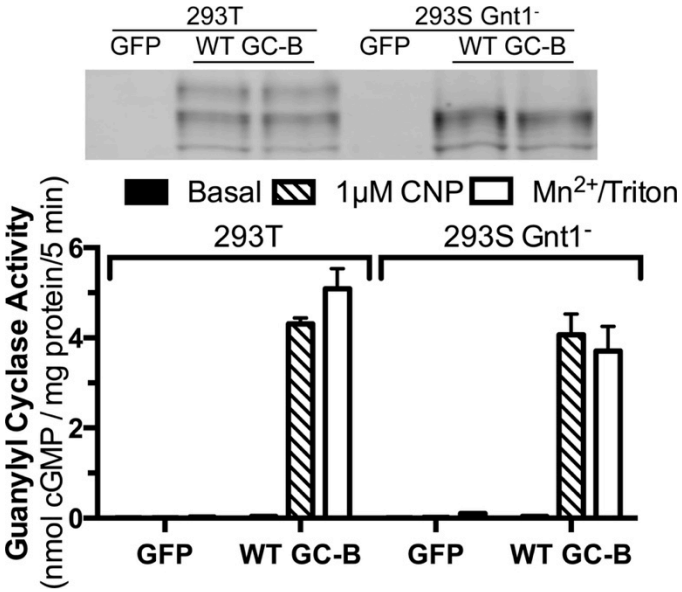

Figure 9. Enzymatic deglycosylation after normal processing does not inhibit GC-B activity. A. Crude membranes were prepared from 293T cells stably expressing GC-B, and then GC-B was immunoprecipitated and incubated with or without PNGase F for 15 min at 16 °C. SDS-PAGE-purified receptors were Western-blotted to verify deglycosylation. Guanylyl cyclase activity was assayed in the presence of Mn^{2+}GTP and Triton X-100. B. Crude membranes were treated with or without PNGase F for 15 min at 16 °C and then Western-blotted or assayed for guanylyl cyclase activity as indicated. The enzyme control was from crude membranes that were first denatured by boiling and then treated with PNGase F for 1 h at 37 °C. The total amount of GC-B (center band) cleaved was determined by analyzing the scanned image with ImageJ software.

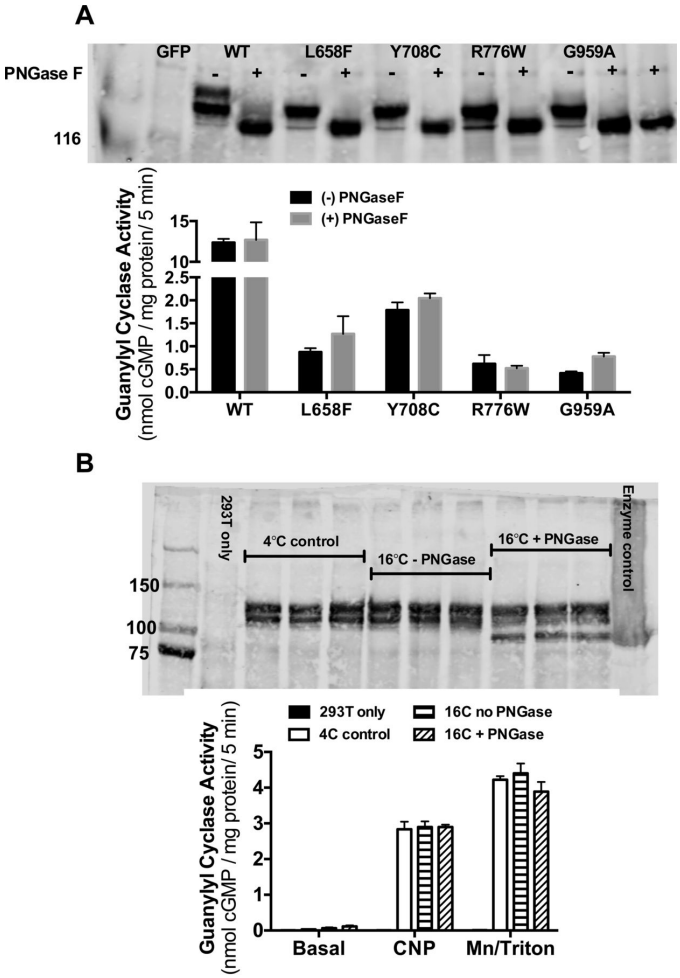

CHAPTER 6:

The pseudokinase domains of guanylyl cyclase-A and -B allosterically increase the affinity of their catalytic domains for substrate.

This chapter is a reprint of an original manuscript accepted pending text revisions, used with permission:

Aaron B. Edmund, Timothy F. Walseth, Nicholas M. Levinson, and Lincoln R. Potter. The pseudokinase domains of guanylyl cyclase-A and -B allosterically increase the affinity of their catalytic domains for substrate. *Science Signaling.* (2019)

Aaron Edmund collected, interpreted, and analyzed data in all figures, created all figures, and contributed heavily to the writing of the manuscript.

SUMMARY

Natriuretic peptides regulate multiple physiologic systems by activating the membrane guanylyl cyclase (GC) receptors, GC-A and GC-B, also known as Npr1 and Npr2. Both enzymes contain an intracellular, phosphorylated, pseudokinase domain (PKD) followed by a cGMP synthesizing GC catalytic domain. Molecular modeling indicated that all the residues in the ATP binding site of protein kinase A except the catalytic aspartate are conserved in the GC PKDs. Kinase inactivating alanine substitutions for the invariant lysine (K535A and K551A) in subdomain II or the aspartate in the DYG-loop (D646A and D662A) of GC-A and GC-B, respectively, failed to decrease enzyme phosphate content, consistent with the PKD lacking kinase activity. In contrast, both mutations reduced enzyme activation by blocking the ability of ATP to decrease the Michaelis constant without affecting NP-dependent activation. The analogous lysine substitution (K551A) in a phosphomimetic, glutamate-substituted mutant of GC-B also reduced enzyme activity, consistent with an allosteric, phosphorylation-independent mechanism. Mutations designed to rigidify the conserved regulatory or catalytic spines within the PKDs increased GC activity (GC-B-I583W), increased sensitivity to NP-stimulation (GC-B-M571F) or reduced the Michaelis constant in the absence of ATP (GC-A-A533W). We conclude that membrane GCs regulate substrate affinity through allosteric mechanisms that are evolutionarily conserved in their PKDs.

INTRODUCTION

There are three natriuretic peptides (NPs) in mammals, and one of two homodimeric single membrane-spanning guanylyl cyclase (GC) receptors mediate the vast majority of the effects of these NPs (*189, 190, 207, 208*). However, cGMP-independent functions have also been described that may be mediated by the NP clearance receptor (*209*). Atrial NP (ANP) and B-type NP activate guanylyl cyclase-A (GC-A), also known as Npr1, which stimulates natriuresis and inhibits cardiac hypertrophy. C-type NP (CNP) activates guanylyl cyclase-B (GC-B), also known as Npr2, which stimulates long bone growth, meiotic arrest in oocytes, and neuronal bifurcation (*102, 207*). GC-A and GC-B are homologous. At the intracellular amino acid level, the two proteins are 78% identical (*43*) and share five phosphorylation sites (*103*).

How NPs activate GC-A and GC-B is incompletely understood, but NP binding is known to cause a 24º counterclockwise rotation in the extracellular domain of one GC-A monomer with respect to the other monomer (*38*). On its way to the catalytic domain, the binding signal travels through a pseudokinase domain (PKD) that is constitutively phosphorylated on at least six residues (*14, 24, 103*). The chemically determined phosphorylation sites identified in rat and human GC-A using rat numbering are S487, S497, T500, S502, S506, S510, and T513 (Fig. 1C) (*103, 210*). The chemically identified phosphorylation sites in rat and human GC-B using rat numbering are S513, T516, S518, S523, S526, and T529 (*103*). Additionally, a functional screen identified a single serine residue in the juxtamembrane region conserved in both GC-A (S473) and GC-B (S489) (*27*). The kinases responsible for phosphorylating these sites are unknown. Phosphorylation of the PKD is absolutely required for propagation of the NP binding signal to the GC catalytic domain of both receptors (*14, 22-24*). Data supporting the essential role of phosphorylation is extensive, ranging from enzymatic dephosphorylation GC-A and GC-B in membranes to the creation of mice expressing phosphomimetic, glutamate substituted, forms of GC-A and GC-B that are resistant to inactivation by dephosphorylation (*22, 23, 27-30, 81, 152, 211*).

In addition to NPs, ATP is required for activation of GC-A and GC-B (*41*). However, understanding of how ATP activates GC-A and GC-B is complicated by the ability of ATP to serve as a substrate for receptor phosphorylation as well as to bind an allosteric site in the catalytic domain (*31, 32*). In substrate-velocity experiments, ATP serves as an allosteric activator that causes a shift from positive cooperative kinetics in the absence of ATP to linear kinetics in the presence of ATP. As a result of binding to an allosteric site, ATP reduces the Michaelis constant an order of magnitude to physiologic GTP concentrations in a NP-dependent manner

(*32*). To identify the ATP binding site, two separate groups covalently cross-linked ATP analogs to the PKD of GC-A and suggested that this process is required for the ability of ATP to increase GC-A activity (*212, 213*). However, the exact ATP binding site in the PKD was not determined. Because protein kinase A (PKA) is the most widely studied mammalian protein kinase, we used knowledge of allosteric activation of PKA and other kinases and pseudokinases to better understand how the intrinsic PKD's regulate the enzymatic activity of GC-A and GC-B.

In PKA the transition from inactive to active state occurs through phosphorylation of the activation loop. The phosphorylated activation loop then forms a salt-bridge with a His residue in the αC-helix located in the N-terminal lobe of the kinase. The regulatory (R)-spine, a network of internal hydrophobic amino acids, is then assembled into a rigid structure which orients all the necessary components for catalysis in the active site. Upon ATP binding to the kinase active site, the adenine ring docks between the N-terminal lobe and the C-terminal lobe of the kinase, thus fusing another network of hydrophobic amino acids called the catalytic (C)-spine (*71*). The triphosphate tail and associated Mg^{2+}cations form interactions with multiple polar and charged amino acids lining the active site. The most notable of these are the invariant lysine in subdomain II and the Mg^{2+}-chelating aspartate in the DFG-loop. Both residues are conserved in GC-A and GC-B and alanine mutants of these residues provided critical data supporting the conclusions of this paper. Because both spines are docked on the αF-helix in the C-terminal lobe, the assembly of both spines rigidifies the entire kinase domain with coordinated motion in the most catalytically competent state (*63*). In pseudokinases, phosphotransferase activity is markedly diminished or absent due to the loss of residues required for catalysis, but ATP-dependent allostery is often maintained (*68-70, 214*).

We created a homology model that revealed that the PKDs of GC-A and GC-B contain the conserved hydrophobic regulatory and catalytic spine elements common to known protein kinases and pseudokinases (Fig. 1B), which implies that the allosteric activation mechanisms of protein kinases and pseudokinases may be conserved receptor GCs as well. In addition, the PKDs in GC-A and GC-B contain all of the ATP binding residues conserved in most protein kinases with the exception of the catalytic aspartate, which suggests that these domains in GC-A and GC-B lack intrinsic phosphotransferase activity (Fig. 1A) (*215*). However, low kinase activity was observed for the putative pseudokinase ErbB3/HER3 and the JH2 domain of JAK2 that also lack the conserved catalytic aspartate, which suggested that the PKDs of GC-A and GC-B may also contain muted, but regulatory, levels of phosphotransferase activity (*216, 217*).

Here, we investigated why the PKD is conserved in receptor GCs beginning with the possibility that the PKD of GC-A has intrinsic autophosphorylating activity by making single amino acid inactivating mutations that disrupt the activity of most protein kinases. However, these mutations failed to reduce the phosphate content of GC-A or GC-B. In contrast, these same mutations markedly decreased the ability of NPs to decrease the Michaelis constant of GC-A and GC-B in an ATP-dependent manner. Finally, a dynamic hydrophobic core model of allostery common to kinases and pseudokinases was developed and used to evaluate how these PKDs stimulate receptor guanylyl cyclase activity.

RESULTS

Canonical ATP-interacting and hydrophobic core residues are conserved in GC-A and GC-B

We generated a homology model for the PKD of GC-A based on the human Lck structure, which has the greatest amino acid identity (32%) to the PKD of GC-A of all known protein kinases (Fig. 1). The residues required for binding of ATP and catalysis in PKA (K72, E91, D166, K168, N171, and D184) are shown beside the homology model of the ATP binding pocket in GC-A (Fig. 1A). Except for D166, the catalytic base in PKA, all residues that directly interact with ATP in PKA are conserved in the PKDs in GC-A and GC-B (Fig 1A and Table 1). We also generated space-filling models that demonstrate that residues composing the R-spine and C-spine are conserved in GC-A and GC-B (Fig 1B and Table 1). Thus, the structural framework required for ATP binding and allosteric transmission of the ATP binding signal in PKA is conserved in NP-stimulated GCs. The GC-A and GC-B phosphorylation sites mutated in the alanine-substituted non-phosphorylated constructs and glutamate-substituted phosphomimetic constructs of GC-A and GC-B are identified for reference (Fig. 1C). To more thoroughly compare our homology model of the PKD of GC-A, we performed a structural alignment in PyMol using our GC-A homology model and the structures of reference kinases (PKA, PDB:1ATP; BRAF, PDB: 1UWH; LCK, PDB: 3LCK) (Fig. 2) and depict it as a linear sequence alignment. Previously, many researchers had assumed the G-x-G-x-x-x-G motif in the PKDs of GC-A and GC-B (G503-G509 in GC-A) fulfilled the role of the glycine-rich (G)-loop of protein kinases found between the β1 and β2 strands. However, when these glycines were mutated to alanine to prevent the backbone flexibility necessary for their function in protein kinases there was no effect on GC activity (*34*). In our model of GC-A, we observed that the glycine to alanine substitutions actually preceded or were within the β1 strand, not in the β1-β2 loop as previously predicted. In the β1-β2 loop of our model of GC-A, there is a degraded G-loop motif, which is expected to decrease ATP affinity and may explain why high concentrations of ATP are necessary to fully activate GC-A and GC-B (*32*).

Alanine substitutions for the conserved K in subdomain II or D in DYG-loop inactivate GC-A and GC-B

Because the most commonly used kinase inactivating mutations (K72 and D184 in PKA) are conserved in GC-A (K535 and D646) and GC-B (K551 and D662), we used alanine substitutions at these sites to investigate the effects of hypothesized decreased ATP binding to the PKD on GC activity. We prepared crude membranes from cells transfected with plasmids

encoding wild type (WT)-GC-A, GC-A-7A, a non-phosphorylated mutant containing alanine substitutions for all known phosphorylation sites, and the single alanine substitution mutants GC-A-K535A and GC-A-D646A (Fig. 3A). We then assayed the membranes for GC activity under maximal physiologic activation conditions (5mM $MgCl_2$, 1mM ATP and 1μM ANP) or under synthetic conditions that yield near maximal activity independently of enzyme phosphorylation or NP binding (5mM $MnCl_2$ and 1% Triton X-100) and are used as a measure of properly folded and active catalytic domain. Activation by manganese and Triton is thought to result from disruption of hydrophobic autoinhibitory interactions (*218*). We observed severe reductions in NP-dependent guanylyl cyclase activity for the GC-A-K535A and GC-A-D646A mutants compared to the activity of the WT enzymes. However, we also observed substantial reductions in detergent-dependent activity for each mutant (Fig. 3A). To confirm the observed effects were due to changes in conserved mechanisms in the receptor GC family, we performed GC assays on the homologous receptor, GC-B, and its analogous mutants GC-B-K551A and GC-B-D662A (Fig. 3B). Again, we observed reductions in NP-dependent guanylyl cyclase activity for GC-B-K551A and GC-B-D662A. Unlike the GC-A mutants, we did not detect significant reductions in detergent-dependent activity of the GC-B mutants, which allowed us to rule out reductions in GC-B protein as a possible explanation for the reductions in CNP-dependent enzymatic activity for these mutant enzymes.

Reduced NP-dependent GC activity in the GC-A-K535A/GC-B-K551A and GC-A-D646A/GC-B-D662A mutants is not explained by reduced levels of fully processed protein or decreased phosphorylation

Theoretically, the alanine mutations could reduce the activity of GC-A and GC-B by decreasing: 1) the amount of fully processed enzyme (*17*), 2) receptor phosphorylation (*22, 23*), or 3) allosteric activation. To determine why the K535A/K551A and D646A/D662A mutations reduce GC activity, we measured protein and phosphate levels on the same samples. Protein abundance was determined by western blotting of lysates or by SYPRO Ruby staining of immunopurified proteins (Fig. 3C, D). We determined the stoichiometry of phosphorylation by first measuring phosphate levels by ProQ Diamond staining followed by SYPRO Ruby staining of the same gel to determine protein concentrations (Fig. 3C, D) (*136, 199*).

We detected phosphorylated WT-GC-A and GC-B as dark diffuse bands when stained with ProQ Diamond, consistent with migration of multiple phosphorylated species that differ in molecular weight due to differing levels of glycosylation and phosphorylation (*199*). Very low or

no staining of GC-A-7A with alanine substitutions for known phosphorylation sites demonstrated that ProQ Diamond dye is specific for phosphate. SYPRO Ruby staining of the same gel used for phosphate detection indicated similar expression of the WT and mutant proteins. Comparable levels of ProQ Diamond and SYPRO Ruby staining for each protein indicated that the stoichiometry of phosphorylation is similar between WT receptors and the two alanine mutants. Again, these data are consistent with the PKD's of GC-A and GC-B lacking intrinsic autophosphorylating activity. To quantify the relative stoichiometry of phosphorylation of GC-A and GC-B, the ratio of ProQ Diamond signal divided by SYPRO Ruby signal for the upper band of GC-A and GC-B was calculated and plotted (Fig. 3E, F). The relative stoichiometry of phosphorylation of the Lys and Asp mutants was not different from each other or their WT counterparts. These data indicate that the decrease in GC activity observed for both ATP binding site mutations cannot be explained by decreased receptor phosphorylation.

Although we observed reductions in the detergent-dependent GC activity and the amount of fully glycosylated and phosphorylated enzyme for the GC-A-K535A and GC-A-D646A mutants, none of these decreases could account for the reduction in ANP and ATP-dependent GC activity. In contrast, both the detergent-dependent GC activity and the species migrating as the upper band were not different between WT-GC-B, GC-B-K551A, and GC-B-D662A, but CNP and ATP-dependent GC activity was markedly reduced by the mutations. Together, these data indicate that both the K535A and D646A mutations in GC-A and the K551A and D662A mutations in GC-B inactivate these enzymes by a process that cannot be explained by reductions in the fully glycosylated, phosphorylated forms of these enzymes.

To further rule out confounding effects of changes in phosphorylated residues, we performed GC activity assays on the glutamate-substituted, phosphomimetic mutant of GC-B called GC-B-7E which behaves kinetically identical to WT-GC-B (*27*). We observed similar decreases in NP-dependent GC activity as a result of the K551A mutation in both WT-GC-B and GC-B-7E with no change in detergent-dependent GC activity (Fig. 4A) or abundance of the species migrating as the upper band as denoted by the arrow (Fig. 4B). These data are consistent with K551 participating in the ATP dependent activation of GC-B in a manner that does not require changes in GC-B protein concentrations or known phosphorylation sites.

The Lys and Asp substitutions specifically reduce ATP, but not NP, activation of GC-A and GC-B

We also investigated the ability of mutations in the PKDs of GC-A and GC-B to specifically inhibit activation by ATP but not NP. Crude membranes from cells transfected with

plasmids expressing the indicated receptors were assayed for 10 seconds, 2 minutes, or 10 minutes with physiologic (100 μM) concentrations of GTP in the absence of both NP and ATP (basal), with only 1μM NP, or with both 1μM NP and 1mM ATP, conditions that mimic physiologic activation (Fig. 5). We observed higher activity for WT versions of GC-A (Fig. 5A) and GC-B (Fig. 5B) when assayed in the presence of NP and ATP at all time points compared to activities measured for any mutant (Fig. 5C-F). Activity of WT-GC-A and WT-GC-B was substantially activated by NP in the absence of ATP (insets to Fig. 5A, B). Fold activation observed with ATP as determined by activity measured in the presence of ANP and ATP divided by activity measured in the presence of only ANP increased with time for WT GC-A and GC-B, but not for any of the mutants tested. Fold activation by ATP was 46-fold for WT GC-A at 10 minutes but was only 3-fold for the GC-A-D646A mutant and less than 2-fold for the GC-A-K535A mutant at 10 minutes (Fig. 5G) with similar patterns observed for WT GC-B and the analogous GC-B-K551A and GC-B-D662A mutants (Fig. 5H).

We also determined fold-activation by NP alone by measuring activity in the presence of only NP divided by activity determined in the absence of NP (Basal). We hypothesized that this ratio would decrease if the single alanine mutations were not specific for ATP binding and were globally affecting the structural integrity of the PKD (Fig. 5I, J). We observed no difference in fold activation by ANP in WT or mutant GC-A and only small differences in activation by CNP in WT or mutant GC-B. Fold activation by CNP of GC-B-D662A was significantly different from WT-GC-B (p=0.01) but was not on the same order as the differences observed in fold activation by ATP. These data indicate that canonical mutations in protein kinases or pseudokinases that diminish ATP-mediated activation also diminish the ability of ATP to activate GC-A and GC-B with little or no effect due to altered stability of the PKD.

Loss of cooperativity occurs through ATP binding to an allosteric site in the catalytic domain

Ill-defined allosteric regulatory sites have been reported for the PKD (*212, 213*) as well as in the catalytic domain of GC-A (*31, 32, 219*). To determine which site is responsible for the cooperative effects on enzyme activity, substrate-velocity assays were performed on membranes prepared from cells expressing a construct of GC-A containing the GC domain but lacking the PKD (Fig. 6A, B) (*12*). Using this construct, we observed a Hill slope of 1.4 in the absence of ATP that was reduced to 1.1 when ATP was added to the reaction mixture (Fig. 6C). However, we failed to observe a substantial decrease in Km upon the addition of ATP in the presence of 1μM ANP as observed for the full length WT version of GC-A (Fig. 6C) (*32*). These data indicate

that ATP binding to the allosteric site in the catalytic domain mediates the positive cooperative effects but is not sufficient to decrease the Km, which requires NP-binding to the extracellular domain (*32*) and may require ATP binding to the canonical ATP binding site in the PKD.

The K535A and D646A mutations prevent the ATP-dependent reduction in the Michaelis constant of GC-A

To determine if the conserved ATP binding site in the PKD of GC-A and GC-B is required for the ATP-dependent reduction in the Km, we assayed crude membranes from 293T cells transiently transfected with plasmids expressing WT-GC-A, GC-A-K535A, GC-A-D646A, WT-GC-B, GC-B-K551A, or GC-B-D662A with saturating concentrations of NP and increasing substrate concentrations in the presence or absence of 1mM ATP (Fig. 7A-F). ATP reduced the Michaelis constant of WT-GC-A 10.1-fold and reduced the Michaelis constant of WT-GC-B 10.6-fold consistent with previous reports (Fig. 7G) (*34*). In contrast, ATP failed to reduce the Km of the GC-A-K535A and GC-A-D646A (Fig. 7C, E) as well as GC-B-K551A and GC-B-D662A (Fig. 7D, F). These data indicate that ATP binding to the conserved binding site in the PKD of GC-A is required for allosteric activation of these enzymes.

To directly determine the effect of the ATP binding site mutations on ATP binding, the catalytic domain was removed from N-terminally FLAG-tagged versions of WT-GC-B and each mutant and the ability of 8-azido-2'/3'-biotinyl-ATP to bind to WT-GC-B and each mutant was assayed as originally described for ATP binding to the PKD of GC-A by De Lean and colleagues (*213*). Unfortunately, non-specific binding to each construct was too high to determine any changes in ATP binding (Fig. S1). We also employed the method used by Jaleel, et. al using soluble GC-A intracellular domain constructs bound to ATP-agarose (*220*). Unfortunately, control WT constructs did not demonstrate substantial binding to the ATP-agarose resin using effective ATP concentrations of 250μM. Furthermore, the weak binding observed was not reduced by the addition of 1mM ATP (Fig. S2). The lack of ATP binding in our assay is not surprising considering that the EC_{50} for activation of GC-A and GC-B by ATP is approximately 0.1mM (*34*). If this EC_{50} is indicative of the dissociation constant, then these results are not surprising and suggest that conventional non-equilibrium ATP-binding assays used for kinases are not likely to work for these enzymes with low affinity for ATP. Also, because mutations at the invariant lysine (K72 in PKA) have failed to inhibit ATP binding in other kinases (*221, 222*), two explanations for the loss of ATP-dependent functions are possible. The first is that mutations reduce binding to ATP, whereas the second possibility is that the mutation does not affect direct

ATP binding, but rather inhibits the ability of ATP to transfer the allosteric effects of ATP binding.

Mutations designed to rigidify the R- and C-spines in the PKD increase allosteric activation

Because large protein segments can contribute to enzyme dynamics, loss-of-function mutations can be misleading since amino acids that do not directly contribute to allostery can inhibit transfer of the allosteric signal. Therefore, we used gain of function mutations that increase the transmission of hypothesized signals through the PKD to test our argument that conserved allosteric mechanisms of the PKD participate in the regulation of these enzymes. In kinases and pseudokinases, the assembly and disassembly of R-spine and C-spine are important for the conformational dynamics that transmit the allosteric signal to the effector module (*56, 71, 73*). Therefore, we generated three individual mutants in these motifs, which are described below.

First, GC-A-A533W, and the analogous mutant, GC-B-A549W, contain a tryptophan for a C-spine alanine in the N-terminal lobe of the PKD (green sidechain in Fig. 8A). The increased bulk of the tryptophan side chain is hypothesized to partially fill the adenine binding pocket of the ATP binding site, which is envisioned to partially mimic an ATP-bound state and rigidify the C-spine. Others used a similar Ala-to-aromatic mutation at this site to engineer a kinase that is catalytically dead but capable of allosterically activating binding partners (*223*). As predicted, GC-A-A533W reduced the Km in the absence of ATP compared to the Km for WT-GC-A (Fig. 8B, C). These data are consistent with activation of GC-A and GC-B by transmission of the allosteric signal through the C-spine as described for other kinases and pseudokinases.

The second unique mutation, GC-B-M571F, lies at the RS3 position (Fig. 9A), which is the residue in both the αC-helix and the R-spine that upon assembly of the R-spine stabilizes the αC-helix in an active conformation (*224, 225*). GC-B-M571F is analogous to the BRAF L505F activating mutation (Table 1) (*224*). The R-spine residues in the N-lobe in GC-A and GC-B are similar to those found in the RAF kinases, which are located close to GC-A and GC-B in the phylogenetic tree of the human kinome (*55*). As predicted, we observed increased GC activity at sub-saturating CNP concentrations for GC-B-M571F mutant (Fig. 9B). Activity of the GC-B-M571F mutant was reduced but this was explained by reduced abundance of the completely processed form of the receptor indicated by arrowheads (Fig. 9B, inset). These data suggest that the EC_{50} for CNP activation of GC-B is modulated by the conformation of the αC-helix and that the R-spine is involved in transmitting the NP binding signal to the catalytic domains of GC-A and GC-B.

The third mutation is GC-B-I583W that is found immediately C-terminal to the final R-spine residue (RS4) and is positioned to strengthen interactions between the R and C spines (Fig. 10A). We hypothesize that this residue rigidifies and increases the transmission of both the ATP and the NP binding signals to the catalytic domain. Consistent with this notion, we observed increased GC activity from the GC-B-I583W by more than 300% in the presence of ATP alone compared to WT-GC-B. Saturating concentrations of CNP in the absence of ATP increased activity of the GC-B-I583W mutant almost 250% compared to WT-GC-B. However, activity measured for GC-B-I583W in the presence of saturating concentrations of ATP and CNP only mildly increased to 130% of WT-GC-B activity (Fig. 10B). Together, these data suggest that R-spines and the C-spines are present in GC-A and GC-B and function as allosteric regulatory modules as observed for *bona fide* kinases and pseudokinases.

DISCUSSION

PKDs are highly conserved from C. elegans to humans in the receptor GC family (*9, 42*), and phylogenetic data indicate that the PKD domains and GC domains coevolved (*16*). Despite being the first PKD to be identified (*70, 226*), the exact function of these domains in GCs has yet to be determined (*16*). Initial studies by Chinkers and Garbers reported that removal of the PKD from GC-A led to maximum activity of the enzyme in the absence ANP or ATP. Hence, they suggested that the PKD represses the GC domain (*40*). Subsequently, groups led by Sharma and DeLean reported that ATP binds the PKD but neither group determined exactly where ATP binds nor whether it uses the highly conserved ATP binding site in the PKD for this purpose (*212, 213*). The Van Den Akker group working on purified hinge-catalytic domain (*31*), and our group working on the full-length receptor (*32*), reported evidence of an additional allosteric site in the catalytic domain, which results in positive cooperativity or linear kinetics in the absence or presence of ATP, respectively. Thus, with multiple ATP-binding sites it has been particularly challenging to determine which effect of ATP is due to which ATP-binding site. For the first time, we used strategic loss-of-function coupled to gain-of-function mutations in the PKDs of GC-A and GC-B to demonstrate that these domains are conserved to allosterically stimulate catalytic activity in a manner consistent with the known ability of pseudokinase domains to allosterically affect other enzymatic activities (*227*).

ATP in broken cell preparations stimulates GC linked receptors by serving as a source of phosphate for the receptor phosphorylation by an unknown kinase as well as by binding an allosteric site that decreases the Michaelis constant (Km) of the receptor (*33, 34, 37*). The PKDs of GC-A and GC-B lack the catalytic Asp responsible for deprotonation of the substrate hydroxyl group, but other kinase domains lacking the same residue retain small amounts of phosphotransferase activity (*216, 217*). Thus, we investigated whether the PKDs in GC-A and GC-B contain phosphotransferase activity based on conservation of the canonical protein kinase domain. However, inactivation mutations in functionally critical residues failed to reduce the stoichiometry of phosphorylation of GC-A. Hence, we were unable to test the hypothesis suggesting that the PKDs of GC-A and GC-B possess intrinsic autophosphorylating protein kinase activity. Nonetheless, from these experiments, we can conclude that if GC-A and GC-B do contain phosphotransferase activity, they do not adhere to canonical kinase mechanisms because they show no requirement for three conserved residues (K72, D166 and D184 in PKA) that are critical for phosphate transfer for most protein kinases.

Results from GC assays are consistent with a critical role for ATP binding to the PKD in the allosteric stimulation of GC activity. It is unknown if the PKD retains its repressive function on the catalytic domain in the absence of the extracellular and transmembrane domains or if any repressive function can be relieved, so the intracellular constructs of GC-A used in our ATP-agarose assays may exist in a form which has even weaker affinity for ATP than the already weak EC_{50} of approximately 0.1 mM for ATP on the full-length enzymes. However, with intracellular concentrations of ATP in the 1-10 millimolar range, weak affinity is still sufficient to elicit full allosteric activity of the PKD's of GC-A and GC-B. Because we observed little or no difference in NP activation of WT or mutant enzymes but observed large decreases in the activation of the mutant enzymes by ATP, we conclude that the reduced activity of the mutant enzymes is due to reduced interactions with ATP, not due to destabilization of domain structure. Regarding the activating mutations, we observe that GC-A-A533W does not completely mimic the ATP-bound state. This is not surprising as the full effect of ATP binding in kinases includes electrostatic interactions involving the triphosphate tail that would not be accounted for by this tryptophan substitution. Furthermore, these proteins are known to be highly dynamic so we would not expect the tryptophan substitution to completely fill the adenine binding pocket, thus leaving the possibility for ATP binding despite a partially occluded active site. Because intracellular concentrations of ATP are generally high, we do not believe ATP concentrations are likely to be regulatory through this process. In contrast, we suggest that these ATP-dependent allosteric processes are required to reduce the Km of the enzymes to physiologic GTP concentrations of 0.1mM as a result of NP binding to the extracellular domain.

ATP also stimulates GC-C and GC-E. Both of these receptors contain PKDs that lack the catalytic base but retain the invariant lysine (K535 in GC-A) and the Mg^{2+}-chelating aspartate (D646 in GC-A) and are known to be activated by ATP in guanylyl cyclase assays mimicking physiologic conditions (*214, 220, 228, 229*). Furthermore, both the entire R-spine and C-lobe portion of the C-spine are both conserved in GC-C and GC-E. Substrate-velocity assays for GC-C revealed that the Vmax of the enzyme increased under both basal and peptide-stimulated conditions with the addition of ATP-γ-S with no change in Km as observed with GC-A and GC-B (*230*). This subtle difference in allosteric regulation is not surprising because the PKD of GC-C is not phosphorylated and cannot substitute for the PKD of GC-A in chimeric GC constructs (*13*). Additionally, the PKDs coevolved with the corresponding GC domains (*16*) indicating the PKD of GC-C evolved specific interactions to activate its own GC domain, not the GC domain in GC-A and GC-B. This suggests that mechanisms used by kinases and pseudokinases to allosterically

activate their partner proteins are used to transfer activation signals to the GC domains in the entire mammalian membrane GC receptor family, not only for GC-A and GC-B, although the exact mechanisms of allosteric signal transfer may differ between proteins.

Allostery in protein kinases occurs through changes in the dynamics of the protein that begin with large-scale motions involving key motifs like the R- and C-spines that are assembled and ultimately transition to more ordered, small-scale elements within the protein (*56, 71, 73*). Because many amino acids are involved in stabilizing the overall structure of a given protein, mutations in far-reaching segments of the protein may have negative effects on allosteric regulation through their effects on the overall stability and dynamics of the protein. As such, we emphasize mutations that were unlikely to impair the overall stability of the PKD and would promote allosteric functions in a manner consistent with what is known about other kinases and PKDs. For the first time, we designed activating mutations in GC-A and GC-B that mimic allosteric functions in known kinases and pseudokinases. This led to a model wherein the PKDs of GC-A and GC-B integrate allosteric inputs from ATP and NP's and provide a single, unified output to the catalytic domain based on the allosteric dynamics of the PKD. We hypothesize that in the basal state the PKD is dynamic, nonsynchronous, and has large-scale motions that preclude the catalytic domain from adopting the most active conformation. In the presence of both NP and ATP, the PKD transitions to more small-scale vibrations that increases the probability that the catalytic domain will adopt the most active conformation. Future mechanistic studies describing how the R-spine and C-spine interact with each other and are assembled in GC-A and GC-B may explain how known mutations activate or inactivate membrane GCs (*17, 151, 178, 214, 231*).

EXPERIMENTAL PROCEDURES

Reagents

Cyclic GMP RIA kit was from Perkin Elmer and cGMP Direct ELISA kit was from Enzo. NPs were from Sigma Aldrich. Protease inhibitors and microcystin were from Roche and Cayman Chemical Company, respectfully. 8-azido-ATP was from Jena Biosciences (Jena, Germany). Innova Biosciences γ-linked ATP-agarose was purchased from Novus Biologicals. The pSVL-GC-A-Δkin plasmid expressing the PKD deleted version of rat GC-A and the pSVL-FLAG-GC-A-INT plasmid expressing a soluble rat GC-A intracellular domain were kind gifts from Dr. Michael Chinkers at the University of South Alabama (*12*).

Homology Modeling of the PKD of GC-A and Alignment

A BLAST search identified the Src-family kinases as possessing some of the highest sequence similarity with the PKD sequence among human protein kinases. We therefore used the X-ray structure of the Src-family kinase Lck (PDB ID: 3LCK) to create a homology model of the pseudokinase domain, using the SWISS-MODEL server. The initial homology model spanned residues Gly^{516} in the putative G-loop of the PKD, through Phe^{772} in the terminal alpha helix of the domain (helix αI). The homology model is missing what would be the first beta strand of the kinase domain (prior to the G-loop), due to poor sequence homology in this region. This strand is conserved in eukaryotic protein kinases, and we noted that the absence of this segment in the PKD model leaves a hydrophobic surface exposed on the top of the N-terminal lobe of the PKD, comprised of residues F521, V534, Y527, C577, and L579, which are conserved in GC-As. To create a putative model for this N-terminal segment, which includes the known phosphorylation sites, we manually docked the corresponding segment from LCK (residues 239-253) into the homology model of the PKD using PyMOL and mutated the sequence to match that of the PKD. This speculative model of the N-terminal segment positions the regulatory phosphorylation sites immediately N-terminal to the PKD, on the back surface in the vicinity of the α C-helix, which is an allosteric hotspot in protein kinases. To generate the alignment (Fig. 2) we aligned the structures of PKA, BRAF, and LCK (PDBs: 1ATP, 1UWH, 3LCK, respectively) with the homology model of GC-A's PKD using the align function in PyMol. The sequence for the PKD of GC-B was aligned to GC-A using Clustal Omega (http://www.ebi.ac.uk/Tools/msa/clustalo/).

Cell culture and transfections

293T cells and were maintained and transfected using the calcium and phosphate method as previously described (*232*). Cos7 cells were maintained as previously described (*40*) and transfected using Lipofectamine 2000 from Invitrogen.

Guanylyl Cyclase assays

Cos7 cells were used when pSVL expression plasmids were used because proteins encoded by pSVL plasmids express better in Cos7 cells. 293T cells were used for all other experiments. Ten-cm plates of cells were washed twice with cold PBS and scraped into 600µl of phosphatase inhibitor buffer. Cells were lysed by sonication at 40% power for 5 seconds, then the insoluble membrane fraction was pelleted by centrifugation at 25,000 x *g* for 15 minutes. The supernatant was aspirated and membranes washed with 400µl phosphatase inhibitor buffer before being resuspended in phosphatase inhibitor buffer for GC assay. Activity assays were performed as described previously (*17*) using 20µl of prepared crude membranes, 20µl of a 5X activation mix containing the divalent metal (Mg^{2+}or Mn^{2+}) as well as any other activators used (ATP, ANP, CNP, or Triton X-100) and adding 60µl of prewarmed reaction cocktail to final reaction conditions of 25mM HEPES pH 7.4, 50mM NaCl, 500mM isobutyl-methyl-xanthine, 0.5µM microcystin, 1mM EDTA, 5mM creatine phosphate and 0.1µg/ml creatine kinase as a nucleotide triphosphate regeneration system, and 0.1% BSA. If not indicated, GTP and ATP concentrations were 0.1 mM and 1 mM, respectively. Cyclic GMP content in single-substrate concentration assays was determined by radioimmunoassay (*40*) or by ELISA by diluting NaOAc-buffered guanylyl cyclase assay samples in 0.1N HCl and following the manufacturer's instructions. Cyclic GMP content in substrate-velocity assays was determined by radioimmunoassay as previously described (*32*) or by purification followed by ELISA estimation of cGMP concentrations. Substrate Velocity assays tested by ELISA were terminated in 110mM ZnOAc and 110 mM Na_2CO_3 and purified on acidified alumina as previously described (*233*) with the exception of eluting in 3ml 200mM ammonium formate to separate ATP and GTP from cGMP. Eluent was used undiluted in ELISA measurements according to manufacturer's instructions with the exception of being performed in 200mM ammonium formate rather than 0.1N HCl. Data were normalized to a control value [Vmax for WT GC-A (1mM ATP)] in Fig 8 due to variations in transfection efficiency. To remove this confounding error associated with transfection efficiency and preserve all differences due to the treatments or mutations we expressed all activity data in Fig 8B as a percentage of the Vmax for WT-GC-A (1mM ATP).

Immunoprecipitations, SDS-PAGE, and Gel staining

Transfected cells from the indicated number of 10-cm plates were lysed in 1ml per 10-cm plate of immunoprecipitation buffer (*37*) containing protease and phosphatase inhibitors, aliquots of pre-cleared lysates were taken for loading controls, and the indicated proteins were immunoprecipitated with 2µl of rabbit 6325 antiserum per 10-cm plate for GC-A proteins or 2µl of rabbit 6327 antiserum per 10-cm plate for GC-B proteins and 25µl of a 50% slurry of Protein-A-agarose beads per 10-cm plate overnight. The beads were washed three times with immunoprecipitation buffer lacking NaCl. After boiling for 5 minutes in 2X reducing sample buffer, samples were fractionated on 8% resolving gels. The gel was first stained with ProQ-Diamond and then stained with SYPRO Ruby protein stain as previously described (*17*). Lysates used for full length GC-A or GC-B western blots were fractionated on 8% resolving gels and lysates used for β-actin or soluble GC-A intracellular domains were fractionated on 10% resolving gels.

Western Blotting

Resolving gels were blotted to an Immobilon-FL PVDF membrane. Membranes were blocked with Odyssey Blocking Buffer diluted 1:1 with PBS and probed with either a 1:5000 dilution of rabbit 6325 antiserum for GC-A western blots or rabbit 6327 antiserum for GC-B western blots followed by 1:15,000 goat anti-rabbit IRDye 680-conjugated secondary antibody. FLAG western blots were probed using a 1:5000 dilution of FLAG-M2 monoclonal antibody followed by 1:15000 goat anti-mouse IRDye 800-conjugated secondary antibody. Actin western blots were probed using a 1:2000 dilution of a monoclonal mouse β-actin antibody (Sigma) followed by 1:15000 goat anti-mouse IRDye 800-conjugated secondary antibody. All western blots were visualized on a LiCor instrument as described previously (*234*).

Densitometry and ratio calculations

Images from gel staining and western blotting were quantified in LiCor ImageStudio. Ratios of arbitrary units were calculated by dividing the ProQ-Diamond signal by the SYPRO Ruby signal from the same band on the same gel.

Statistical analysis

All statistical analysis was performed in Graphpad Prism. Differences among measured values in groups of two were analyzed by unpaired t-test. Differences among measured values in groups of

three or more were analyzed first by ANOVA or two-way ANOVA (if multiple variables were present in the experiment) to determine if any significant differences are present in the data. We then computed specific *p*-values of any significant differences using Tukey's test to correct for multiple comparisons. $p < 0.05$ were considered significant. *, **, and *** indicate statistical significance at $p<0.05$, $p<0.01$, and $p<0.005$ respectively.

SUPPLEMENTARY MATERIALS AND METHODS

8-Azido-2'/3'-Biotinyl-ATP Synthesis and Binding

Biotin was esterified to the ribose ring of 8-azido-ATP similar to the method used by Schafer and de Lean with the following modifications (*213, 235*). A 2.5-fold molar excess of carbonyldiimidazole over biotin was used to activate the biotin carboxyl group, and 8-azido-ATP was added as a 10mM stock in buffer as supplied by Jena Biosciences with a 22.5-fold molar excess of biotin over 8-azido-ATP. The reaction was allowed to incubate until precipitates were clarified into solution. No further reaction was observed after this point. The completed reaction was purified by HPLC using a 1.5x15cm column of AGMP-1(anion exchange resin) and a concave-upward gradient of trifluoroacetic acid from 3-300mM at 3ml/minute over 60 minutes. The eluted nucleotides were detected using a Beckman 166 UV detector set at 280nm. The biotinylated product eluted at 56.1 minutes and was collected and dialyzed against ultrapure water in 500 MWCO dialysis tubing at 4^0C to remove trifluoroacetic acid. After dialysis, samples were lyophilized and stored at -20ºC until use. Unreacted 8-azido ATP was collected (elution time 48.1 minutes), dialyzed as above, and used for further rounds of synthesis and purification of the biotinylated product. By analysis of HPLC peak intensities, the reactions yielded 40% product. Membranes were prepared from transfected 293T cells and resuspended in a binding buffer consisting of 50mM HEPES pH 7.4, 100mM NaCl, 50mM NaF, 0.5µM CNP, 20% glycerol, 2mM MgCl2, 1µM Microcystin-LR, 1x Roche Complete Protease Inhibitors, and with or without 1mM ATP. Samples were incubated at room temperature 1 hour to allow hormone binding and competitive ATP binding, then 100µM 8-azido-2'/3'-biotinyl-ATP was added. Samples were vortexed briefly and incubated on ice for 10 minutes before crosslinking in a Stratalinker 2400 for 3 minutes. The samples were centrifuged at 25K x g for 15 minutes at 4ºC to pellet the membranes, supernatants were aspirated, and pellets were solubilized in 1ml immunoprecipitation buffer. Solubilized samples were immunoprecipitated overnight using 20µl of FLAG-M2-agarose beads, fractionated by SDS-PAGE, and samples were split to run on two identical 8% resolving gels. Both gels were transferred to Immobilon-FL PVDF membrane and blocked with Odyssey Blocking Buffer diluted 1:1 with PBS. One blot detected total protein abundance by blotting against the N-terminal FLAG epitope as described above, and one-blot detected biotin using a 1:2000 LiCor IRDye-800 Streptavidin in blocking buffer plus 0.15% Tween-20 and 0.08% SDS.

ATP-agarose binding assay

Soluble FLAG-tagged intracellular domain samples of wild type GC-A were prepared by detaching transiently transfected Cos7 cells from four 10-cm plates per construct using PBS supplemented with 5mM EDTA for 10 minutes at 37ºC. Total lysate controls were prepared by solubilizing one 10-cm plate in RIPA buffer as with the immunoprecipitations. Intact cells in PBS/EDTA were pelleted by centrifugation at 300x*g* for 3 minutes. Supernatants were aspirated and the cell pellet resuspended in ATP-agarose interaction buffer (50mM HEPES pH 7.4, 150mM NaCl, 10mM $MgCl_2$). Cells were lysed by sonication for 10 seconds at 40% power. The insoluble fraction was pelleted by centrifugation at 25K x *g*, and the soluble fraction used for further analysis. Endogenous ATP from cells was removed using Pall Nanosep 10K MWCO spin filters to retain our protein of interest but elute ATP in the flow through. Successive rounds of concentration and dilution in the same ATP-agarose interaction buffer were used until 99% of the endogenous ATP had been removed. Buffer exchanged soluble fraction was incubated with ATP-agarose resin (effective ATP concentration = 250μM) with or without the addition of 1mM ATP for 90 minutes at 4ºC with rotation. Agarose beads were briefly washed with ATP-agarose interaction buffer prior to boiling in 2x reducing sample buffer for fractionation by SDS page. The appropriate band was verified by western blotting against the GC-A C-terminus in whole cell lysates and soluble fraction of GC-A transfected cells where it is expected to be present, and in the insoluble fraction of GC-A transfected cells or lysates from GFP-transfected cells where it is not expected to be present. Buffer exchange controls to demonstrate the retention of the GC-A intracellular constructs were further verified by western blotting against the N-terminal FLAG epitope. The band was detected at 60 kDa in agreement with its published molecular weight (*12*).

FIGURES AND TABLES

Figure 1. The regulatory and catalytic spines and residues that directly bind and transmit the allosteric ATP-binding signal in PKA are conserved in the PKD of GC-A.

A. Homology modeling demonstrates that all of the residues that interact with ATP in the active site (red) except for the catalytic base (D166) in PKA, which is N628 in GC-A (yellow), are conserved in GC-A. **B.** The residues composing the regulatory (red) and catalytic (green) spines as well as the shell (blue) in PKA are also conserved in PKD of GC-A. The F-helix is depicted in yellow. **C.** Serines and threonines mutated in non-phosphorylated or phosphomimetic constructs are indicated with their position numbers. Ser/Thr in red are phosphorylation sites that were chemically determined (*103*). The sites in blue were identified by a functional screen (*27*).

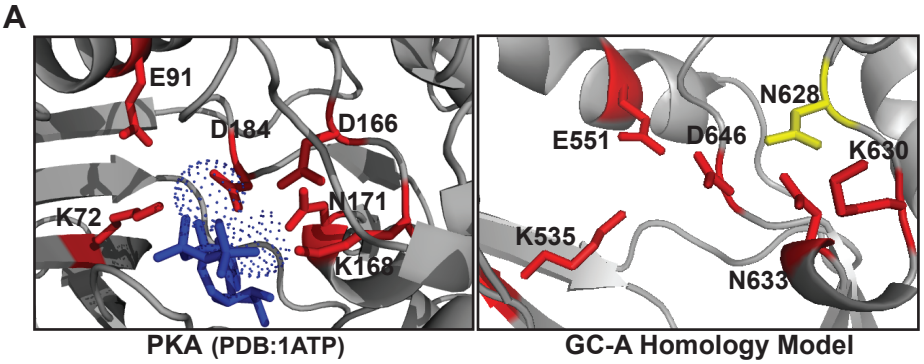

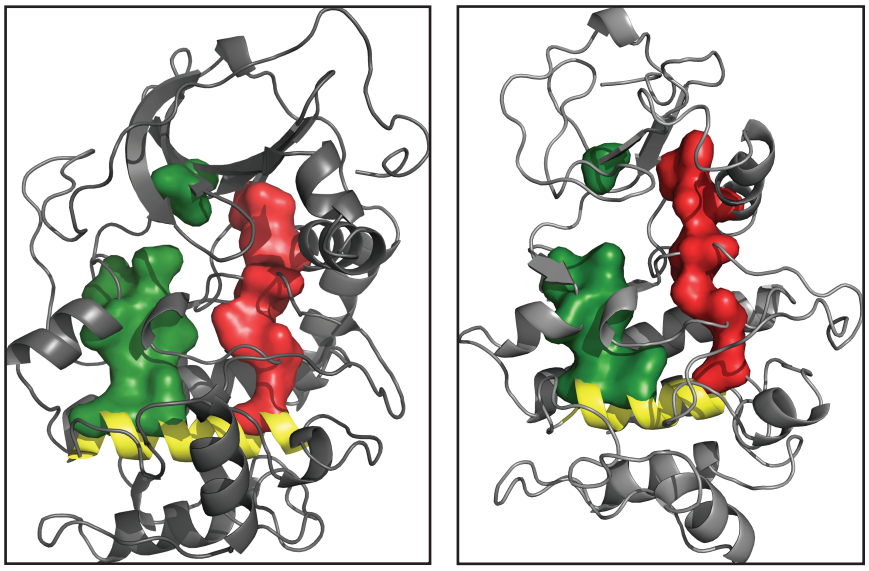

C

```
                 473                 487                 497 500 502     506     510 513
GC-A  SELWRVRWEDLQPSSLERHLRSAGSRLTLSGRGSNYGSLLT
GC-B  SMLWRIRWEELQFGNSDRYHKGAGSRLTLSLRGSSYGSLMT
                 489                 513 516 518     523     526 529
```

Figure 2. Structural alignment of the PKD of GC-A with crystal structures from other kinases.

The homology model of the PKD of GC-A and the structures of PKA, BRAF, and LCK were aligned in PyMol. A linear representation of this structural alignment is shown with secondary structure features annotated above the alignment and specific residues numbered in Table 1 for the R-spine (red), C-spine (cyan), and ATP-interacting amino acids (gray) highlighted.

```
                    β1----      β2--------    β3------
PKA   32    TPSQNTAQLDQFDRIKTLGTGSFGRVM--LVKHKESGNHYAMKILD-K-QKVVKL  82
BRAF  447   --DDWEIPDGQITVGQRIGSGSFGTVY--KGKWH---GDVAVKML--N-VTAPTP  491
LCK   234   WEDEWEVPRETLKLVERLGAGQFGEVW--MGYYNGH-TKVAVKSL--KQGSM-SP  282
GC-A  496   GSRLTLSGRGSNYGSLLTTEGQFQ-VFAKTAYYKGN-L-VAVKRVNRKRIEL-TR  546
GC-B  512   GSRLTLSLRGSSYGSLMTAHGKYQ-IFANTGHFKGN-V-VAIKHVNKKRIEL-TR  562

            αC--------------        β4----   β5----      αD--------
PKA   83    KQIEHTL-NEKRILQAVNFPFLVKLEFSFKDNSNLYMVMEYVPGGEMFSHLR-RI  135
BRAF  492   QQLQA-FKNEVGVLRKTRHVNILLFMGYST-KPQLAIVTQWCEGSSLYHHLHIIE  544
LCK   283   ---DAFL-AEANLMKQLQHQRLVRLYAVVT-QEPIYIITEYMENGSLVDFLK-TP  331
GC-A  547   ---KV-L-FELKHMRDVQNEHLTRFVGACTDPPNICILTEYCPRGSLQDILE-NE  595
GC-B  563   ---QV-L-FELKHMRDVQFNHLTRFIGACIDPPNICIVTEYCPRGSLQDILE-ND  611

                αE------------------   β6--       β7----- β8---
PKA   136   -G-RFSEPHARFYAAQIVLTFEYLHSLDLI-YRDLKPENLLIDQQGYIQVTDFGF  187
BRAF  545   T--KFEMIKLIDIARQTAQGMDYLHAKSII-HRDLKSNNIFLHEDLTVKIGDFGL  596
LCK   332   SGIKLTINKLLDMAAQIAEGMAFIEERNYI-HRDLRAANILVSDTLSCKIADFGL  385
GC-A  596   S-ITLDWMFRYSLTNDIVKGMLFLHNGAICSHGNLKSSNCVVDGRFVLKITDYGL  649
GC-B  612   S-INLDWMFRYSLINDLVKGMAFLHNSIISSHGSLKSSNCVVDSRFVLKITDYGL  665

            Act. Loop----- P+1 Loop---                αF----------
PKA   188   AKRV-KG----RTWTLCGTPEYLAPEIILSKG---Y----NKAVDWWALGVLIYE  230
BRAF  597   ATVKSRWSGSHQFEQLSGSILWMAPEVIRMQDKNPY----SFQSDVYAFGIVLYE  647
LCK   386   ARLI-EDNEYTAREGAKFPIKWTAPEAIN-YG--TF----TIKSDVWSFGILLTE  432
GC-A  650   ESFR-D-LDPEQGHTVYAKKLWTAPELLRMAS---PPVRGSQAGDVYSFGIILQE  699
GC-B  666   ASFR-STAEPDDSHALYAKKLWTAPELLSGNP---LPTTGMQKADVYSFGIILQE  716

            ---              αG-------                  αH--------
PKA   231   MAA--GYPPFF-ADQ-PIQIYEKIVSG-K-VRF-PS----HF-S-SDLKDLLRNL  272
BRAF  648   LMT--GQLPYSNINN-RDQIIFMVGRGYLSPDLSKV----RSNCPKAMKRLMAEC  695
LCK   433   IVTH-GRIPYPGM-T-NPEVIQNLERG-YRMVR-PD----NC-P-EELYQLMRLC  478
GC-A  700   IALRSGVFHVEGLDLSPKEIIERVTRGEQPPFR-PSLALQSH-L-EELGLLMQRC  751
GC-B  717   IALRSGPFYLEGLDLSPKEIVQKVRNGQRPYFR-PSIDRTQL-N-EELVLLMERC  768

                      αI-------
PKA   273   LQVDLTKRFGNLKNGVNDIKNHKWFAT  299
BRAF  696   LKKKRDERP-----LFPQILASIELLA  717
LCK   479   WKERPEDRP-----TFDYLRSVLEDFF  500
GC-A  752   WAEDPQERP-----PFQQIRLTLRKFN  773
GC-B  769   WAQDPAERP-----DFGQIKGFIRRFN  790
```

Figure 3. Decreased NP-dependent guanylyl cyclase activity in Lys and Asp mutants is not explained by changes in protein abundance or phosphorylation.

A. Guanylyl cyclase activity measured in membranes from transfected 293T cells for 5 minutes in the presence of 100µM GTP, 1 µM ANP, 1mM ATP, and 5mM $MgCl_2$ (ANP/ATP) or 1% Triton X-100 and 5mM $MnCl_2$ (Mn^{2+}/Triton) stimulation. *n* = 8 independent experiments. **B.** Guanylyl cyclase activity measured in membranes from transfected 293T cells for 5 minutes in the presence of 100µM GTP, 1 µM CNP, 1mM ATP, and 5mM $MgCl_2$ (ANP/ATP) or 1% Triton X-100 and 5mM $MnCl_2$ (Mn^{2+}/Triton) stimulation. *n* = 3 independent experiments. **C.** ProQ Diamond Phosphopreotein Gel Stain and SYPRO Ruby Protein Gel Stain of immunoprecipitated wild type and mutant GC-A, and immunoblot (IB) of the same samples used for GC activity assays in A. The arrowhead indicates the fully processed form of GC-A. Data are representative of *n* = 7 independent experiments. **D.** ProQ Diamond Phosphopreotein Gel Stain and SYPRO Ruby Protein Gel Stain of immunoprecipitated wild type and mutant GC-B, and immunoblot of the same samples used for GC activity assays in B. The arrowhead indicates the fully processed form of GC-B. Data are representative of *n* = 3 independent experiments. **E.** Gel staining images from experiments in C were quantified using Image Studio Lite, and ratios were calculated by dividing the ProQ Diamond intensity by the SYPRO Ruby intensity. *n* = 7 independent experiments. **F.** Gel staining images from experiments in C were quantified using Image Studio Lite, and ratios were calculated by dividing the ProQ Diamond intensity by the SYPRO Ruby intensity. *n* = 3 independent experiments. Error bars represent the SEM.

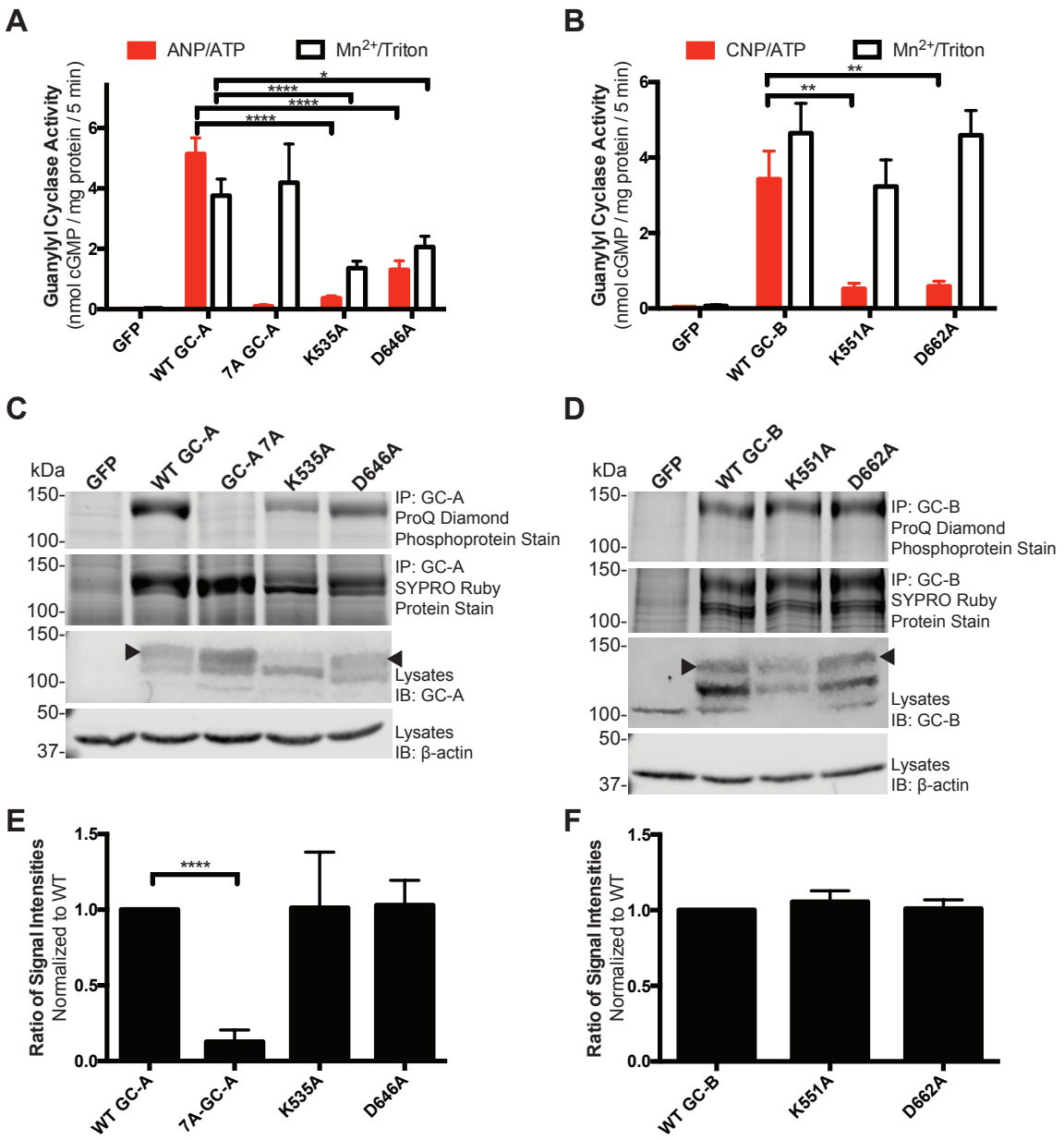
A
ANP/ATP
Mn2+/Triton
Guanylyl Cyclase Activity
(nmol cGMP / mg protein / 5 min)
GFP
WT GC-A
7A GC-A
K535A
D646A
B
CNP/ATP
Mn2+/Triton
Guanylyl Cyclase Activity
(nmol cGMP / mg protein / 5 min)
GFP
WT GC-B
K551A
D662A
C
kDa
GFP
WT GC-A
GC-A 7A
K535A
D646A
IP: GC-A
ProQ Diamond
Phosphoprotein Stain
IP: GC-A
SYPRO Ruby
Protein Stain
Lysates
IB: GC-A
Lysates
IB: β-actin
D
kDa
GFP
WT GC-B
K551A
D662A
IP: GC-B
ProQ Diamond
Phosphoprotein Stain
IP: GC-B
SYPRO Ruby
Protein Stain
Lysates
IB: GC-B
Lysates
IB: β-actin
E
Ratio of Signal Intensities
Normalized to WT
WT GC-A
7A-GC-A
K535A
D646A
F
Ratio of Signal Intensities
Normalized to WT
WT GC-B
K551A
D662A

Figure 4. The GC-B-K551A mutant has reduced CNP-dependent GC activity that is not explained by changes in phosphorylation or protein levels.

A. GC activity measured in membranes from 293T cells transfected with the indicated GC-B receptors for 5 minutes with 0.1 mM GTP, 1µM CNP, 1mM ATP, and 5mM $MgCl_2$ (CNP/ATP) or with 1% Triton X-100 and 5mM $MnCl_2$ (Mn^{2+}/Triton) stimulation. n = 5 independent experiments. (**B**) Immunoblot (IB) against GC-B showing abundance of GC upper band (indicated with arrowhead) to indicate even expression. Data are representative of n = 3 experiments. Error bars represent the SEM.

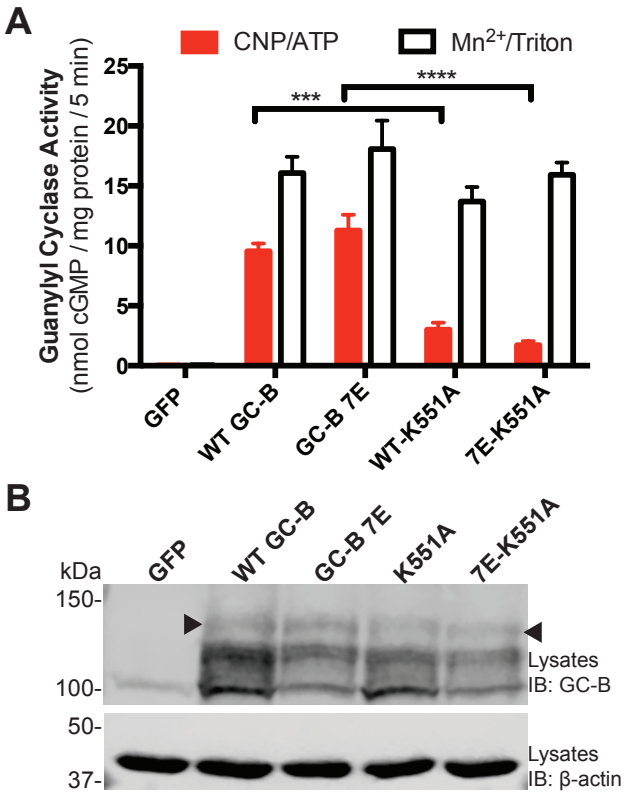

Figure 5. Conserved Lys and Asp residues in PKD's are required for activation of GC-A and GC-B by ATP but not NP.

A. GC activity measured in membranes from 293T cells transfected with wild type GC-A for 10 sec, 2 minutes, or 10 minutes with 0.1 mM GTP in the presence of 5mM $MgCl_2$ (Basal), 1µM ANP and 5mM $MgCl_2$ (ANP), or 1µM ANP, 1mM ATP, and 5mM $MgCl_2$ (ANP/ATP) stimulation. The inset displays the basal and ANP activity. *n* = 3 independent experiments. **B.** GC activity measured in membranes from 293T cells transfected with WT-GC-B for 10 sec, 2, or 10 minutes with 0.1 mM GTP in the presence of 5mM $MgCl_2$ (Basal), 1µM CNP and 5mM $MgCl_2$ (CNP), or 1µM CNP, 1mM ATP, and 5mM $MgCl_2$ (CNP/ATP) stimulation. The inset displays the basal and ANP activity. *n* = 3. **C.** GC activity measurements as in A for GC-A K535A. *n* = 3 independent experiments. **D.** GC activity measurements as in B for GC-B-K551A. *n* = 3 independent experiments. **E.** GC activity measurements as in A for GC-A-D646A. *n* = 3 independent experiments. **F.** GC activity measurements as in B for GC-B-D662A. *n* = 3 independent experiments. **G.** Fold Stimulation by ATP was calculated by dividing activity from A, C, and E measured with ANP and ATP by activity measured with only ANP and plotted as a function of time. *n* = 3 independent experiments. **H.** Fold Stimulation by ATP was calculated by dividing activity from B, D, and F measured with CNP and ATP by activity measured with only CNP and plotted as a function of time. *n* = 3 independent experiments. **I.** Fold Stimulation by ANP was calculated by dividing activity from A, C, and E measured with ANP alone by activity measured without ANP or ATP and plotted as a function of time. *n* = 3 independent experiments. **J.** Fold Stimulation by CNP was calculated by dividing activity from B, D, and F measured with CNP alone by activity measured without CNP or ATP and plotted as a function of time. *n* = 3 independent experiments. Error bars represent the SEM.

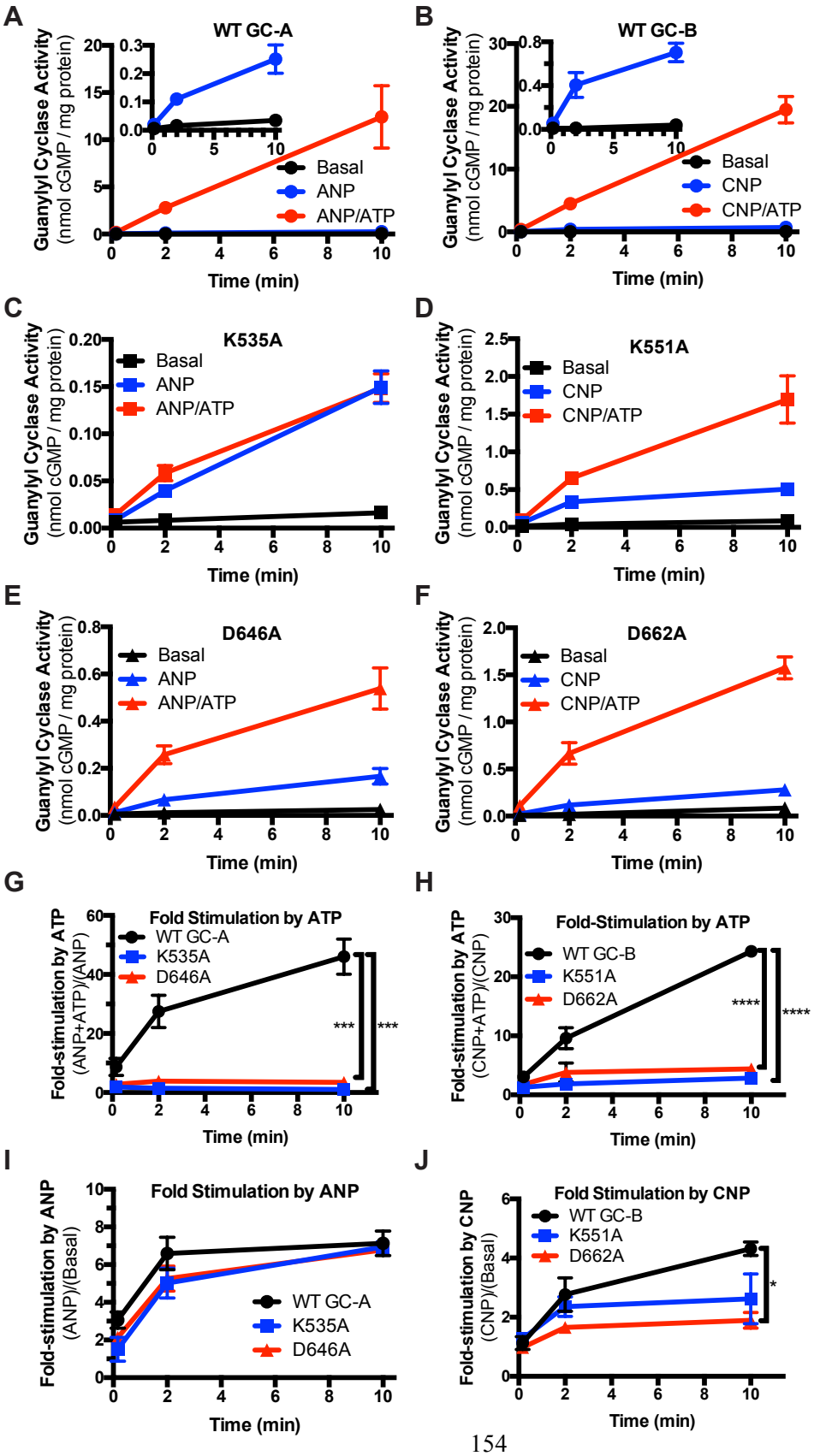
A
WT GC-A
Guanylyl Cyclase Activity
(nmol cGMP / mg protein)
Basal
ANP
ANP/ATP
Time (min)
B
WT GC-B
Basal
CNP
CNP/ATP
C
K535A
D
K551A
E
D646A
F
D662A
G
Fold Stimulation by ATP
Fold-stimulation by ATP
(ANP+ATP)/(ANP)
WT GC-A
K535A
D646A
***
H
Fold-Stimulation by ATP
(CNP+ATP)/(CNP)
WT GC-B
K551A
D662A
****
I
Fold Stimulation by ANP
Fold-stimulation by ANP
(ANP)/(Basal)
J
Fold Stimulation by CNP
Fold-stimulation by CNP
(CNP)/(Basal)
*

Figure 6. A GC-A mutant lacking the pseudokinase domain contains a cooperative, ATP binding, allosteric site.

A. GC activity measured in membranes from transfected Cos7 cells for 5 minutes with increasing concentrations of GTP in the presence of 1µM ANP and 5mM $MgCl_2$ with or without the addition of 1mM ATP. *n* = 4 independent experiments. **B.** An enlarged portion of A to better demonstrate the concave upward shape of the activity curve observed without ATP. *n* = 4 independent experiments. **C.** A table showing the measured hill slope (h) and K_{half} of the plots in A and B in the absence and presence of ATP and their respective *p*-values. Error bars represent the SEM.

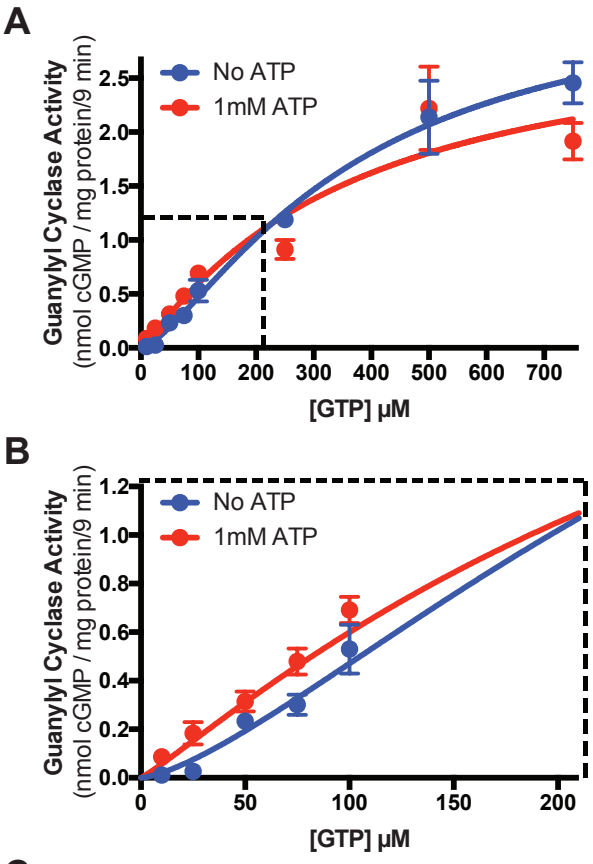

C

	No ATP	1mM ATP	*p*-value
h	1.452	1.146	0.018
Khalf (µM)	378.3	361.5	ns

Figure 7. The Lys and Asp mutations increase the Michaelis constants for GC-A and GC-B. **A.** GC activity measured in membranes from 293T cells transfected with wild type GC-A for 5 minutes with increasing concentrations of GTP, 5mM $MgCl_2$ and 1µM ANP with or without 1mM ATP. *n* = 4 independent experiments. **B.** GC activity measured in membranes from 293T cells transfected with WT-GC-B for 5 minutes with increasing concentrations of GTP, 5mM $MgCl_2$ and 1µM CNP with or without 1mM ATP. *n* = 3 independent experiments. **C.** GC activity as in A for GC-A-K535A. *n* = 4 independent experiments. **D.** GC activity as in B for GC-B-K551A. *n* = 3 independent experiments. **E.** GC activity as in A for GC-A-D646A. *n* = 4 independent experiments. **F.** GC activity as in B for GC-B-D662A. *n* = 3 independent experiments. **G.** A table showing the measured Michaelis constants in the absence and presence of ATP and their associated *p*-values. Error bars represent the SEM.

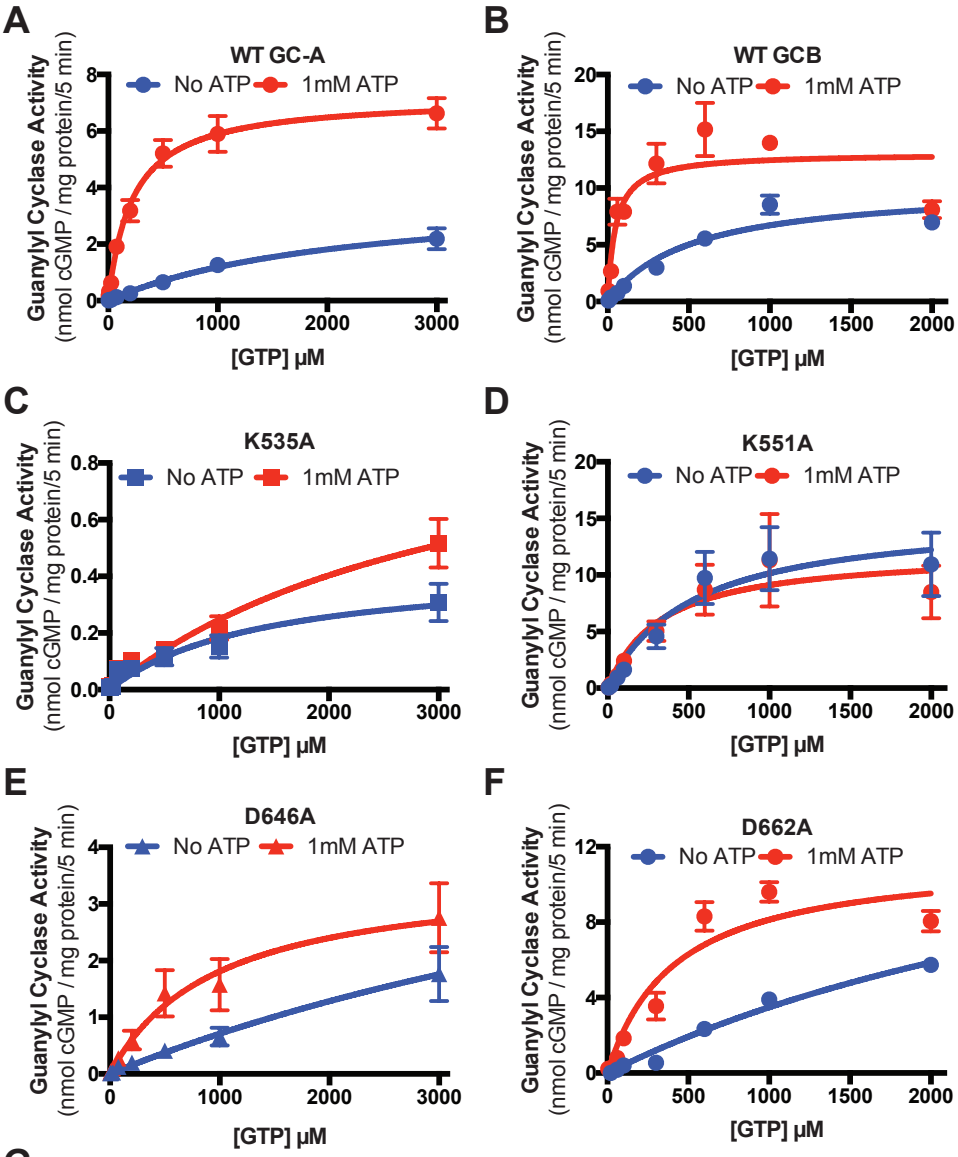

G

		WT GC-A	K535A	D646A	WT GC-B	K551A	D662A
Km (SEM) µM	**No ATP**	2236 (457.7)	1874 (611.4)	7620 (1780)	609.6 (67.47)	437.3 (82.75)	4750 (1725)
	1mM ATP	251.5 (48.85)	5450 (2749)	1341 (493.4)	59.60 (3.163)	361.8 (53.90)	425.9 (134.7)
	***p*-value**	0.0478	ns	ns	0.0146	ns	ns

Figure 8. The GC-A-A533W mutation partially mimics the ATP bound state of GC-A. **A.** A model demonstrating how ATP (orange) rigidifies the C-spine in PKA and how the Trp in GC-A-A533W (A533:space-filling/chartreuse, A533W:sticks) docks into the same pocket. **B.** Substrate-velocity assays measured in membranes from transfected 293T cells for 5 minutes with increasing GTP concentrations, 5mM $MgCl_2$ and 1µM ANP with or without 1mM ATP. $n = 4$ independent experiments. **C.** A table showing the measured Michaelis constants and their associated *p*-values. Error bars represent the SEM.

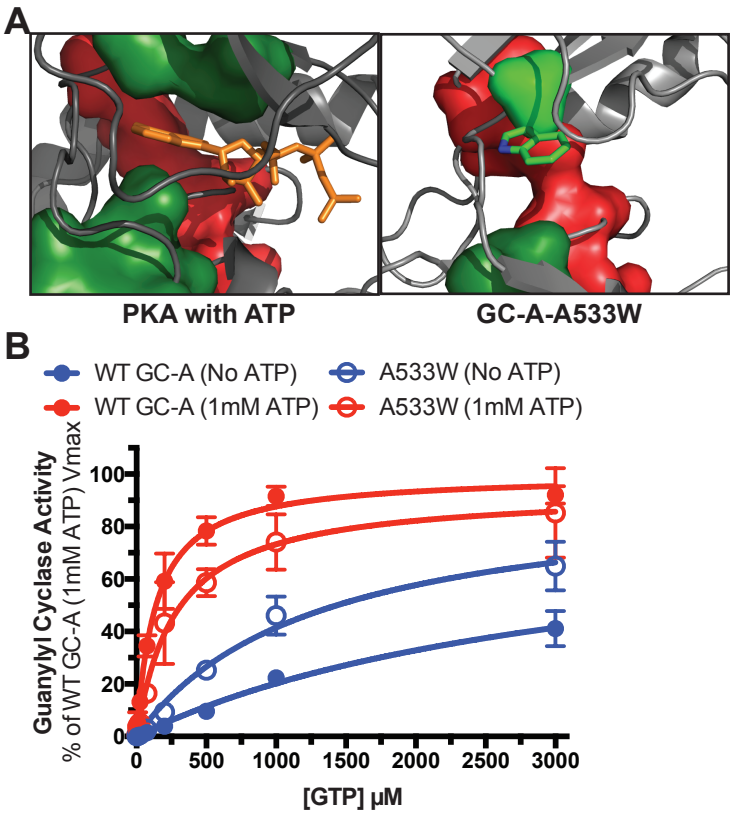

C

	WT GC-A	A533W	*p*-value
Km (SEM) µM			
No ATP	3762	1335	0.014
1mM ATP	140.8	283.2	ns

Figure 9. The GC-B-M571F mutation increases GC activity at sub-saturating concentrations of CNP.

A. A homology model indicating the location of M571F in the R-spine and C-helix. The R-spine residues RS2, RS3, and RS4 are red with red mesh surfaces. The RS3 mutant is yellow. **B.** GC activity measured in membranes from transfected 293T cells for 5 minutes with 0.1mM GTP, 5 mM $MgCl_2$, 1mM ATP and 0 nM (Basal), 50 nM or 1000 nM CNP. *n* = 3 independent experiments. Inset: GC-B Immunoblot shows that the upper species denoted by arrowheads in the GC-B-M571F mutant is reduced in accordance with the corresponding reduction GC activity measured with 1000 nM CNP. *n* = 3 independent experiments. Error bars represent the SEM.

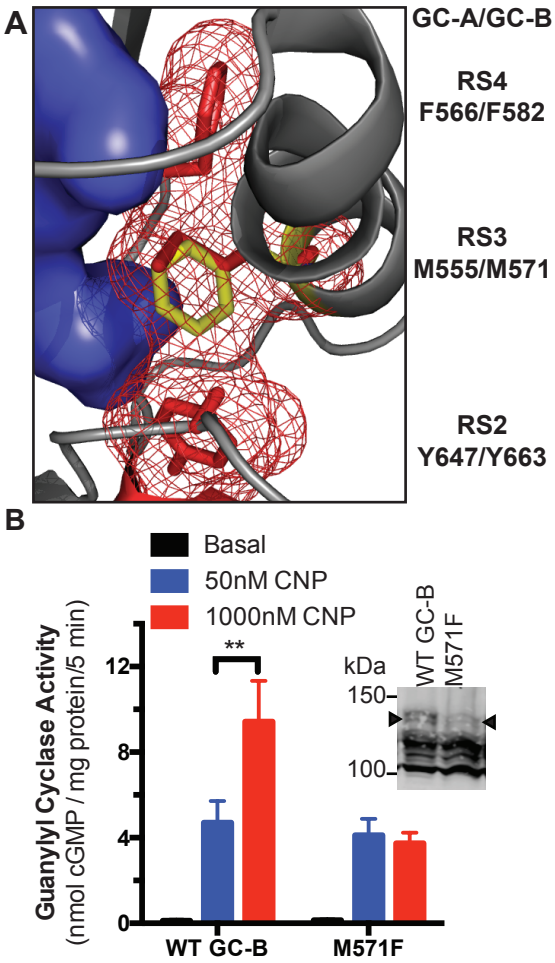

Figure 10. The GC-B-I583W mutation increases stimulation by either ATP or ANP alone. **A.** A homology model of GC-A shows the location of the V567W substitution that is analogous to the I583W substitution in GC-B. Yellow spheres represent the substituted Trp. This model suggests that the substituted Trp serves as a bridge between the R- and C-spines and increases activity of GC-B in the absence of either CNP or ATP. **B.** GC activity measured in membranes from transfected 293T cells for 5 minutes with 0.1mM GTP and 5 mM $MgCl_2$, under the indicated conditions. For $Mn^{2+/}$Triton conditions, 5 mM $MnCl_2$ was substituted for 5 mM $MgCl_2$. n = 3 independent experiments. Error bars represent the SEM.

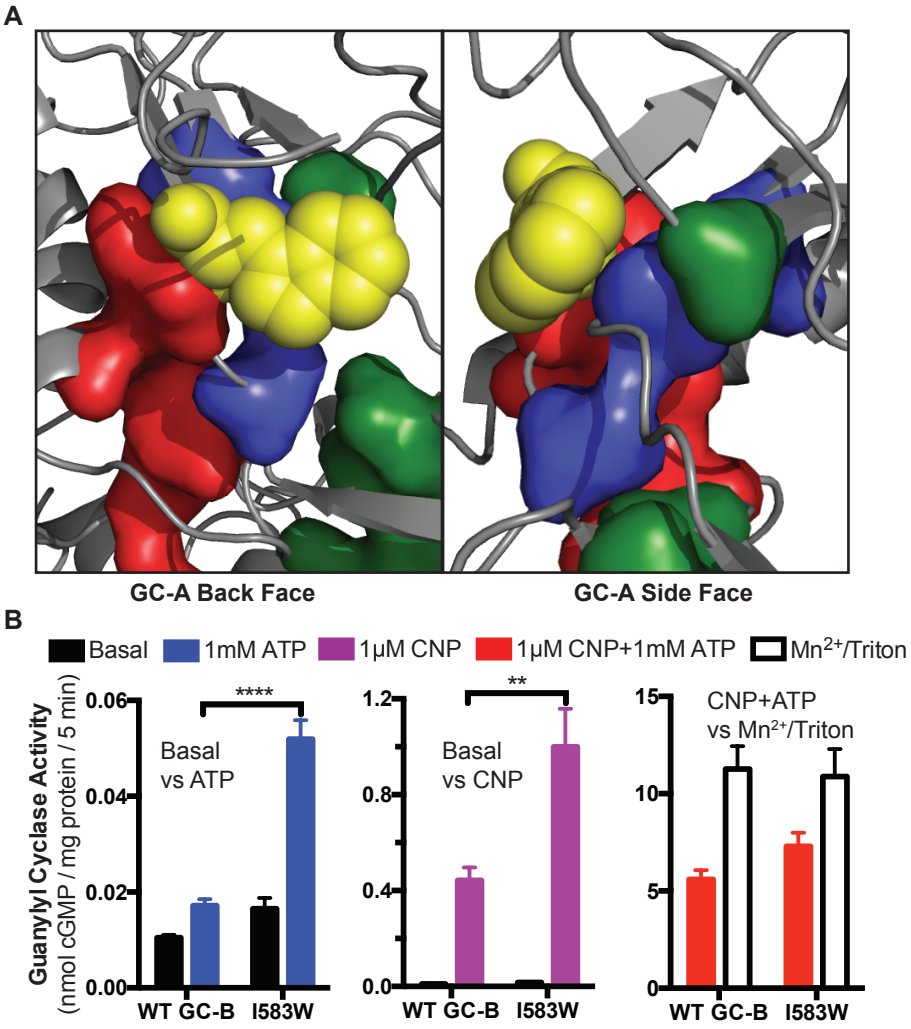

Table 1. Amino acids that are important for ATP binding and allosteric transmission of the ATP binding signal are conserved between PKA and GC-A and GC-B. PKA is an example of a Ser/Thr kinases. BRAF is an example of a Tyr-like Ser/Thr kinases, and Lck is an example of a Tyr kinases and was the source of the homology model.

PKA	BRAF	Lck	GC-A	GC-B
ATP-Interacting Amino Acids				
K72	K483	K273	K535	K551
E91	E501	E288	E551	E567
D166	D576	D364	N628	S644
K168	K578	R366	K630	K646
N171	N581	N369	N633	N649
D184	D594	D382	D646	D662
Regulatory (R)-Spine				
L106 (RS4)	F516	L303	F566	F582
L95 (RS3)	L505	M292	M555	M571
F185 (RS2)	F595	F383	Y647	Y663
Y164 (RS1)	H574	H362	H626	H642
D220 (RS0)	D638	D422	D689	D706
Catalytic (C)-Spine				
V57	V471	V259	L511	L527
A70	A481	A271	A533	A549
M128	L537	L324	L588	L604
L172	I582	I370	C634	C650
L173	F583	L371	V635	V651
I174	L584	V372	V636	V652
L227	V601	L429	I696	I713
M231	L605	I433	I700	I717

Supplementary Figure S1. 8-azido-2'/3'-biotinyl-ATP binding.

Membranes from 293T cells transiently transfected with the indicated constructs were incubated with 1µM ANP and 250µM 8-azido-2'/3'-biotinyl-ATP and crosslinked under UV light (300mJ/sample). Membranes were then solubilized and GC-B was immunopurified using the N-terminal FLAG epitope and fractionated by SDS-PAGE. ATP binding was visualized by a Streptavidin-IRDye-800CW conjugate. Protein content was visualized by western blotting against the FLAG epitope. Data are representative of $n = 5$ independent experiments.

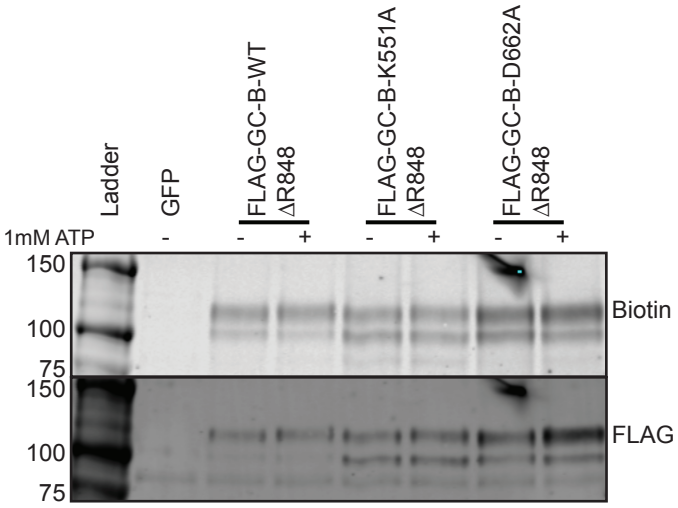

Supplementary Figure S2. ATP-agarose interaction assay.

A. Western blot of wild type GC-A soluble intracellular domains to verify solubility of the protein and specificity of the western blotting. Data are representative of *n* = 3 independent experiments. **B.** Western blot of endogenous ATP removal by 10K MWCO spin filtration. Data are representative of *n* = 3 independent experiments. **C.** Western blot of wild type and K535A ATP-Agarose pulldown samples including a competition by 1mM ATP. Data are representative of *n* = 3 independent experiments.

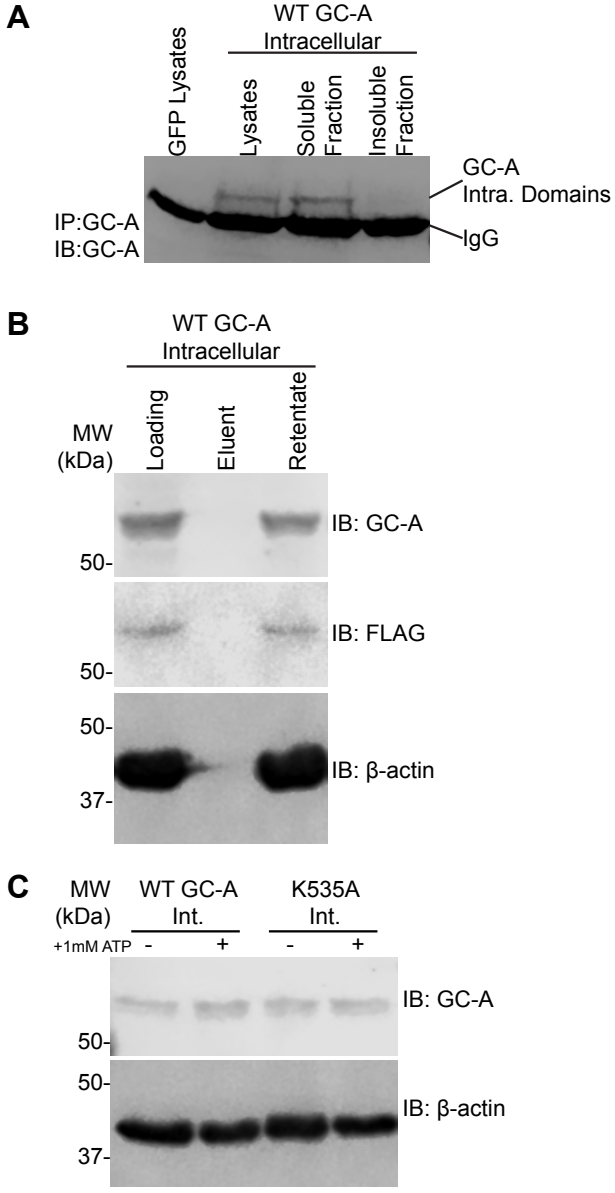

CHAPTER 7:
Conclusions and Future Directions

CONCLUSIONS

My first project in the laboratory involved an ongoing collaboration with Dr. Laurinda Jaffe's laboratory at the University of Connecticut Health Center. Here, we investigated the role and regulation of GC-B in the resumption of meiosis of the oocyte in response to Luteinizing Hormone (LH) from the pituitary gland. In this project, I performed *in vitro* GC activity assays on membranes from either rat or mouse ovarian follicles with or without a 20 or 30 minute LH treatment. I also performed GC assays on ovarian follicle membranes incubated with or without various phosphatase inhibitors. The first study in rat ovarian follicles identified two separate processes that decrease guanylyl cyclase activity in response to LH. First, GC-B is rapidly dephosphorylated by an unidentified phosphoprotein phosphatase (PPP). This is detected at 10 minutes post-LH treatment and reaches its maximal effect at 30 minutes post-LH treatment. Second, CNP is decreased 4 hours after treatment with LH. Experiments employing phosphatase inhibitors have narrowed the possible phosphatases that dephosphorylate GC-B to the PPP family, with gene expression analysis further narrowing the possible phosphatases to PPP1, PPP2, and/or PPP6 as the most likely candidates for causing the observed GC-B dephosphorylation in response to LH treatment. This was the first study to demonstrate that dephosphorylation of NPRs, which is known to be regulatory in *in vitro* settings, is a *de facto in vivo* regulatory mechanism. My experiments directly contributed to the validation and calibration of this rat model system compared to the mouse system used in previous studies and revealed a role for phosphodiesterases (PDEs) in the LH-induced decrease in follicle cGMP content. This study was published in *Development* in 2014 (*152*). Subsequently, our coauthors continued this project and demonstrated that both PDE5 and PDE1 contribute to the decrease in follicle cGMP content required for resumption of meiosis (*236*).

The second study in mouse ovarian follicles introduced a novel mouse model based on a glutamate-substituted form of GC-B called GC-B-7E that was engineered by Andrea Yoder, a previous graduate student in the Potter laboratory, that contains glutamate substitutions for all known and putative phosphorylation sites (*27*).This mutant form of GC-B is activated by CNP like the wild type phosphorylated form of GC-B, but has more CNP-dependent activity *in vivo* because more of the protein contains negative charge since it receives the charge as a result of translation, not post-translationally by phosphorylation (*17*). Also, it is not inactivated by dephosphorylation, since the negative charge of the glutamates cannot be removed as it can by dephosphorylating the phosphorylated wild type receptor. Hence, by examining the phenotype of

the GC-B$^{7E/7E}$ mouse, we determined which physiologic responses are regulated by changes in GC-B phosphorylation.

My experiments directly validated the model system by demonstrating that the initial activation of GC-B in follicles from GC-B$^{7E/7E}$ mice is similar, if not identical, to GC-B activity determined in follicle membranes from GC-B$^{WT/WT}$ mice. In contrast to the wild type receptor, which was dephosphorylated and inhibited by LH, we found that GC-B in follicles from GC-B$^{7E/7E}$ mice was completely unaffected by LH. These data definitively demonstrated that dephosphorylation is required for the LH-dependent inhibition of GC-B in wild type mice. We went on to show that the inability to inactivate GC-B by dephosphorylation was associated with a delay in the resumption of meiosis by 5 hours in follicles from the GC-B$^{7E/7E}$ mice compared to follicles from wild type mice (*28*). Nonetheless, there was no effect on the fertilization rate. This is likely due to the remaining signaling elements activated by LH aside from PPP activation such as increased PDE activity reducing follicle cGMP content, decreasing CNP leading to less activation of GC-B present in granulosa cells, and decreased expression of GC-B over time following LH receptor stimulation. These results were published in *Developmental Biology* in 2016 (*28*).

My next project was a part of a collaboration with the groups of Drs. Sophie Wang at the Genome Institute of Singapore, Andrew Dauber at Boston Children's Hospital, and Matthew Warman at Harvard Medical School that investigated and characterized the role of GC-B mutations in idiopathic short stature (ISS) patients and was published in *Human Mutation* in 2015 (*195*). While homozygous or compound heterozygous GC-B inactivating mutations that result in AMDM are rare, heterozygous GC-B inactivating mutations are more prevalent and lead to a variety of growth impairments in the general population. This may be, in part, due to their milder phenotype attracting less attention to their underlying genetic differences. Importantly, this study was the first to sequence individuals of average height to control for naturally occurring variants that do not have any obvious phenotypic effects. In this project, I performed western blot analysis and *in vitro* guanylyl cyclase activity assays on wild type and mutant forms of GC-B recombinantly expressed in 293 cells. The various missense mutations were identified either in short stature patient cohorts or bio-bank samples from individuals at the known extremes for short stature or tall stature. Sixteen variants were found in idiopathic short stature cohorts or bio-bank extremes that were not previously identified. Of these, I characterized eight missense mutations that result in amino acid substitutions. Of these mutations, four (A48S, E389D, I494S, R562Q) were determined to likely be pathogenic in causing a change in the individual's stature. Of those

four, one variant (I494S) had altered processing and expression. Three (N247D, A549T, and R787W) were not found to be pathogenic, and one (A164G) yielded varied results of unknown significance. *In vitro* GC activity assays that I performed, determined that three variants (A48S, A164G, and E389D) were normally processed but had significant reductions in hormone-stimulated activity. Interestingly, three additional mutations that I characterized (A549T, R562Q, and R787W) were also sites of interest in my future projects. The mutation that was most significant to my research (R562Q) was found in the FINRISK bio-bank tall extreme and represents the fourth known activating mutation in GC-B. Unfortunately, because of the lack of patient data to characterize the skeletal effects of this mutation, this activating mutation has gone largely under-appreciated.

Next, I worked on a project spanning the entire Potter laboratory evaluating the effects of altered glycosylation on both the wild type and the mutant 7E versions of GC-B as well as understanding the mechanisms underlying AMDM mutations (*17*). In this project, I evaluated the role of glycosylation in regulation of GC-B activity. Specifically, I determined the differential effects of ER-mediated N-glycosylation and Golgi-mediated N-glycosylation on GC-B processing and enzymatic activity. I did this by performing western blot analysis and guanylyl cyclase activity assays on membranes from cells expressing WT or mutant GC-B incubated in the presence or absence of tunicamycin to interrupt ER-dependent N-glycosylation or from cells lacking the Golgi N-acetylglucosaminyl transferase 1 enzyme, which disrupts N-glycosylation in the Golgi apparatus. We found that the receptors with the AMDM mutations are on the cell surface and bind CNP, which was the opposite finding reported by another group in a highly cited paper (*197*). Instead, we found that the mutant receptors were unable to transduce the CNP binding signal to the GC domain. We also showed that inhibition of N-linked glycosylation in the ER, but not the Golgi yields a form of the receptor that cannot be activated. This is consistent with ER-mediated N-glycosylation's role in promoting chaperone interactions to properly fold the GC-B polypeptide. The AMDM mutant forms of GC-B tested, GC-B-L658F and GC-B-G959A, had activity profiles similar to those of WT-GC-B expressed in the presence of tunicamycin, which is predicted to cause improper folding due to a lack of chaperone interaction as a result of inhibited ER-mediated glycosylation. Thus, AMDM mutants likely destabilize the overall structure of GC-B and result in a receptor that is improperly folded and inactive. This study also indicated for the first time that in cells not lacking glycosyltranferase enzymes, the only band observed on western blots that has guanylyl cyclase activity is the upper, most heavily glycosylated band, which is also the only band found to contain phosphate.

My longest and primary project in the Potter laboratory is to investigate why the pseudokinase domains of receptor guanylyl cyclases are evolutionarily conserved in natriuretic peptide activated GCs. I initially evaluated the potential for low-level intrinsic protein kinase activity in the PKDs of GC-A and GC-B to phosphorylate their own or the other subunit's phosphorylation sites. My approach for these studies was to use single amino acid kinase-inactivating, loss-of-function mutations that are known to inactive most *bona fide* protein kinases. Instead of observing decreased receptor phosphorylation as predicted, I observed no change in the stoichiometry of phosphorylation. Rather, the mutations designed to inactivate the kinase and reduce the stoichiometry of phosphorylation unexpectedly reduced ATP-dependent allosteric reductions in the Michaelis constant (Km). While these experiments do not allow us to definitively rule out kinase activity in the PKDs of GC-A and GC-B, we can say that if kinase activity is present in these domains, it does not follow the canonical reaction mechanism because three residues that are highly conserved and required for catalytic function in most protein kinases are not required for the phosphorylation of GC-A and GC-B. This led me to evaluate the role of the well-known dynamic hydrophobic core in other protein kinases in the PKDs of GC-A and GC-B using newly designed gain-of-function mutations that either mimic the allosterically active state or enhance the hypothesized allosteric transmission networks.

We showed that the PKDs of GC-A and GC-B are evolutionarily conserved for their molecular switch properties intrinsic to the protein kinase family by designing three allosterically activating mutations that mimicked the ATP-bound state (GC-A-A533W), increased activity at low concentrations of CNP (GC-B-M571F), or increased activity in the presence of either CNP or ATP alone with comparatively little effect when both activators are present (GC-B-I583W). The dynamic assembly and disassembly of the hydrophobic core elements known as the R-spine and the C-spine mediate these molecular switch functions in the protein kinase family and are present in the PKD of GC-A and GC-B as well. Allostery had previously been assumed but had not been tested because of the delicate conditions necessary to produce biologically meaningful results with GC-A and GC-B. Without Mg^{2+} as the metal cofactor and the proper membrane environment activity assays do not reflect a physiologically relevant state of the enzyme, suggesting that the structure and/or dynamics of the protein are altered in these conditions. Thus, purified protein preparations, which require detergent solubilization, are unlikely to provide accurate information about the native state of GC-A and GC-B. This new model of the intracellular domain interactions and dynamics necessary for maintenance of low activity in the basal state as well as the mechanism of NP binding-dependent signal transduction to the GC catalytic domain may

reveal the underlying mechanisms to explain over-activation or under-activation mutations of GC-A and GC-B in disease states as well as provide new pharmacologic sites for allosteric activators or inhibitors.

FUTURE DIRECTIONS

Evaluating the dynamics of GC-A and GC-B by FRET

While my projects have advanced the field by showing how various natural mutations, phosphorylation and ATP binding affect particulate GC activity, many questions remain unanswered regarding the activation and inactivation of GC-A and GC-B as well as the entire receptor guanylyl cyclase family. The allostery model for the PKDs of GC-A and GC-B relies on their dynamic properties as molecular switches. The primary tools available for study of protein dynamics are nuclear magnetic resonance (NMR), electron paramagnetic resonance (EPR), and fluorescence-based techniques such as Förster/fluorescence resonance energy transfer (FRET). Given the delicate conditions necessary to obtain information relevant to the biological transitions associated with function, FRET emerges as the most feasible tool to further study the dynamics of GC-A and GC-B because it is the only tool that does not require extensive purification when encoded fluorescent proteins are used for the donor/acceptor pair and because it can be used in live cells.

Fluorescent proteins in the donor/acceptor pair can be inserted into surface exposed loops or tagged to the termini of proteins to generate a protein with intrinsic FRET properties dependent on the structure and dynamics. Many insertion points and donor/acceptor pairs may need to be evaluated to generate one polypeptide in which both donor and acceptor fluorescent proteins are present without disrupting the necessary interactions for GC activity and allosteric regulation. Studies identifying these insertion points would also be beneficial towards understanding the molecular interactions necessary for GC activity and allosteric regulation. Once a FRET-competent construct of wild-type GC-A or GC-B is developed, one could measure the donor-acceptor distance in cells. This approach was employed by Dave Thomas's laboratory at University of Minnesota using an RFP/GFP pair (*237*). Changes in dynamics upon NP binding are hypothesized to modify the donor-acceptor distance or narrow the distribution of distances observed. This system lends itself to studies examining the intracellular effects of extracellular NP binding as well as studies investigating changes in dynamics resulting from allosterically activating mutations in the most biologically intact state.

A salt-bridge mechanism for regulation by phosphorylation

Another project that would build upon my findings was initially begun by a former postdoctoral fellow, Dr. Neil Otto, which focuses on determining why phosphorylation of the PKDs of GC-A and GC-B is required for allosteric activation of these enzymes by their

respective NP's. One of the primary structural roles of acidic residues such as phosphorylated serines and threonines is to form salt-bridges with basic amino acids like lysine and arginine (*238*). Because we can mimic the effect of the phosphorylation sites with single or double glutamate substitutions, this suggested that the primary role of the phosphate was to provide a region of localized negative charge, possibly for salt bridge formation with an arginine or lysine. When sequence conservation was mapped onto the same homology model used in my studies of allosteric activation of GC-A and GC-B a conserved surface-exposed patch of four arginines and lysines was found that could be the site of salt-bridge interactions with the phosphorylated serines and threonines of GC-A and GC-B (GC-A K613, R766, R770, K771, Fig 1D). Further modeling of GC-B on the I-TASSER server identified a fifth basic amino acid with similar orientation and conservation to those identified in GC-A (GC-A K774, Fig 1D). The majority of this patch is found on the αI-helix in the α-helical GHI subdomain; a well-known allosteric regulatory region in eukaryotic protein kinases not found in the less-regulated eukaryotic-like kinases (*56, 239*). Furthermore, if the PKDs of GC-A and GC-B adopt a BRAF-like dimerization state this would put the phosphorylation sites of GC-A and GC-B within interaction distance of the basic patch (Fig. 1).

I then mutated these Arg/Lys sites to Ala and observed similar kinetic effects as observed when the corresponding phosphorylation sites hypothesized to interact with the basic residues were mutated to Ala (Fig. 2). In single Ala substitutions of the first four basic sites identified in GC-A, I made two observations: 1) Ala substitutions at Arg residues reduced GC activity more than Ala substitutions at Lys residues and 2) Ala substitutions at the N-terminal sites (Fig. 2A, open markers) inactivated GC-A more than Ala substitutions at the C-terminal sites (Fig. 2A, filled markers). I then sequentially compounded the four Ala substitutions beginning at either the N-terminal basic site (GC-A K613, Fig. 2B) or the C-terminal basic site (GC-A K771, Fig. 2C). The differences between the double Ala-substituted constructs relative to their WT and quadruple Ala-substituted controls further validated my second observation. Because the GC activity of the GC-A-K613A/R766A mutant was more harshly affected than the GC-A-R770A/K771A mutant relative to their WT and quadruple Ala-substituted controls, this suggests that the N-terminal sites are more important to our hypothesized salt-bridge model of regulation by phosphorylation. These data are the first to suggest a molecular mechanism to explain how the phosphorylation sites of GC-A and GC-B exert their regulatory effect over the transmission of the NP-binding signal to the GC catalytic domain. Further experiments to test this hypothesis involve making "charge-switch" mutations wherein we mutate the basic patch to acidic residues and mutate the

phosphorylation sites to basic residues to recreate the same regulatory interactions using amino acids of opposite charge. These studies would further refine the model of allostery that I generated through the incorporation of another important regulatory element; phosphorylation. With a comprehensive model describing how NP binding stimulates turnover of GTP to cGMP in an ATP-dependent manner in only the phosphorylated state, we gain a new level of understanding of these enzymes, which could lead to the development of small molecule inhibitors or activators of GC-A or GC-B that can be used to treat cardiovascular or skeletal diseases.

αC Helix modulation of NP activation

I have now implemented a model for the transition from an allosterically inactive state to an allosterically active state within the PKD that is initiated by the rotation of the extracellular domains as a result of NP binding. However, we do not yet understand how the NP-binding signal is propagated across the membrane to initiate this transition in the PKD. Combining functional GC activity assay data from multiple mutations yielded a site of regulation by hormone activation: the αC-helix. Three mutations along this helix increased activity at sub-saturating concentrations of NP (R562Q, F566L, M571F; Fig. 3) and structural analysis showed that all three mutations are predicted to move the αC-helix, a highly important regulatory element in all known protein kinases and pseudokinases, towards the helix-in state (Fig. 3A). The helix-in state is a hallmark of allosterically active kinases and pseudokinases (*56, 240-242*). What interactions outside of the PKD are mediating this αC-helix motion? The two key roles of Arg in protein structure are salt-bridge electrostatic interactions and planar stacking interactions with aromatic amino acid residues. Because R562 and F566 exist on the same face of the αC-helix, we further analyzed these two mutations and combined both the F566L and R562Q mutations to make the double mutant GC-B R562Q/F566L in preliminary experiments. The F566L mutation had lower activating effects than the R562Q mutant, and R562Q/F566L was no different from R562Q (Fig. 4), indicating that R562 is the primary residue in this interaction, and F566 is involved in positioning R562 for interaction with either aromatic amino acids or negatively charged amino acids.

Because the phosphorylated activation loop commonly forms salt-bridge interactions with the αC-helix in most protein kinases, we investigated if negatively charged amino acids in the activation loop form any interaction with R562. The activation loops of GC-A and GC-B do not contain any known phosphorylation sites, but they do contain three conserved aspartates or glutamates in the spread of five amino acids that could substitute in this charge interaction. If this

region of concentrated negative charge interacts with R562, then mutation of all three acid sites to their corresponding amides in GC-B would be expected to mimic the effects of the R562Q mutation. In contrast, this failed to have any effect on receptor activation (Fig. 5) indicating that these amino acids are not salt-bridge interaction partners with R562. Other conserved acidic motifs in GC-A and GC-B are found in the linker region preceding the PKD and in the coiled-coil hinge region preceding the cyclase domain, which have yet to be tested.

Extending the allostery model beyond the PKD

The effects and positions of R562Q and F566L mutations both lend themselves to a hypothesized Arg/aromatic stack along the outer edge of the αC-helix. Both R562 and F566 are invariant in GC-A's and GC-B's and any surface-exposed aromatic amino acids that interact alongside R562 and F566 to form a contiguous stack or a cluster of interaction are predicted to also be highly conserved or invariant. Mutations at these conserved aromatic amino acids are predicted to have similar increases in GC activity at sub-saturating concentrations of NP. Combinations of mutations at this novel interaction site may also prove to be constitutively activating if these mutations result in the αC-helix being locked in the helix-in state. Similarly, mutations at these sites to change to a different mechanism of interaction, such as Van der Waal's interactions in aliphatic hydrophobic packing, may restore the enzyme to a more wild-type-like state. An invariant W-R-ψ-R-W (ψ = aliphatic hydrophobic by the convention standardized in (*243*)) motif is present in the linker region between the transmembrane helix and PKD in GC-A and GC-B. An example of a potential mode of interaction with R562 and F566 are shown (Fig. 6A). Models of this linker region and the PKD of GC-B generated on the I-TASSER protein structure prediction server (*244-246*), which has been cited over 2400 times since its development, do not show this linker region adopting clear secondary structure or localization. Because the distance between amide nitrogens in protein structures is approximately 3.5 Å and the distance to be covered between the modeled N-terminus and F566 in the opposite subunit is 34.8 Å a minimum of 10 amino acids would be required for the WRψRW motif to reach F566. Thus, it is reasonable that the 16 amino acids between the modeled N-terminus and the WRψRW motif in this linker region are sufficient to allow interaction with the αC-helix of the opposite subunit in the GC-B homodimer based on the BRAF-like dimerization model (Fig. 6B).

Similarly, how does the transition from an allosterically inactive state to an allosterically active state within the PKD propagate to the GC domain to increase turnover of GTP to cGMP? Given our hypothesized BRAF-like PKD dimerization state and the recent structure of the

adenylyl cyclase domain with the preceding helical domain from *Mycobacterium intracellulare* (PDB:5O5K), this leaves only 28 amino acids structurally unaccounted for and a well-defined space to fill to develop a model to address this question. Within 15 models of GC-A and 25 models of GC-B generated on the I-TASSER protein structure prediction server(*244-246*) 28 models cluster this area of primary sequence into one of two potential positions, both of which are predominantly α-helical and traverse the side face of the PKD. Twenty-one of these models dock this helix between the αF-αG and αG-αH loops with two primary orientations (Fig. 7, blue and cyan), and seven models dock this helix between the αD-αE and β6-β7 loops (Fig. 7, red). The transition observed in other kinases from fully open in the apo state to fully closed in the most activated state could clamp down on this helix in either interaction site and as such, these interaction sites are hypothesized to participate in transmitting the NP-binding signal to the helical and cyclase domains following the PKDs of GC-A and GC-B, which would extend our model of allosteric activation for these enzymes.

FIGURES:

Figure 1. A conserved patch of basic residues in the PKD is positioned to interact with known phosphorylation sites in a hypothesized BRAF-like dimer.

A. A homology model generated by Dr. Nick Levinson of the PKD of GC-A based on the structure of Lck with α-carbons of the identified basic sites (blue) and known phosphorylation sites (red) to highlight their potential interaction in a hypothesized BRAF-like dimer. B. A model of the PKD of GC-B generated on the I-TASSER server with the known phosphorylation sites and conserved basic residues indicated with spheres in a BRAF-like dimer similar to GC-A. C. The dimer interface of the GC-B dimer model. D. Identification of the conserved basic sites identified in the GC-A homology model.

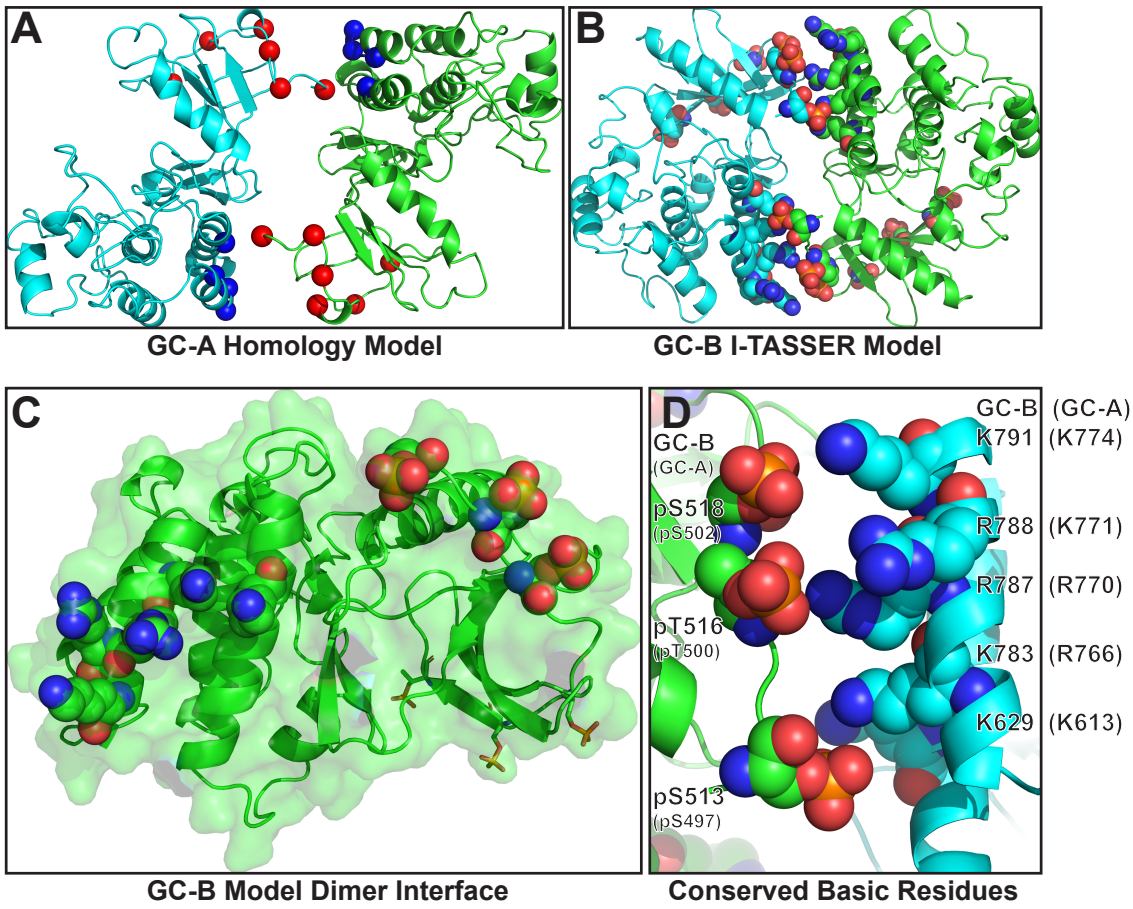

Figure 2. Mutation of conserved basic sites reduces activation similar to dephosphorylation. **A, B, C.** GC activity measured for 5 minutes in membranes with increasing concentrations of GTP, 5mM $MgCl_2$, 1µM ANP, and 1mM ATP from 293T cells transfected with wild type or mutant GC-A. *n* = 2.

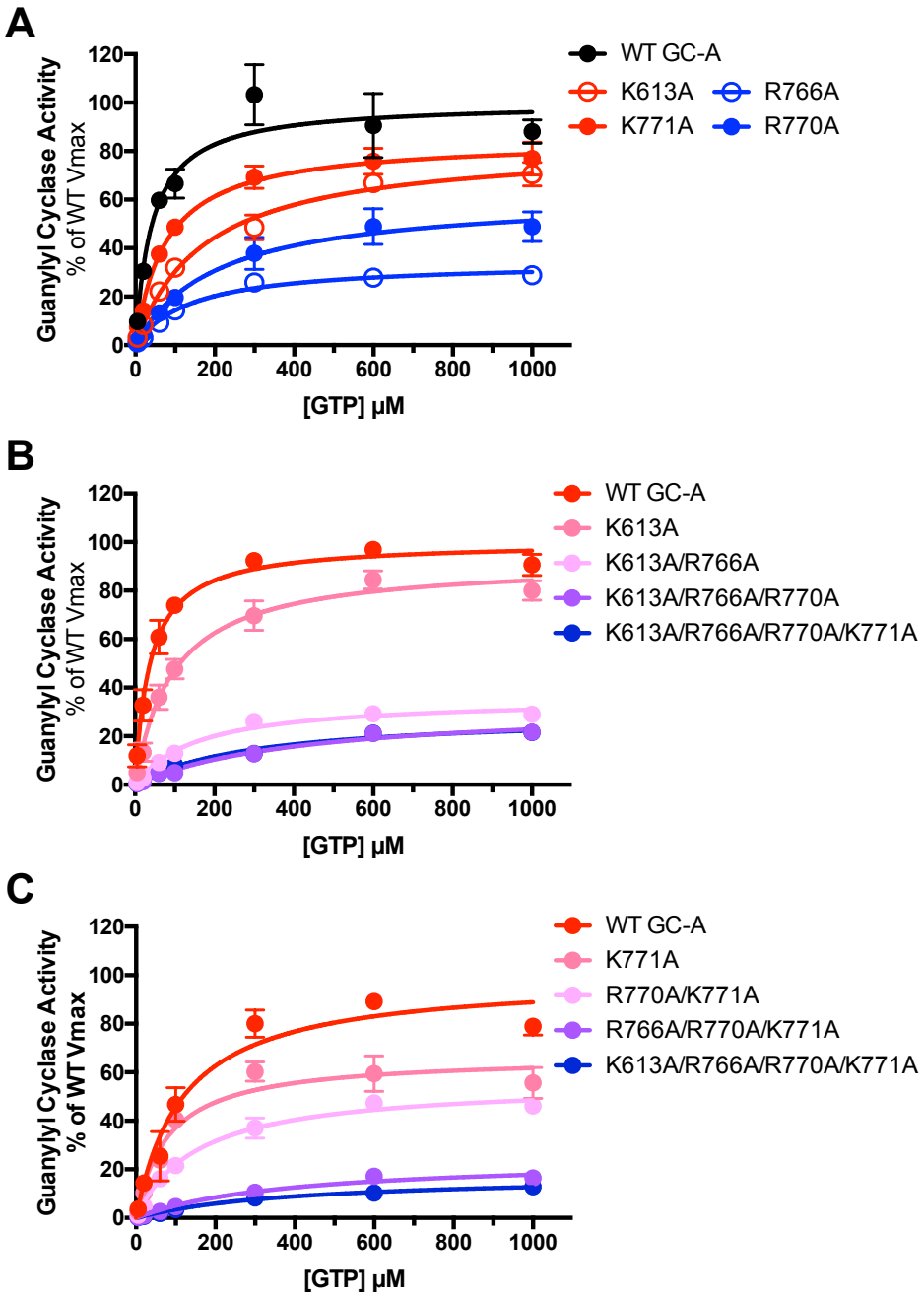

Figure 3. Preliminary data suggests αC-helix motion controls NP sensitivity.

A. The αC-helix of GC-B viewed from the bottom. Sites of three mutations are indicated and their hypothesized effects on αC-helix motion are briefly explained. B, C, D. Guanylyl cyclase activity assays without CNP expressed as a percent of saturating (1μM) CNP stimulation for GC-B R562Q, F566L, and M571F respectively. Activities are plotted separately as the different mutants were not assayed in the same experiments. R562Q; n = 4, F566L; n = 2, M571F; n = 3. E, F, G. Guanylyl cyclase activity assays with sub-saturating (50nM) CNP concentrations expressed as a percent of saturating (1μM) CNP stimulation for GC-B R562Q, F566L, and M571F respectively. Activities are plotted separately as the different mutants were not assayed in the same experiments. R562Q; n = 4, F566L; n = 2, M571F; n = 3.

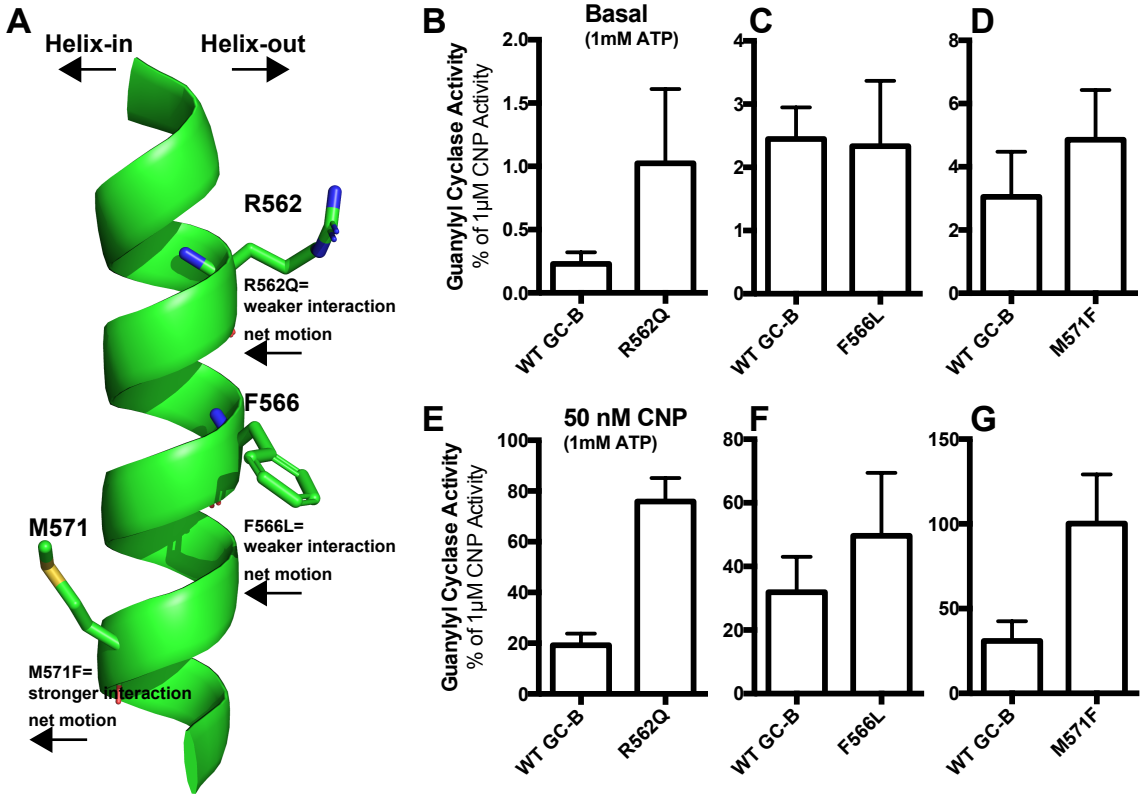

Figure 4. Preliminary data shows F566 positions R562 for optimal regulatory interactions. We performed guanylyl cyclase activity assays on membranes from cells transiently transfected with the indicated receptors in the presence of 1mM ATP, 0.1mM GTP, and the indicated concentrations of CNP to estimate the EC_{50} for CNP-dependent activation of GC-B.

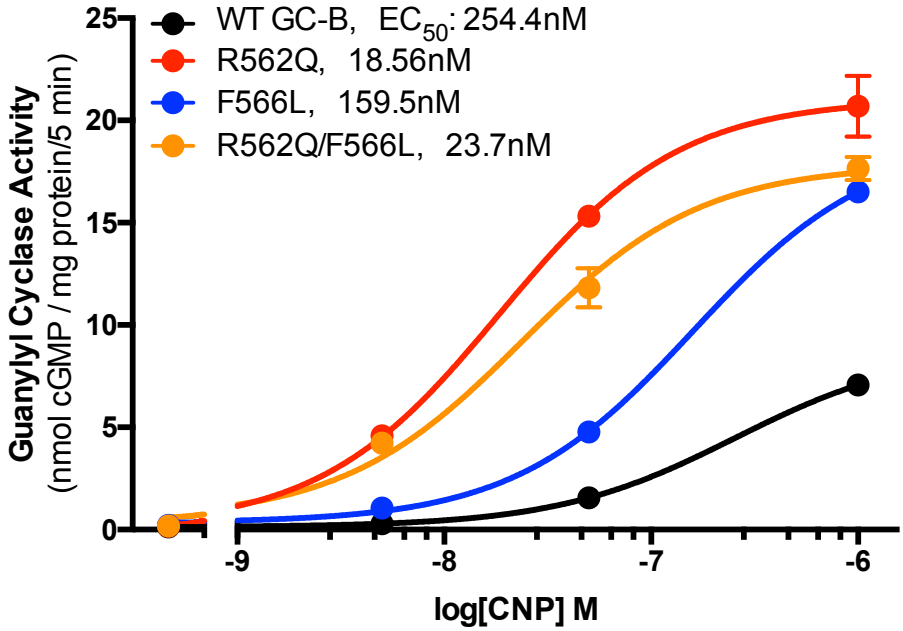

Figure 5. Preliminary data shows removing negative charge in the activation loop does not mimic the R562Q mutation.

Guanylyl cyclase activity assays either without CNP (ATP Only) or sub-saturating concentrations of CNP (50nM) expressed as a percent of activity measured in the presence of saturating concentrations of CNP (1μM) and ATP stimulation for WT or mutant GC-B. n = 2.

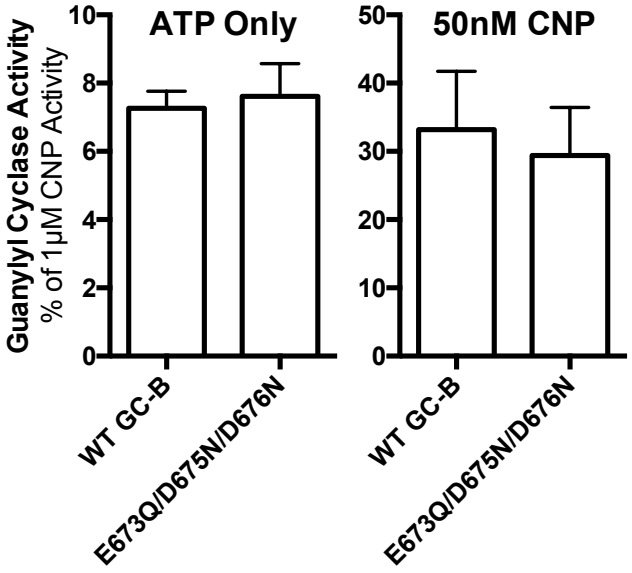

Figure 6. Hypothesized interactions between the N-terminal Linker and the PKD.
A. A model generated in PyMol for how conserved tryptophans could interact with the R562/F566 stack. B. A model showing how the N-terminal linker region may interact with αC-helix of the opposite subunit.

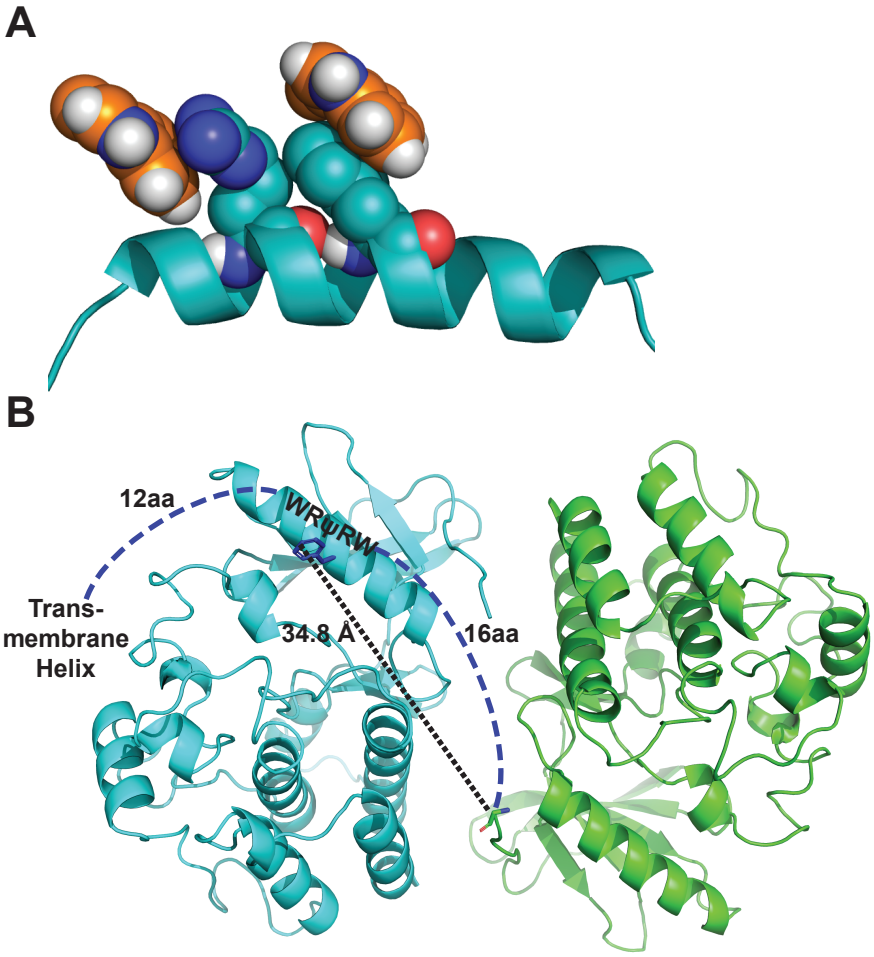

Figure 7. Representative models of the PKD C-terminal hinge helix.

Models of the PKDs of GC-A and GC-B and hinge helix were generated on the I-TASSER server and representative structures of clustered models are shown aligned with a model of the PKD. Twenty-one models of 40 generated cluster to the helices in blue and cyan. Seven models cluster to the helix in red. The loops interacting with these helices are indicated in the same color as the helix.

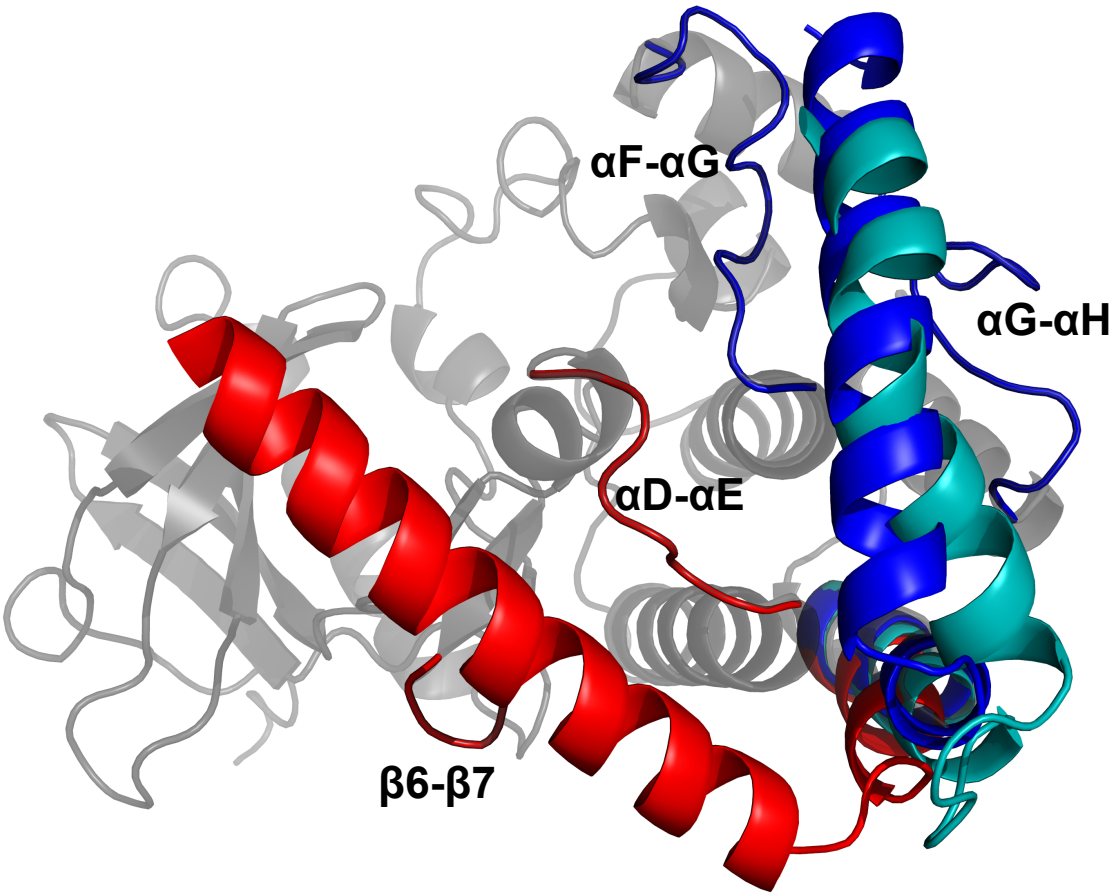

Bibliography

1. A. J. de Bold, H. B. Borenstein, A. T. Veress, H. Sonnenberg, A rapid and potent natriuretic response to intravenous injection of atrial myocardial extract in rats. *Life Sci* **28**, 89-94 (1981).
2. T. Sudoh, N. Minamino, K. Kangawa, H. Matsuo, C-type natriuretic peptide (CNP): a new member of natriuretic peptide family identified in porcine brain. *Biochem Biophys Res Commun* **168**, 863-870 (1990).
3. T. Sudoh, K. Kangawa, N. Minamino, H. Matsuo, A new natriuretic peptide in porcine brain. *Nature* **332**, 78-81 (1988).
4. R. A. Rose, W. R. Giles, Natriuretic peptide C receptor signalling in the heart and vasculature. *J Physiol* **586**, 353-366 (2008).
5. T. Kuno *et al.*, Co-purification of an atrial natriuretic factor receptor and particulate guanylate cyclase from rat lung. *J Biol Chem* **261**, 5817-5823 (1986).
6. R. Takayanagi *et al.*, Two distinct forms of receptors for atrial natriuretic factor in bovine adrenocortical cells. Purification, ligand binding, and peptide mapping. *J Biol Chem* **262**, 12104-12113 (1987).
7. S. Meloche, N. McNicoll, B. Liu, H. Ong, A. De Lean, Atrial natriuretic factor R1 receptor from bovine adrenal zona glomerulosa: purification, characterization, and modulation by amiloride. *Biochemistry* **27**, 8151-8158 (1988).
8. M. Chinkers *et al.*, A membrane form of guanylate cyclase is an atrial natriuretic peptide receptor. *Nature* **338**, 78-83 (1989).
9. D. G. Lowe *et al.*, Human atrial natriuretic peptide receptor defines a new paradigm for second messenger signal transduction. *Embo J* **8**, 1377-1384 (1989).
10. K. J. Koller *et al.*, Selective activation of the B natriuretic peptide receptor by C-type natriuretic peptide (CNP). *Science* **252**, 120-123 (1991).
11. S. Schulz *et al.*, The primary structure of a plasma membrane guanylate cyclase demonstrates diversity within this new receptor family. *Cell* **58**, 1155-1162 (1989).
12. M. Chinkers, E. M. Wilson, Ligand-independent oligomerization of natriuretic peptide receptors. Identification of heteromeric receptors and a dominant negative mutant. *The Journal of biological chemistry* **267**, 18589-18597 (1992).
13. K. J. Koller, F. J. de Sauvage, D. G. Lowe, D. V. Goeddel, Conservation of the kinaselike regulatory domain is essential for activation of the natriuretic peptide receptor guanylyl cyclases. *Mol Cell Biol* **12**, 2581-2590 (1992).
14. L. R. Potter, T. Hunter, Phosphorylation of the kinase homology domain is essential for activation of the A-type natriuretic peptide receptor. *Molecular and cellular biology* **18**, 2164-2172 (1998).
15. E. M. Wilson, M. Chinkers, Identification of sequences mediating guanylyl cyclase dimerization. *Biochemistry* **34**, 4696-4701 (1995).
16. K. H. Biswas, A. R. Shenoy, A. Dutta, S. S. Visweswariah, The evolution of guanylyl cyclases as multidomain proteins: conserved features of kinase-cyclase domain fusions. *J Mol Evol* **68**, 587-602 (2009).
17. D. M. Dickey *et al.*, Catalytically Active Guanylyl Cyclase B Requires Endoplasmic Reticulum-mediated Glycosylation, and Mutations That Inhibit This Process Cause Dwarfism. *J Biol Chem* **291**, 11385-11393 (2016).
18. D. G. Lowe, B. M. Fendly, Human natriuretic peptide receptor-A guanylyl cyclase. Hormone cross- linking and antibody reactivity distinguish receptor glycoforms. *J Biol Chem* **267**, 21691-21697 (1992).
19. J. M. Heim, S. Singh, R. Gerzer, Effect of glycosylation on cloned ANF-sensitive guanylyl cyclase. *Life Sci* **59**, PL61-68 (1996).

20. M. Miyagi, X. Zhang, K. S. Misono, Glycosylation sites in the atrial natriuretic peptide receptor Oligosaccharide structures are not required for hormone binding. *Eur J Biochem* **267**, 5758-5768 (2000).
21. R. Kumar, N. Grammatikakis, M. Chinkers, Regulation of the atrial natriuretic peptide receptor by heat shock protein 90 complexes. *J Biol Chem* **276**, 11371-11375 (2001).
22. L. R. Potter, Phosphorylation-dependent regulation of the guanylyl cyclase-linked natriuretic peptide receptor B: dephosphorylation is a mechanism of desensitization. *Biochemistry* **37**, 2422-2429 (1998).
23. L. R. Potter, D. L. Garbers, Dephosphorylation of the guanylyl cyclase-A receptor causes desensitization. *The Journal of biological chemistry* **267**, 14531-14534 (1992).
24. L. R. Potter, T. Hunter, Identification and characterization of the major phosphorylation sites of the B-type natriuretic peptide receptor. *The Journal of biological chemistry* **273**, 15533-15539 (1998).
25. L. R. Potter, D. L. Garbers, Protein kinase C-dependent desensitization of the atrial natriuretic peptide receptor is mediated by dephosphorylation. *The Journal of biological chemistry* **269**, 14636-14642 (1994).
26. L. R. Potter, T. Hunter, Activation of protein kinase C stimulates the dephosphorylation of natriuretic peptide receptor-B at a single serine residue: a possible mechanism of heterologous desensitization. *The Journal of biological chemistry* **275**, 31099-31106 (2000).
27. A. R. Yoder *et al.*, A Functional Screen Provides Evidence for a Conserved, Regulatory, Juxtamembrane Phosphorylation Site in Guanylyl Cyclase A and B. *PLoS ONE* **7**, e36747 (2012).
28. L. C. Shuhaibar *et al.*, Dephosphorylation of juxtamembrane serines and threonines of the NPR2 guanylyl cyclase is required for rapid resumption of oocyte meiosis in response to luteinizing hormone. *Dev Biol* **409**, 194-201 (2016).
29. J. W. Robinson *et al.*, Dephosphorylation is the mechanism of fibroblast growth factor inhibition of guanylyl cyclase-B. *Cell Signal* **40**, 222-229 (2017).
30. L. C. Shuhaibar *et al.*, Dephosphorylation of the NPR2 guanylyl cyclase contributes to inhibition of bone growth by fibroblast growth factor. *Elife* **6**, (2017).
31. P. Pattanaik, L. Fromondi, K. P. Ng, J. He, F. van den Akker, Expression, purification, and characterization of the intra-cellular domain of the ANP receptor. *Biochimie* **91**, 888-893 (2009).
32. J. W. Robinson, L. R. Potter, Guanylyl cyclases a and B are asymmetric dimers that are allosterically activated by ATP binding to the catalytic domain. *Science signaling* **5**, ra65 (2012).
33. D. C. Foster, D. L. Garbers, Dual role for adenine nucleotides in the regulation of the atrial natriuretic peptide receptor, guanylyl cyclase-A. *J Biol Chem* **273**, 16311-16318 (1998).
34. L. K. Antos, L. R. Potter, Adenine nucleotides decrease the apparent Km of endogenous natriuretic peptide receptors for GTP. *American journal of physiology. Endocrinology and metabolism* **293**, E1756-1763 (2007).
35. M. Chinkers, S. Singh, D. L. Garbers, Adenine nucleotides are required for activation of rat atrial natriuretic peptide receptor/guanylyl cyclase expressed in a baculovirus system. *J Biol Chem* **266**, 4088-4093 (1991).
36. C. H. Chang *et al.*, Characterization of ATP-stimulated guanylate cyclase activation in rat lung membranes. *Biochim Biophys Acta* **1052**, 159-165 (1990).

37. L. K. Antos, S. E. Abbey-Hosch, D. R. Flora, L. R. Potter, ATP-independent activation of natriuretic peptide receptors. *The Journal of biological chemistry* **280**, 26928-26932 (2005).
38. H. Ogawa, Y. Qiu, C. M. Ogata, K. S. Misono, Crystal structure of hormone-bound atrial natriuretic peptide receptor extracellular domain: rotation mechanism for transmembrane signal transduction. *J Biol Chem* **279**, 28625-28631 (2004).
39. X. He, D. Chow, M. M. Martick, K. C. Garcia, Allosteric activation of a spring-loaded natriuretic peptide receptor dimer by hormone. *Science* **293**, 1657-1662 (2001).
40. M. Chinkers, D. L. Garbers, The protein kinase domain of the ANP receptor is required for signaling. *Science* **245**, 1392-1394 (1989).
41. L. R. Potter, Regulation and therapeutic targeting of peptide-activated receptor guanylyl cyclases. *Pharmacology & Therapeutics* **130**, 71-82 (2011).
42. E. J. Baude, V. K. Arora, S. Yu, D. L. Garbers, B. J. Wedel, The cloning of a Caenorhabditis elegans guanylyl cyclase and the construction of a ligand-sensitive mammalian/nematode chimeric receptor. *J Biol Chem* **272**, 16035-16039 (1997).
43. S. Schulz, C. K. Green, P. S. Yuen, D. L. Garbers, Guanylyl cyclase is a heat-stable enterotoxin receptor. *Cell* **63**, 941-948 (1990).
44. M. V. Roque, M. Camilleri, Linaclotide, a synthetic guanylate cyclase C agonist, for the treatment of functional gastrointestinal disorders associated with constipation. *Expert review of gastroenterology & hepatology* **5**, 301-310 (2011).
45. R. Bhandari *et al.*, Functional inactivation of the human guanylyl cyclase C receptor: modeling and mutation of the protein kinase-like domain. *Biochemistry* **40**, 9196-9206 (2001).
46. I. V. Peshenko, E. V. Olshevskaya, A. M. Dizhoor, Dimerization Domain of Retinal Membrane Guanylyl Cyclase 1 (RetGC1) Is an Essential Part of Guanylyl Cyclase-activating Protein (GCAP) Binding Interface. *J Biol Chem* **290**, 19584-19596 (2015).
47. I. V. Peshenko, E. V. Olshevskaya, A. M. Dizhoor, Evaluating the role of retinal membrane guanylyl cyclase 1 (RetGC1) domains in binding guanylyl cyclase-activating proteins (GCAPs). *J Biol Chem* **290**, 6913-6924 (2015).
48. W. A. Gorczyca, J. P. Van Hooser, K. Palczewski, Nucleotide inhibitors and activators of retinal guanylyl cyclase. *Biochemistry* **33**, 3217-3222 (1994).
49. J. G. Aparicio, M. L. Applebury, The photoreceptor guanylate cyclase is an autophosphorylating protein kinase. *J Biol Chem* **271**, 27083-27089 (1996).
50. G. Bereta *et al.*, A functional kinase homology domain is essential for the activity of photoreceptor guanylate cyclase 1. *J Biol Chem* **285**, 1899-1908 (2010).
51. G. BURNETT, E. P. KENNEDY, The enzymatic phosphorylation of proteins. *J Biol Chem* **211**, 969-980 (1954).
52. E. G. KREBS, E. H. FISCHER, Phosphorylase activity of skeletal muscle extracts. *J Biol Chem* **216**, 113-120 (1955).
53. M. RABINOWITZ, F. LIPMANN, Reversible phosphate transfer between yolk phosphoprotein and adenosine triphosphate. *J Biol Chem* **235**, 1043-1050 (1960).
54. D. R. Knighton *et al.*, Crystal structure of the catalytic subunit of cyclic adenosine monophosphate-dependent protein kinase [see comments]. *Science* **253**, 407-414 (1991).
55. G. Manning, D. B. Whyte, R. Martinez, T. Hunter, S. Sudarsanam, The protein kinase complement of the human genome. *Science* **298**, 1912-1934 (2002).
56. S. S. Taylor, A. P. Kornev, Protein kinases: evolution of dynamic regulatory proteins. *Trends Biochem Sci* **36**, 65-77 (2011).
57. J. A. Adams, Kinetic and catalytic mechanisms of protein kinases. *Chem Rev* **101**, 2271-2290 (2001).

58. J. Zheng *et al.*, Crystal structure of the catalytic subunit of cAMP-dependent protein kinase complexed with MgATP and peptide inhibitor. *Biochemistry* **32**, 2154-2161 (1993).
59. J. R. Knowles, Enzyme-catalyzed phosphoryl transfer reactions. *Annu Rev Biochem* **49**, 877-919 (1980).
60. K. Mukherjee *et al.*, CASK Functions as a Mg2+-independent neurexin kinase. *Cell* **133**, 328-339 (2008).
61. P. A. Cole, P. Burn, B. Takacs, C. T. Walsh, Evaluation of the catalytic mechanism of recombinant human Csk (C-terminal Src kinase) using nucleotide analogs and viscosity effects. *J Biol Chem* **269**, 30880-30887 (1994).
62. R. Qamar, M. Y. Yoon, P. F. Cook, Kinetic mechanism of the adenosine 3',5'-monophosphate dependent protein kinase catalytic subunit in the direction of magnesium adenosine 5'-diphosphate phosphorylation. *Biochemistry* **31**, 9986-9992 (1992).
63. J. Kim *et al.*, A dynamic hydrophobic core orchestrates allostery in protein kinases. *Sci Adv* **3**, e1600663 (2017).
64. B. Nolen, S. Taylor, G. Ghosh, Regulation of protein kinases; controlling activity through activation segment conformation. *Mol Cell* **15**, 661-675 (2004).
65. L. R. Masterson, A. Mascioni, N. J. Traaseth, S. S. Taylor, G. Veglia, Allosteric cooperativity in protein kinase A. *Proc Natl Acad Sci U S A* **105**, 506-511 (2008).
66. L. G. Ahuja, A. P. Kornev, C. L. McClendon, G. Veglia, S. S. Taylor, Mutation of a kinase allosteric node uncouples dynamics linked to phosphotransfer. *Proc Natl Acad Sci U S A* **114**, E931-E940 (2017).
67. T. Rajakulendran, M. Sahmi, M. Lefrançois, F. Sicheri, M. Therrien, A dimerization-dependent mechanism drives RAF catalytic activation. *Nature* **461**, 542-545 (2009).
68. H. M. Hammarén *et al.*, ATP binding to the pseudokinase domain of JAK2 is critical for pathogenic activation. *Proc Natl Acad Sci U S A* **112**, 4642-4647 (2015).
69. E. Zeqiraj *et al.*, ATP and MO25alpha regulate the conformational state of the STRADalpha pseudokinase and activation of the LKB1 tumour suppressor. *PLoS Biol* **7**, e1000126 (2009).
70. J. M. Murphy *et al.*, A robust methodology to subclassify pseudokinases based on their nucleotide-binding properties. *Biochem J* **457**, 323-334 (2014).
71. A. P. Kornev, N. M. Haste, S. S. Taylor, L. F. Eyck, Surface comparison of active and inactive protein kinases identifies a conserved activation mechanism. *Proc Natl Acad Sci U S A* **103**, 17783-17788 (2006).
72. H. S. Meharena *et al.*, Deciphering the structural basis of eukaryotic protein kinase regulation. *PLoS Biol* **11**, e1001680 (2013).
73. A. P. Kornev, S. S. Taylor, L. F. Ten Eyck, A helix scaffold for the assembly of active protein kinases. *Proc Natl Acad Sci U S A* **105**, 14377-14382 (2008).
74. V. Reiterer, P. A. Eyers, H. Farhan, Day of the dead: pseudokinases and pseudophosphatases in physiology and disease. *Trends Cell Biol* **24**, 489-505 (2014).
75. R. P. Norris *et al.*, Cyclic GMP from the surrounding somatic cells regulates cyclic AMP and meiosis in the mouse oocyte. *Development* **136**, 1869-1878 (2009).
76. S. Vaccari, J. L. Weeks, M. Hsieh, F. S. Menniti, M. Conti, Cyclic GMP signaling is involved in the luteinizing hormone-dependent meiotic maturation of mouse oocytes. *Biol Reprod* **81**, 595-604 (2009).
77. M. Bortolussi, G. Marini, A. Dal Lago, Autoradiographic study of the distribution of LH(HCG) receptors in the ovary of untreated and gonadotrophin-primed immature rats. *Cell Tissue Res* **183**, 329-342 (1977).

78. R. M. Rajagopalan-Gupta, M. L. Lamm, S. Mukherjee, M. M. Rasenick, M. Hunzicker-Dunn, Luteinizing hormone/choriogonadotropin receptor-mediated activation of heterotrimeric guanine nucleotide binding proteins in ovarian follicular membranes. *Endocrinology* **139**, 4547-4555 (1998).
79. M. Zhang, Y. Q. Su, K. Sugiura, G. Xia, J. J. Eppig, Granulosa cell ligand NPPC and its receptor NPR2 maintain meiotic arrest in mouse oocytes. *Science* **330**, 366-369 (2010).
80. K. Kawamura *et al.*, Pre-ovulatory LH/hCG surge decreases C-type natriuretic peptide secretion by ovarian granulosa cells to promote meiotic resumption of pre-ovulatory oocytes. *Human reproduction* **11**, 3094-3101 (2011).
81. J. W. Robinson *et al.*, Luteinizing hormone reduces the activity of the NPR2 guanylyl cyclase in mouse ovarian follicles, contributing to the cyclic GMP decrease that promotes resumption of meiosis in oocytes. *Developmental biology* **366**, 308-316 (2012).
82. T. Tsuji, C. Kiyosu, K. Akiyama, T. Kunieda, CNP/NPR2 signaling maintains oocyte meiotic arrest in early antral follicles and is suppressed by EGFR-mediated signaling in preovulatory follicles. *Mol Reprod Dev* **79**, 795-802 (2012).
83. K. A. Geister *et al.*, A novel loss-of-function mutation in Npr2 clarifies primary role in female reproduction and reveals a potential therapy for acromesomelic dysplasia, Maroteaux type. *Hum Mol Genet* **22**, 345-357 (2013).
84. J. Törnell, H. Billig, T. Hillensjö, Regulation of oocyte maturation by changes in ovarian levels of cyclic nucleotides. *Hum Reprod* **6**, 411-422 (1991).
85. J. Y. Peng *et al.*, Identification and gene expression analyses of natriuretic peptide system in the ovary of goat (Capra hircus). *Gene* **524**, 105-113 (2013).
86. Y. Hiradate, Y. Hoshino, K. Tanemura, E. Sato, C-type natriuretic peptide inhibits porcine oocyte meiotic resumption. *Zygote* **22**, 372-377 (2014).
87. W. Zhang *et al.*, Brain natriuretic peptide and C-type natriuretic peptide maintain porcine oocyte meiotic arrest. *J Cell Physiol* **230**, 71-81 (2015).
88. X. Liu, F. Xie, A. M. Zamah, B. Cao, M. Conti, Multiple pathways mediate luteinizing hormone regulation of cGMP signaling in the mouse ovarian follicle. *Biol Reprod* **91**, 9 (2014).
89. M. Conti, M. Hsieh, A. M. Zamah, J. S. Oh, Novel signaling mechanisms in the ovary during oocyte maturation and ovulation. *Mol Cell Endocrinol* **356**, 65-73 (2012).
90. D. Clift, M. Schuh, Restarting life: fertilization and the transition from meiosis to mitosis. *Nat Rev Mol Cell Biol* **14**, 549-562 (2013).
91. J. E. Holt, S. I. Lane, K. T. Jones, The control of meiotic maturation in mammalian oocytes. *Curr Top Dev Biol* **102**, 207-226 (2013).
92. L. M. Mehlmann, in *Oogenesis,* D. F. A. G. Cotticchio, and L. De Santis, Ed. (Springer-Verlag, London, 2013), pp. 171-182.
93. M. Hunzicker-Dunn, K. Mayo, in *Knobil and Neill's Physiology of Reproduction,* T. M. Plant, A. J. Zeleznik, Eds. (Academic Press, San Diego, 2015), pp. 895-945.
94. L. M. Mehlmann, T. L. Jones, L. A. Jaffe, Meiotic arrest in the mouse follicle maintained by a Gs protein in the oocyte. *Science* **297**, 1343-1345 (2002).
95. L. M. Mehlmann *et al.*, The Gs-linked receptor GPR3 maintains meiotic arrest in mammalian oocytes. *Science* **306**, 1947-1950 (2004).
96. K. Horner *et al.*, Rodent oocytes express an active adenylyl cyclase required for meiotic arrest. *Dev Biol* **258**, 385-396 (2003).
97. M. Hinckley, S. Vaccari, K. Horner, R. Chen, M. Conti, The G-protein-coupled receptors GPR3 and GPR12 are involved in cAMP signaling and maintenance of meiotic arrest in rodent oocytes. *Dev Biol* **287**, 249-261 (2005).

98. C. Ledent *et al.*, Premature ovarian aging in mice deficient for Gpr3. *Proc Natl Acad Sci U S A* **102**, 8922-8926 (2005).
99. E. A. Bornslaeger, P. Mattei, R. M. Schultz, Involvement of cAMP-dependent protein kinase and protein phosphorylation in regulation of mouse oocyte maturation. *Dev Biol* **114**, 453-462 (1986).
100. M. Kovo *et al.*, An active protein kinase A (PKA) is involved in meiotic arrest of rat growing oocytes. *Reproduction* **132**, 33-43 (2006).
101. J. Gutkowska *et al.*, Hormonal regulation of natriuretic peptide system during induced ovarian follicular development in the rat. *Biol Reprod* **61**, 162-170 (1999).
102. L. R. Potter, S. Abbey-Hosch, D. M. Dickey, Natriuretic peptides, their receptors, and cyclic guanosine monophosphate-dependent signaling functions. *Endocrine reviews* **27**, 47-72 (2006).
103. A. R. Yoder, M. D. Stone, T. J. Griffin, L. R. Potter, Mass spectrometric identification of phosphorylation sites in guanylyl cyclase a and B. *Biochemistry* **49**, 10137-10145 (2010).
104. M. Jankowski *et al.*, C-type natriuretic peptide and the guanylyl cyclase receptors in the rat ovary are modulated by the estrous cycle. *Biol Reprod* **56**, 59-66 (1997).
105. R. P. Norris, M. Freudzon, V. O. Nikolaev, L. A. Jaffe, Epidermal growth factor receptor kinase activity is required for gap junction closure and for part of the decrease in ovarian follicle cGMP in response to LH. *Reproduction* **140**, 655-662 (2010).
106. L. R. Potter, T. Hunter, A constitutively "phosphorylated" guanylyl cyclase-linked atrial natriuretic peptide receptor mutant is resistant to desensitization. *Molecular biology of the cell* **10**, 1811-1820 (1999).
107. S. E. Abbey, L. R. Potter, Lysophosphatidic acid inhibits C-type natriuretic peptide activation of guanylyl cyclase-B. *Endocrinology* **144**, 240-246 (2003).
108. M. Cargnello *et al.*, Phosphorylation of the eukaryotic translation initiation factor 4E-transporter (4E-T) by c-Jun N-terminal kinase promotes stress-dependent P-body assembly. *Mol Cell Biol* **32**, 4572-4584 (2012).
109. K. J. Koller, M. T. Lipari, D. V. Goeddel, Proper glycosylation and phosphorylation of the type A natriuretic peptide receptor are required for hormone-stimulated guanylyl cyclase activity. *The Journal of biological chemistry* **268**, 5997-6003 (1993).
110. E. Kinoshita, E. Kinoshita-Kikuta, K. Takiyama, T. Koike, Phosphate-binding tag, a new tool to visualize phosphorylated proteins. *Mol Cell Proteomics* **5**, 749-757 (2006).
111. J. McTague *et al.*, Different signaling mechanisms are involved in the norepinephrine-stimulated TORC1 and TORC2 nuclear translocation in rat pinealocytes. *Endocrinology* **153**, 3839-3849 (2012).
112. F. X. Yu *et al.*, Protein kinase A activates the Hippo pathway to modulate cell proliferation and differentiation. *Genes Dev* **27**, 1223-1232 (2013).
113. E. Kinoshita, E. Kinoshita-Kikuta, T. Koike, in *Protein Kinase Technologies,* H. Mukai, Ed. (Humana Press, New York, 2012), pp. 13-34.
114. J. W. Robinson, L. R. Potter, ATP Potentiates Competitive Inhibition of Guanylyl Cyclase A and B by the Staurosporine Analog, Go6976: RECIPROCAL REGULATION OF ATP AND GTP BINDING. *The Journal of biological chemistry* **286**, 33841-33844 (2011).
115. M. Swingle, L. Ni, R. E. Honkanen, Small-molecule inhibitors of ser/thr protein phosphatases: specificity, use and common forms of abuse. *Methods Mol Biol* **365**, 23-38 (2007).
116. T. W. Cohen, in *Protein Phosphatases,* J. Anno, D. R. Alexander, Eds. (Springer-Verlag, Berlin, 2004), pp. 1-20.

117. S. R. Pereira, V. M. Vasconcelos, A. Antunes, The phosphoprotein phosphatase family of Ser/Thr phosphatases as principal targets of naturally occurring toxins. *Crit Rev Toxicol* **41**, 83-110 (2011).
118. Y. M. Li, C. Mackintosh, J. E. Casida, Protein phosphatase 2A and its [3H]cantharidin/[3H]endothall thioanhydride binding site. Inhibitor specificity of cantharidin and ATP analogues. *Biochem Pharmacol* **46**, 1435-1443 (1993).
119. Y. Wang, F. Santini, K. Qin, C. Y. Huang, A Mg(2+)-dependent, Ca(2+)-inhibitable serine/threonine protein phosphatase from bovine brain. *J Biol Chem* **270**, 25607-25612 (1995).
120. R. E. Honkanen, Cantharidin, another natural toxin that inhibits the activity of serine/threonine protein phosphatases types 1 and 2A. *FEBS Lett* **330**, 283-286 (1993).
121. J. D. Corbin, I. V. Turko, A. Beasley, S. H. Francis, Phosphorylation of phosphodiesterase-5 by cyclic nucleotide-dependent protein kinase alters its catalytic and allosteric cGMP-binding activities. *Eur J Biochem* **267**, 2760-2767 (2000).
122. S. D. Rybalkin, I. G. Rybalkina, R. Feil, F. Hofmann, J. A. Beavo, Regulation of cGMP-specific phosphodiesterase (PDE5) phosphorylation in smooth muscle cells. *J Biol Chem* **277**, 3310-3317 (2002).
123. A. Tsafriri, in *Biology of Fertilization,* C. B. Metz, A. Monroy, Eds. (Academic Press, Orlando, 1985), vol. 1, pp. 221-252.
124. H. Rime, R. Ozon, Protein phosphatases are involved in the in vivo activation of histone H1 kinase in mouse oocyte. *Dev Biol* **141**, 115-122 (1990).
125. R. P. Norris *et al.*, Luteinizing hormone causes MAP kinase-dependent phosphorylation and closure of connexin 43 gap junctions in mouse ovarian follicles: one of two paths to meiotic resumption. *Development* **135**, 3229-3238 (2008).
126. I. Granot, N. Dekel, Phosphorylation and expression of connexin-43 ovarian gap junction protein are regulated by luteinizing hormone. *J Biol Chem* **269**, 30502-30509 (1994).
127. S. Sela-Abramovich, E. Chorev, D. Galiani, N. Dekel, Mitogen-activated protein kinase mediates luteinizing hormone-induced breakdown of communication and oocyte maturation in rat ovarian follicles. *Endocrinology* **146**, 1236-1244 (2005).
128. S. M. Breen *et al.*, Ovulation involves the luteinizing hormone-dependent activation of G(q/11) in granulosa cells. *Mol Endocrinol* **27**, 1483-1491 (2013).
129. M. P. Flynn *et al.*, Luteinizing hormone receptor activation in ovarian granulosa cells promotes protein kinase A-dependent dephosphorylation of microtubule-associated protein 2D. *Mol Endocrinol* **22**, 1695-1710 (2008).
130. J. Y. Park *et al.*, EGF-like growth factors as mediators of LH action in the ovulatory follicle. *Science* **303**, 682-684 (2004).
131. M. Hsieh, K. Thao, M. Conti, Genetic dissection of epidermal growth factor receptor signaling during luteinizing hormone-induced oocyte maturation. *PLoS One* **6**, e21574 (2011).
132. H. Ashkenazi *et al.*, Epidermal growth factor family members: endogenous mediators of the ovulatory response. *Endocrinology* **146**, 77-84 (2005).
133. Y. Reizel, J. Elbaz, N. Dekel, Sustained activity of the EGF receptor is an absolute requisite for LH-induced oocyte maturation and cumulus expansion. *Mol Endocrinol* **24**, 402-411 (2010).
134. S. E. Abbey, L. R. Potter, Vasopressin-dependent inhibition of the C-type natriuretic peptide receptor, NPR-B/GC-B, requires elevated intracellular calcium concentrations. *The Journal of biological chemistry* **277**, 42423-42430 (2002).

135. T. D. Chrisman, D. L. Garbers, Reciprocal Antagonism Coordinates C-type Natriuretic Peptide and Mitogen-signaling Pathways in Fibroblasts. *J Biol Chem* **274**, 4293-4299 (1999).
136. R. Potthast *et al.*, Calcium-dependent dephosphorylation mediates the hyperosmotic and lysophosphatidic acid-dependent inhibition of natriuretic peptide receptor-B/guanylyl cyclase-B. *The Journal of biological chemistry* **279**, 48513-48519 (2004).
137. S. E. Abbey-Hosch, D. Smirnov, L. R. Potter, Differential regulation of NPR-B/GC-B by protein kinase c and calcium. *Biochemical pharmacology* **70**, 686-694 (2005).
138. I. R. Thompson *et al.*, Homologous and heterologous desensitization of guanylyl cyclase-B signaling in GH3 somatolactotropes. *Cell Tissue Res* **355**, 425-436 (2014).
139. N. Tamura *et al.*, Critical roles of the guanylyl cyclase B receptor in endochondral ossification and development of female reproductive organs. *Proc Natl Acad Sci U S A* **101**, 17300-17305 (2004).
140. A. Yasoda *et al.*, Overexpression of CNP in chondrocytes rescues achondroplasia through a MAPK-dependent pathway. *Nat Med* **10**, 80-86 (2004).
141. R. C. Olney, C-type natriuretic peptide in growth: a new paradigm. *Growth hormone & IGF research : official journal of the Growth Hormone Research Society and the International IGF Research Society* **16 Suppl A**, S6-14 (2006).
142. K. Miura *et al.*, An Overgrowth Disorder Associated with Excessive Production of cGMP Due to a Gain-of-Function Mutation of the Natriuretic Peptide Receptor 2 Gene. *PloS one* **7**, e42180 (2012).
143. H. Chusho *et al.*, Dwarfism and early death in mice lacking C-type natriuretic peptide. *Proc Natl Acad Sci U S A* **98**, 4016-4021 (2001).
144. G. Ter-Avetisyan, F. G. Rathjen, H. Schmidt, Bifurcation of axons from cranial sensory neurons is disabled in the absence of Npr2-induced cGMP signaling. *J Neurosci* **34**, 737-747 (2014).
145. J. R. Becker *et al.*, Differential activation of natriuretic peptide receptors modulates cardiomyocyte proliferation during development. *Development* **141**, 335-345 (2014).
146. S. Holm, A simple sequentially rejective multiple test procedure. *Scand. J. Stat.* **6**, 65-70 (1979).
147. P. M. Bryan, L. R. Potter, The atrial natriuretic peptide receptor (NPR-A/GC-A) is dephosphorylated by distinct microcystin-sensitive and magnesium-dependent protein phosphatases. *The Journal of biological chemistry* **277**, 16041-16047 (2002).
148. L. C. Shuhaibar *et al.*, Intercellular signaling via cyclic GMP diffusion through gap junctions restarts meiosis in mouse ovarian follicles. *Proc Natl Acad Sci U S A* **112**, 5527-5532 (2015).
149. M. Schuh, J. Ellenberg, Self-organization of MTOCs replaces centrosome function during acentrosomal spindle assembly in live mouse oocytes. *Cell* **130**, 484-498 (2007).
150. M. Zhang *et al.*, Estradiol promotes and maintains cumulus cell expression of natriuretic peptide receptor 2 (NPR2) and meiotic arrest in mouse oocytes in vitro. *Endocrinology* **152**, 4377-4385 (2011).
151. C. F. Bartels *et al.*, Mutations in the transmembrane natriuretic peptide receptor NPR-B impair skeletal growth and cause acromesomelic dysplasia, type Maroteaux. *Am J Hum Genet* **75**, 27-34 (2004).
152. J. R. Egbert *et al.*, Dephosphorylation and inactivation of NPR2 guanylyl cyclase in granulosa cells contributes to the LH-induced decrease in cGMP that causes resumption of meiosis in rat oocytes. *Development* **141**, 3594-3604 (2014).
153. X. N. Wang, G. S. Greenwald, Hypophysectomy of the cyclic mouse. II. Effects of follicle-stimulating hormone (FSH) and luteinizing hormone on folliculogenesis, FSH

and human chorionic gonadotropin receptors, and steroidogenesis. *Biol Reprod* **48**, 595-605 (1993).
154. M. Thunemann *et al.*, Transgenic mice for cGMP imaging. *Circ Res* **113**, 365-371 (2013).
155. J. J. Eppig, The relationship between cumulus cell-oocyte coupling, oocyte meiotic maturation, and cumulus expansion. *Dev Biol* **89**, 268-272 (1982).
156. A. Salustri, M. Yanagishita, C. B. Underhill, T. C. Laurent, V. C. Hascall, Localization and synthesis of hyaluronic acid in the cumulus cells and mural granulosa cells of the preovulatory follicle. *Dev Biol* **151**, 541-551 (1992).
157. N. B. Gilula, M. L. Epstein, W. H. Beers, Cell-to-cell communication and ovulation. A study of the cumulus-oocyte complex. *J Cell Biol* **78**, 58-75 (1978).
158. M. Hsieh *et al.*, Luteinizing hormone-dependent activation of the epidermal growth factor network is essential for ovulation. *Mol Cell Biol* **27**, 1914-1924 (2007).
159. X. Du *et al.*, Velvet, a dominant Egfr mutation that causes wavy hair and defective eyelid development in mice. *Genetics* **166**, 331-340 (2004).
160. N. Andric, M. Thomas, M. Ascoli, Transactivation of the epidermal growth factor receptor is involved in the lutropin receptor-mediated down-regulation of ovarian aromatase expression in vivo. *Mol Endocrinol* **24**, 552-560 (2010).
161. A. Ozasa *et al.*, Complementary antagonistic actions between C-type natriuretic peptide and the MAPK pathway through FGFR-3 in ATDC5 cells. *Bone* **36**, 1056-1064 (2005).
162. M. Russwurm *et al.*, Design of fluorescence resonance energy transfer (FRET)-based cGMP indicators: a systematic approach. *Biochem J* **407**, 69-77 (2007).
163. E. C. Lee *et al.*, A highly efficient Escherichia coli-based chromosome engineering system adapted for recombinogenic targeting and subcloning of BAC DNA. *Genomics* **73**, 56-65 (2001).
164. S. Noll, G. Hampp, H. Bausbacher, N. Pellegata, H. Kranz, Site-directed mutagenesis of multi-copy-number plasmids: Red/ET recombination and unique restriction site elimination. *Biotechniques* **46**, 527-533 (2009).
165. R. Behringer, M. Gertsenstein, K. Vintersten, A. Nagy, *Manipulating the mouse embryo: A laboratory manual*. (Cold Spring Harbor Laboratory Press, Cold Spring Harbor, ed. 4, 2014), pp. 502.
166. S. H. Tang, F. J. Silva, W. M. Tsark, J. R. Mann, A Cre/loxP-deleter transgenic line in mouse strain 129S1/SvImJ. *Genesis* **32**, 199-202 (2002).
167. D. Muller, M. Hildebrand, J. Lubberstedt, M. Kuhn, R. Middendorff, The membrane receptors guanylyl cyclase-A and -B undergo distinctive changes in post-translational modification during brain development. *J Neurochem* **115**, 1024-1034 (2010).
168. N. Amano *et al.*, Identification and Functional Characterization of Two Novel NPR2 Mutations in Japanese Patients with Short Stature. *J Clin Endocrinol Metab*, jc20133525 (2014).
169. D. Calebiro *et al.*, Persistent cAMP-signals triggered by internalized G-protein-coupled receptors. *PLoS Biol* **7**, e1000172 (2009).
170. T. S. Lawrence, N. Dekel, W. H. Beers, Binding of human chorionic gonadotropin by rat cumuli oophori and granulosa cells: a comparative study. *Endocrinology* **106**, 1114-1118 (1980).
171. S. Schulz, C-type natriuretic peptide and guanylyl cyclase B receptor. *Peptides* **26**, 1024-1034 (2005).
172. P. Krejci *et al.*, Interaction of fibroblast growth factor and C-natriuretic peptide signaling in regulation of chondrocyte proliferation and extracellular matrix homeostasis. *Journal of cell science* **118**, 5089-5100 (2005).

173. V. Mericq, J. A. Uyeda, K. M. Barnes, F. De Luca, J. Baron, Regulation of fetal rat bone growth by C-type natriuretic peptide and cGMP. *Pediatr Res* **47**, 189-193 (2000).
174. R. Bocciardi *et al.*, Overexpression of the C-type natriuretic peptide (CNP) is associated with overgrowth and bone anomalies in an individual with balanced t(2;7) translocation. *Hum Mutat* **28**, 724-731 (2007).
175. A. Moncla *et al.*, A cluster of translocation breakpoints in 2q37 is associated with overexpression of NPPC in patients with a similar overgrowth phenotype. *Hum Mutat* **12**, 1183-1188 (2007).
176. K. Miura *et al.*, Overgrowth syndrome associated with a gain-of-function mutation of the natriuretic peptide receptor 2 (NPR2) gene. *Am J Med Genet A* **164**, 156-163 (2014).
177. S. E. Hannema *et al.*, An activating mutation in the kinase homology domain of the natriuretic Peptide receptor-2 causes extremely tall stature without skeletal deformities. *J Clin Endocrinol Metab* **98**, E1988-1998 (2013).
178. J. W. Robinson *et al.*, A human skeletal overgrowth mutation increases maximal velocity and blocks desensitization of guanylyl cyclase-B. *Bone* **56**, 375-382 (2013).
179. R. C. Olney *et al.*, Heterozygous mutations in natriuretic peptide receptor-B (NPR2) are associated with short stature. *The Journal of clinical endocrinology and metabolism* **91**, 1229-1232 (2006).
180. G. A. Vasques *et al.*, Heterozygous mutations in natriuretic peptide receptor-B (NPR2) gene as a cause of short stature in patients initially classified as idiopathic short stature. *J Clin Endocrinol Metab* **98**, E1636-1644 (2013).
181. S. R. Wang *et al.*, Large-scale pooled next-generation sequencing of 1077 genes to identify genetic causes of short stature. *J Clin Endocrinol Metab* **98**, E1428-1437 (2013).
182. M. J. Rock *et al.*, Gain-of-function mutations in TRPV4 cause autosomal dominant brachyolmia. *Nat Genet* **40**, 999-1003 (2008).
183. R. J. Kuczmarski *et al.*, 2000 CDC Growth Charts for the United States: methods and development. *Vital Health Stat 11*, 1-190 (2002).
184. E. Vartiainen *et al.*, Thirty-five-year trends in cardiovascular risk factors in Finland. *Int J Epidemiol* **39**, 504-518 (2010).
185. L. Leitsalu *et al.*, Cohort Profile: Estonian Biobank of the Estonian Genome Center, University of Tartu. *Int J Epidemiol* **44**, 1137-1147 (2015).
186. M. A. Rivas *et al.*, Deep resequencing of GWAS loci identifies independent rare variants associated with inflammatory bowel disease. *Nat Genet* **43**, 1066-1073 (2011).
187. G. R. Abecasis *et al.*, A map of human genome variation from population-scale sequencing. *Nature* **467**, 1061-1073 (2010).
188. A. R. Yoder, A. C. Kruse, C. A. Earhart, D. H. Ohlendorf, L. R. Potter, Reduced ability of C-type natriuretic peptide (CNP) to activate natriuretic peptide receptor B (NPR-B) causes dwarfism in lbab -/- mice. *Peptides* **29**, 1575-1581 (2008).
189. L. R. Potter, Natriuretic Peptide Metabolism, Clearance and Degradation. *The FEBS Journal* **278**, 1808-1817 (2011).
190. L. R. Potter, Guanylyl cyclase structure, function and regulation. *Cellular signalling* **23**, 1921-1926 (2011).
191. H. Schmidt *et al.*, The receptor guanylyl cyclase Npr2 is essential for sensory axon bifurcation within the spinal cord. *J Cell Biol* **179**, 331-340 (2007).
192. L. R. Potter, T. Hunter, Guanylyl cyclase-linked natriuretic peptide receptors: structure and regulation. *The Journal of biological chemistry* **276**, 6057-6060 (2001).
193. R. Hachiya *et al.*, Intact kinase homology domain of natriuretic peptide receptor-B is essential for skeletal development. *J Clin Endocrinol Metab* **92**, 4009-4014 (2007).

194. S. Khan *et al.*, Novel mutations in natriuretic peptide receptor-2 gene underlie acromesomelic dysplasia, type maroteaux. *BMC medical genetics* **13**, 44 (2012).
195. S. R. Wang *et al.*, Heterozygous Mutations in Natriuretic Peptide Receptor-B (NPR2) Gene as a Cause of Short Stature. *Hum Mutat* **36**, 474-481 (2015).
196. A. Hisado-Oliva *et al.*, Heterozygous NPR2 Mutations Cause Disproportionate Short Stature, Similar to Léri-Weill Dyschondrosteosis. *J Clin Endocrinol Metab* **100**, E1133-1142 (2015).
197. A. N. Hume *et al.*, Defective cellular trafficking of missense NPR-B mutants is the major mechanism underlying acromesomelic dysplasia-type Maroteaux. *Hum Mol Genet* **18**, 267-277 (2009).
198. W. Wang *et al.*, Acromesomelic dysplasia, type maroteaux caused by novel loss-of-function mutations of the NPR2 gene: Three case reports. *Am J Med Genet A* **170A**, 426-434 (2016).
199. P. M. Bryan *et al.*, A sensitive method for determining the phosphorylation status of natriuretic peptide receptors: cGK-Ialpha does not regulate NPR-A. *Biochemistry* **45**, 1295-1303 (2006).
200. J. A. Prescher, C. R. Bertozzi, Chemical technologies for probing glycans. *Cell* **126**, 851-854 (2006).
201. S. I. Patterson, J. H. Skene, Novel inhibitory action of tunicamycin homologues suggests a role for dynamic protein fatty acylation in growth cone-mediated neurite extension. *J Cell Biol* **124**, 521-536 (1994).
202. R. Fenrick, N. Bouchard, N. McNicoll, A. De Lean, Glycosylation of asparagine 24 of the natriuretic peptide receptor-B is crucial for the formation of a competent ligand binding domain. *Mol Cell Biochem* **173**, 25-32 (1997).
203. A. Tannous, G. B. Pisoni, D. N. Hebert, M. Molinari, N-linked sugar-regulated protein folding and quality control in the ER. *Semin Cell Dev Biol* **41**, 79-89 (2015).
204. D. Fan, P. M. Bryan, L. K. Antos, R. J. Potthast, L. R. Potter, Down-regulation does not mediate natriuretic peptide-dependent desensitization of natriuretic peptide receptor (NPR)-A or NPR-B: guanylyl cyclase-linked natriuretic peptide receptors do not internalize. *Molecular pharmacology* **67**, 174-183 (2005).
205. P. J. Reeves, N. Callewaert, R. Contreras, H. G. Khorana, Structure and function in rhodopsin: high-level expression of rhodopsin with restricted and homogeneous N-glycosylation by a tetracycline-inducible N-acetylglucosaminyltransferase I-negative HEK293S stable mammalian cell line. *Proc Natl Acad Sci U S A* **99**, 13419-13424 (2002).
206. D. R. Flora, L. R. Potter, Prolonged atrial natriuretic peptide exposure stimulates guanylyl cyclase-A degradation. *Endocrinology* **151**, 2769-2776 (2010).
207. M. Kuhn, Molecular Physiology of Membrane Guanylyl Cyclase Receptors. *Physiol Rev* **96**, 751-804 (2016).
208. T. Duda, P. Yadav, R. K. Sharma, Allosteric modification, the primary ATP activation mechanism of atrial natriuretic factor receptor guanylate cyclase. *Biochemistry* **50**, 1213-1225 (2011).
209. A. J. Moyes *et al.*, Endothelial C-type natriuretic peptide maintains vascular homeostasis. *J Clin Invest* **124**, 4039-4051 (2014).
210. J. Schroter *et al.*, Homologous desensitization of guanylyl cyclase A, the receptor for atrial natriuretic peptide, is associated with a complex phosphorylation pattern. *FEBS J* **277**, 2440-2453 (2010).

211. N. M. Otto, W. G. McDowell, D. M. Dickey, L. R. Potter, A Glutamate-Substituted Mutant Mimics the Phosphorylated and Active Form of Guanylyl Cyclase-A. *Mol Pharmacol* **92**, 67-74 (2017).
212. B. Burczynska, T. Duda, R. K. Sharma, ATP signaling site in the ARM domain of atrial natriuretic factor receptor guanylate cyclase. *Mol Cell Biochem* **301**, 93-107 (2007).
213. S. Joubert, C. Jossart, N. McNicoll, A. De Lean, Atrial natriuretic peptide-dependent photolabeling of a regulatory ATP-binding site on the natriuretic peptide receptor-A. *FEBS J* **272**, 5572-5583 (2005).
214. V. Mishra, R. Goel, S. S. Visweswariah, The regulatory role of the kinase-homology domain in receptor guanylyl cyclases: nothing 'pseudo' about it! *Biochem Soc Trans*, (2018).
215. L. R. Potter, Domain analysis of human transmembrane guanylyl cyclase receptors: implications for regulation. *Frontiers in bioscience : a journal and virtual library* **10**, 1205-1220 (2005).
216. F. Shi, S. E. Telesco, Y. Liu, R. Radhakrishnan, M. A. Lemmon, ErbB3/HER3 intracellular domain is competent to bind ATP and catalyze autophosphorylation. *Proc Natl Acad Sci U S A* **107**, 7692-7697 (2010).
217. D. Ungureanu *et al.*, The pseudokinase domain of JAK2 is a dual-specificity protein kinase that negatively regulates cytokine signaling. *Nat Struct Mol Biol* **18**, 971-976 (2011).
218. M. J. Knape *et al.*, Divalent metal ions control activity and inhibition of protein kinases. *Metallomics* **9**, 1576-1584 (2017).
219. S. Joubert, N. McNicoll, A. De Lean, Biochemical and pharmacological characterization of P-site inhibitors on homodimeric guanylyl cyclase domain from natriuretic peptide receptor-A. *Biochem Pharmacol* **73**, 954-963 (2007).
220. M. Jaleel, S. Saha, A. R. Shenoy, S. S. Visweswariah, The kinase homology domain of receptor guanylyl cyclase C: ATP binding and identification of an adenine nucleotide sensitive site. *Biochemistry* **45**, 1888-1898 (2006).
221. M. J. Robinson *et al.*, Mutation of position 52 in ERK2 creates a nonproductive binding mode for adenosine 5'-triphosphate. *Biochemistry* **35**, 5641-5646 (1996).
222. G. H. Iyer, S. Garrod, V. L. Woods, S. S. Taylor, Catalytic independent functions of a protein kinase as revealed by a kinase-dead mutant: study of the Lys72His mutant of cAMP-dependent kinase. *J Mol Biol* **351**, 1110-1122 (2005).
223. J. Hu *et al.*, Mutation that blocks ATP binding creates a pseudokinase stabilizing the scaffolding function of kinase suppressor of Ras, CRAF and BRAF. *Proc Natl Acad Sci U S A* **108**, 6067-6072 (2011).
224. J. Hu *et al.*, Allosteric activation of functionally asymmetric RAF kinase dimers. *Cell* **154**, 1036-1046 (2013).
225. S. S. Taylor, A. S. Shaw, N. Kannan, A. P. Kornev, Integration of signaling in the kinome: Architecture and regulation of the αC Helix. *Biochim Biophys Acta* **1854**, 1567-1574 (2015).
226. S. Singh *et al.*, Membrane guanylate cyclase is a cell-surface receptor with homology to protein kinases. *Nature* **334**, 708-712 (1988).
227. P. A. Eyers, J. M. Murphy, The evolving world of pseudoenzymes: proteins, prejudice and zombies. *BMC Biol* **14**, 98 (2016).
228. R. Bhandari, K. Suguna, S. S. Visweswariah, Guanylyl cyclase C receptor: regulation of catalytic activity by ATP. *Biosci Rep* **19**, 179-188 (1999).
229. A. Yamazaki *et al.*, A critical role for ATP in the stimulation of retinal guanylyl cyclase by guanylyl cyclase-activating proteins. *J Biol Chem* **278**, 33150-33160 (2003).

230. H. Gazzano, H. I. Wu, S. A. Waldman, Activation of particulate guanylate cyclase by Escherichia coli heat-stable enterotoxin is regulated by adenine nucleotides. *Infect Immun* **59**, 1552-1557 (1991).
231. D. M. Dickey, N. M. Otto, L. R. Potter, Skeletal overgrowth-causing mutations mimic an allosterically activated conformation of guanylyl cyclase-B that is inhibited by 2,4,6,-trinitrophenyl ATP. *J Biol Chem* **292**, 10220-10229 (2017).
232. H. C. Champion *et al.*, Gene transfer of endothelial nitric oxide synthase to the penis augments erectile responses in the aged rat. *Proceedings of the National Academy of Sciences of the United States of America* **96**, 11648-11652 (1999).
233. S. E. Domino, D. J. Tubb, D. L. Garbers, Assay of guanylyl cyclase catalytic activity. *Methods Enzymol* **195**, 345-355 (1991).
234. G. F. Schreiner, A. A. Protter, B-type natriuretic peptide for the treatment of congestive heart failure. *Curr Opin Pharmacol* **2**, 142-147 (2002).
235. H. J. Schäfer *et al.*, 8-N(3)-3'-biotinyl-ATP, a novel monofunctional reagent: differences in the F(1)- and V(1)-ATPases by means of the ATP analogue. *Biochem Biophys Res Commun* **286**, 1218-1227 (2001).
236. J. R. Egbert, S. P. Yee, L. A. Jaffe, Luteinizing hormone signaling phosphorylates and activates the cyclic GMP phosphodiesterase PDE5 in mouse ovarian follicles, contributing an additional component to the hormonally induced decrease in cyclic GMP that reinitiates meiosis. *Dev Biol* **435**, 6-14 (2018).
237. S. J. Gruber *et al.*, Discovery of enzyme modulators via high-throughput time-resolved FRET in living cells. *J Biomol Screen* **19**, 215-222 (2014).
238. N. Errington, A. J. Doig, A phosphoserine-lysine salt bridge within an alpha-helical peptide, the strongest alpha-helix side-chain interaction measured to date. *Biochemistry* **44**, 7553-7558 (2005).
239. S. S. Taylor, M. M. Keshwani, J. M. Steichen, A. P. Kornev, Evolution of the eukaryotic protein kinases as dynamic molecular switches. *Philos Trans R Soc Lond B Biol Sci* **367**, 2517-2528 (2012).
240. L. Palmieri, G. Rastelli, αC helix displacement as a general approach for allosteric modulation of protein kinases. *Drug Discov Today* **18**, 407-414 (2013).
241. D. Fabbro, S. W. Cowan-Jacob, H. Moebitz, Ten things you should know about protein kinases: IUPHAR Review 14. *Br J Pharmacol* **172**, 2675-2700 (2015).
242. D. A. Johnson, P. Akamine, E. Radzio-Andzelm, M. Madhusudan, S. S. Taylor, Dynamics of cAMP-dependent protein kinase. *Chem Rev* **101**, 2243-2270 (2001).
243. R. Aasland *et al.*, Normalization of nomenclature for peptide motifs as ligands of modular protein domains. *FEBS Lett* **513**, 141-144 (2002).
244. J. Yang *et al.*, The I-TASSER Suite: protein structure and function prediction. *Nat Methods* **12**, 7-8 (2015).
245. A. Roy, A. Kucukural, Y. Zhang, I-TASSER: a unified platform for automated protein structure and function prediction. *Nat Protoc* **5**, 725-738 (2010).
246. Y. Zhang, I-TASSER server for protein 3D structure prediction. *BMC Bioinformatics* **9**, 40 (2008).